UTS UNIVERSITY OF TECHNOLOGY SYDNEY

Thermal Performance of Heat Exchanger for Hydrogen Energy Storage: An Advanced Computational Fluid Dynamics (CFD) Approach

by Puchanee Larpruenrudee

Thesis submitted in fulfilment of the requirements for the degree of

Doctor of Philosophy

under the supervision of Dr Saidul Islam and A/Prof Nick Bennett

University of Technology Sydney
Faculty of Engineering and Information Technology

February 2025

Required wording for the certificate of original authorship

CERTIFICATE OF ORIGINAL AUTHORSHIP

I, *Puchanee Larpruenrudee*, declare that this thesis is submitted in fulfilment of the requirements for the award of *Doctor of Philosophy*, in the *School of Mechanical and Mechatronic Engineering* at the University of Technology Sydney.

This thesis is wholly my own work unless otherwise referenced or acknowledged. In addition, I certify that all information sources and literature used are indicated in the thesis.

This document has not been submitted for qualifications at any other academic institution.

This research is supported by the Australian Government Research Training Program.

Production Note:
Signature: Signature removed prior to publication.

Date: 17/02/25

Abstract

Metal hydride hydrogen energy storage system is one of the solid storage technologies for hydrogen storage. This storage has been recently used worldwide because of its advantages, which provide a large hydrogen storage capacity and high safety. However, the main disadvantage of this storage is the metal hydride material, which generally has a low thermal conductivity. This negatively affects the hydrogen kinetic reactions, resulting in slow hydrogen absorption and desorption reactions. This problem significantly influences the overall storage system performance. For these purposes, several techniques have been applied to enhance the overall storage system performance under the improvement of hydrogen kinetic reaction. These techniques include the improvement of heat transfer performance of the storage system by using heat exchangers, the selection of the metal hydride materials/heat transfer fluid, and the appropriate selection of operating conditions for the metal hydride storage system. Therefore, the aim of this study is to enhance the overall storage system performance. The objective is divided into several main points to achieve the study's aim based on heat transfer enhancement and appropriate operating condition selection. The new internal heat exchanger, namely a semi-cylindrical coil heat exchanger, is proposed to improve the heat transfer performance. This heat exchanger is then further developed to enhance its performance by combining itself with a central return tube. Moreover, the other existing heat exchangers are combined as the external heat exchangers to further enhance the hydrogen kinetic reaction. These external heat exchangers include the cooling jacket and phase change material. Under the phase change material configuration, the new configuration, namely the phase change material capsule, is first proposed instead of the existing configurations. In addition, the new internal fin heat exchanger, namely the triple-branched fin is designed to be combined with an internal straight tube for heat transfer enhancement purposes, which is mainly considered the effect of the pressure losses during the heat transfer fluid circulating inside the storage. The various heat exchanger parameters are analysed for the new heat exchanger design to optimise their performance under the effect of these parameters on the average metal hydride bed temperature and hydrogen kinetic reaction during absorption/desorption. Finally, the initial operating conditions of the storage system and heat transfer fluid are investigated to obtain the appropriate operating condition value for the new storage system configurations. The key findings of the present study will provide a better understanding of the heat transfer enhancement for hydrogen kinetic reaction during the absorption and desorption processes under the new heat exchanger designs, which can be useful for hydrogen storage applications, especially in mobile applications. Moreover, the modelling principle, as well as the fundamental analysis of the heat exchanger designs and their performance, can be useful for several engineering applications.

Acknowledgements

Firstly, I would like to express my deep and sincere gratitude to my principal supervisor, Dr Mohammad S. Islam, for his valuable guidance, inspiration, and constant encouragement. I have had the opportunity to apply for my PhD because of his encouragement and his advice. I have decided to study for my PhD because of receiving his inspiration. Without his help, I would not be able to get a scholarship from the University of Technology Sydney (UTS).

I would like to convey my gratitude to my co-supervisor, Dr Nick S. Bennett, for his support throughout my PhD journey. I would like to acknowledge him for his valuable insight, continuous encouragement, motivation and belief in my ability to keep working in the academic field. The collaboration work throughout my PhD project significantly motivated me to pay high attention to research projects.

I would like to express my gratitude to the University of Technology Sydney for the International Research Scholarship (IRS) to cover my tuition fees and the UTS President's Scholarship (UTSP) to assist with general living costs. Without this great opportunity, I would not be able to apply for my PhD and complete the course at this time. Special thanks to the Postgraduate Research Scholarship for the HDR WiEIT Award. This special scholarship motivated me to keep improving my academic profile with high-quality publications. The high-performance computing facility in UTS (UTS iHPC) is also acknowledged as most of my works were based on computation simulation.

A special thanks to all of my colleagues for their encouragement and support. Their words motivated me to keep working on my PhD project.

Lastly, my greatest appreciation goes to my family members, especially my father, my mother, my sister, and my aunt, for their endless support throughout my PhD journey. Their support greatly encouraged me to keep working on my PhD project. Their words and suggestions significantly helped me when I was confronted with difficult situations during my PhD journey.

List of Publications

Research Paper:

1. **Larpruenrudee, P.,** Bennett, N.S., Gu, Y., Fitch, R., & Islam, M.S., (2022). Design Optimization of a magnesium-based metal hydride hydrogen energy storage system. **Scientific Reports,** 12, 13436. https://doi.org/10.1038/s41598-022-17120-3. **SJR: 0.973 [Q1], IF: 4.997**

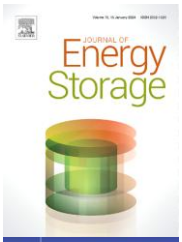

2. **Larpruenrudee, P.,** Bennett, N.S., Luo, Z., Fitch, R., Sauret, E., & Islam, M.S., (2023). A novel design for faster hydrogen storage: a combined semi-cylindrical and central return tube heat exchanger. **Journal of Energy Storage**, 71, 108018. https://doi.org/10.1016/j.est.2023.108018. **SJR: 1.456 [Q1], IF: 9.4**

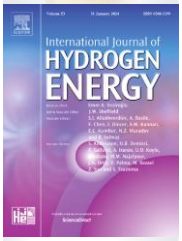

3. **Larpruenrudee, P.,** Bennett, N.S., Fitch, R., Sauret, E., Gu, Y., & Islam, M.S., (2024). Investigation of metal hydride hydrogen storage performance using phase change materials. **International Journal of Hydrogen Energy**, 60, 996-1019. https://doi.org/10.1016/j.ijhydene.2024.02.057. **SJR:1.318 [Q1], IF: 7.2**

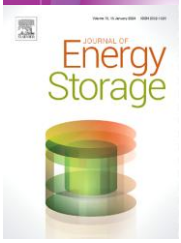

4. **Larpruenrudee, P.,** Bennett, N.S., Fitch, R., Sauret, E., Gu, Y., Hossain, M.J., & Islam, M.S., (2025). The enhancement of metal hydride hydrogen storage performance using novel triple-branched fin. **Journal of Energy Storage**, 123, 116659. https://doi.org/10.1016/j.est.2025.116659. **SJR: 1.456 [Q1], IF: 9.4**

Review Paper:

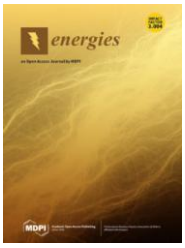

1. **Larpruenrudee, P.,** Bennett, N.S., Luo, Z., Hossain, M.J., Haque, N., Sauret, E., Fitch, R., Islam, M.S., 2025. A review on the overall performance of metal hydride-based hydrogen storage systems. **Energies**, 18, 1291. https://doi.org/10.3390/en18051291. **SJR:0.65 [Q1], IF: 3**

Peer Review Conference Paper:

1. **Larpruenrudee, P.,** Bennett, N.S., Hossain, M.J., Fitch, R., Islam, M.S. Hydrogen energy storage system: how does the semi-cylindrical helical coil heat exchanger affect metal hydride beds' thermal conductivity?. In Proceeding of the 23rd Australasian Fluid Mechanics Conference., eds C. Lei, B. Thornber, and S. Armfield. Sydney, Australia, 4-8 December 2022, 421.

Table of Contents

List of Figures

List of Tables

Nomenclature

CFD	Computational fluid dynamics
ETC	Effective thermal conductivity
HCHE	Helical coil heat exchanger
HSC	Hydrogen storage capacity
HTC	Heat transfer coefficient
HTF	Heat transfer fluid
MH	Metal hydride
MHHS	Metal hydride hydrogen storage system
ML	Machine learning
PCM	Phase change material
SCHE	Semi-cylindrical coil heat exchanger
SCHE-CR	Semi-cylindrical coil heat exchanger with central return tube
A_m	Velocity of mushy zone, kg m^{-3} s^{-1}
C_a	Absorption rate constant, s^-
C_d	Desorption rate constant, s^-
C_p	Specific heat, J kg^{-1} K^{-1}
$\frac{\partial X}{\partial t}$	Hydrogen kinetic reaction
E_a	Activation energy for absorption, J mol^{-1}
E_d	Activation energy for desorption, J mol^{-1}
G_{k_t}	Generation of turbulent kinetic energy due to mean velocity gradients
G_b	Generation of turbulent kinetic energy due to mean velocity gradients buoyancy
h_f	Heat transfer coefficient, W m^{-2} K^{-1}
I	Turbulent intensity
K	Permeability, m^2
k_t	Turbulent kinetic energy
L_{PCM}	Latent heat capacity, J kg^{-1}
M	Molecular weight, g mol^{-1}
Nu	Nusselt number
$\vec{n}$	Normal vector
P	Pressure, Pa
Pr	Prandtl number
R	Universal gas constant, J K^{-1} mol^{-1}
Re	Reynolds number
T	Temperature, K
t	time, s
U	Time-averaged velocity, m s^{-1}
u_i'	Fluctuating velocity, m s^{-1}
X	Absorbed hydrogen amount, *wt%*
x_f	Maximum absorbed hydrogen amount
Y_M	Contribution of the fluctuating dilatation in compressible turbulence to the overall dissipation rate
wt	Maximum mass content of hydrogen in the metal, wt%
ΔH	Enthalpy of reaction, J mol^{-1}
ΔS	Entropy of reaction, J mol^{-1} K^{-1}

Greek Symbols

Greek Symbols

β	Thermal expansion coefficient, K^{-1}
ε	Porosity
ε_t	Turbulent dissipation rate
σ_{ε_t}	Turbulent Prandtl number for ε_t
σ_{k_t}	Turbulent Prandtl number for k_t
λ	Thermal conductivity, W m^{-1} K^{-1}
$\lambda_{e,MH}$	Effective thermal conductivity of metal hydride, W m^{-1} K^{-1}
μ	Dynamic viscosity, Pa s
v	Kinematic viscosity, m^2 s^{-1}
ρ	Density, kg m^{-3}
ρ_{MH}	Hydride density, kg m^{-3}
$\rho_{ss,MH}$	Density of saturated metal hydride, kg m^{-3}

Subscript

0	Initial or exerting condition
a	Ambient or absorption
e	Effective
eq	Equilibrium
f	Fluid or liquid fraction
H_2	Hydrogen
i	Inner or Cartesian coordinate
J	Cartesian coordinate
in	Inlet
l	Liquid
M	Metal
ref	Reference
s	Static or solid

Chapter 1 – Introduction

1.1 Background

Hydrogen has been proposed as the most promising energy carrier to store renewable energy for both stationary and mobile applications. Thermal energy storage techniques store hydrogen for the purpose of producing electricity. The main advantages of hydrogen for energy storage are its characteristics, portability and its ability to offer high energy capacity per unit mass, which is even higher than fossil fuels. To meet the demand, large amounts of hydrogen have to be safely stored at a low cost. Refer to hydrogen storage in stationary applications; these include stationary power generation, on-site storage for utilisation, and on-site production. Regarding hydrogen storage in mobile applications, these include hydrogen transportation and vehicle fuel, such as automotive, aerospace, and maritime industries.

Basically, hydrogen energy storage can be classified into three main types, which are compressed gas, liquid storage, and solid storage/material based. For the first technique, hydrogen is stored by being compressed into a selected container, such as steel and carbon fibre cylinders. However, the technique suffers from either low capacity or high cost of the containers. Another point is the heat transfer issue during the compressing process, which can degrade the composite materials. Liquid storage is also another type of hydrogen storage. The hydrogen can be stored in a liquid state at ambient temperature. This technique allows the hydrogen to be stored in a small volume with a volumetric density of approximately 70.8 kg/m^3. In contrast, solid storage can store hydrogen with approximately 70.6 kg/m^3 of a volumetric density. Although the amount of hydrogen that can be stored in liquid storage is similar to that in solid storage, the liquid storage technique usually requires high energy consumption and operating time for the liquefaction process, which leads to a 40% energy loss. Therefore, storing hydrogen as a solid is the most efficient technique that has been widely used around the world. Solid storage includes metal hydrides, complex hydrides, chemical hydrides, and adsorbents. Complex hydrides and chemical hydrides are primarily used to store hydrogen by absorption. However, the main problems of these techniques are the lack of reversibility and the complexity of the reaction process to extract hydrogen. For the absorbents, porous materials will be employed to absorb hydrogen. This technique provides better thermal management in the charging and discharging processes than another three techniques, including metal hydride, chemical hydride, and complex hydride. However, this technique negatively affects the storage capacity when focusing on large-scale commercialisation.

Metal hydride (MH) has recently attracted significant interest as it offers a high hydrogen capacity, low material cost for storage applications, and high safety performance. The metal hydride hydrogen storage system (MHHS) has been applied to several applications, such as fuel cells, concentrating solar, thermal power, and water pumping systems. However, the main disadvantage of this storage is the MH materials which generally have a low thermal conductivity. This leads to a slow hydrogen kinetic reaction. In other words, it causes slow hydrogen absorption and desorption, which negatively affects the overall storage performance. Due to the chemical reaction between the metal hydride and hydrogen injection, the metal hydride temperature rapidly increases at the initial moment when the hydrogen is first injected into the storage system. The storage system must be cooled down to control the hydrogen charging flow at the desired rate with the maximum storage capacity. For the hydrogen desorption process, the metal hydride temperature rapidly decreases at the initial moment when the hydrogen is first released from the storage system. The storage system must be heated up to achieve maximum storage performance. Therefore, the enhancement of thermal performance inside the storage system is the key aspect to improve the hydrogen kinetic reaction. For the absorption process, the faster heat removal from the storage system significantly results in a faster hydrogen absorption reaction. For the desorption process,

faster additional heat supplied to the storage system directly results in a faster hydrogen desorption reaction.

1.2 Research Aims and Objectives

1.2.1 Research Aims:

The aim of this study is to enhance the thermal performance of the metal hydride hydrogen storage system by considering the heat exchanger structure under the computational fluid dynamics (CFD) method. The novel heat exchangers are designed and developed for this purpose.

1.2.2 Research Objectives:

To achieve the aims of this study, the following objectives have been achieved;

i. To enhance the storage thermal performance by proposing the new design of an internal heat exchanger
ii. To further enhance the thermal performance of the storage and heat exchanger by further developing the new internal heat exchanger structure from the objective i.
iii. To further enhance the thermal performance of the storage and heat exchanger by combining the new internal heat exchanger (from objective ii) with the external heat exchanger under an active thermal management technique
iv. To further enhance the thermal performance of storage and heat exchanger by combining the new internal heat exchanger (from objective ii) with the external heat exchanger under a passive thermal management technique
v. To enhance the thermal performance of the storage and heat exchangers by proposing a new internal heat exchanger design. The effect of pressure losses during the heat transfer fluid circulating inside the storage is considered.
vi. To identify an appropriate initial value for each operating parameter of the metal hydride storage system under the new storage configurations and heat exchangers. The operating parameters include;
    - Operating condition of the metal hydride storage system under the activation temperature and hydrogen pressure
    - Operating condition of the heat transfer fluid under the flow rate, initial temperature, and heat transfer coefficient

1.3 Significance and Innovation

The comprehensive understanding of the heat transfer performance inside the MHHS under the different configurations and operating conditions is the key factor to analyse and improve the thermal performance of the MHHS. The various MHHS configurations include the heat exchanger designs, the initial operating conditions of the MHHS and the heat transfer fluid (HTF) as well as the use of heat exchanger materials. For this purpose, the investigations of the average bed temperature inside the MHHS and hydrogen concentration during the hydrogen absorption/desorption process are mainly considered in the present study. Finally, the prediction of one complete duration for the hydrogen absorption-desorption cycle is proposed under the use of different heat exchanger designs and other selected parameters under the MHHS and HTF operating conditions. These new MHHS configurations would be beneficial for the industrial setting and advancements in hydrogen storage applications. Regarding hydrogen storage applications, the MHHS can be applied for both stationary and mobile applications. However, the weight of the overall MHHS is the key factor for mobile applications, while the hydrogen storage capacity is the key factor for stationary applications. The work from this present

study is only focused on hydrogen storage for mobile applications, such as vehicle fuel cells. Therefore, the additional comparison regarding the overall volumetric and gravimetric of the MHHS is analysed in this study under the new heat exchanger design.

The innovation of this study is to propose new heat exchangers to enhance the MHHS thermal performance. These new heat exchangers are designed by considering the improvement of their thermal performance when combined with the MHHS. Moreover, the thermal performance is also improved when combining these new heat exchangers with other existing heat exchangers. Firstly, the new heat exchanger, namely the semi-cylindrical coil heat exchanger (SCHE) is first designed and proposed in this study. This SCHE is developed from the conventional helical coil heat exchanger (HCHE), which is known as one of the best heat exchanger designs, compared to other heat exchanger types. Secondary, The SCHE is then further developed to enhance the heat transfer performance by combining itself with the central return tube (SCHE-CR). Under the combination of heat exchangers, it includes the use of a cooling jacket, and phase change material (PCM) as the external heat exchanger. To investigate the new heat exchanger performance when combining with other heat exchangers, the effect of PCM configuration after combining with the new heat exchanger is comprehensively analysed under the liquid fraction and average bed temperature of the MH and PCM. To further enhance the thermal performance, the new PCM configuration, namely the PCM capsule is proposed to combine with the SCHE-CR. Moreover, the new internal fin, namely the triple-branched fin, is designed and enhanced its performance for the last study in this thesis. This triple-branched fin is designed to connect with the straight tube, which contains the HTF. The purpose of this fin design is to minimise the pressure losses from the HTF during circulation throughout the heat exchanger tube. In general, increasing heat transfer surface area by using complex heat exchanger structures significantly improves the heat transfer performance. However, the drawback of these heat exchangers is the huge pressure losses. This can negatively affect the overall system's efficiency and cause system failure. To maintain the overall system/heat exchanger performance, the heat exchange efficiency and pressure drop should be balanced. In order to enhance the heat transfer rate from the HTF straight tube, the new triple-branched fin is developed for the last study of this thesis. The effect of pressure losses during the use of the HTF throughout different complex heat exchanger structures is investigated to ensure that the pressure losses are minimised before applying the HTF straight tube to the new fin design. Furthermore, the new fin performance is investigated by comparing it with other conventional fin designs. Lastly, various fin parameters are considered to improve this new fin efficiency. From the above mentioned, the parametric study under operating conditions is performed for all studies. This is to ensure that an appropriate initial value for each operating parameter is selected when having the new heat exchangers and storage configurations. The more details regarding the work from this study can be seen in Figure 1.1 under the thesis outline.

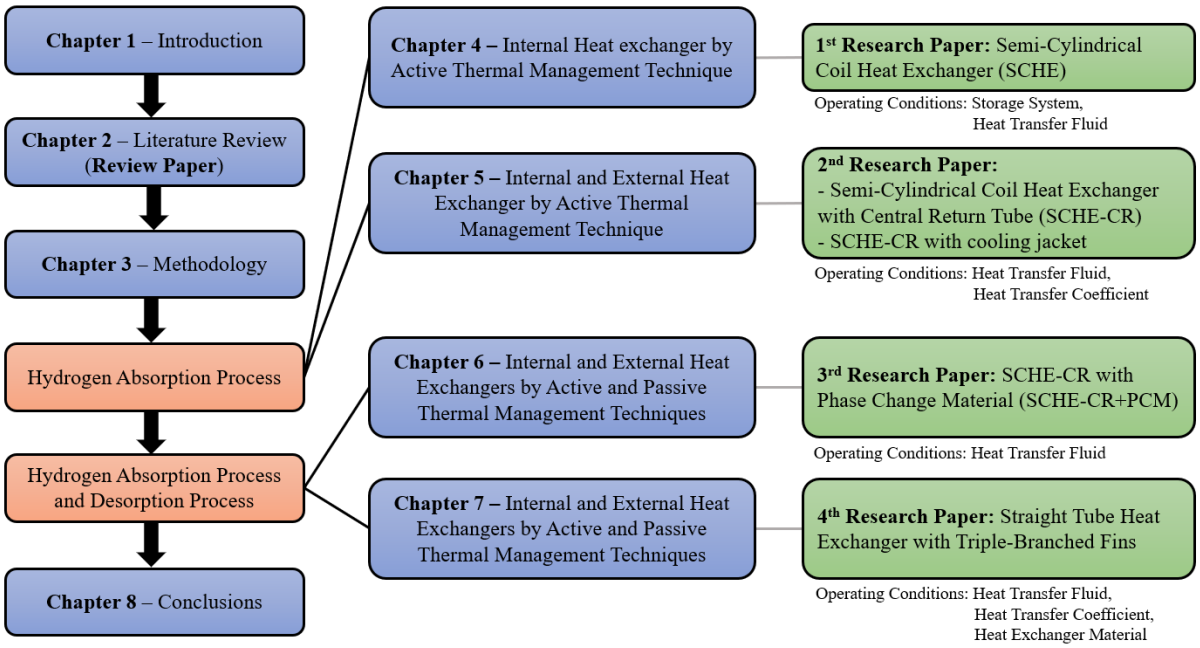

Figure 1.1 Flowchart of the thesis

1.4 Thesis Outline

This thesis contains eight chapters, including the introduction as Chapter 1, the literature review or review paper as Chapter 2, the methodology, which is applied to all main research papers, as Chapter 3, and the conclusion of all works as Chapter 8. The main research papers are divided into two main parts, which can be seen in Figure 1.1. Chapter 4 and Chapter 5 are the first two research papers that mainly focus on the hydrogen absorption process under the use of new heat exchangers (SCHE and SCHE-CR). The following Chapter 6 and Chapter 7 are the third and fourth research papers which mainly focus on the complete process of the hydrogen absorption-desorption cycle under the use of the new heat exchangers (SCHE, SCHE-CR, PCM capsule, and triple-branched fin).

The detailed framework of this present study is presented in Figure 1.2. The computational fluid dynamics (CFD) is applied to analyse the heat transfer performance and achieve the research aim for all main research papers. Under the pre-processing, SolidWorks software is used to generate the 3D models for all research papers. ANSYS Meshing is used to perform the grid refinement test. For the solver based on numerical simulation, ANSYS Fluent is used to simulate and work to fulfil the research aim and objectives. The hydrogen kinetic reaction for hydrogen absorption and desorption processes is the key parameter for the CFD simulation. The energy model is used for the convection heat transfer between the heat transfer fluid (HTF) and metal hydride (MH) bed. The viscous model with turbulent flow under transient conditions is used for the HTF. The main purpose is to cool down the MHHS during the hydrogen absorption process and to heat up the MHHS during the hydrogen desorption process. Under the post-processing, all selected models are validated against the experimental works from available literature before starting the new simulation of the new works for this study. The model validation can be found under the “Chapter 3 – Methodology” section.

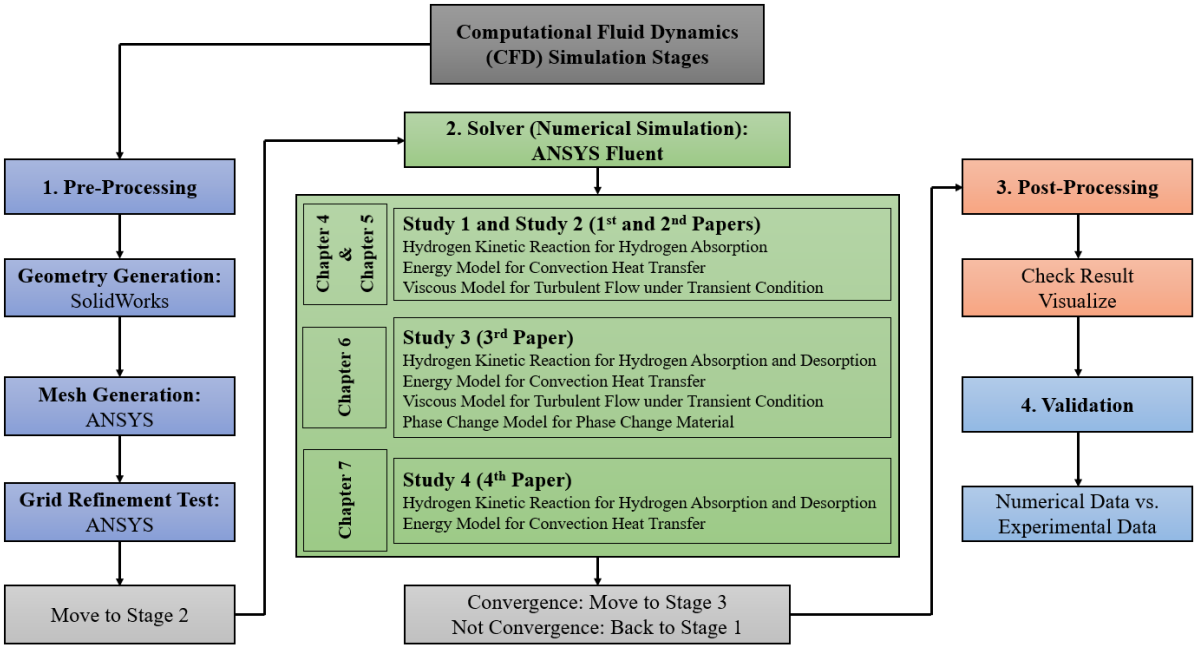

Figure 1.2 Framework of the present thesis

Chapter 2 – Literature Review: A Review on the Overall Performance of Metal Hydride-based Hydrogen Storage Systems

Review Paper: **Larpruenrudee, P.,** Bennett, N.S., Luo, Z., Hossain, M.J., Haque, N., Sauret, E., Fitch, R., Islam, M.S., 2025. A review on overall performance of the metal hydride-based hydrogen storage systems. **Energies**, 18, 1291. https://doi.org/10.3390/en18051291. **SJR:0.65 [Q1], IF: 3**

2.1 Summary

The overall performance of the MHHS is summarised and prepared as the review paper. The thermal performance of the MHHS can be significantly affected by several aspects, including the MHHS configuration under the heat exchanger designs, the selection of the MH materials and the HTF, and the operation parameters. The contents in this section are divided into three main parts, including the metal hydride materials, heat exchanger design optimisation for thermal management, and operating conditions. The structure of this work/chapter is as follows;

- Metal hydride material: Machine learning techniques for investigation of metal hydride materials' properties, Hydrogen storage capacity, Effective thermal conductivity, and Density and raw cost materials
- Heat exchanger design optimisation for thermal management: Design optimisation for active thermal management method, Design optimisation for passive thermal management method, Design optimisation based on the combination of various heat exchanger methods, Comparison between various heat exchanger methods and performances, and Heat transfer fluids
- Operating conditions: Initial condition of metal hydride storage under the initial temperature of the storage and hydrogen loading pressure, Initial condition of the heat transfer fluid under the initial temperature and fluid flow velocity, Other operating conditions and comparison of the operating parameters.

From above mentioned, the main research chapters (four research papers) are performed under the following points

i. The MH material, namely Mg_2Ni is selected as this material offers a high hydrogen storage capacity, compared to other MH materials. However, this MH material offers a low thermal conductivity compared to other MH materials such as $LaNi_5$. To solve this problem, the improvement of the hydrogen kinetic reaction rate is required instead. This can be done by the enhancement of the heat transfer performance.

ii. The new internal heat exchanger is designed and optimised under various heat exchanger parameters, such as coil pitch, tube diameter, fin angle, fin height, fin width, etc. The main consideration is to reduce the hydrogen absorption/desorption duration that is caused by the improvement of the heat transfer performance due to the new heat exchanger structure.

iii. The combination of various heat exchanger types is proposed to enhance the heat transfer performance as well as the overall storage performance. This includes the use of an external heat exchanger, such as a cooling jacket and phase change material, as well as the use of the new internal heat exchanger.

iv. The appropriate selection of operating conditions under the new heat exchanger designs are considered as parametric studies to reduce the hydrogen absorption/desorption duration.

2.2 Abstract

Metal hydride-based hydrogen storage (MHHS) has been used for several applications, including mobile and stationary applications. In general, the overall MHHS performance for both applications depends on three main factors, which are appropriate selections of metal hydride material uses, design configurations of the MHHS based on heat exchanger, and overall operating conditions. However, there are different specific requirements for these two applications. The weight of the overall MHHS is the key requirement for mobile applications, while hydrogen storage capacity is the key requirement for stationary applications. Based on these requirements, several techniques have been recently used to enhance the MHHS performance by mostly considering the faster hydrogen absorption/desorption reaction. Considering the metal hydride (MH) materials, the low thermal conductivity of MH materials significantly impacts the hydrogen absorption/desorption reaction. For this purpose, a comprehensive understanding of these three main factors and the hydrogen absorption/desorption reaction is critical and it should be up to date to obtain the suitable MHHS performance for all related applications. Therefore, this article reviews the key techniques, which are recently been applied for the enhancement of the MHHS performance. From the review, it has been demonstrated that the design and layout of the heat exchanger greatly affect the performance of the internal heat exchanger. The initial temperature of the heat transfer fluid and hydrogen supply pressure are the main parameters to increase the hydrogen sorption rate and specific heating power. The higher supply pressure results in the improvement of specific heating power. For the metal hydride material selection under the consideration of mobile applications and stationary applications, it is important to strike trade-offs between hydrogen storage capacity, weight, material cost, and effective thermal conductivity.

Keywords: Metal hydride, Hydrogen storage, Hydrogen absorption and desorption, Thermal design, Heat transfer enhancement, Heat exchanger

2.2.1 Graphical Abstract

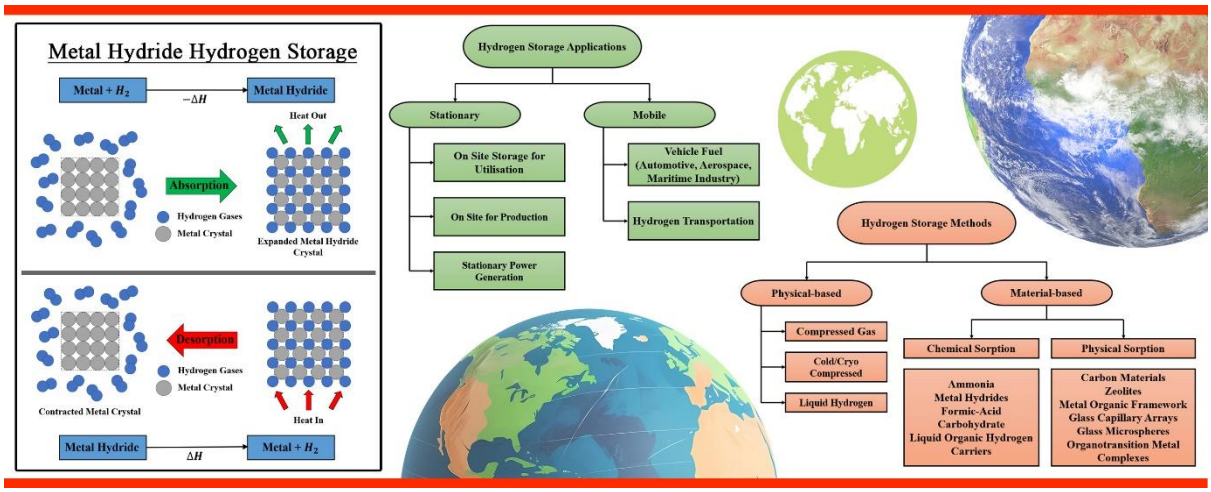

Figure 2.1 Graphical abstract for the review paper

2.3 Introduction

Thermal energy storage techniques store hydrogen for the purpose of producing electricity. Hydrogen has been proposed as the most promising energy carrier to store renewable energy for both stationary and mobile applications. Under hydrogen storage in stationary applications, these include stationary power generation, on-site storage for utilisation, and on-site storage for production. For hydrogen storage in mobile applications, these include hydrogen transportation and vehicle fuel, such as automotive, aerospace, and maritime industries.

The main advantages of hydrogen for energy storage are its characteristics and portability and its ability to offer high energy capacity per unit mass, which is significantly higher than that of fossil fuels (Tang et al., 2011). For this purpose, hydrogen energy storage has been applied for both small-scale and large-scale applications. Focusing on the high demand for hydrogen, underground hydrogen storage is one of the suitable options as this storage offers a large volume to store hydrogen with several options such as deep aquifers, salt caverns, depleted deposits of natural gas and oil, and others (Yue et al., 2021).

The recent advancement in subsurface hydrogen farming significantly highlights the importance of biotic and abiotic processes to convert the indigenous components, gases, and nutrients into hydrogen (Hassanpouryouzband et al., 2024). To prevent leakage and ensure efficient hydrogen production, stability of surrounding geological materials is required (Hassanpouryouzband et al., 2025). Furthermore, clay minerals also can withstand the conditions required for subsurface hydrogen generation. This greatly supports the development of safe and effective hydrogen production technologies (Hassanpouryouzband et al., 2025). To meet the demand, large amounts of hydrogen must be safely stored at low costs.

In general, hydrogen energy storage can be classified into three main types, which are compressed gas, liquid storage, and solid /material-based storage. For the first method, hydrogen is stored by compression into a selected container, such as steel and carbon fibre cylinders. Liquid storage is also another type of hydrogen storage. Using this technique, hydrogen can be stored in a liquid state at ambient temperature (Dagdougui et al., 2018). Comparing to other storage types, the solid storage requires less energy consumption and operating time (Colozza 2002). Therefore, storing hydrogen as a solid is the most efficient technique that has been widely used around the world.

Considering the solid storage, this technique includes metal hydrides, complex hydrides, chemical hydrides, and adsorbents.

- Complex hydrides and chemical hydrides: These two techniques are primarily used to store hydrogen by absorption. However, the main problems of these techniques are the lack of reversibility and the complexity of the reaction process to extract hydrogen (Yue et al., 2021).

- Absorbents: The porous materials will be employed to absorb hydrogen. This technique provides better thermal management in the charging and discharging processes than another three techniques, including metal hydride, chemical hydride, and complex hydride (Moradi & Groth 2019). However, this technique negatively affects the storage capacity when focusing on large-scale commercialisation (Marnellos et al., 2008).

- Metal hydride: Metal hydride (MH) has recently attracted significant interest as it offers a high hydrogen capacity, low material cost for storage applications, and high safety performance (Sakintuna et al., 2007; Jain et al., 2010; Rusman & Dahari 2016).

Figure 2.2 presents the different technologies of hydrogen storage that have been widely used in various fields.

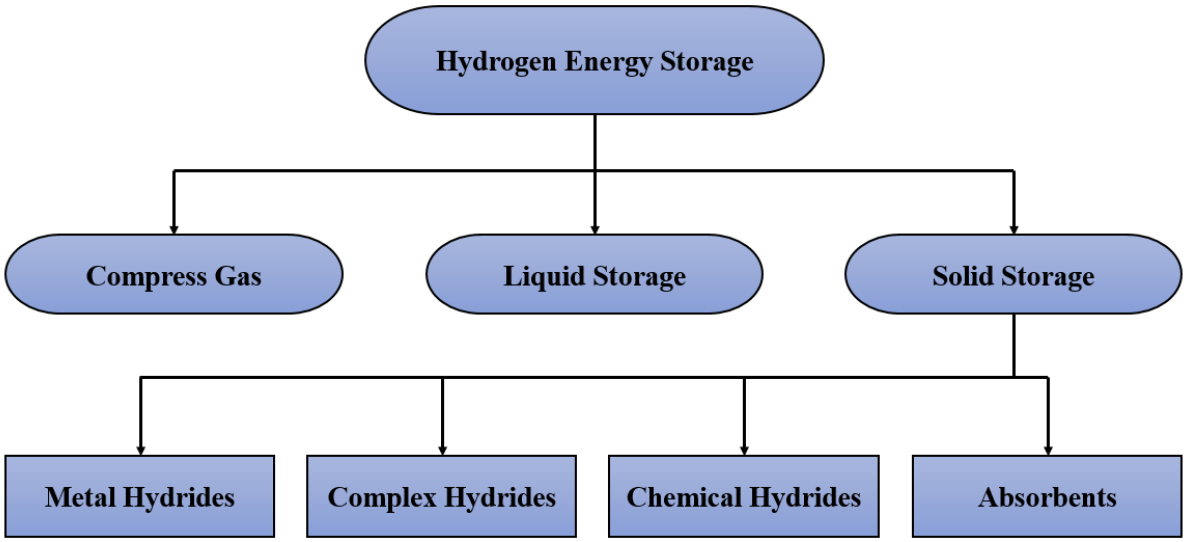

Figure 2.2 Different technologies of hydrogen energy storage

Basically, metal hydrides are powders. When metal powders absorb hydrogen to form hydrides, heat is released. When hydrogen is released from a hydride, heat is absorbed instead. The processes are provided in Figure 2.3

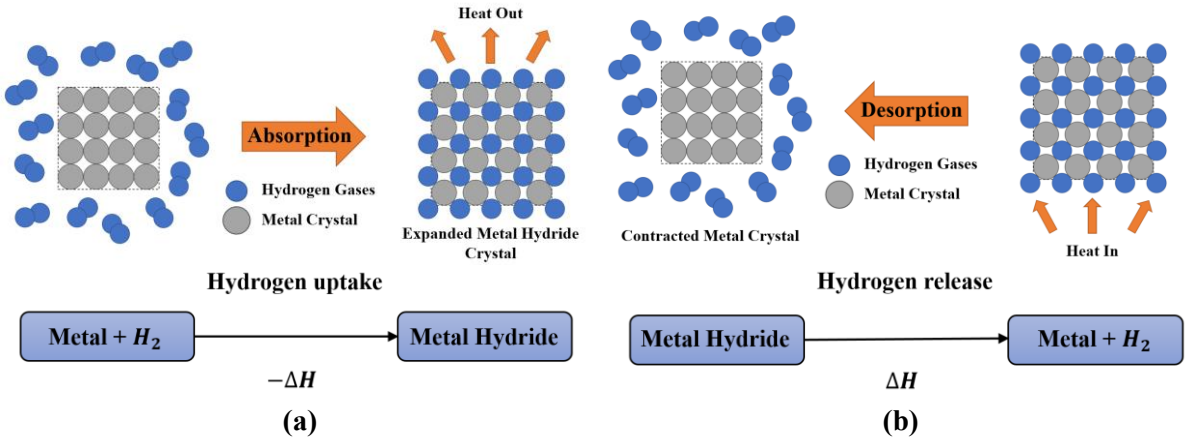

Figure 2.3 Absorption and desorption processes of metal hydride; (a) hydrogen absorption process and (b) hydrogen desorption process

The hydrogen reaction for absorption and desorption is generally expressed as:

$$\frac{2}{n}M(solid) + H_2(gas, P) \leftrightarrow \frac{2}{n}MH_n(solid) + \Delta H \quad (2.1)$$

In general, it is the chemical reaction between metal alloys and hydrogen. The hydrogen can be stored or released from the storage by absorption and desorption processes. This chemical reaction is reversible as it is the exothermic reaction for hydrogen absorption and the endothermic reaction for hydrogen desorption (from Equation (2.1)).

The amount of hydrogen (X) that is absorbed and desorbed on a metal surface can be expressed in weight percentage (wt%). The rate of this sorption is associated with the kinetic reaction, according to the following equations.

For hydrogen absorption (Chung & Lin 2009),

$$\frac{dX}{dt} = C_a \cdot exp^{\left(\frac{-E_a}{RT}\right)} \cdot \left(\frac{P_{H_2} - P_{eq}}{P_{eq}}\right) \cdot (X_{max} - X) \tag{2.2}$$

where C_a denotes the absorption rate constant and E_a refers to the activation energy for hydrogen absorption. P_{H_2} is the hydrogen supply pressure. X_{max} is the maximum amount of hydrogen which is considered as 1 for the full amount of hydrogen reaction fraction. X refers to the current amount of hydrogen in reaction fraction term ranges from 0-1.

For hydrogen desorption (Chung & Lin 2009),

$$\frac{dX}{dt} = C_d \cdot exp^{\left(\frac{-E_d}{RT}\right)} \cdot \left(\frac{P_{H_2} - P_{eq}}{P_{eq}}\right) \cdot (X) \tag{2.3}$$

where C_d is the desorption rate constant and E_d is the activation energy for hydrogen desorption.

The equilibrium pressure (P_{eq}) inside the MH storage for absorption and desorption can be determined by using Van't Hoff equation as (Wu et al., 2014):

$$\ln \frac{P_{eq}}{P_{ref}} = \frac{\Delta H}{RT} - \frac{\Delta S}{R} \tag{2.4}$$

where P_{ref} is the reference pressure. ΔH and ΔS are the enthalpy of reaction and entropy of reaction, respectively. R refers to the universal gas constant.

The hydrogen reaction kinetics (refer to Equation (2.2) and Equation (2.3)) are mainly influenced by the heat transfer rate inside the storage system as the limitation of MH performance is the slow reaction kinetics to absorb and desorb the hydrogen due to a low thermal conductivity of MH material (Zhao et al., 2020). This mainly affects the overall metal hydride-based hydrogen storage (MHHS) performance. Therefore, the design optimisation of MHHS under various techniques has been considered for the improvement of MHHS performance.

One of the most effective methods to enhance the overall MHHS performance is appropriate thermal management to control the hydrogen flow rate during absorption and desorption (Nguyen & Shabani 2022). This significantly improves the hydrogen reaction kinetics. A faster MH bed temperature reduction leads to faster hydrogen absorption. In contrast, a higher MH bed temperature is required for the hydrogen desorption process. The enhancement of heat transfer performance techniques has been used to fulfil this limitation based on the design and optimisation of heat exchangers. Not only the development of these heat exchangers, but the overall MHHS performance is also affected by other factors. In general, the overall MHHS performance for each specific application is depended on the three main factors. Appropriately selecting the overall operating conditions, material uses, and design configurations of the MHHS based on heat exchangers are essential requirements as these factors can positively or negatively affect the overall system performance, such as the volumetric and gravimetric properties of the storage system and the hydrogen reaction kinetic.

Considering the storage applications, there are different requirements of the MHHS configurations between the MHHS for mobile applications and the MHHS for stationary applications. The weight of the overall MHHS is the key factor for mobile applications, while the hydrogen storage capacity is the key factor for the MHHS in stationary applications. However, both storage applications also require the superior hydrogen reaction kinetics to store and release the hydrogen when its needed. For these purposes, the comprehensive understanding of these three factors (operating condition, material uses,

and heat exchanger design configurations) and hydrogen reaction kinetic on the overall MHHS performance for both mobile and stationary applications should be prioritised and up to date. Therefore, the main objective of this paper is to review the current trends in the use of MH materials, heat exchanger design configurations, as well as the selected parameters for operating conditions by considering the effect of these factors on the hydrogen reaction kinetics under the overall requirement of the MHHS for both mobile and stationary applications. The MH materials are reviewed under heat transfer performance, cost, density, and their effect on the overall MHHS performance for both mobile and stationary applications. The design and optimisation of heat exchangers, choice of heat transfer fluids (HTF), and operation parameters are considered as the key techniques to improve the reaction kinetic, resulting in the enhancement of the overall MHHS performance. The heat exchanger configurations based on thermal management methods, including active and passive methods, are considered in this article under both inner and outer heat exchanger structures that affect the hydrogen absorption/desorption reaction and overall volumetric/gravimetric of the MHHS. In addition, the operating conditions for the MHHS and the HTF are analysed by focusing on the hydrogen absorption/desorption duration and its improvement under the different MHHS configurations.

2.4 Metal Hydride Materials

The main component of MHHS is the MH material. An appropriate selection of MH material is one of the most important parameters that can significantly impact overall MHHS performance for both mobile and stationary applications. Difference metal alloys will have different thermos-physical properties that will influence the hydrogen absorption/desorption, storage capacity, etc. The metal alloys should offer high hydrogen storage capacity and high thermal conductivity, fast reaction kinetic, short refuelling time, low cost, easy availability and high cyclic stability (Muthukumar et al., 2018). The low gravimetric density of MH material is important for automobile applications as the size of MHHS and vehicle must be suitable to provide an appropriate driving range. In contrast, the high volumetric density of MH is required for stationary applications as the weight of the overall storage system will not affect the storage efficiency (Rahnama et al., 2019a). This section summarises the main characteristics of MH materials that affect the overall MHHS performance for both mobile and stationary applications. These include the hydrogen storage capacity, effective thermal conductivity, density and raw cost materials. Under the MH material sections, several techniques have been widely used to study MH materials and their properties such as experimental work and numerical work based on the computational fluid dynamics (CFD) method and machine learning method.

2.4.1 Machine Learning Techniques for Investigation of Metal Hydride Materials' Properties

In general, machine learning (ML) is used to predict future outcomes based on previous data which can be from different sources such as the CFD method and experimental works (Mocanu et al., 2016; Hameed et al., 2022). A large dataset is the first requirement for training of ML technique. Then, the appropriate selection of related parameters (descriptors) is the key factor for the ML algorithm to efficiently learn from previous data and then predict an accurate outcome (Hirscher et al., 2020). Some studies also used ML to analyse and predict the thermal performance of pin fin heat exchangers by considering several related parameters. These included the fin space, thickness, material, and conductive heat transfer coefficient (Krishnayatra et al., 2020; Kim et al., 2022; Ostanek 2014; Balachandar et al., 2015; Beigzadeh et al., 2016; Lee et al., 2021). For the development of hydrogen technologies, ML has been used to predict the results in various applications, including hydrogen production (Yu et al., 2021; Vo et al., 2021), hydrogen storage (Jian et al., 2021; Witman et al., 2020), and hydrogen conversion in fuel cells (Sun et al., 2021; Guarino et al., 2021). In recent years, ML has been well-known as a useful method for analysing MH databases to classify the materials' uses and

their properties as these factors play an important role in the requirement of MHHS properties (Suwarno et al., 2022).

Several models for ML methods have been applied to hydrogen applications, especially to the MHHS. The study by Rahnama et al. (2019b) employed ML to predict the hydrogen storage capacity in weight percentage and identify the most conducive MH material for the use of efficient way for fuel cell application. The database based on more than 1600 references was collected from the International Energy Agency Hydrogen Implementing Agreement that was funded by the U.S. Department of Energy (https://www.energy.gov/eere/fuelcells/databases). The MH classes from the database included Mg alloys (373 samples), complex hydrides (234 samples), solid solution alloys (263 samples), AB (179 samples), A_2B (140 samples), AB_2 (625 samples), AB_5 (477 samples), and Misc intermetallic compounds (431 samples). For hydrogen weight percentage, the correlations were made based on the relationship between the hydrogen weight percentage, temperature, heat formation, material class, composition formulas, and pressure. The results from these studies proved that the ML-boosted decision tree algorithm obtained the best performance with a 0.83 of coefficient of determination compared to other models, including the Bayesian linear (0.56), neural network (0.60), and linear regression (0.50). However, for the classification of materials used by considering the heat of formation and hydrogen content, the neural network provided a better performance to obtain the hydrogen weight percentage with a 0.80 accuracy compared to logistic regression (0.47 of accuracy), decision forest (0.60 of accuracy) and decision jungle algorithms (0.62 of accuracy). Withman et al. **(2020)** also employed a similar database to analyse the relationship between the alloys and MH properties. The results from Withman et al. **(2020)** found that the molecular volume of alloys is the most important factor for thermodynamic predictors. This finding also supported the results from other previous studies (Lundin et al., 1977; Mendelsohn et al., 1979; Reilly et al., 1999). However, the database from HydPARK (refer to U.S. Department of Energy) contained data from the previous study and only up to 2004. Therefore, the recent study from Suwarno et al. **(2022)** was based on the database of AB_2-based MH classes from 1998 to 2019. The 314 pairs of AB_2 alloys were taken with their own hydrogen storage properties, including heat formation, phase abundance, and hydrogen storage capacity. This study proved that Ni, Cr, and Mn significantly affected the hydrogen properties, while only the Cr element significantly influenced the phase fraction (refer to phase abundance). The uses of ML for MH properties' prediction and its accuracy outcome are summarised in Figure 2.4 and Table 2.1.

Figure 2.4 Machine learning techniques for metal hydride properties' prediction

Table 2.1 Comparison of a coefficient of determination (R^2) between various machine learning algorithms for different parameters of AB_2-based MH properties

ML algorithms	Coefficient of determination (R^2)			Reference
	Hydrogen storage capacity (in wt%)	Phase abundance	Heat formation	
Multivariate regression	0.667	0.448	0.367	

Decision tree	0.498	0.785	0.346	Suwarno et al., 2022
Random forest	0.688	0.832	0.647	
Boosted decision tree regression	0.830	-	-	Rahnama et al., 2019a, b
Baysian linear regression	0.569	-	-	
Neural network regression	0.608	-	-	
Linear regression	0.502	-	-	

Note: It should be noted that the investigation of these factors is based on the actual dataset of hydrogen weight percentage, heat formation, operating temperature and pressure.

It can be seen that the accuracy of predicted results is usually based on the selection of the ML algorithm. An appropriate selection of ML algorithms is required to obtain accurate results. However, the ML techniques are currently applied for the study of MH materials' properties only. From these studies, hydrogen storage capacity, phase abundance, and heat formation are only considered under the AB_2-based MH materials. Furthermore, the maximum hydrogen storage capacity under these studies is still less than 0.9 wt%.

2.4.2 Hydrogen Storage Capacity

According to the target of the American Department of Energy (DOE), the hydrogen storage capacity (HSC) for commercialisation is expected at 6.5 wt% with a low decomposition temperature ranging from 60-120 ℃. However, this target has still not been achieved as the metal alloys with the low operating temperature usually obtain a low HSC of less than 2 wt%. In contrast, metal alloys with high HSC usually require a high operating temperature to activate the system. Table 2.2 summarises the operating condition ranges and the HSC of some commonly used metal alloys.

Table 2.2 Operating conditions and hydrogen capacity (wt%) of some commonly used metal alloys

Metal alloy	Operating temperature (K)	Operating pressure (MPa)	Hydrogen capacity (wt%)	Reference
$LaNi_5$	293	2.00	0.25	Aoyagi et al., 1995
	0-373	5.00	1.44	Corre et al., 1998
	285	0.1	1.37	Principi et al., 2009
$LaNi_{4.7}Al_{0.3}$	193-413	0.00-6.00	1.43	Hahne & Kallweit 1998
Mg_2Ni	573	2.90	3.20	Singh et al., 1995
	573	1.16	3.50	Zaluski et al., 1995
	553	0.10-0.20	3.53	Abdellaoui 1998;
	553	0.10-1.50	4.10	Abdellaoui 2006
	528	0.1	3.59	Vija et al., 2005
				Principi et al., 2009
$MmNi_{4.5}Al_{0.5}$	298	0.38	1.2	Muthukumar et al., 2018
NaAl	353-453	7.60-9.10	5.00	Zaluski et al., 1995
$Ti_{1.1}CrMn$	293	3.3	1.80	Kojima et al., 2006
TiFe	298	0.41	1.86	Muthukumar et al., 2018
$TiMn_{1.5}$	298	0.84	1.9	Muthukumar et al., 2018

Several metal alloys have been developed to improve storage performance. Light metals, such as Li, Be, Na, Mg, B, and Al, are mainly used to form a large variety of MH compounds. Metal alloys can be classified into two main types: complex hydrides and intermetallic compounds. Complex hydrides are lightweight storage materials. Among other elements, sodium (Na), lithium (Li), and beryllium (Be) are the three elements that are lighter than magnesium and can be used as MH materials (Sakintuna et al., 2007). Sodium aluminium or NaAl-based alloys are one of the considerable choices as they obtain a

high HSC, which is up to 5 wt%. However, the limitations of complex hydrides are kinetic and thermodynamic. Intermetallic compounds are widely used as MH materials as these alloys only require low temperature and pressure ranges for system activation that is close to ambient temperature (293 K or 20 ℃) and pressure. Normally, these compounds are determined based on their crystal structures, such as AB_2, AB_5, and Ti-based body-centred cubic. Among intermetallic compounds, lanthanum nickel or $LaNi_5$-based alloys are the most popular alloys which have been recently used for several applications. However, the main problem of these alloys is the HSC with around 1.4 wt% at the maximum. The $LaNi_5$-based alloys and the storage capacity of other intermetallic compounds is also less than 2 wt%. Magnesium hydride is well known as a lightweight material for solid-state storage applications with a high storage capacity of 7.6 wt% (Rusman & Dahari 2016; Aburto & Orgaz 2007; Shao et al., 2008). However, it has slow kinetics and requires high temperature ranges for absorption and desorption. Therefore, several magnesium-based or Mg-based alloys have been developed for storage applications. The advantages of these alloys are a high storage capacity, excellent heat resistivity and good recyclability (Rusman & Dahari 2016; Liang 2004). Among several Mg-based alloys, magnesium-nickel alloys (Mg_2Ni) have received much more attention as they provide a considerable HSC of up to 6 wt% and faster reaction kinetics for hydrogen sorption compared to magnesium hydride (Friedlmeier et al., 1996). However, these alloys still require a high-temperature range to activate the system at around 523-603 K or 250-330 ℃.

2.4.3 Effective Thermal Conductivity

Effective thermal conductivity (ETC) is the main parameter that directly affects the heat and mass transfer performance within the MH beds. In general, the main problem of the MHHS is the low ETC (between 0.1 W/mK and 1.5 W/mK) which leads to the slow heat transfer rate. This problem will negatively affect hydrogen absorption and desorption. The operating conditions and ETC of some commonly used metal alloys are provided in Table 2.3.

Table 2.3 Operating conditions and effective thermal conductivity of some commonly used metal alloys

Metal alloy	Operating temperature (K)	Operating pressure (MPa)	Effective thermal conductivity (W/mK)	Reference
$LaNi_5$	293-333	0-1.0	0.1-1.5	Pons et al., 1993; Pons et al., 1994; Pon et al., 1991
$LaNi_{4.7}Al_{0.3}$	253-413	0.0-6.0	0.1-1.1	Hahne & Kallweit 1998
Mg_2Ni	308-473 373	0.1-4.0 0.2-4.5	0.35-0.75 0.66-0.83	Ishido et al., 1982 Suissa et al., 1984
$MlNi_{4.5}Mn_{0.5}$	313-333	0.1-3.0	0.7-1.3	Sun & Deng 1990
$MmNi_{4.5}Al_{0.5}$	273-373	0-5.0	0.1-1.2	Kumar et al., 2011
$MmNi_4Fe$	273	0.2-4.5	0.8-1.05	Suissa et al., 1984
NaAl	303-473	0-5.0	0.25-1.2	Christopher 2006; Dedrick et al., 2005; Ahluwalia 2007
$Ti_{1.1}CrMn$	293-300	0.3-25.3	0.3-0.7	Flueckiger et al., 2010
TiFe	298	-	1.49	Goodell 1980
$TiFe_{0.85}Mn_{0.15}$	273-373	0-5.5	0.1-1.5	Kempf & Martin 1986
$TiMn_{1.5}$	294, 311	0.1-5.0	0.2-1.3	Suda et al., 1980; Suda et al., 1981

From Table 2.3, the maximum ETC from intermetallic compounds and complex hydrides (such as $LaNi_5$ and Ti-based alloys) is over 1 W/mK, while the maximum ETC from the magnesium-nickel-

based alloys (Mg_2Ni) is less than 1 W/mK. However, most of them require a high operating temperature (over 333 K or 60 ℃) to achieve the maximum ETC, except $LaNi_5$, $MlNi_{4.5}Al_{0.5}$, $MmNi_4Fe$, and TiFe alloys. Similarly, most metal alloys also require a high operating pressure to reach the maximum ETC, except $LaNi_5$ alloy. The operating pressure range varies, but it is at least 0-3 MPa for most of them, except $LaNi_5$ alloy, which requires only 0-1 MPa.

2.4.4 Density and Raw Cost Materials

The material's weight and raw cost materials are the main parameters for on-board hydrogen storage. The magnesium-based alloys are well-known as lightweight and low-cost materials compared to other alloys. The summary of density and raw cost materials from some commonly used metal alloys are presented in Figure 2.5 and Figure 2.6, respectively. From Figure 2.5, the density of Mg_2Ni alloy is lower than other alloys as there is only 3.6 g/cc, while the density of Ti-based alloy is over 6.4 g/cc. The density of mischmetal (Mm) alloys is over 8.1 g/cc, which is similar to $LaNi_5$ with 8.3 g/cc of density. However, the lanthanum-nickel alloys based on $LaNi_{4.7}Al_{0.3}$ has 7.6 g/cc of density.

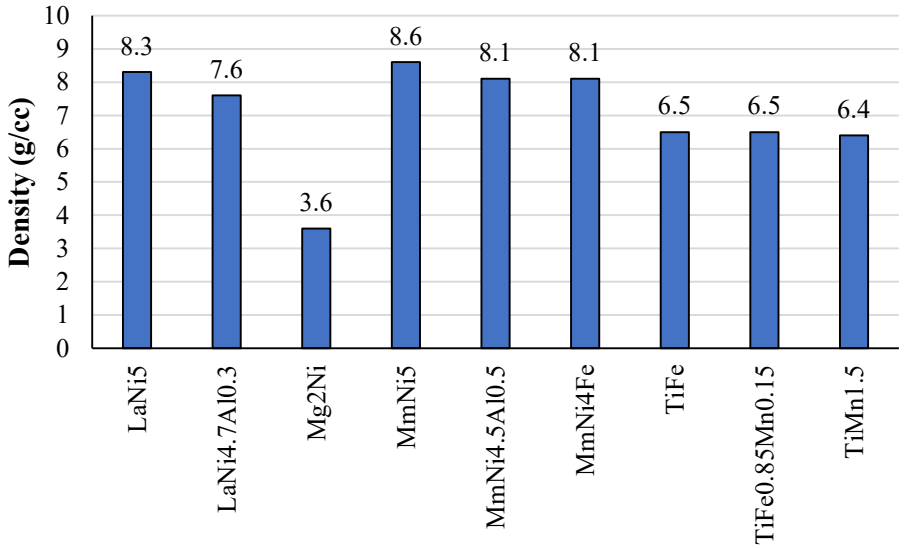

Figure 2.5 Comparison of density between some commonly used metal alloys (Sandrock 1999)

From available literature, the lanthanum-nickel-based alloys have the highest cost, which is over 9 $/kg. Therefore, the cheaper element mixture mischmetal (Mm) was used instead of lanthanum in $LaNi_5$ alloy (Sandrock 1979). The raw cost reduces from 9 $/kg to 7 $/kg when using Mm-based alloy instead of La-based alloy. However, it is still higher than other alloys, especially the Mg-based and Ti-based alloys. The raw cost of Ti-based alloys is lower than other alloys as it is less than 5 $/kg, while the raw cost of Mg_2Ni alloy is 6.26 $/kg. It should be noted that the raw material cost from the available literature in this article is from 1996. The cost of raw materials might be higher in the present.

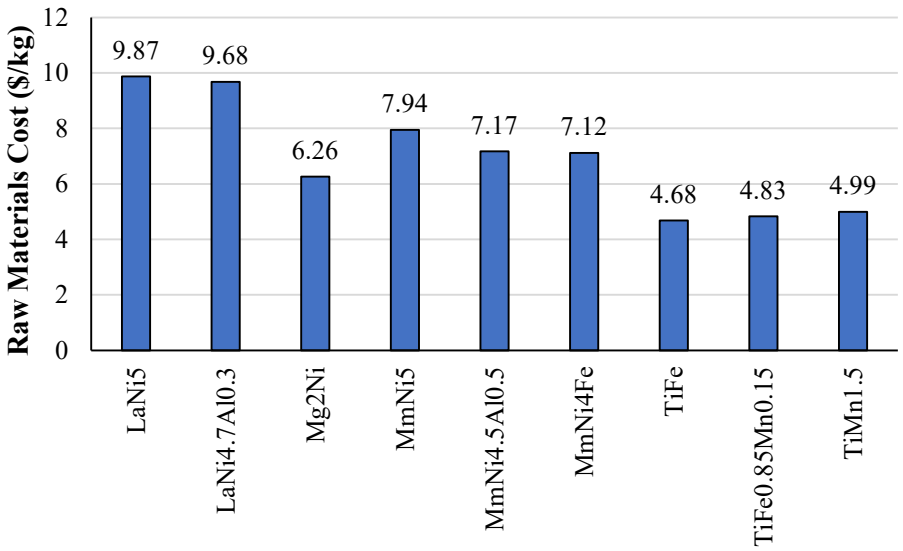

Figure 2.6 Comparison of raw materials cost between some commonly used metal alloys (price basis: mid-1996) (Sandrock 1999; Chandra et al., 2011; Sandrock et al., 1997; Reilly & Wiswall 1972)

From these comparisons (refer to sections 2.2 to 2.4), magnesium-based metal alloys mostly have a high HSC, lightweight, and low cost, but they have a low ETC. Intermetallic compounds, such as lanthanum nickel-based and titanium-based alloys, usually have a low HSC but they have a high ETC. Mischmetal-based alloys have a lower density and cost among intermetallic compounds than lanthanum nickel-based alloys. However, these alloys' density and raw material cost are still higher than titanium-based alloys.

Focusing on the MH material, the low-cost MH material is also important for eco-nomic purposes. Most MH materials, which offer a high HSC and being lightweight, usually have a low ETC. In contrast, most MH materials, which have a high ETC, usually have a heavy weight and low HSC. Therefore, the HSC and cost should be optimised, while the ETC should be enhanced for the MH materials. A low ETC negatively affects the hydrogen reaction kinetics, resulting in a decrease in the overall MHHS performance. Considering the specific requirements of both small and large-scale MHHS applications, the magnesi-um-based metal alloys seem to be the most suitable MH material for both applications. As these alloys offer a lightweight for compact MHHS applications, and a high HSC for large-scale MHHS applications. However, the slow hydrogen reaction kinetic rate due to the low ETC is the main problem of these alloys. One of the most effective ways to improve the hydrogen reaction kinetic rate is the enhancement of the heat transfer performance inside the MHHS. This can be done by the design and optimisation of the heat exchanger configurations. Furthermore, the heat exchanger configurations should be designed with consideration of volumetric and gravimetric parameters of the overall MHHS.

2.5 Heat Exchanger Design Optimisation for Thermal Management

The heat exchanger configuration is one of the key factors to improve the MHHS performance, as it significantly improves the heat transfer performance inside the storage system. Among MHHS studies from the 90s and before 2020, 40% focused on experimental studies, while the rest focused on numerical studies (Sreeraj et al., 2022). Most recent works from 2020 still employed numerical simulation to perform their studies by considering the design optimisation of the heat exchanger configurations. Therefore, several heat exchanger configurations have been designed and optimised based on numerical simulations, especially the computational fluid dynamics (CFD) method.

Several designs for heat exchangers have been proposed and optimised for thermal management in active and passive methods. The improvement of heat transfer performance based on various heat

exchanger types leads to the enhancement of hydrogen reaction kinetic, resulting in the enhancement of the overall MHHS performance. This section summarises the heat exchanger types under the active and passive methods that have been used for the MHHS on a small scale and large scale. The active heat exchanger design optimisations of the MHHS include an internal and external heat exchanger, such as a cooling/heating tube and cooling/heating jacket. The schematic diagram of MHHS with external and internal heat exchangers is provided in Figure 2.7. For both techniques, the HTF and hydrogen are injected from opposite directions during the absorption process as this will increase the heat transfer rate compared to the case with the same direction. The HTF is injected from the bottom part, while the hydrogen is injected from the top surface of the reactor. For the external heat exchanger based on the cooling jacket, there is heat transfer between the outer MH bed as this area is directly close to the HTF which covers around the MHHS. The MHHS will be cooled down starting from the outer MH bed area first. However, the MHHS will be cooled down starting from the inner MH bed area first when having the internal heat exchanger inside the system. For the desorption process, the hydrogen is released from the top surface with the heating fluid to supply the required heat instead. Considering the passive thermal management method, the passive heat exchanger design optimisations include inner/outer fins and phase change materials (PCM) (Mazzucco et al., 2014). The schematic diagram of MHHS with these heat exchangers under this method is provided in Figure 2.8. From this figure, the PCM is used to cover the MH bed as the external heat exchanger. There is the heat transfer between these two parts. The PCM directly absorbs the heat from the MH bed during the hydrogen absorption and releases the heat during the hydrogen desorption. To improve the heat transfer rate, the metal fins are integrated with the PCM and MH bed. The heat is then transferred from the MH bed to the metal fin as well as from the metal fin to PCM. The comparison of heat exchangers' performance in regard to the hydrogen sorption and heat transfer as well as reduction in volumetric and gravimetric parameters of the overall MHHS is provided in "2.5.4".

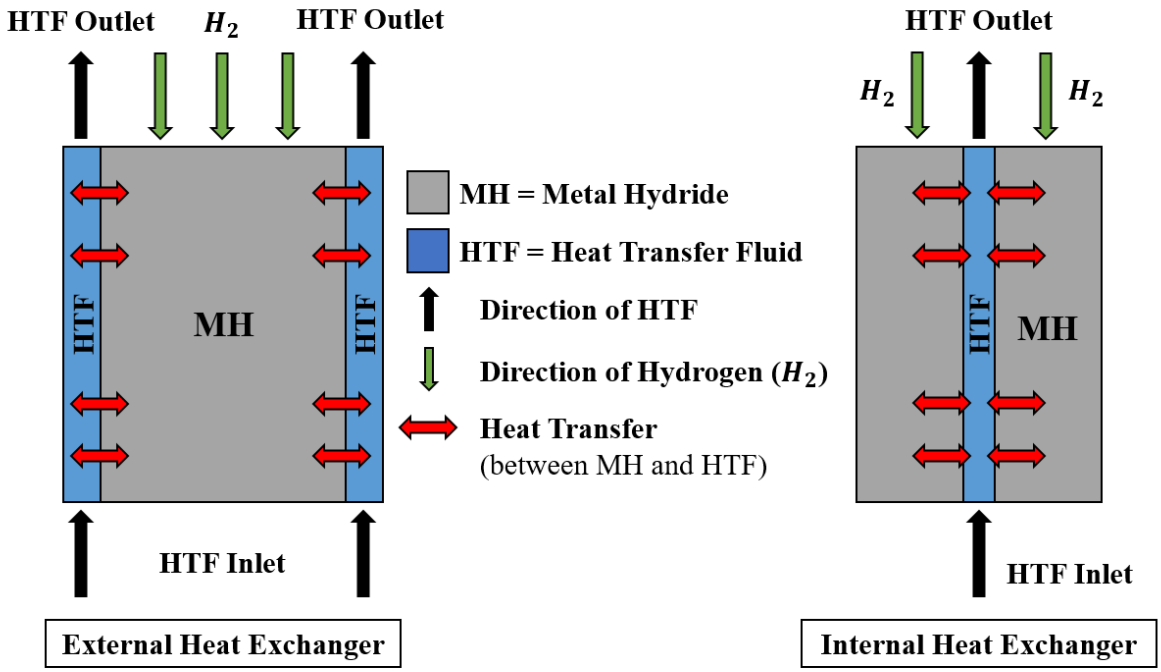

Figure 2.7 Schematic diagram of metal hydride storage system with external and internal heat exchangers for active thermal management technique

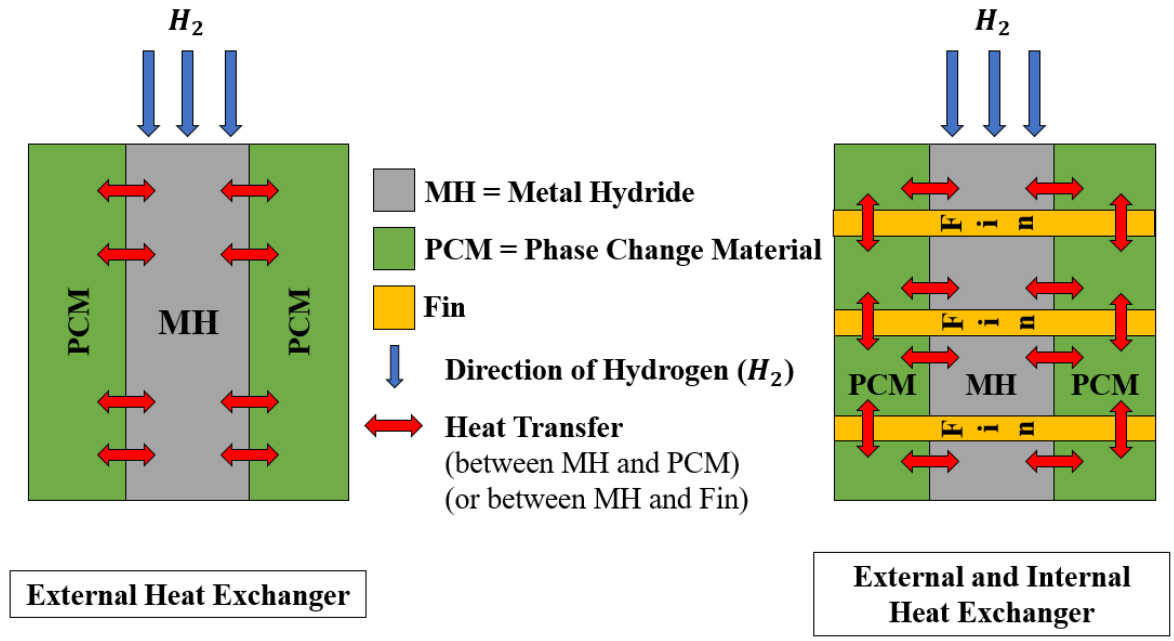

Figure 2.8 Schematic diagram of metal hydride storage system with external and internal heat exchangers for passive thermal management method.

2.5.1 Design Optimisation for Active Thermal Management Method

The active thermal management method requires external power to control the heat transfer rate. This method uses the HTF, such as air or water, to remove the heat during the hydrogen absorption and provide the heat during the hydrogen desorption. The main advantages of the active method are the ability to control the temperature of the storage system and faster heat removal/addition than the passive method. There are two main types of heat exchanger configurations for the active method, which are external and internal heat exchangers.

- *External Heat Exchanger*

The cooling/heating fluid is used as an external heat exchanger to cover the outer wall of the MH bed. Figure 2.9 presents an example of this heat exchanger design.

- Cooling/heating jacket

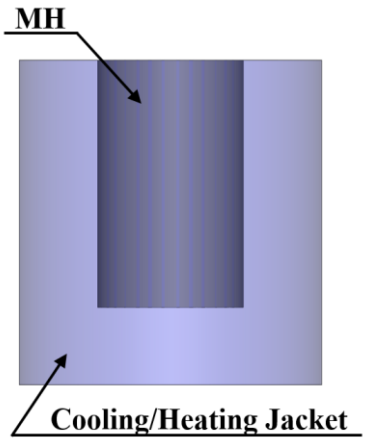

Figure 2.9 Examples of an external heat exchanger design

The reactor with the cooling jacket is widely used because of having simple structure and better heat transfer performance (Chung & Ho 2009; Valizadeh et al., 2016; Wang et al., 2009; Nam et al., 2012;

Yoo et al., 2014; Patil & Gopal 2013; Urunkar & Patil 2021; Yiotis et al., 2015). From the study of Chung & Ho (2009), the expansion volume was used instead of porous media and located on the top of the MH bed, which was covered by water as a heating/cooling fluid. This study found that thermal resistance was increased by having an expansion volume inside the storage system. The two-dimensional MHHS with a cooling jacket was proposed by Patil & Gopal (2013). They found that supply pressure and initial HTF temperature affected hydrogen sorption rates. For the fuel cell application, the poor thermal conductivity of the MH powder is the main problem for the high electrical power ratings of this application (Yiotis et al., 2015). Although this technique is widely used due to the simple structure, the heat transfer areas are only nearly the outer wall of the MH bed which is connected to the cooling jacket. Therefore, this technique is usually combined with other internal heat exchanger techniques to increase the heat transfer performance. The comparison between these heat exchangers and their performance is provided in Sections "2.5.3" and "2.5.4".

- Tube coil

Moreover, an external tube coil was developed for a hydrogen storage canister with hot water as the HTF (Hwang & Chang 2012). The hydrogen discharge rate was improved due to the hot water that was circulated around the $LaNi_5$ MH tank. Weiss-Ungethum et al. (2014) performed an experimental study to investigate the effect of liquid cooling on the fuel cell stack by considering the various origins of heat loss. The three inner tubes were used to contain the $NaAlH_4$ material as MH powders covering the external helical coil tube. Their study indicated that the amount of heat loss that was rejected from the stack throughout the cooling fluid slightly exceeded the heat demand for the hydrogen discharging process. Therefore, comprehensive studies are required to design and optimise this heat exchanger for further improvement.

Although using an external heat exchanger also significantly increases the heat transfer rate, this only applies to the outer wall of the MH bed which directly contacts the external heat exchanger wall. Therefore, various internal heat exchangers are developed for better heat transfer distribution inside the MH bed's purpose.

- Internal Heat Exchanger

The heat transfer surface area is generally increased by inserting the heat exchanger inside the MHHS, which increases the heat and mass transfer mechanisms (Wu et al., 2016). Several studies have optimised the heat exchanger performance by considering the development of multiple internal heat exchanger configurations to transfer cooling/heating fluid inside the MHHS. These include straight tubes, U-shape tube, mini-channel tubes, helical coil/spiral tubes, and semi-cylindrical coils. Figure 2.10 presents examples of different internal heat exchangers.

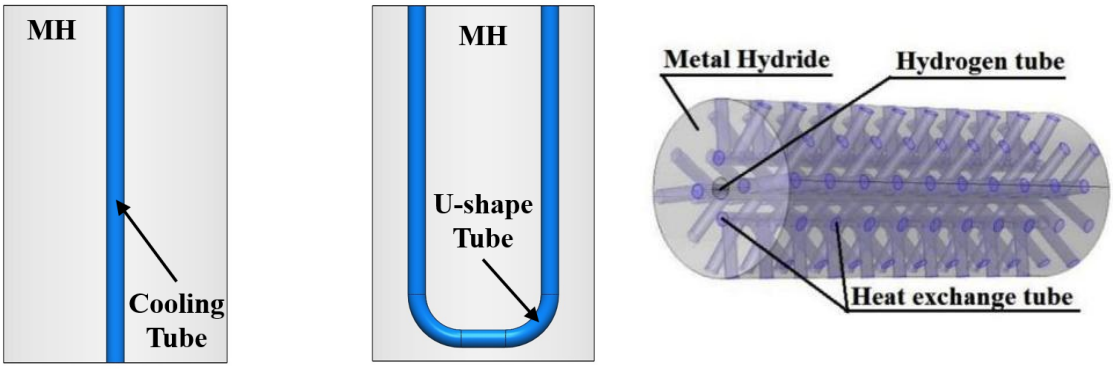

(a) (b) (c)

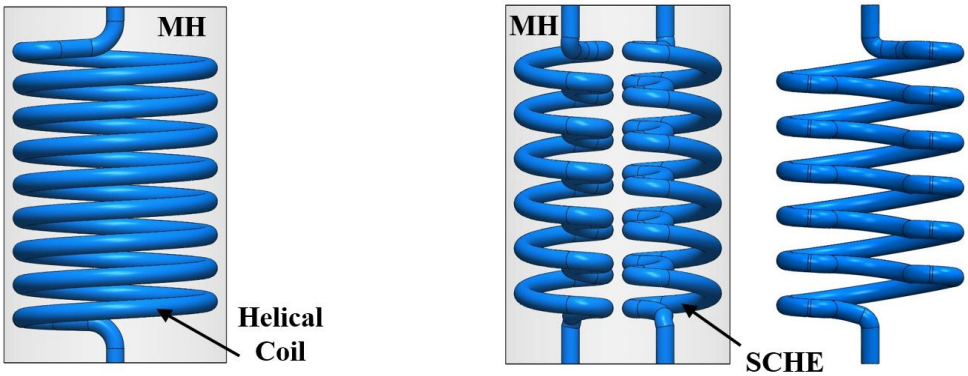

(d) (e)

Figure 2.10 Examples of various internal heat exchanger designs; (a) Straight tube, (b) U-shape tube, (c) Mini-channel tubes (Wang et al., 2019), (d) Helical coil, and (e) Semi-cylindrical coil.

- Cooling/heating tube

The reactor is equipped with an internal straight-tube heat exchanger for the HTF (Anbarasu et al., 2014a; Bao et al., 2013a; Mellouli et al., 2009; Raju & Kumar 2011; Hardy & Anton 2009; Bhouri et al., 2015; Mohan et al., 2007; Kumar et al., 2019; Raju et al., 2019a), as presented in Figure 2.10a. The HTF will act as a cooling/heating fluid to transfer generated heat or supply the required heat inside the MH bed during the hydrogen absorption or desorption. The straight tube was embedded inside the $LaNi_5$ MH storage based on the combination of aluminium foam and hydride (Mellouli et al., 2009). This study proved that using a metal foam exchanger and a concentric heat exchanger tube improved heat transfer performance, resulting in a 60% improvement in absorption duration. The absorption duration decreased when using several straight tubes as the internal heat exchanger (Raju & Kumar 2011). Multiple heat exchanger tubes were used for the heat transfer investigation during the hydrogen sorption by employing a hierarchical methodology (Hardy & Anton 2009). The combination of two materials ($LaNi_{4.3}Al_{0.4}Mn_{0.3}$ and Li-Mg-N-H) was used and filled inside the reactor by Bhouri et al. (2015). The design optimisation for the number and thickness of tubes was evaluated under the absorption process. However, the study by Mohan et al. (2007) proved that the thickness of several heat exchanger tubes had a minor effect on the absorption and desorption time. Using several HTF tubes greatly influenced the MHHS rather than the HTF flow rate (Kumar et al., 2019; Raju et al., 2019a). However, more uniform heat transfer distributions are still required from this technique. Therefore, the other complex HTF structures have been performed to fulfil this requirement.

- U-shaped tube

Some researchers developed a U-shaped tube to increase the heat transfer area when it was inserted inside the tank. An example of this design can be seen in Figure 2.10b. A U-shape tube incorporated with radial circular copper fins was placed inside $LaNi_5$ MH storage (Singh et al., 2017a, b; Singh et al., 2015). Water was used as the HTF and also used to reduce the MH bed temperature during the absorption process. This study proved that the improvement of hydrogen charging time significantly depended on the number of fins, the thickness of fins, and the diameter of the heat exchanger tube. For the hydrogen absorption of 12 g, the absorption was reduced by 48% when increased the number of fins from 4 to 13. Increasing the diameter of the heat exchanger tube from 3.4 mm to 5.4 mm reduced the absorption time by 27.6%. Increasing the fin thickness from 0.5 mm to 1.5 mm also improved the absorption duration. However, these studies found that increasing the number of fins from 13 to 34 and reducing the fin thickness and pitch instead, resulting in a 32% reduction of absorption time compared to the case with 13 fins. The ratio of fins' numbers, pitch, and thickness was calculated under the constant volume of fins. The MHHS with a U-shape tube should be incorporated with 34 radial circular fins with a pitch of 3.83 mm and a thickness of 0.19 mm. Therefore, under the constant volume of fins, the number of fins is the key parameter to improve the heat transfer performance inside the MHHS. Recently, Yang et al. (2025) performed a numerical study to further improve the heat transfer and reaction rate performances. They combined the U-shape tube with radial circular fins and additional bottom curved fins. The results from these combinations proved that the heat transfer performance significantly improved especially around the bend section of the U-shape tube due to the additional

bottom curved fins. The absorption rate significantly improved by 50% compared to the case without additional bottom-curved fins.

- Mini-channel tubes

The mini-channel tubes, were designed as shown in Figure 2.10c. This technique contains multiple straight tubes (with a small diameter of 2-4 mm) inside the reactor for the HTF. The MH reactor, with the addition of mini-channel tubes based on the spiral tube design, was designed by Li et al. (2015). This study found that increasing the radius of the spiral tube resulted in a faster reaction rate due to an increase in heat transfer surface area. Meng et al. (2013) performed both numerical and experimental studies on the $LaNi_5$-based storage system based on multi-straight tubes. The comparison between various parameters, such as the number of straight tubes, hydrogen supply and discharge pressures, was performed. The results from this study indicated that the new reactor configuration improved the reaction rate for absorption and desorption processes compared to the traditional MHHS. The slim radiation tubes were designed for the HTF (Wang et al., 2019; Wang et al., 2021). All radial heat exchange tubes were designed to connect to the cooling jacket around the MH bed. The MHHS with a radiation tube was compared to other reactors with different configurations, such as straight and spiral tubes. The numerical results from their study indicated that using a radiation tube as a heat exchanger provided the best MHHS performance compared to other configurations. This was because of an increase in heat transfer surface area, resulting in having more uniform temperature distributions inside the MHHS.

- Spiral/helical coil tube

Figure 2.10d provides an example of the spiral/helical coil tube. From this design, the secondary circulations of the coil tube significantly increase the heat transfer rate inside the MHHS as it offers more heat transfer surface area between the MH and the HTF compared to straight tubes (Wu et al., 2014; Fernández et al., 2018). Furthermore, it also generates the turbulence flow of the HTF during circulation along the HTF tube (Raju et al., 2012). The more uniform temperature distribution inside the MHHS is the key factor for heat transfer enhancement by this technique (Fernández et al., 2018). A higher heat transfer coefficient was found in this method as well as it was easier to manufacture (Shafiee & McCay 2016). Under the constant HTF tube volume, the hydrogen absorption duration was improved by 34.6% when using the spiral coil tube compared to the case with a straight tube (Wang et al., 2019). Improving the absorption reaction by increasing the heat transfer coefficient was confirmed by Wang et al. (2012). Mellouli et al. (2007) studied the effect of a spiral tube heat exchanger on the hydrogen absorption time when embedded in the MHHS. The inlet and outlet of this tube were designed to have the same direction to increase the tube length. Around the coolant tube, there was a faster hydrating reaction rate (Bhogilla 2017). Reduction in coolant temperature resulted in faster hydrogen filling times (Visaria & Mudawar 2012a, b). A helical coil tube was used to circulate the supercritical water to heat the MHHS during the desorption instead of the electrical system (Dong et al., 2017). The HTF's thermal diffusion technique was studied and applied by using the superheated water for the MHHS with a helical coil tube (Mathew et al., 2021). This study proved that thermal conductivity in MH has less effect on the performance of the MHHS. The helical coil's characteristics also play a significant role in the enhancement of the heat transfer mechanism in the MHHS (Tiwari & Sharma 2021). These include a smaller ratio of helical pitch to the helical diameter and non-dimensional pitch (Wu et al., 2014), increasing the number of flat spiral tube planes (Ardahaie et al., 2021), a lower pitch of the helical coil and a higher coil diameter (Eisapour et al., 2021a). Moreover, using the duplex helical elliptical tube (Wang et al., 2020) and a helical coil with a central return tube (Eisapour et al., 2021a) greatly increased the heat removal rate between the HTF and MH bed. However, it should be noted that the helical coil characteristics and their ratio are based on the MHHS scale.

- Semi-cylindrical coil tube

A semi-cylindrical coil tube from Figure 2.10e was developed from the helical coil tube to enhance the heat transfer rate (Larpruenrudee et al., 2022a). Two semi-cylindrical coil tubes were embedded inside the MHHS as internal heat exchangers. Due to the better heat transfer surface area arrangement of these heat exchangers, which resulted in having more uniform temperature distribution, the average bed temperature of the MHHS reduced faster than the case with conventional helical coil tube. Under

constant volume of MH bed and HTF tube, the absorption duration significantly reduced by 59% compared to the storage with helical coil case. Moreover, the semi-cylindrical coil tube also obtained a higher turbulence level of the HTF than the helical coil tube, resulting in faster heat removal (Larpruenrudee et al., 2022b). Moreover, when combining the semi-cylindrical coil tube with the central return tube, the heat transfer performance was greatly improved, resulting in faster hydrogen absorption/desorption (Larpruenrudee et al., 2023; (Larpruenrudee et al., 2024). The duration of the absorption-desorption cycle was reduced by 50% when using this heat exchanger, compared to the case with the helical coil case. There was a 31% reduction in the duration of the absorption-desorption cycle when using this heat exchanger with a central return tube, compared to the case without this central return tube.

From the above mentioned, to improve the overall MHHS performance, there are several internal heat exchanger configurations that have been designed instead of the conventional straight tube. Most recent studies have been focused on the internal heat exchanger rather than the external heat exchanger. This might be because the internal heat exchanger offers a higher heat transfer surface area. The enhancement of heat transfer performance by the internal heat exchanger usually depends on the well arrangement of the heat exchanger structure, which increases more heat transfer surface area and obtains more uniform temperature distribution. Furthermore, the complex heat exchanger structure also results in a higher turbulent flow, which significantly leads to faster heat transfer However, all of these heat exchangers are obtained using the active thermal management method, which requires additional energy to transfer the heat. The other heat exchanger designs under the passive technique are provided in the next section. It is worth mentioning that the comparison between various internal heat exchangers and their performance can be found in “2.5.4”.

2.5.2 Design Optimisation for Passive Thermal Management Method

Passive thermal management is a method that does not require any additional energy to improve the heat transfer rate. This method normally uses natural convection, which can be done by adding fins or phase change materials to the inner or outer surface of the MHHS. This technique usually requires materials with a high conductivity that leads to an increase in heat transfer surface area. The main advantages of the passive method are easier implementation and lower cost to produce compared to the active method. This section provides a summary of the three main types that are usually applied to this method. These include the metal fins, metal foam, and phase change material (PCM).

- *Fins*

Using fins as the external or internal heat exchangers is also one of the effective techniques to enhance the heat transfer performance. The examples of fin heat exchanger designs are provided in **Figure 10**.

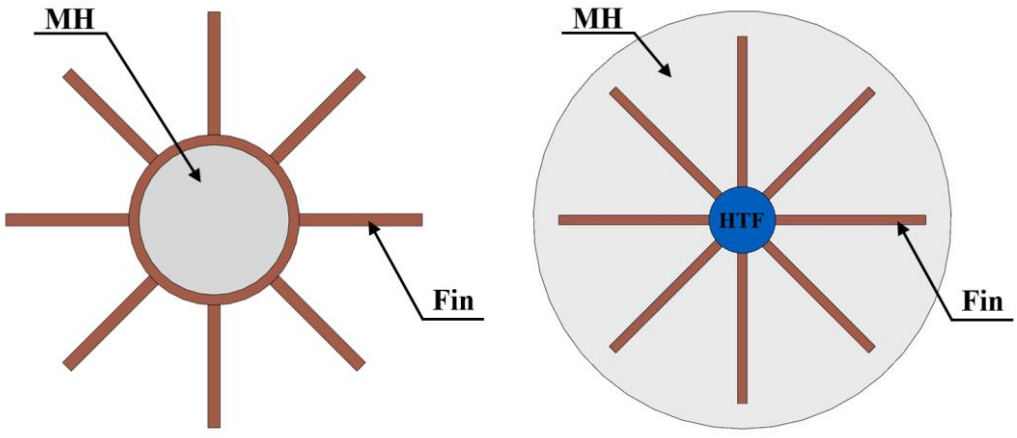

(a) **(b)**

Figure 2.11 Examples of heat exchanger design and optimisation by using fins; (a) External fins and (b) Internal fins.

- External fins

Adding metal fins on the outer wall of the MH bed as an external heat exchanger is one of the external heat exchanger configurations, which can increase the convective heat transfer area. An example of this design is provided in Figure 2.11a. An experimental study from Andreasen et al. (2013) found that using axial fins as the external heat exchanger of the MH tank incorporated with internal disk-shaped metal foils significantly improved heat exchange with the environment. The MH reactor's performance mainly depended on the fin and tube arrangements (MacDonald & Rowe 2006). Adding fins significantly affects the pressure of the hydrogen and the overall heat transfer inside the reactor (Veerraju & Gopal 2010). The three full cycles of hydrogen sorption (both absorption and desorption) were achieved in 15 minutes by the case with fins, while there was only one hydrogen desorption for the case without fins (Veerraju & Gopal 2010). This means that there was an 83% improvement in hydrogen sorption when using fins compared to the case without fins. Although the sorption times can be further enhanced by increasing the fins area, this can increase the overall volumetric and gravimetric of the MHHS. Although external fins can provide a larger heat transfer area, there is only an increase in heat transfer area outside the MHHS reactor. Therefore, inserting fins inside the reactor as an internal heat exchanger is another way to improve the MH performance by maintaining natural convection conditions (Keshari & Maiya 2018; Nyamsi et al., 2012; Keshari & Maiya 2020; Garrison et al., 2012; Muthukumar et al., 2012).

- Internal fins

Figure 2.11b provides an example of this design. The internal fin arrangement leads to a more uniform temperature distribution inside the storage system. Therefore, the local thermal conductivity of the MH bed can be improved because of an increase in the heat transfer area (Muthukumar et al., 2012). Keshari & Maiya (2018) designed a new heat exchanger by using a copper pin fin for $LaNi_5$-based storage. Each pin fin was designed to attach them at the centre using side-by-side techniques. They concluded that the number of fins and fin diameter are the key parameters for pin fin heat exchanger design. Increasing the pin fin diameter and the number of fins increased more heat transfer surface areas, resulting in a higher heat transfer rate. Krishna et al. (2024b) introduced the fin efficiency technique to optimise the conventional longitudinal fin performance. This study used the fin performance index to investigate the fin effect on hydrogen absorption/desorption. From their study under the total fin weight constant, the configuration with 8 fins obtained the best performance compared to other fin numbers from 4 to 12. The fin performance index significantly increases from 0.58 to 0.96 when increasing the fin numbers from 4 to 8. However, the fin performance index only increases from 0.96 to 1.1 when increasing the fin numbers from 8 to 12.

From this technique, increasing the fin number is the key parameter to improve the heat transfer rate. However, the drawback of this technique also relates to the weight of overall MHHS, especially for mobile applications. Furthermore, this technique is usually combined with an internal cooling tube as it provides better heat transfer performance, instead of having a natural convective heat transfer by using fins only. The well arrangement of the heat exchanger designs based on the fins and internal cooling tubes might be another option to reduce the weight of the overall storage system. These combinations are discussed in section "2.5.3".

- Metal Form

Metal alloys (before forming the MH) usually have a low thermal conductivity, negatively affecting the hydrogen reaction kinetics. Therefore, adding the metal foam will improve the effective thermal properties of the MH bed. In general, the selected metal foam should have high thermal conductivity, and its porosity should be over 90% (Sreeraj et al., 2022). The comparison of the use of metal foam for the MH storage system was proposed under the different metal materials, including aluminium, copper and zinc (Mellouli et al., 2009). The numerical calculation was done for the $LaNi_5$-based storage under the operating condition at 293 K of the temperature and 0.1 MPa of supply pressure with the cooling

fluid for the convective heat transfer. This study proved that adding metal foam significantly improved the hydrogen ab-sorption reaction. Absorption duration was improved by 55% in the case when zinc foam was added, 63% in the case when copper foam was added, and 66% in the case when aluminium foam was added compared to the case without metal foam. Figure 2.12 summarises the hydrogen absorption duration at 13 g of hydrogen/kg of hydride corresponding to the use of metal foams.

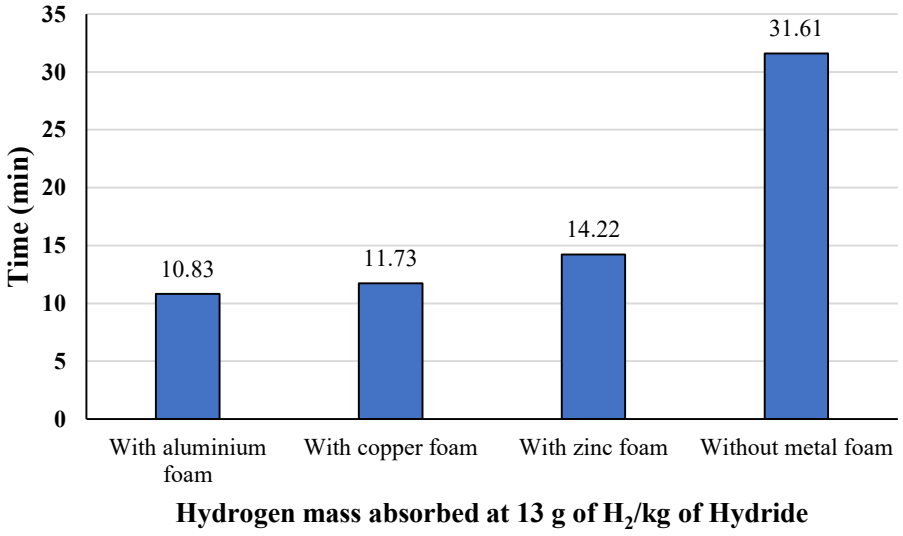

Figure 2.12 The hydrogen absorption duration from the use of metal foams to increase effective thermal conductivity by the study of Mellouli et al. (2009).

Other studies also focused on adding aluminium foam for ETC improvement as this material offered higher thermal conductivity and lower thermal mass than other metal foams (Mellouli et al., 2016; Alqahtani et al., 2020a; Alqahtani et al., 2020b; Afzal & Sharma 2018; Minko et al., 2015). The overall ETC based on the aluminium foam addition was improved by 4 W/mK for the $MmNi_{4.5}Al_{0.5}$ storage (Suda 1985) and up to 10 W/mK for the $LaNi_5$ storage (Laurencelle & Goyette 2007). The porosity size also affected the hydrogen reaction kinetics as the overall ETC significantly increased from 4.95 W/mK to 24.15 W/mK when reducing the porosity from 98% to 90% (Ferekh et al., 2015). However, the MHHS with metal foam is usually combined with a simple heat exchanger such as internal straight tubes (Bao et al., 2013), phase change material jacket (Darzi et al., 2016), inner tubes and cooling jacket (Mellouli et al., 2009; Afzal & Sharma 2018). This is because of the metal foam's structure and porosity. Moreover, enhancing the ETC by adding metal foam directly increases the weight of the overall storage system and reduces the hydrogen storage capacity, which directly affects the overall MHHS performance in all MHHS scales. The disintegration of itself during the hydrogen absorption/desorption is also the main problem of this technique (Nguyen & Shabani 2021). Therefore, the most recent studies mainly focus on the improvement of the heat transfer performance by the management of heat exchanger configurations rather than adding metal foam. One of the passive thermal methods that has been recently used for the MHHS is the use of PCM.

- *Phase Change Materials*

Phase change materials (PCMs) have been used to improve the cooling and heating of the MHHS during the absorption and desorption processes due to their ability to provide high thermal energy storage capacity, chemical stability, and low costs (Nguyen & Shabani 2021). Therefore, various PCMs have been applied in MHHS and several thermal management applications, such as the cooling of electronic devices (Kalbasi 2021; Ren et al., 2020), and the thermal management of batteries and buildings (Adilkhanova et al., 2021; Qu et al., 2021; Ling et al., 2014). One of the key advantages of using PCMs is their ability to recover the waste heat during the hydrogen sorption as the PCM will absorb the generated heat during the hydrogen absorption and release it as the required heat during the hydrogen desorption (Cui et al., 2022). In general, PCMs such as paraffin and sodium nitrate ($NaNO_3$) have a low

thermal conductivity, resulting in the limitation of heat transfer rates. Therefore, several PCMs with high thermal conductivity have been proposed to solve this problem such as $LiNO_3$-$3H_2O$, $Mg_{69}Zn_{28}Al_3$, and $Na_2CO_3 \cdot 10H_2O$. In general, these PCMs have their own melting point temperatures and other thermo-physical properties. For this purpose, the different melting temperatures play a significant role in selecting which PCM to use with a specific metal alloy. Table 2.4 summarises the selection of PCMs and their thermo-physical properties that have been used to improve the overall MHHS performance.

Table 2.4 Summary of selected phase change materials and their thermo-physical properties for some commonly used metal alloys

Metal Alloy	**PCM**					
Type	**Type of selected PCM**	**Melting temperature (K)**	**Density (kg/m^3)**	**Specific heat (J/kg K)**	**Thermal conductivity (W/m K)**	**Latent heat of fusion (kJ/kg)**
$LaNi_5$	Rubitherm (Salt) SP29Eu (Darzi et al., 2016;Nyamsi et al., 2019)	302.15-304.15	2000	2500	0.6	175
$LaNi_5$	Paraffin RT35 (Tong et al., 2019a; Tong et al., 2021)	308.15	880	1800	0.2	157
$LaNi_5$	Paraffin (Yao et al., 2020a)	308.15	850	2160	0.25	220
$LaNi_5$	Paraffin RT28 (El Mghari et al., 2020)	301	880	1800	0.2	245
$LaNi_5$	$LiNO_3$-$3H_2O$ (El Mghari et al., 2020; El Mghari et al., 2019; Lewis & Chippar 2021; Maad et al., a, b)	303.3-305.3	2140	1730	1.32	296
$LaNi_5$	$Na_2CO_3 \cdot 10H_2O$ (El Mghari et al., 2020)	305	1460	1880	1.25	267
$LaNi_5$	$Na_2SO_4 \cdot 10H_2O$ (El Mghari et al., 2020)	305.5	1485	1440	1.23	251
$LaNi_5$	$CaCl_2 \cdot 6H_2O$ (El Mghari et al., 2020)	302.6	1802	1430	1.09	192
Mg	$Mg_{69}Zn_{28}Al_3$ (Garrier et al., 2013;Mellouli et al., 2015)	607	2900	1100	10	175
Mg_2Ni	$NaNO_3$ (Ardahaie et al., 2021; Mellouli et al., 2016; Alqahtani et al., 2020a; Mellouli et al., 2017; Nguyen & Shabani 2020; Ye et al., 2020;	579-580	2260	1820	0.48	174

	Larpruenrudee et al., 2024)					
Mg_2Ni	NaOH (Alqahtani et al., 2020b)	590-591	2100	2080	0.92	165
Mg_2Ni	$Mg_{69}Zn_{28}Al_3$ (Maad et al., 2018)	607	2900	1100	10	175
MmNiMnCo	RT35HC (Nguyen & Shabani 2020)	308.15	880	2000	0.2	240

From Table 2.4, there are only four metal alloys that have been incorporated with PCMs. A $LaNi_5$ alloy is mostly used as MH material, followed by Mg_2Ni alloy. The $LaNi_5$ alloy has a high thermal conductivity of up to 1.5 W/mK and requires a low operating temperature as around the room temperature at 293 K to activate the system. However, this alloy has a low hydrogen storage capacity of up to 1.4 wt%. The Mg_2Ni offers a high hydrogen storage capacity with up to 6 wt% but it requires a high operating temperature of around 573 K to activate the system. Furthermore, this alloy also has a low thermal conductivity with less than 1 W/mK. A higher operating temperature range of Mg-based material must be used with a high melting temperature PCM such as $NaNO_3$. The MH materials and their thermal physical properties are provided in sections "2.4.2" to "2.4.4".

The design configurations using PCM also influence the overall MHHS performance. Several PCM configurations have been designed to optimise the PCM performance. These can be classified into four main types: pool bed PCM, jacket bed PCM, spherical bed, partition arrangement PCM, and sandwich bed PCM. Figure 2.12 provides the example of these configurations.

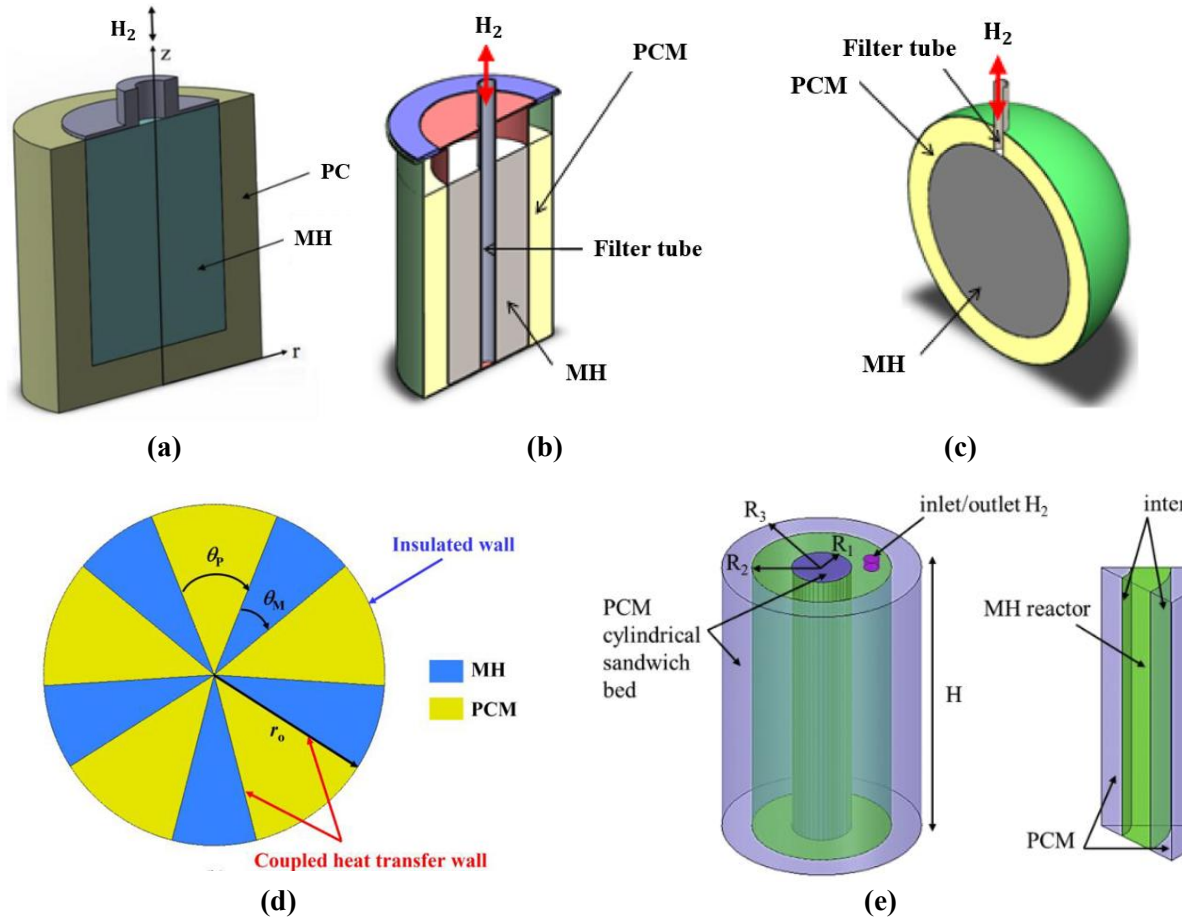

Figure 2.13 Design optimisation for various configurations of using phase change materials; (a) Pool bed (El Mghari et al., 2020), (b) Jacket bed (Mellouli et al., 2015), (c) Spherical bed (Mellouli et al., 2015), (d) Partition arrangement (Dai et al., 2024) and (e) Sandwich bed (Alqahtani et a., 2020a).

- Pool bed

The MHHS is designed by having a PCM covered around the MH bed except for the top side as the pool bed. The MHHS with PCM pool bed can be seen in Figure 2.13a as an example. Maad et al. (2016a, b) used $LiNO_3$-$3H_2O$ as the PCM to improve heat and mass transfer during the absorption of $LaNi_5$ MH storage. They found that the PCM's thermal conductivity and melting enthalpy were mostly affected by the hydrating rate and the capacity of MHHS. Then, this reactor was further used with Mg_2Ni as MH powder and $Mg_{69}Zn_{28}Al_3$ as the PCM (Maad et al., 2018). This study summarised that a specific melting temperature, a high melting, and latent heat were essential for selecting PCM during hydrogen desorption. Due to the low thermal conductivity of the PCM, the metal foam was composited with PCM to improve the heat transfer performance (Darzi et al., 2016; Tong et al., 2019a; El Mghari et al., 2020). The results from these studies proved that inserting metal foam in the PCM improved the thermal conductivity and reduced the hydrogen sorption duration. Using copper foam with PCM obtained better MH storage performance, compared to the PCM with aluminium foam (El Mghari et al., 2020). Moreover, increasing PCM thermal conductivity positively improved the storage system (Tong et al., 2019a). Several PCMs were tested for the $LaNi_5$ MH storage by Mghari et al. (2020). These included Paraffin RT28, $LiNO_3$-$3H_2O$, $Na_2CO_3 \cdot 10H_2O$, $Na_2SO_4 \cdot 10H_2O$, and $CaCl_2 \cdot 6H_2O$. They summarised that the use of $LiNO_3$-$3H_2O$ as PCM obtained better storage performance compared to other PCMs, as the storage with $LiNO_3$-$3H_2O$ obtained a faster hydrogen absorption. The $LaNi_5$-based MH storage with paraffin enhanced storage efficiency by 47% (Tong et al., 2021).

- Jacket bed

Unlike pool bed PCM, the jacket bed PCM only covers the MH bed like the outer cooling heat exchanger. Figure 2.13b presents an example of the MH reactor with a PCM jacket. Nguyen & Shabani (2020) proposed MHHS for a solar system using PCM. They employed MmNiMnCo as the MH alloy and paraffin as a PCM. They stated that the thermal conductivity of PCM must be improved to 1.5 W/mK as a minimum value. With this minimum value, thermal management could be more practical. Lewis & Chippar (2021) analysed the effect of the PCM on the MHHS during absorption and desorption processes. They used $LiNO_3$-$3H_2O$ as the jacket PCM and $LaNi_5$ as the MH alloy. In addition, they also investigated the effect of metal foam that was added to the PCM. This study proved that adding metal foam into PCM significantly improved storage performance.

- Spherical bed

A PCM configuration was designed to cover the MH bed as a spherical shape in the study by Melloui et al. (2015), which is presented in Figure 2.13c. This configuration was compared to the base case with a PCM jacket bed. This study employed Mg as the MH powder and $Mg_{69}Zn_{28}Al_3$ as a PCM. This study showed that using the spherical tank to contain the PCM obtained higher storage performance. The hydrogen sorption time improved by 22% with the use of a spherical tank compared to a jacket tank.

- Partition arrangement

Recently, the study by Dai et al. (2024) proposed the new PCM configuration with the constant PCM and MH volumes by focusing on the effect of partition arrangement of the MH and PCM on the hydrogen absorption performance. This can be seen in Figure 2.13d. The results from this study proved that when increasing the number of partitions from 2 to 5, the hydrogen absorption duration was reduced by 23.8%. However, the hydrogen absorption duration was significantly reduced by 67.13% when using the 5 PCM partitions instead of the PCM jacket.

- Sandwich bed

Increasing the PCM layer is also one of the effective techniques that can improve storage performance. The MH bed is placed in the middle between PCM beds, which can be seen in Figure 2.13e. A comparison between the MHHS with a PCM cylindrical jacket and the MHHS with a PCM cylindrical sandwich bed was performed by Alqahtani et al. (2020a). The Mg_2Ni was employed as the MH material and $NaNO_3$ as the PCM bed. The results from this study proved that using a PCM sandwich bed obtained a better heat transfer rate. Under the same PCM volumes, the durations of hydrogen absorption and desorption from the case with the sandwich bed were reduced by 81.5% and 73%, compared to the case with the jacket bed. Ye et al. (2021a, b) used the PCM, which was placed in the middle between two MH disks for heat recovery during the hydrogen desorption process. This study employed Mg as the MH powder and $NaNO_3$ as the PCM. When using PCM as a sandwich bed, desorption significantly improved by 21.8% compared to the case when PCM was used as a jacket bed. The design configuration of the PCM sandwich was then improved by using two different PCM materials with different melting points that were placed separately as two layers covering around the MH bed (Alqahtani et al., 2020b). The NaOH PCM was placed next to the MH bed as the first layer, followed by $NaNO_3$ PCM as the second layer. This study proved that having two PCM layers with different PCM types improved the hydrogen absorption duration by 26% and desorption duration by 51%, compared to the PCM sandwich bed with the same PCM types. However, this design was suggested for use with large-scale stationary storage (i.e. concentrated solar power applications) when considering the weight of the overall storage system and hydrogen storage capacity. Table 2.5 provides the summary of MH reactor configurations by using PCM.

Table 2.5 Summary of the configuration designs for using phase change materials with a metal hydride storage system

Metal alloy	**PCM**	**Configuration of PCM**	**Reference**
$LaNi_5$	Rubitherm (Salt) SP29Eu	Pool bed	Darzi et al., 2016; Nyamsi et al., 2019
$LaNi_5$	Paraffin RT35	Pool bed	Tong et al., 2019a; Tong et al., 2021
$LaNi_5$	Paraffin	Pool bed	Yao et al., 2020a
$LaNi_5$	Paraffin RT28	Pool bed	El Mghari et al., 2020
$LaNi_5$	$LiNO_3$-$3H_2O$	Pool bed	El Mghari et al., 2020; El Mghari et al., 2019; Lewis & Chippar 2021; Maad et al., 2016a, b
$LaNi_5$	$LiNO_3$-$3H_2O$	Jacket bed	Ye et al., 2021b
$LaNi_5$	$Na_2CO_3 \cdot 10H_2O$	Pool bed	El Mghari et al., 2020
$LaNi_5$	$Na_2SO_4 \cdot 10H_2O$	Pool bed	El Mghari et al., 2020
$LaNi_5$	$CaCl_2 \cdot 6H_2O$	Pool bed	El Mghari et al., 2020
Mg	$Mg_{69}Zn_{28}Al_3$	Pool bed	Garrier et al., 2013
Mg	$Mg_{69}Zn_{28}Al_3$	Jacket bed, Spherical bed	Mellouli et al., 2015
MgH_2	$NaNO_3$	Sandwich bed	Fernández et al., 2018
Mg_2Ni	$NaNO_3$	Jacket bed	Yehui et al., 2022; Nguyen & Shabani 2020; Larpruenrudee et al., 2024
Mg_2Ni	$NaNO_3$	Sandwich bed	Alqahtani et al., 2020a; Ye et al., 2020
Mg_2Ni	$NaNO_3$	Capsule bed	Larpruenrudee et al., 2024
Mg_2Ni	$NaNO_3$+NaOH	Cascaded sandwich bed	Alqahtani et al., 2020b

Mg_2Ni	$Mg_{69}Zn_{28}Al_3$	Pool bed	Maad et al., 2018
MmNiMnCo	RT35HC	Jacket bed	Nguyen & Shabani 2020

Several types of PCM have been used for the MHHS with various metal alloys. The PCM sandwich bed obtains the best heat transfer performance of the MHHS as the generated heat from the MH bed will transfer via two interfaces of the PCM. There is over 22% improvement of hydrogen absorption/desorption based on the PCM sandwich bed compared to the case with the PCM jacket bed and pool bed. There is over 26% improvement in hydrogen sorption when using two types of PCMs compared to only a single PCM under the PCM sandwich configuration design. Adding metal foam to the PCM is also another technique to increase the PCM performance. However, using the PCM as a heat exchanger will require a large amount of PCM to absorb the removal heat during the hydrogen absorption and release the heat during the hydrogen desorption. The weight of PCM and metal foam has a drawback that affects the overall MHHS weight. Therefore, having the appropriate amount of PCM and metal foam is one of the key challenges for the overall MHHS design and optimisation.

From the above mentioned, there are several types of heat exchangers for both external and internal types under the passive thermal management method. The overall weight of MHHS is the main problem of this method. This method generally requires a high amount of PCM to store the heat and release when it needed. Using a high number of fins also negatively affects the overall MHHS weight. Therefore, to further improve the MHHS performance by considering the overall MHHS weight, the combination of the heat exchangers between the active and passive thermal management methods has been recently proposed. The summary of this combination can be seen in the next section, 2.5.3.

2.5.3 Design Optimisation based on the Combination of various Heat Exchanger Methods

To further improve the heat transfer performance as well as the overall MHHS performance, some studies have been focused on the combination of various heat exchanger types under active and passive thermal management methods. These include the internal and internal heat exchangers, internal and external heat exchangers. Figure 2.14 provides examples of some heat exchanger combinations.

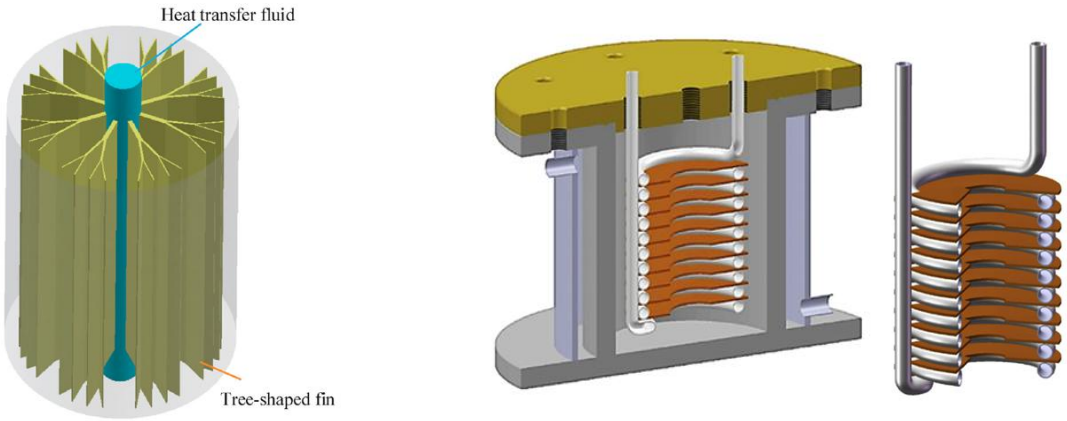

(a) (b)

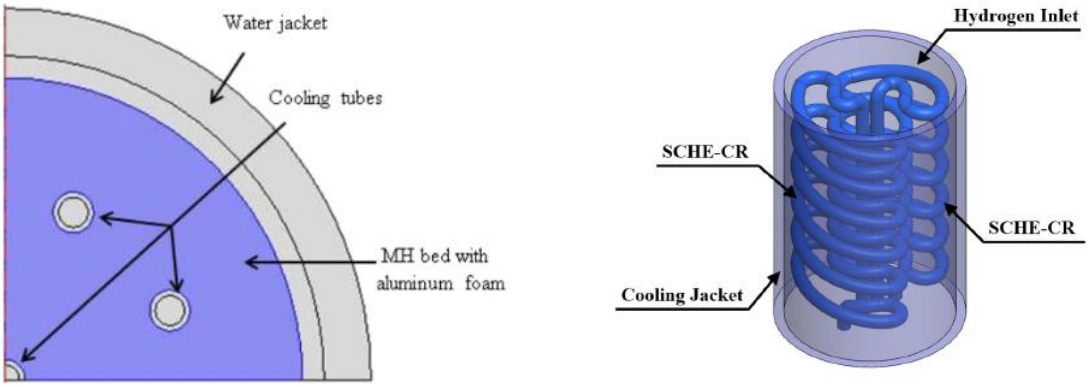

(c) (d)

Figure 2. 14 The example of the combination of various heat exchangers; (a) Central straight tube and fins (Bai et al., 2021), (b) Helical coil and fins (Souahila et al., 2014), (c) Internal cooling tubes and cooling jacket (Afzal & Sharma 2018), and (d) Semi-cylindrical coil with central return tube and cooling jacket (Larpruenrudee et al., 2023).

- Active and passive thermal management methods

From Figure 2.14a, b, an internal straight tube or helical coil tube is combined with internal fins to improve the heat transfer performance and hydrogen reaction kinetics. Ma et al. (2014) and Mallik & Sharma (2021) developed the MHHS with multiple tubes combined with fins. This study found that the fin number was the key parameter that affected hydrogen absorption, compared to fin radius and fins thickness. Refer to Figure 2.14a, tree-shaped fins were first introduced and embedded with a central heat exchanger tube by Bai et al. (2021). This design decreased the absorption time by 20.7% compared to the case with radial fins. Furthermore, increasing the length ratio of these fins increased the heat transfer performance of the MHHS. A variable cross-section annular fin was embedded with the MHHS's cooling tube to improve the inhomogeneous reaction phenomenon (Liu et al., 2021). This study proved that using this fin effectively resolved the inhomogeneous reaction phenomenon in the hydrogen reaction process. Ayub et al. (2020) performed a numerical simulation of the MHHS with annular truncated hollow conical fins that were attached to the central cooling tube. They summarised that various fin parameters affected the performance of the MHHS. These included fin angle, fin radius, number of fins, fin spacing, and fin thickness. The studies of Krishna et al. (2024b, c) proved that the appropriate selection of the fin's number significantly affected the heat transfer, while the fin shape obtainedless effect on the heat transfer performance. The fin thickness of 3 mm was recommended for the use of a precisely radial tapering fin. The helical coil tubes incorporated fins proposed by Dhaou et al. (2011) and Souahila et al. (2014). This combination indicated that the absorption duration was two times less than the case with helical coil only. Figure 2.14b indicates the MH reactor with a helical coil tube and fins. Mellouli et al. (2010) employed a spiral-coil tube with additional circular fins that were embedded at the innermost turn. There was a 66% improvement in the absorption time in the case of those equipped with spiral-coil tubes and circular fins compared to those without fins. Krisha et al. (2024a) proposed a new internal heat exchanger, namely a flat coil tube heat exchanger that was integrated with a spiral fin. From this combination, the hydrogen absorption duration reduced by 35.3% and 16.7%, compared to the case with a helical coil tube and double helical coil tube only.

- Active and active thermal management methods

The development of the MHHS with internal and external heat exchangers has been considered. Internal cooling tubes incorporating an external cooling jacket obtained better reaction kinetics (Freni et al., 2009; Karmakar et al., 2021). The combination of internal straight tubes and an external cooling jacket was applied to a large-scale stationary application with Ti-Mn-based MHHS by Afzal & Sharma (2018). This combination design can be seen in Figure 2.14c. This study summarised that a 14-MH multi-tube MH reactor had the best performance for the absorption and desorption processes, with the maximum reaction fraction at 1600 s, while the maximum reaction fraction from other cases was around 2700-3400 s. Larpruenrudee et al., (2023) combined an internal semi-cylindrical coil heat exchanger and central return tube with a cooling jacket (Figure 2.14d). This combination significantly improved the

heat transfer performance, resulting in a faster hydrogen absorption reaction. The absorption duration was reduced by 51% when using these heat exchangers, compared to the case without a cooling jacket.

Some studies also combine PCM with other heat exchanger types. The combination of PCM and inserting a heat exchanger into the MHHS also increases the storage performance instead of adding metal foam into the PCM only. Figure 2.14 presents the examples of these combinations.

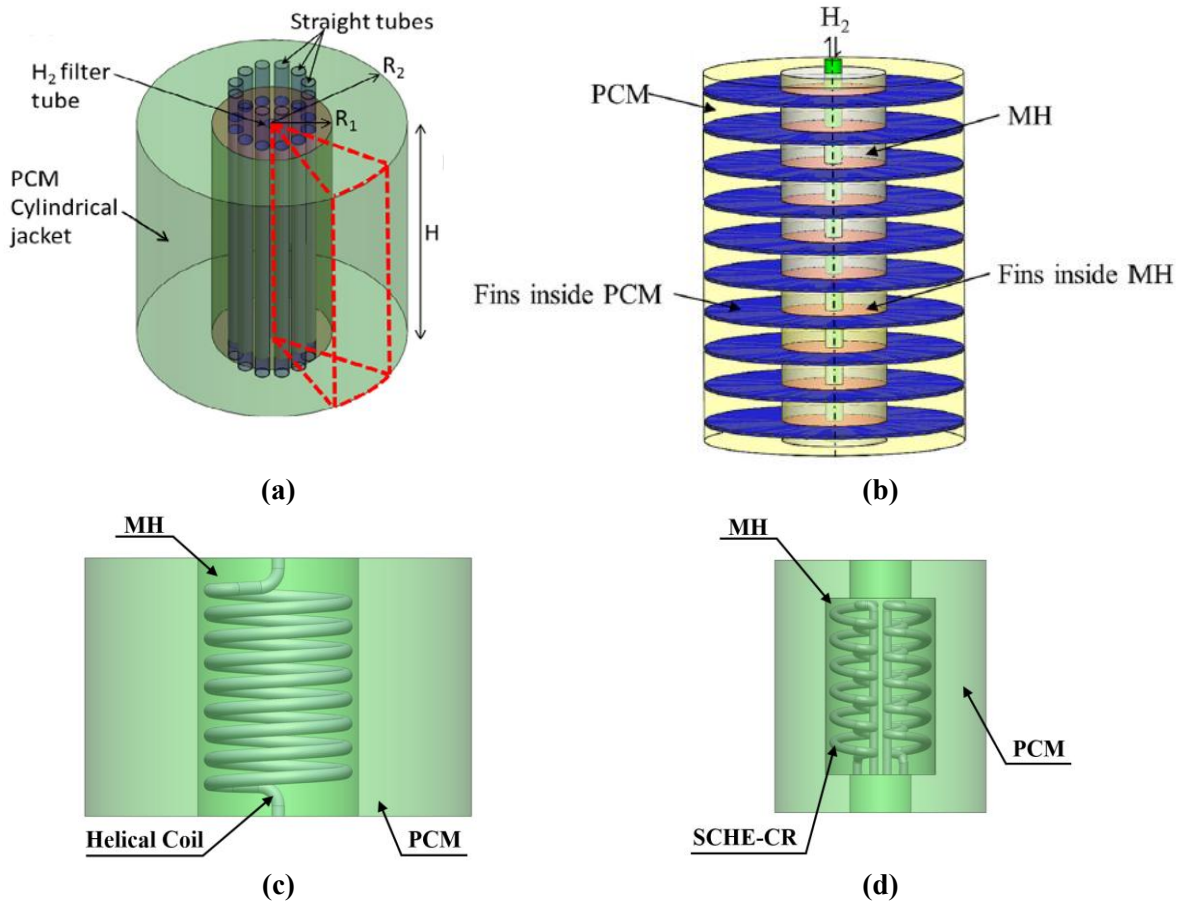

Figure 2.15 The combination of using phase change material and internal heat exchanger; (a) External PCM bed with internal cooling tube (Melloui et al., 2017), (b) External PCM bed with fins (Shrivastav et al., 2024), (c) External PCM bed with internal helical coil tube, and (d) External PCM capsule with internal semi-cylindrical coil tube.

Melloui et al. **(2017)** studied the HTF tube's effect when embedded inside the MHHS that was covered by PCM. The new design of this MHHS configuration can be seen in Figure 2.15a. Multiple tubes were added to the MH bed to improve the heat transfer rate. The numerical simulation was performed based on Mg_2Ni as MH material and $NaNO_3$ as the PCM. This study proved that the combination of these techniques (PCM jacket and internal cooling tube) improved the hydrogen absorption time by a 94% reduction compared to the base storage covered by PCM only. From Figure 2.15b, this MHHS with outer PCM was combined with the inner copper fins to improve the heat transfer performance (Shrivastav et al., 2024). The small MH parts were separated by the integration of inner copper fins in this study. This study concluded that using at least 10 copper fins reduced the hydrogen absorption rate by at least 86.5%, compared to the case without fins. Figure 2.15c shows the new MHHS configuration, which includes the outer PCM and inner helical coil. Tong et al. (2021) analysed the effect of using PCM with an internal cooling tube on the hydrogen desorption process. The helical coil tube was equipped with the MH bed ($LaNi_5$) covered by PCM (Paraffin RT35). Ardahaie et al. (2021) employed the $NaNO_3$-based PCM jacket incorporating the internal spiral tube as the heat exchanger for the Mg_2Ni-

based MHHS. This study summarised that employing a PCM jacket improved the hydrogen absorption and desorption time by 44% and 20%, respectively, compared to the base case without a PCM jacket. The $LiNO_3$-$3H_2O$-based PCM was employed for a $LaNi_5$-based storage system with the concentric finned tube heat exchanger (a combination of straight tube and finned disc) (Ye et al., 2021b). This study proved that using jacket bed PCM reduced the absorption and desorption time by 50% compared to the case with a concentric finned tube heat exchanger only. Larpruenrudee et al. (2024) developed the new PCM configuration, namely the PCM capsule (see Figure 2.15d). The purpose of this development was to incorporate the internal heat exchanger, namely a semi-cylindrical coil heat exchanger with a central return tube. The results from this study proved that the duration of the hydrogen absorption-desorption cycle was reduced by at least 63% when using these heat exchangers, compared to the case with PCM only. When using these heat exchangers, there was at least a 39% reduction in the duration of the absorption-desorption cycle, compared to the case without PCM. This study also concluded that using the PCM capsule instead of the PCM jacket and PCM pool bed obtained better heat transfer performance. This is because of the well arrangement of the PCM capsule, which increases more heat transfer surface areas around the top and the bottom parts of the MH bed. Furthermore, this study also analysed the effect of PCM volume on the heat transfer/storage capacity and reaction of heat recovery rate. From the combination of these heat exchangers, 4/8 of the total PCM volume obtained the best performance with the heat transfer/storage capacity at 108.66 kJ of PCM and 146.71 kJ of the HTF and the heat recovery rate of the PCM at 42.55%. However, this study only analysed the effect of PCM volumes when having additional heat exchangers on the heat transfer/storage capacity. The effect of these volumes on the hydrogen absorption/desorption reaction rate has still not been considered.

From this section, it can be summarised that the overall heat transfer performance as well as the overall MHHS performance are significantly improved when combining several heat exchanger types. The combination of internal heat exchangers has its own drawback in that it can reduce the MH volume. Recently, the PCM has been used as the external heat exchanger. The required amount of PCM is mostly calculated based on the assumption and its ability to store all the generated heat from the MH bed. In most studies, when combining the PCM with other internal heat exchangers, the relationships between the MH bed volume and the required amount of PCM (based on the heat exchanger combinations) are still not available yet. The proportional volume of PCM, MH bed, and HTF tube should be further considered to optimise the MHHS performance. The effect of the proportional volume of these factors should be considered with the hydrogen absorption/desorption reaction rate.

To understand the effect of different heat exchanger designs on heat transfer performance, some studies performed the comparison between various heat exchanger designs. This can be seen in the next section.

2.5.4 Comparison between various Heat Exchanger Methods and Performances

An appropriate selection of heat exchanger type is one of the key factors to increase the overall MHHS performance. The enhancements of hydrogen reaction kinetics as well as the heat transfer mechanism are also achieved based on this factor. Several studies have been performed to compare the MHHS performance under various heat exchanger types. The comparison between the effect of a cooling jacket and 22 circular fins on the MH performance was comprehensively investigated by Kaplan (2009). The results indicated that a higher hydrogen absorption rate was found when incorporated with a cooling jacket, as it significantly reduced the MH bed temperature. The reactor with a cooling jacket obtained the highest effective thermal conductivity at 113 W/m^2K, while the case with external fins obtained only 35 W/m^2K. The study by Wu et al. (2016) proved that the helical coil obtained the best performance to improve the heat and mass transfer rates compared to a straight tube and fins. The average reaction conversion for the desorption from the helical coil case reached 0.4 within 4000 s. The average reaction conversion for other cases was still less than 0.4 at 10000 s. Another study by Tong et al. (2019b) also indicated that using a double-coiled tube obtained a higher heat transfer rate than a straight tube and

single spiral tube. Askri et al. (2009) performed a numerical simulation to compare the performance of various heat exchanger configurations. Their results indicated that employing both cooling tube and fins essentially reduced the absorption time by 80%. However, using the internal cooling tube individually resulted in faster absorption time than using external fins only. Raju & Kumar (2012) performed the comparison between three heat exchanger configurations; (1) a cooling jacket with internal straight tubes and fins, (2) a cooling jacket with internal helical coil tubes, and (3) a cooling jacket with straight tubes that were placed horizontally. They proved that the MHHS with a cooling jacket and internal helical coil tube had better gravimetric and volumetric densities compared to other cases.

Various heat exchanger configurations for the MHHS were designed to compare the performance and their effect on the hydrogen storage capacity (Sekhar et al., 2015). The designs included an inner straight tube, inner helical coil, and cooling jacket with and without fins, which are presented in Figure 2.16a. Compared to other cases, the storage with an inner straight tube obtained a lower improvement of the dynamics of hydrogen absorption, followed by the case with a cooling jacket without additional fins. However, there was a similar absorption rate from the storage with an inner helical coil and a cooling jacket with additional fins. Under the same operating conditions at 3 MPa of supply pressure and 303 K of storage temperature, the cases with helical coil and external cooling jacket with fins achieved an average hydrogen concentration of over 70% within 400 s, while the average hydrogen concentration from other cases was around 40-60% within 500 s. However, using an internal heat exchanger significantly reduced the hydrogen storage capacity. The comparison of MH volume and the reduction of storage capacity can be found in Figure 2.16b. The MH volume from the case with the internal helical coil was around 1 L, while the MH volume from other cases was around 1.2-1.4 L. The storage capacity was reduced by 23.7% when using an internal helical coil, while there was only an 8.1% reduction of storage capacity when using an internal straight tube and fins.

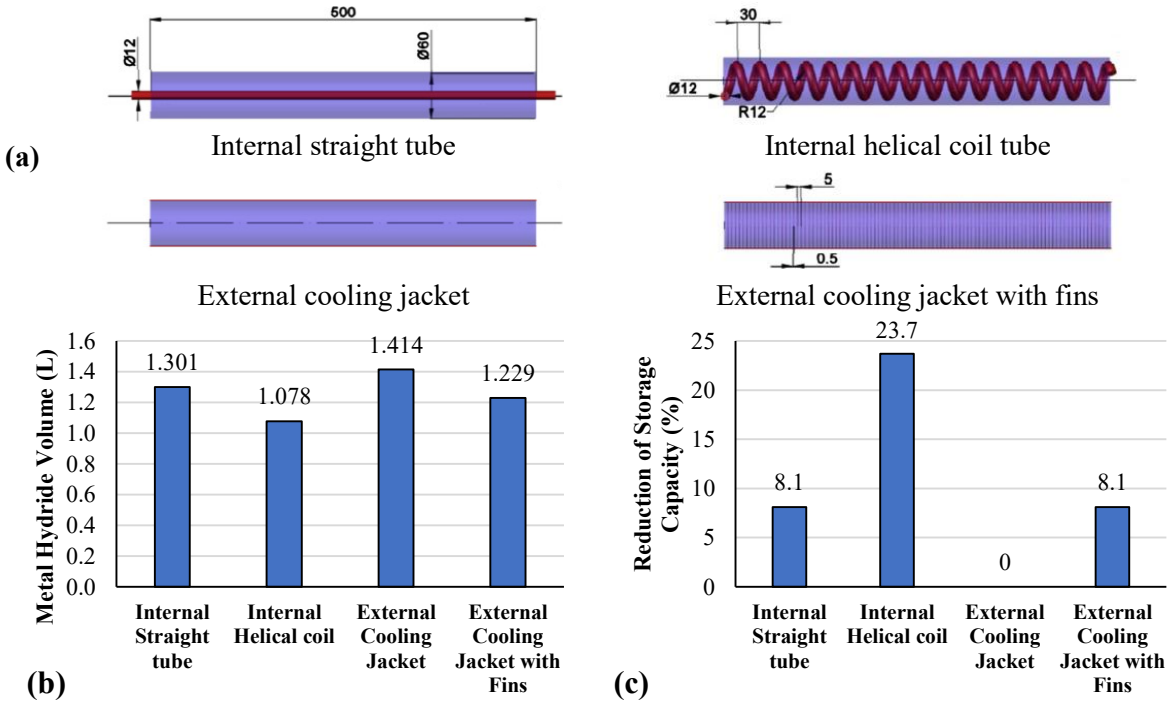

Figure 2.16 Main characteristics of four heat exchanger configurations by Sekhar et al. (2015); (a) Four main heat exchanger designs, (b) Metal hydride volume, and (c) Reduction of hydrogen storage capacity.

Wang et al. (2019) proposed the new $LaNi_5$-based MHHS design that was incorporated with radiation tubes (considered as mini-channel tubes). They investigated the mini-channel tubes' performance by comparing this heat exchanger with other heat exchangers, including inner straight tube, convergent-divergent tube, spiral tube, conjugate spiral tube, coupling network spiral tube, and the case without

heat exchanger. These designs are provided in Figure 2.17. These heat exchangers were designed under the constant tube volume and MH bed volume with the operating conditions as 1 MPa of supply pressure and 293 K of initial temperature. At 0.83 of reaction fraction, the absorption duration from the case without a heat exchanger was at 2500 s, while it was only 1550 s from the cases with an inner straight tube and with the convergent-divergent tube. There was a 38% reduction in hydrogen absorption duration when using an inner straight tube compared to the case without a heat exchanger. However, the complete hydrating process was achieved within 1200 s by the case with a radiation tube. This resulted in 52% and 37% reductions in absorption duration when compared to the cases with a straight tube and a spiral tube, respectively. The absorption duration from the cases with other spiral tubes (conjugate and coupling network designs) was similar to the case with the normal spiral tube. Furthermore, the absorption duration was significantly reduced by 77% when using the radiation tube, compared to the case without a heat exchanger. This study concluded that the key reduction of the hydrogen absorption from this study was the new arrangement of radial heat exchanger tubes, which improved the heat transfer mechanism in the radial section rather than the axial section of the MH bed instead.

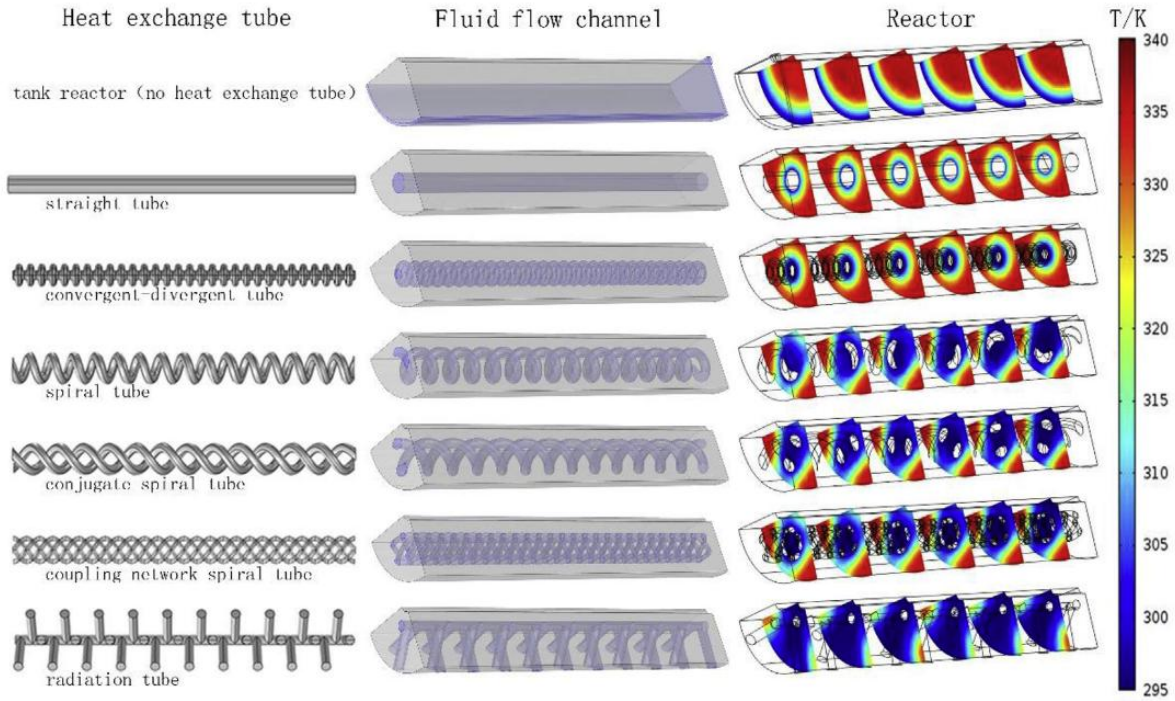

Figure 2.17 Comparisons of storage performance under various heat exchangers during the hydrogen absorption process of LaNi5-based MHHS (Wang et al., 2019). (including the case without heat exchanger, straight tube, convergent-divergent tube, spiral tube, conjugate spiral tube, coupling network spiral tube, and radiation tube).

Zheng et al. (2023) proposed the new MHHS design with primary and secondary helical tubes. The hydrogen tube was located at the central area of the MHHS to transport the hydrogen during the absorption and desorption. The performance of this heat exchanger was analysed by comparing it with other heat exchanger designs, including the cooling jacket, mini-channel tubes, spiral mini-channel tube, duplex helical circular tube, and duplex helical elliptical tube. Compared with the base case as the use of a cooling jacket, the hydrogen absorption duration at 90% of concentration significantly reduced by 61%, 77%, and 83% when using a spiral mini-channel tube, duplex helical circular tube, duplex helical elliptical tube instead of the use of cooling jacket, respectively. However, the absorption duration was significantly reduced by 95% when using the primary and secondary helical tubes instead. This is due to the secondary spiral tube which accelerates both hydrating and heat transfer rate nearly the central area of the hydrogen tube.

In these comparisons, several heat exchangers and their performances have been compared to optimise the MHHS performance under the consideration of hydrogen reaction kinetics and heat transfer rate. These include internal and external heat exchangers such as inner/outer cooling tubes under different shapes (straight, helical coil, mini-channel tubes) and fins. From these studies, it can be summarised that the heat transfer rate and hydrogen reaction kinetics are based on the well arrangement/layout of the heat exchanger structure. This leads to a more uniform temperature distribution, resulting in more reaction fraction distribution inside the MHHS. The active thermal management technique using the HTF throughout the heat ex-changer tube (internal/external tube) significantly improves heat transfer efficiency in contrast to the passive thermal management technique such as fin and PCM. However, the drawback of internal heat exchanger tube with complex structures based on active thermal management technique is the pressure losses. Huge pressure losses are usually a result of the curvature ratio of the complex HTF tube. This can negatively affect the overall MHHS performance. The amount of pressure losses from the heat exchanger should be stabilised to maintain the overall storage/heat exchanger performance (Guan et al., 2014; Zhang & Liu 2022). Furthermore, the comparison between these heat exchangers and U-shape tube or semi-cylindrical coil tube is still not available yet. Moreover, the combination of PCM configuration and these heat exchangers is also not available. As mentioned previously, the relationship between the required PCM volume, heat exchanger volume, and MH volume should be taken into account when combining the PCM with other internal heat exchangers as this can directly affect the MHHS performance, especially for mobile applications. To optimise the MHHS, the effect of the proportional volume of these parameters should be considered with the hydrogen absorption/desorption reaction rate. The design optimisation of MHHS and heat exchangers usually depends on the MHHS application and its scale which are based on the weight of the overall storage system and hydrogen storage capacity. However, it is not only heat exchanger design and configuration that affect the overall MHHS performance and heat transfer rates; heat transfer fluids (HTFs) also affect heat transfer performance. This is due to their thermo-physical properties that conduct heat. The next section provides the discussion based on the different HTFs on the heat transfer performance under the hydrogen reaction kinetics.

2.5.5 Heat Transfer Fluids

Appropriate selection of HTFs affects heat transfer performance as well as hydrogen reaction kinetics. Several types of HTFs have been used for thermal energy storage. However, for MH storage, air and water are generally used as the HTF due to having a low cost and less environmental impact. For the MH alloys, which require the operating temperature as the room temperature at 298 K (i.e. $LaNi_5$), water is usually used as the HTF. However, the air is generally used with the MH alloys, which require a higher operating temperature (i.e. Mg, Mg_2Ni) at 573 K. The effect of selecting HTF on the hydrogen absorption performance was investigated by Mellouli et al. (2017). HTFs in this study included air, water, oil, and molten salt. The Mg_2Ni was employed as the MH powder, and $NaNO_3$ as the PCM. The investigation was performed under the operating temperature of the storage system and HTF at 579 K and supply pressure at 1.5 MPa. Thermo-physical properties of these HTFs and the results of this investigation are summarised and provided in Table 2.6 and Figure 2.18.

Table 2.6 Thermo-physical properties of heat transfer fluids (Vignarooban et al., 2015)

Type of HTF	Melting point (K)	Viscosity (Pa s)	Thermal conductivity (W/mK)	Heat capacity (kJ/kgK)
Air	-	0.00003	0.06	1.12
Water/steam	273	0.00133	0.08	2.42
Thermal oil	253	0.014	0.136	2.25
Molten Salt	368	0.007	0.654	1.44

From Figure 2.18a, air and water require longer hydrogen absorption time compared to oil and molten salt. The absorption time for the cases with air and water is over 400 mins, while using molten salt requires the absorption time lower than 300 minutes. In contrast, from Figure 2.18b, using molten salt requires a large cost of approximately \$0.62-\$0.81 per kilogram, while using oil also requires a high cost, around \$0.3 per kilogram. However, air and water are then preferred as there is no cost.

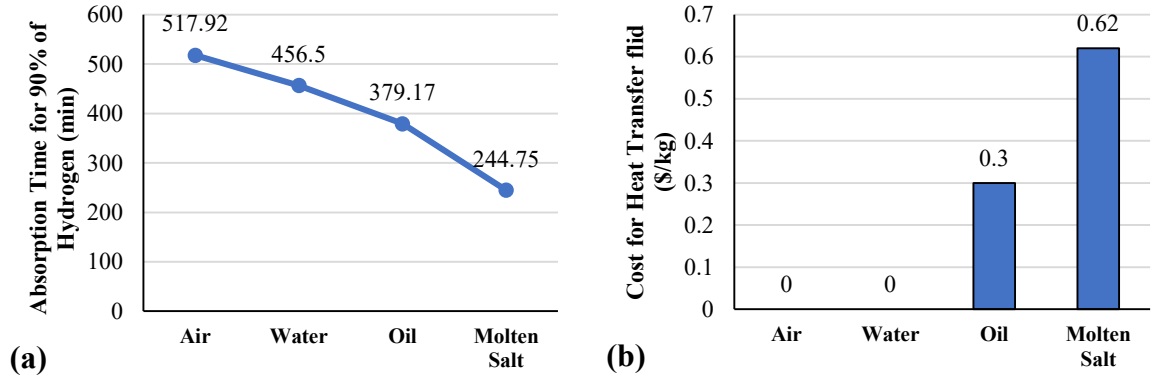

Figure 2.18 Comparison of the hydrogen absorption time and cost between various heat transfer fluids (a) Absorption time for 90% of hydrogen and (b) Cost for heat transfer fluids per kilogram (Mellouli et al., 2017; Vignarooban et al., 2015)

2.6 Operating Conditions

The operating parameters during the reaction process are the main factors that can positively or negatively influence the hydrogen reaction kinetics as well as the overall MHHS performance in actual utilisation. The range of operating conditions can be varied due to the MH materials that have different thermos-physical properties. Therefore, the enhancement of the MHHS performance for both small- and large-scale operation has been considered based on the optimisation of operating parameters. The operating parameters basically include the initial temperature of MH storage, hydrogen loading pressure, initial temperature and flow rate of the HTF, heat transfer coefficient (HTC), effective thermal conductivity (ETC), and particle size.

2.6.1 Initial Condition of the Metal Hydride Storage

Appropriate selecting initial temperature and supply pressure plays a significant role in the hydrogen reaction kinetics during absorption and desorption. The initial temperature directly affects the driving force when producing the hydride reaction. For the hydrogen absorption process, decreasing the initial temperature results in faster absorption at the initial moment of the process. A lower initial temperature directly causes a lower equilibrium pressure. The hydrogen is then absorbed faster with a larger difference in pressure between exerted and equilibrium pressure. Therefore, a higher exerted pressure also leads to faster hydrogen absorption (Wu et al., 2014). In general, the metal alloys significantly absorb the hydrogen at the initial moment of hydrogen absorption due to a larger difference between these two pressures (Afzal & Sharma 2021a; Afzal & Sharma 2021b). However, the opposite way is

applied to the hydrogen desorption process. From the previous discussion under the introduction section, due to the exothermic reaction for the hydrogen absorption process and the endothermic reaction for the hydrogen desorption process, a higher initial temperature usually results in faster desorption. The operating condition ranges for both temperature and pressure for some commonly used metal alloys can be seen in Table 2.2.

Various types of heat exchanger designs have been proposed recently. Among the heat exchanger designs using the HTF, some studies focus on improving MHHS performance based on the operating conditions of the system. As mentioned earlier, the operating temperature and pressure ranges are dependent on the MH materials, which have different operating ranges. The investigation of various initial temperatures of the storage was done by a few studies based on the Mg_2Ni alloy due to the operating temperature ranges of MH materials. The initial temperature at 573 K and 673 K were the best values for hydrogen absorption and desorption, respectively (Wu et al., 2016; Larpruenrudee et al., 2022). The loading pressure also varies depending on the MH materials. Only three types of metal alloys have been used to compare the MH performance by focusing on loading pressure. These include $LaNi_5$, Mg_2Ni, and $MmNi_{4.6}Al_{0.4}$. The heat exchanger types are only the external cooling/heating jacket and internal heat exchanger tube that require the HTF. The best case of $LaNi_5$-based storage incorporating with mini-channel heat exchanger was found when using the supply pressure at 1 MPa and 0.1 MPa for hydrogen absorption and desorption, respectively. The supply pressure at 1.2-1.6 MPa is the best value for the absorption and 0.025 MPa for the desorption based on the $LaNi_5$-based storage with an external cooling jacket (Chung & Ho 2009; Valizadeh et al., 2016; Nam et a., 2012). The best value for Mg_2Ni-based storage during the absorption was 1.8 MPa for multi-zone configuration (Eisapour et al., 2021b) and semi-cylindrical coil (Larpruenrudee et al., 2022), while the best value for the desorption was 0.8 MPa for helical coil (Wu et al., 2016). The best values of supply pressure during the absorption and desorption for the $MmNi_{4.6}Al_{0.4}$-based storage with an external heating/cooling jacket were 3 MPa and 1 MPa, respectively (Patil & Gopal 2013). Table 2.7 summarises the initial condition of the MHHS based on the initial temperature and loading pressure that affect the hydrogen absorption and desorption duration.

Table 2.7 Summary of initial conditions of metal hydride storage on the improvement of hydrogen sorption duration

Initial temperature of metal hydride storage						
Metal alloy	**Heat exchanger types**	**Hydrogen sorption**	**Temperature range of storage (K)**	**Improvement of hydrogen sorption (%)**	**Best case (K)**	**Reference**
$LaNi_{4.7}Al_{0.3}$	Straight tubes	Absorption	293-308	< 1	293	Raju et al., 2019b
Mg_2Ni	Helical coil	Absorption	523-673	NA	523	Wu et al., 2014
Mg_2Ni	Helical coil	Desorption	573-673	NA	673	Wu et al., 2016
Mg_2Ni	Helical coil with central return tube	Absorption	523-673	NA	523	Eisapour et al., 2021a
Mg_2Ni	Semi-cylindrical coil	Absorption	473-623	11-24	573	Larpruenrudee et al., 2022
Loading pressure						
Metal alloy	**Heat exchanger types**	**Hydrogen sorption**	**Pressure range of storage (MPa)**	**Improvement of hydrogen sorption (%)**	**Best case (MPa)**	**Reference**
$LaNi_5$	Mini-channel	Absorption Desorption	0.5-2.5 0.0-0.2	42-62 21-63 (RF=0.1)	1.0 0.1	Wang et al., 2021
$LaNi_5$	Mini-channel	Absorption	0.7-1.6	43-65 (RF=0.8)	1.0	Wang et al., 2020
$LaNi_5$	Heating/cooling jacket	Absorption Desorption	0.4-1.6 0.025-0.1	58-63 (RF=0.9) 37-50 (RF=0)	1.6 0.025	Chung & Ho 2009

$LaNi_5$	Heating jacket	Desorption	0.025-0.1	31-66	0.025	Valizadeh et al., 2016
$LaNi_5$	-	Absorption	0.6-1.2	19-38	1.2	Nam et al., 2012
$LaNi_5$	U-shape tube and fin	Absorption	1.0-1.8	42.4	1.8	**Yang et al., 2025**
$LaNi_5$	PCM Partition arrangement	Absorption	0.8-1.6	41.23	1.6	**Dai et al., 2024**
$LaNi_{4.7}Al_{0.3}$	Straight tubes	Absorption Lower values could not reach 1.28 *wt%*	2.5-3.5	30 (Cap=1.28 *wt%*)	2.5	Raju et al., 2019b
Mg_2Ni	Helical coil	Absorption	0.6-1.8	62-75 (RF=0.7)	1.8	Eisapour et al., 2021a
Mg_2Ni	Helical coil	Desorption	0.8-1.6	35-76 (RF=0.1)	0.8	Wu et al., 2016
Mg_2Ni	Multi-zone configuration	Absorption	1.0-1.8	38-48	1.8	Eisapour et al., 2021b
Mg_2Ni	Semi-cylindrical coil	Absorption	1.2-3.0	32-42	1.8	Larpruenrudee et al., 2022
$MmNi_{4.6}Al_{0.4}$	Heating/cooling jacket	Absorption Desorption	1.0-3.0 1.0-3.0	45-72 (RF=0.9) 20-53 (RF=0.1)	3.0 1.0	Patil & Gopal 2013

Note: RF = Reaction fraction (maximum reaction fraction that could be achieved for hydrogen absorption and minimum reaction fraction that could be achieved for hydrogen desorption by specific values) and Cap = Hydrogen storage capacity.

From these parameters, it is obvious that the different MH materials also have different initial temperatures and loading pressure ranges to activate the system. The lower initial temperature of MHHS usually obtains better performance for the absorption process, while the higher initial temperature is better for the desorption process. In contrast, a higher loading pressure is usually better for absorption, while a lower loading pressure is suitable for desorption. However, it should be noted that appropriate range selection of these two parameters is required, especially when using the new MH materials as these parameters can significantly affect the hydrogen storage capacity (Muthukumar et al., 2018; Larpruenrudee et al., 2022).

2.6.2 Initial Condition of the Heat Transfer Fluid

Several types of HTFs have been used for thermal energy storage. However, for the MHHS, air and water are generally used as the HTF due to their low cost and less environmental impact. A lower/higher HTF temperature directly improves the heat transfer rate during the hydrogen absorption/desorption process. This results in faster hydrogen reaction kinetics in both absorption and desorption processes. The study from Ardahaie et al. (2021) proved that reducing the HTF temperature from 573 K to 373 K improved the absorption duration by 47%, while increasing the HTF temperature from 643 K to 843 K improved the desorption duration by 43%. The turbulence level of the HTF flow rate also plays an important role in removing the generated heat during hydrogen absorption and supplying the required heat during hydrogen desorption (Wang et al., 2021). A high turbulence level is caused by a high HTF flow rate that circulates through the HTF tube. The study of Anbarasu et al. (2014a, b, c, d) found that the operating pressure, the temperature of the cooling fluid, and the ETC of the MH impacted the MH reactor performance. A faster hydrogen absorption/desorption reaction was observed when increasing the HTF flow rate (Singh et al., 2015). However, a higher number of HTF tubes obtained a greater MH performance compared to the HTF flow rate (Kumar et al., 2019; Raju et al., 2019). The initial HTF temperature should be lower than the initial MHHS temperature for the hydrogen absorption process. In contrast, the initial HTF temperature should be higher than the initial MHHS temperature for the hydrogen desorption process. As for faster hydrogen reaction kinetics, the MHHS must be cooled down during the absorption, while the MHHS must be heated up during the desorption.

Table 2.8 summarises the initial conditions of the HTF and their effects on the improvement of hydrogen sorption duration under various heat exchanger types. The lower HTF temperature usually results in a higher hydrogen absorption reaction. In contrast, a higher initial temperature of the HTF leads to a higher hydrogen desorption reaction instead. The lowest initial temperatures for the hydrogen absorption at 283 K and 298 K are used for $LaNi_5$-based storage and $MmNi_{4.6}Al_{0.4}$-based storage, while the highest initial temperatures for the desorption process at 353 K and 400 K are used for these storages. The minimum initial temperature for the absorption at 373 K and the highest initial temperature for the desorption at 843 K are used for the Mg_2Ni-based storage. However, some studies focus on improving the storage system by using various flow rates and Reynolds numbers (Re). In general, the flow rate and Re are varied depending on the heat exchanger tube's diameter. With the tube diameter at 6 mm of the semi-cylindrical coil, the Re at 22000 is the best value for the Mg_2Ni-based storage (Larpruenrudee et al., 2022). When reducing this tube diameter from 6 mm to 4 mm, the Re at 9000 is the best value for this storage type. With the tube diameter of 4 mm of mini-channel, the flow rate of 1 m/s is the best value for the $LaNi_5$-based storage (Wang et al., 2021).

Table 2.8 Summary of initial conditions of a heat transfer fluid on the improvement of hydrogen absorption and desorption duration

Initial temperature of heat transfer fluid

Metal alloy	Heat exchanger types	Hydrogen sorption	Temperature range of HTF (K)	Improvement of hydrogen sorption (%)	Best case (K)	Reference
$LaNi_5$	Mini-channel	Absorption Desorption	273-313 333-373	20-45 25-56	293 353	Wang et al., 2021
$LaNi_5$	Mini-channel	Absorption	273-298	30-65 (RF=0.8)	273	Wang et al., 2020
$LaNi_5$	Heating/cooling jacket	Absorption Desorption	283-323 293-323	38-72 (RF=0.9) 68-86 (RF=0.4)	283 323	Chung & Ho 2009
$LaNi_5$	Heating jacket	Desorption	293-323	34-61	323	Valizadeh et al., 2016
$LaNi_5$	Spiral coil	Absorption Desorption	283-293 303-323	21-38 60-69	288 323	Mellouli et al., 2007
$LaNi_5$	U-shape tube and fin	Absorption	273-313	55	273	**Yang et al., 2025**
Mg_2Ni	Semi-cylindrical coil	Absorption	373-573	20-56	373	Larpruenrudee et al., 2022
Mg_2Ni	Semi-cylindrical coil with central return tube	Absorption	423-573	19-36	423	**Larpruenrudee et al., 2023**
Mg_2Ni	Semi-cylindrical coil with central return tube and PCM capsule	Absorption Desorption	423-573 573-723	15-26 25-38	423 723	**Larpruenrudee et al., 2024**
Mg_2Ni	Spiral coil and PCM ($NaNO_3$)	Absorption Desorption	373-573 643-843	31-47 32-43	373 843	Ardahaie et al., 2021
Mg_2Ni	Semi-cylindrical coil with central return tube and PCM ($NaNO_3$)	Absorption Desorption	423-573 573-723	26-50 39-67	423 723	Larpruenrudee et al., 2024
Mg_2Ni	Multi-zone configuration	Absorption	373-573	50-66	373	Eisapour et al., 2021b
$MmNi_{4.6}Al_{0.4}$	Heating/cooling jacket	Absorption Desorption	298-318 380-400	13-36 (RF=0.9) 15-39 (RF=0.1)	298 400	Patil & Gopal 2013

Flow rate of heat transfer fluid

Metal alloy	Heat exchanger types	Hydrogen sorption	Flow rate range of HTF (m/s)	Improvement of hydrogen sorption (%)	Best case	Reference
$LaNi_5$	Mini-channel	Absorption Desorption	0.1-2.0 (m/s) 0.1-2.0 (m/s)	44 19	1.0 (m/s)	Wang et al., 2021

					1.0 (m/s)	
$LaNi_5$	U-shape tube and fin	Absorption	1.0-3.0 (m/s)	8.2-15.7	2.0 (m/s)	**Yang et al., 2025**
$LaNi_{4.7}Al_{0.3}$	Straight tubes	Absorption	10-35 (lpm)	21-38	20 (lpm)	Raju et al., 2019b

Reynolds number of heat transfer fluid

Metal alloy	Heat exchanger types	Hydrogen sorption	Re range of HTF	Improvement of hydrogen sorption (%)	Best case	Reference
Mg_2Ni	Multi-zone configuration	Absorption	17000-52000	13-19	52000	Eisapour et al., 2021b
Mg_2Ni	Semi-cylindrical coil	Absorption	10000-22000	28-50	22000	Larpruenrudee et al., 2022
Mg_2Ni	Semi-cylindrical coil with central return tube	Absorption	6400-14500	24-44	9000	Larpruenrudee et al., 2023

Note: RF = Reaction fraction (maximum reaction fraction that could be achieved for hydrogen absorption and minimum reaction fraction that could be achieved for hydrogen desorption by specific values and certain time)

From these parameters, it can be seen that a lower initial temperature of the HTF obtains better performance for the absorption process, while a higher initial temperature of the HTF is better for the desorption process. It is worth mentioning that the HTF temperature ranges from these studies might not be applied in reality. Appropriate selection of the HTF temperature ranges should be based on each specific application. For the HTF flow rate and Re, a higher value of these two parameters always obtains the higher heat transfer performance as the heat is always transferred faster based on a faster fluid flow. However, an appropriate selection of this parameter usually depends on the HTF tube diameter. Moreover, in reality, a high-speed flow rate of the HTF or a high coil pitch/curvature ratio of the coil tube usually increases the oscillation level. This significantly affects the heat and mass transfer rate (Schlichting 1979; Claman & Minton 1977; Lin & Ebadian 1997). In some cases, these changes can induce flow instabilities in equipment due to the fluctuation of flow and pressure drop (Pendyala et al., 2008). Therefore, a real experiment is required to test the MHHS system when applying the heat exchanger with the HTF at a high flow rate.

2.6.3 Other Operating Conditions and Comparison of the Operating Parameters

Other operating parameters have been analysed recently. These include the heat transfer coefficient (HTC) between the MH bed and the HTF, effective thermal conductivity (ETC), and particle sizes. Valizadeh et al. (2016) studied the effect of the HTC between the MH bed and HTF for the $LaNi_5$-based storage that was covered by a heating jacket during the desorption process. The HTC varied from 500 W/m^2K to 2000 W/m^2K. They pointed out the suitable value was 500 W/m^2K. Other higher HTC values had less effect on the desorption process. This was due to the limitation of heat capacity inside the MH bed. The study from Wu et al. (2016) and Eisapour et al. (2021a) also proved that among the HTCs between 10 W/m^2K and 1000 W/m^2K, the HTC at 500 W/m^2K was the best value for the desorption process of the Mg_2Ni-based storage system with internal helical coil heat exchanger. Similarly, the study from Larpruenrudee et al. (2023) also reported that using the HTC at 500 W/m^2K with semi-cylindrical coil heat exchangers with central return tube and cooling jacket, obtained the best heat transfer performance, compared to other lower and higher HTC values. Li et al. (2015) studied the effects of operating parameters and spiral mini-channel tubes on the heat transfer efficiency and hydrogen absorption rate of the $LaNi_5$-based storage. The operating parameters included volume fraction, loading pressure, initial temperature, ETC, and HTC. Their study indicated that the HTC had only less effect on the hydrogenation process compared to other parameters. Among the HTC from 500 W/m^2K to 8000 W/m^2K, there is only a 2% improvement in hydrogen absorption duration. In the ETC

ranges from 0.5 W/mK to 7.5 W/mK, the recommendation value was 2.5 W/mK, with the improvement of the absorption reaction at 48% from the ETC at 0.5 W/mK. The improvement of absorption reaction only improved by 29% when increased the ETC from 2.5 W/mK to 7.5 W/mK.

The effect of operating conditions was considered by the numerical study of Raju et al. (2019b). The multi-tube heat exchanger was used as an internal heat exchanger for MH ($LaMi_{4.7}Al_{0.3}$) storage. This study concluded that operating parameters, especially supply pressure, significantly affected the absorption process. The flow rate of the HTF also influenced hydrogen absorption. Several studies (Wang et al., 2012; Bhogilla 2017; Eisapour et al., 2021a; Bai et al., 2021; Visaria & Mudawar 2012c) also proved that the HTF temperature and loading pressure significantly influenced the hydrogen reaction kinetics for both absorption and desorption, compared to other parameters, including volume of MH storage, overall HTC, and initial temperature of the MHHS. Furthermore, the reduction of coolant temperature reduced the hydrating time by approximately 57% compared to the base case (Visaria & Mudawar 2012a, b). The multiple zones of HTF were proposed to improve the hydrogen absorption of the MH (Mg_2Ni) storage (Eisapour et al., 2021b). With this technique, air as the HTF was injected through multi-HTF zones of the MHHS. This study proved that higher loading pressure and airflow Re resulted in a faster absorption rate. Besides, the lower inlet temperature of the HTF led to a faster absorption rate instead. The reduction of the inlet temperature of the fluid was the most effective case for improving the absorption rate. However, the study by Wang et al. (2021) indicated that changing the particle size of MH material had less effect on the hydrogen sorption rate.

The specific heating power also plays an important role as an evaluation indicator to provide the average power output of the system. This parameter has been applied to several thermal storage applications, including heat transformers (Yang et al., 2012), heat pumps (Yang et al., 2010), and thermal batteries (Malleswararao et al., 2021). The sensitivity analysis was performed under various ranges of operating parameters for the absorption process by Mou et al. (2023). These included the hydrogen supply pressure, thermal resistance between the MH and heat exchanger, HTF flow rate and temperature. The MHHS in this study contained the helical coil tube and $LaNi_5$ as the MH powder. Table 2.9 summarises the results of this study.

Table 2.9 Summary of the effect of operating parameters on specific heating power from Mou et al. (2023)

Parameter	Operating range	Specific heating power range ($W.kg^{1}$)	Improvement of specific heating power (%)
Supply pressure	0.8-1.6 MPa	125-209	40%
Heat transfer fluid temperature	285-301 K	143-199	28%
Heat transfer fluid flow rate	18-42 L/h	166-173	4%
Thermal resistance	600-1400 $mm^2 \cdot K/W$	158-186	15%

From Table 2.9, the hydrogen supply pressure significantly affects specific heating power. There is a 40% improvement of the specific heating power when increasing the supply pressure from 0.8 to 1.6 MPa, while there is only a 4% improvement of the specific heating power with the flow rate ranging between 18 and 42 L/h. The specific heating power only improves by 28% and 15% when changing HTF temperature from 285 K to 301 K and thermal resistance from 600 $mm^2 \cdot K/W$ to 1400 $mm^2 \cdot K/W$, respectively.

For comparison purposes, Figure 2.19 compares the improvement of hydrogen sorption duration based on various operating conditions that are taken from Table 2.7 and Table 2.8. The improvement of hydrogen absorption is only 11-24% when changing the initial temperature of the MHHS, while there

is around 13-50% improvement of hydrogen absorption with the different ranges of flow rate and the Re of the HTF. However, the minimum improvement of the hydrogen absorption by changing the hydrogen supply pressure is 20%, while the minimum improvement of the absorption by changing the HTF temperature is 13% only. Besides, the maximum improvement of hydrogen absorption from these two parameters is 72%. It can be summarised that the hydrogen pressure and initial HTF temperature are the main parameters that significantly influence MH storage performance for the absorption process compared to the other two parameters. In contrast, the maximum improvement in hydrogen desorption based on the HTF temperature is 10 % higher than in the cases with supply pressure. The minimum improvements of desorption duration for HTF temperature and supply pressure are 20% and 15%, respectively. For the desorption process, the maximum improvement of this process based on the flow rate is 19%.

It should be noted that the difference in improvement percentage might be because of the difference in selected operating ranges for each operating parameter. However, changing the supply pressure can positively and negatively affect the total mass absorbed (Mellouli et al., 2007). Therefore, an appropriate selection of supply pressure should be considered for each new MH storage application. Moreover, in reality, there is a limitation of the initial value of the HTF inlet temperature during the cyclic application as well as during the hydrogen sorption process.

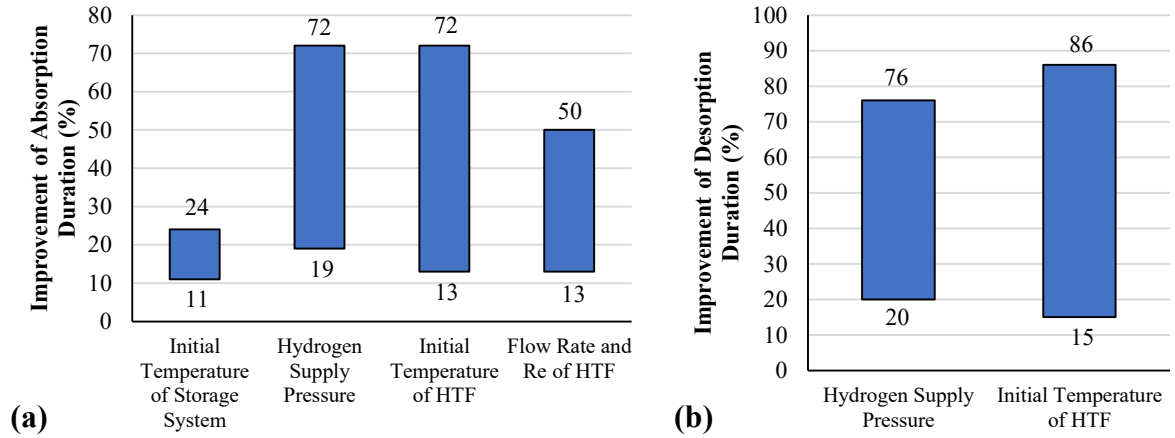

Figure 2.19 Improvement of hydrogen sorption duration based on various operating conditions; (a) Hydrogen absorption and (b) Hydrogen desorption

2.7 Application Requirements and Economic Assessments for Metal Hydride Hydrogen Storage

Most recent studies have been focused on the investigation of MHHS performance with the use of several heat exchanger types, including simple heat exchangers and complex heat exchangers. However, these studies mostly focus on small-scale hydro-gen storage for both experimental and numerical works. There is only 37% of the cur-rent studies focused on large-scale systems, while the rest of the current studies focus on small-scale systems (Afzal et al., 2017). In general, small-scale experiments offer lower cost, lower safety risk, and shorter experiment time with high flexibility compared to large-scale experiments. In other words, small-scale experiments are ideal for initial testing, feasibility studies, and concept validation. However, these experiments present lesser data accuracy and low operational complexity compared to large-scale experiments. Therefore, large-scale experiments are important for validating real-world applicability, long-term performance, and system integration. Similarly, small-scale numerical works such as CFD simulations are ideal for initial testing, conceptual designs, and fast analysis, while these simulations require lower computational costs. On the other hand, large-scale simulations offer more realistic, detailed insights that are important for commercial-scale MHHS.

As per these recent studies, all the heat exchanger types positively affect the hydrogen kinetics reaction due to the improvement in heat transfer performance inside the MHHS. However, the results can be changed when these heat exchangers are used in large-scale applications. When applying the external heat exchanger such as a cooling jacket to large-scale MHHS, this technique can cause hot spots inside the MHHS as the heat only transfers between the walls of the MH bed (Nquyen & Shabani 2021). With the use of internal heat exchangers, the heat transfer coefficient and HTF temperature are the two main parameters that significantly affect heat transfer performance in small-scale applications. This is due to the fact that the heat directly transfers from the core of the MH bed to the wall of the HTF tube without much thermal resistance (Chung & Ho 2009; Jiao et al., 2012). However, when having large-scale hydrogen storage, the amount of MH is significantly larger than in the case with small-scale hydrogen storage. The ability of the heat exchangers from the small-scale application may not be effective enough to transfer the heat. Therefore, increasing the cooling tube number is another option to increase heat transfer performance for use in large-scale applications (Afzal & Shama 2018). Considering real-world applications, this technique is only recommended for cases with several straight internal tubes, not for complex heat exchanger tubes. For the use of a complex heat exchanger tube, this can be combined with other external heat exchangers such as a cooling jacket or PCM. Furthermore, improvement in thermal conductivity of the MH bed might be another option in large-scale applications instead of using complex heat exchangers. This can be achieved by several techniques such as adding metal foam or a network of fins (Afzal & Shama 2018; Laurencelle & Goyette 2007). However, adding metal foam might be the better option for this improvement as metal foam is more uniformly distributed within the MH compared to a network of fins (Ferekh et al., 2015).

In regard to the mobile and stationary applications, the primary driving factor when considering economic assessments is costs. These include the cost of raw materials and manufacturing costs including potential enhancements, quality control, recycling, target profit margins, and others (Sandrock 1997). However, the scale of production/application is the main aspect that significantly affects these costs, especially the manufacturing costs (Klopcic et al., 2023). For the stationary MHHS, this storage always obtains higher energy density compared to the mobile MHHS. However, it requires a significantly higher cost, especially when having multiple heat exchangers or other addition-al equipment.

For the key trade-offs between the energy density, weight, and cost for the MHHS, the MH materials offer high volumetric energy density compared to other hydrogen storage types such as compressed gas. However, the MH materials are usually heavy, which directly increases the overall weight of the MHHS. To achieve higher energy density, specific MH materials with unique properties are required. In contrast, these specific MH materials are rare earth metals, leading to high costs. Raw material cost depends on production costs which could vary depending on abundance and form of the material occurring in nature. Some common materials used for MH are provided in Table 2.10.

Table 2.10 Material used for metal hydride and its environmental factor (Klopcic et al., 2023; Nuss & Eckelman 2014).

Material for MH	Abundance	Most common forms in nature	Extraction/production method of pure form
Al	3rd most abundant in Earth's crust	Bauxite ore	Hall-Heroult process
Fe	4th most abundant in Earth's crust	Minerals – hematite, magnetite, siderite, banded iron formations	Reduction with coke in blast furnace followed by oxidation with air
Na	6th most abundant in Earth's crust	Minerals – NaCl, natron	Electrolysis of molten NaCl
Mg	7th most abundant in Earth's crust	Magnesite, dolomite, brucite, other minerals	Seawater, silicothermic Pidgeon process

Ti	9th most abundant in Earth's crust	Oxides in igneous rock, sediments	Kroll process
Mn	12th most abundant in Earth's crust	Pyrolusite, braunite, psilomelane	Leaching manganese ore with sulphuric acid followed by an electrowinning process
Ni	23rd most abundant in Earth's crust	Combination with sulphur and iron, laterite ore and magmatic sulphide deposits	Extractive metallurgy, conventional roasting and reduction methods
La	28th most abundant in Earth's crust	Rate earth minerals together with other lanthanides	Difficult, time consuming, and expensive multistep processes
Li	32nd most abundant in Earth's crust	Igneous rocks, granitic pegmatites, lithium salts in mineral springs and brine pools, etc	Brine extraction, filtration of leachates in geothermal wells, mining ore

However, the key trade-offs between energy density, weight, and cost for small-scale and large-scale applications as well as the mobile and stationary applications depend on the requirements for each application. To understand these factors, extensive data from the manufacturers for each storage application are required. In general, the manufacturing costs totally depend on the production process/synthesis method and the scale of production. Regarding production methods, important factors include equipment, production time, and costs for additional materials. In some cases, several materials require production steps with high energy demand for ball milling, harsh conditions, long production times, as well as expensive dopants and catalysts to improve the MHHS properties to reach acceptable quality (Klopcic et al., 2023).

The potential degradation of MHs is one of the main factors that affect cyclic loading in the long-term stability of metal hydrides, leading to a decrease in overall MHHS performance. This is due to the difference in the specific volume between a high-thermal-conductivity metallic and MH powder during the hydrogen absorption/desorption cycles. Under different operating temperatures and pressures during the cycling processes, the MH powder frequently experiences expansion and contraction when repeating these cycles. This might result in a decrease in hydrogen storage capacity, swelling, loss of compactness, or crystal cracks (Nquyen & Shabani 2021; Liu et al., 2017; Mirabile et al., 2016; Dieterich et al., 2015; Nemukula et al., 2025). However, different MH materials have their own different characteristics, including cyclic loading in long-term stability. Table 2.11 presents the advantages and disadvantages of some common MH materials. These advantages/disadvantages mainly focus on cycling stability.

Table 2.11 Advantages and disadvantages of metal hydride materials (Klopcic et al., 2023; Fadonougbo et al., 2022).

MH	Advantages	Disadvantages
$LaNi_5$	Low operating temperature and pressure High hydrogenation rate Mild activation condition High volumetric capacity Good cycling stability High resistance towards gas impurities	Low specific energy density Low hydrogen storage capacity at 1.4 *wt%* Expensive Not abundant: rare Earth material Flammable
MgH_2	Inexpensive and abundant High hydrogen storage capacity at 7.6 *wt%* Thermal stability	Sluggish kinetics Poor cycle stability Very slow (first) hydrogenation High desorption temperature and enthalpy High sensitivity towards oxygen
$NaAlH_4$	Inexpensive and abundant Relatively moderate operating temperature for complex hydride	Slow hydrogenation kinetics Poor reversibility Pyrophoric
TiFe	Inexpensive and abundant Simple enhancement by substitution common Good cycling stability at low pressure Mild operating conditions	Demanding conditions for (first) activation Relatively low gravimetric storage capacity Low hydrogenation rate

	Good recyclability	High sensitivity toward gas impurities and oxygen
$TiMn_2$	Good kinetics Inexpensive and abundant Long-term stability/durability Ambient operation temperature Mild activation conditions	Sensitivity towards gas impurities High equilibrium pressure plateau Hysteresis effect Oxygen-affine

From Table 2.11, it is obvious that Mg_2Ni offers cost-effective and abundant MH materials. It also offers a high hydrogen storage capacity of 3.6 wt%. However, the main disadvantages of this material are high operating conditions and slow hydrogen reaction kinetics. Other materials such as TiFe, $TiMn_2$, and $LaNi_5$ have favourable operating condition at near ambient temperatures and low pressures. However, these materials have low gravimetric energy density. Therefore, these materials are more suitable to use with stationary applications. Considering the cost of these materials, $LaNi_5$ is more expensive than the other two materials as La is a rare earth material. In contrast, TiFe and $TiMn_2$ require slightly higher operating conditions to activate the system compared to $LaNi_5$. However, in terms of durability, Mg_2Ni, $LaNi_5$, TiFe, and $TiMn_2$ offer good cycle stability.

2.8 Conclusion

design and optimisation of the MHHS configurations are the key factors, which can positively or negatively affect the overall MHHS performance in both mobile and stationary applications. Based on these key factors, several techniques have been applied to improve the overall MHHS performance for both applications. The hydrogen absorption/desorption reaction is usually the key parameter that has been considered for the overall MHHS enhancement as the MH materials basically have a low thermal conductivity, resulting in slow hydrogen reaction kinetic. Therefore, the comprehensive understanding of the relationship between these key factors and the hydrogen reaction kinetic for absorption/desorption is significant to obtain the suitable MHHS performance for all related applications. The main techniques that have been recently used to enhance the overall MHHS performance must be reviewed and up to date. Therefore, the key findings from this review paper are summarised as follows;

Metal hydride materials

- Mg-based alloys such as Mg_2Ni have a high hydrogen storage capacity, lightweight, and low cost, but they have a low effective thermal conductivity. Intermetallic compounds such as La-based and Ti-based alloys have a high effective thermal conductivity, but they have a low hydrogen storage capacity.
- The volumetric and gravimetric density, effective thermal conductivity, and cost of MH materials should be optimised to meet the overall requirements of mobile/stationary storage applications.

Heat exchanger configurations

- The well arrangement/layout of the heat exchanger structure is the key factor to increase the heat transfer distribution inside the storage system. However, some limitations for manufacturing are likely in reality as most studies are based on numerical simulation.
- The complex HTF tube structure obtains superior heat transfer performance, compared to other heat exchangers. The complex HTF tube structure should be well designed and optimised to prevent a huge pressure loss from the tube inlet throughout the tube outlet and maintain the system's efficiency.
- The heat exchangers' characteristics are important for heat transfer enhancement. The coil pitch and diameter/radius are the key parameters for the helical coil performance, while the number of fins and fins diameter/thickness are the main parameters for fins performance.

- Appropriate design and optimisation of the MHHS configuration is the key factor when combining the MHHS with various heat exchanger types. The design and optimisation should be based on the gravimetric and volumetric of the MHHS for each specific application.
- When considering the gravimetric and volumetric of the MHHS for the mobile/stationary applications, the passive heat exchanger types, such as fins or PCM should be integrated with the HTF tube to improve the heat and mass transfer as well as reduce the overall storage weight.
- When combining the PCM with other heat exchanger types, the proportional PCM/MH/HTF tube volume should be prioritised under the improvement of hydrogen reaction kinetics.

Operating conditions

- The hydrogen supply pressure and the HTF temperature are the main parameters for the improvement of hydrogen absorption/desorption reaction, compared to other parameters. To avoid the reduction of total mass absorbed, appropriate selection of supply pressure should be prioritised and well-studied for each new MHHSS configuration/application.
- The HTC between the MH and HTF has a minor effect on the hydrogen sorption reaction for most MHHS types. The suitable value of the heat transfer coefficient is 500 W/mK with the use of La and Mg-based alloys for both internal and external heat exchangers.
- Changing the supply pressure significantly improves specific heating power by 40%, while other parameters obtain less than 30% improvement in specific heating power.

2.9 Limitation and Recommendation for Future Work

Considering the selection of MH materials for the use of both mobile and stationary storage applications, mg-based alloys might be one of the good options for the MHHS due to its several advantages from above mentioned. To improve the hydrogen reaction kinetic and overall MHHS performance, the heat exchanger should be well designed and optimised instead.

For the MHHS configurations, most studies to date only focused on improving the heat and mass transfer performance inside the MHHS by using various heat exchanger configurations. However, these studies do not consider the relationship between the volume of the heat exchanger/MH and the hydrogen reaction kinetic. To meet the requirement of the MHHS in mobile and stationary applications, the future study should prioritise the comprehensive comparison/combination between various heat exchanger types based on the relationship between the gravimetric/volumetric parameters of the MHHS and how faster hydrogen absorption/desorption reactions.

The pressure losses and fluid flow oscillation from the complex heat exchangers are also the key parameters that can positively or negatively affect the overall MHHS performance. An experimental study is required to investigate the effect of these parameters on the MHHS performance for the hydrogen absorption and desorption process.

Using machine learning techniques is also one of the most effective ways to investigate the MHHS performance. For MHHS applications, machine learning is only applied for the investigation of MH materials' properties. Therefore, this technique can be applied to design and optimise the overall storage performance under heat exchanger design configurations and other related factors

Chapter 3 – Methodology

This section provides all the important governing equations for both hydrogen absorption and desorption processes, phase change process, turbulent flow, and heat transfer of the heat transfer fluid.

To simplify the solution of the hydrogen sorption reaction, the following assumptions are made and provided;

- In the hydrogen sorption, thermo-physical properties of MH and hydrogen are constant (Sekhar et al., 2015). It should be noted that there is a slightly variation in the effective thermal conductivity with loading pressure and concentration.
- The radiation heat transfer is not considered, as the radiative heat flux is considerably lower than the convective heat flux in the storage system (Chung & Lin 2009)
- Local thermal equilibrium conditions are applied for the numerical simulation, considering hydrogen as an ideal gas (Chaise et al., 2009; Jemni et al., 1999).
- The effect of pressure gradient by hydrogen injection is neglected if *N* in Equation (3.1) is lower than 0.01 (dimensionless) (Chaise et al., 2010).

$$N = \frac{\lambda_e M L_{gas}^2 \mu}{P_{a,eq} \frac{\Delta H^2}{RT^2} \rho_g K L_{heat}^2} \quad (3.1)$$

- Where L_{heat} an L_{gas} are the axial height and radius of the tank. When *N* is less than 0.01, the hydrogen flowing inside the system can be considered negligible to the numerical simulation without causing a significant error (Valizadeh et al., 2016). For the current study, the pressure gradients' effect is negligible as *N* is considerably less than 0.01.
- An adiabatic condition is applied for the outer wall of the reactor as the reactor's wall is well insulated (Bao et al., 2013b).
- The liquid PCM is assumed to be highly viscous. Therefore, the convection heat transfer within the PCM subdomain is assumed to be negligible (Mellouli et al., 2017; Mellouli et al., 2015; Tao et al., 2015).
- The effect of expansion and contraction is negligible during the phase transition of PCM (Nyamsi et al., 2019).

- Selection of Metal Hydride (MH) Material

The MH material for the present study is a magnesium-nickel alloy based on Mg_2Ni. This alloy is chosen as it obtains a faster hydrogen kinetic reaction compared to magnesium hydride (Muthukumar et al., 2008). Furthermore, this alloy also offers a high hydrogen storage capacity, lightweight, good recyclability, and excellent heat resistivity (Rusman & Dahari 2016; Liang 2004). From the present study, the maximum mass content of hydrogen that the Mg_2Ni can store is 3.6% of the weight per unit volume (Wu et al., 2014; Wu et al., 2016; Ardahaie et al., 2021).

- Selection of Phase Change Material (PCM)

Appropriate selection of PCM type is also the main factor that affects the overall MHHS performance. The melting temperature of PCM should be higher than the MHHS temperature during the absorption (Ardahaie et al., 2021). For this purpose, the generated heat during the absorption can be stored in the PCM and released from itself during the desorption. The present study uses Mg_2Ni, which has a maximum hydrogen storage capacity of 3.6% when using the activation temperature at 573 K (Muthukumar et al., 2008). In other words, the amount of stored hydrogen in this study is considered as the maximum mass content of hydrogen at 3.6 *wt%.* Therefore, sodium nitrate ($NaNO_3$) is selected as the PCM for this study due to its melting temperature of 580 K, which is higher than the activation

temperature point. Furthermore, $NaNO_3$ also offers a lower mass, lower volume ratio, and higher safety than other PCM types, including $FeCL_3$, NaOH, and KNO_3 (Mellouli et al., 2016).

- *Selection of Heat Transfer Fluid (HTF)*
Among HTFs, air and water are commonly selected as the HTF for the MH reactor due to having a low cost and less environmental impact. Due to a high operating temperature range of magnesium-based alloy, air is selected as the HTF for the present study. Moreover, it also has better flow characteristics compared to other liquid metals and molten salt (Ward et al., 2016).

3.1 Governing Equations

3.1.1 Absorption Process and Desorption Process

The thermal equilibrium between the hydrogen and MH is the key parameter for the energy equation for the absorption and desorption processes. It can be determined as (Wu et al., 2014):

$$\frac{\partial\left(\left(\rho C_p\right)_{e,MH}T\right)}{\partial t} = \nabla\cdot\left(\lambda_{e,MH}\nabla T\right) + \frac{\rho_{MH}wt(1-\varepsilon)\Delta H}{M_{H_2}}\frac{\partial X}{\partial t} \tag{3.2}$$

The effective heat capacity is calculated from the following equation;

$$\left(\rho C_p\right)_{e,MH} = \varepsilon_{MH}\times\rho_{H_2}\times C_{p,H_2} + (1-\varepsilon_{MH})\times\rho_{MH}\times C_{p,MH} \tag{3.3}$$

The effective thermal conductivity is defined as the following equation;

$$\lambda_{e,MH} = \varepsilon_{MH}\times\lambda_{H2} + (1-\varepsilon_{MH})\times\lambda_{MH} \tag{3.4}$$

The reaction of hydrogenation for Mg_2Ni bed (ΔH) is defined as Equation 3.5:

$$Mg_2Ni + 2H_2 \leftrightarrow Mg_2NiH_4 + \Delta H \tag{3.5}$$

X refers to the quantity of hydrogen when it is absorbed (in $wt\%$). It can be obtained from the kinetic equation $\left(\frac{\partial X}{\partial t}\right)$ as Equation 3.6 (Gambini 1994):

$$\frac{\partial X}{\partial t} = C_a\left(\frac{P_{H_2}-P_{a,eq}}{P_{a,eq}}\right)\left(\frac{x-x_f}{x_0-x_f}\right)exp\left(\frac{-E_a}{RT}\right) \tag{3.6}$$

where $P_{a,eq}$ denotes the equilibrium pressure inside storage system for the absorption process. $P_{a,eq}$ is calculated by Van't Hoff equation as follow (Wu et al., 2014):

$$\frac{P_{a,eq}}{P_{ref}} = exp\left(\frac{\Delta H}{RT_m} - \frac{\Delta S}{R}\right) \tag{3.7}$$

where the reference pressure (P_{ref}) is 0.1 MPa. ΔS is the reaction entropy, while ΔH is the reaction enthalpy.

For the first two research papers (Chapter 4 and Chapter 5), the hydrogen kinetic reaction and equilibrium pressure inside the storage system for hydrogen absorption process is calculated based on Equation 3.6 and Equation 3.7. However, the studies from (Mellouli et al., 2016; Wu eat al., 2014; Wu et al., 2016) prove that the hydrogen kinetic reaction and equilibrium pressure for hydrogen absorption process can be calculated based on the following equations.

The kinetic equation for hydrogen absorption is determined as follows (Mellouli et al., 2016):

$$\frac{\partial X}{\partial t} = C_a exp\left(\frac{-E_a}{RT}\right)\left(\frac{P_{H_2}-P_{a,eq}}{P_{a,eq}}\right)(X_{max}-X) \tag{3.8}$$

where C_a denotes the reaction rate for absorption and E_a refers to activation energy for absorption. $P_{a,eq}$ is the equilibrium pressure inside the MHHS for the absorption process which is determined by using Van't Hoff equation as follows (Wu et al., 2014):

$$\ln\frac{P_{a,eq}}{P_{ref}} = -\frac{7618}{T_m} + 14.534 \tag{3.9}$$

where P_{ref} is the reference pressure as 0.1 MPa.

The amount of hydrogen desorption is determined as follows (Wu et al., 2016):

$$\frac{\partial X}{\partial t} = C_d exp\left(\frac{-E_d}{RT}\right)\left(\frac{P_{H_2}-P_{d,eq}}{P_{d,eq}}\right)(1-X) \tag{3.10}$$

where C_d and E_d are the reaction rate for desorption and the activation energy for desorption, while $P_{d,eq}$ is the equilibrium pressure inside the MHHS for the desorption process. The $P_{d,eq}$ is defined as follows (Wu et al., 2016):

$$\ln\frac{P_{d,eq}}{P_{ref}} = -\frac{7614}{T_m} + 14.049 \tag{3.11}$$

Therefore, the studies in Chapter 6 and Chapter 7 (Research Paper 3 and Research Paper 4) use Equation 3.8 and Equation 3.10 to calculate the hydrogen kinetic reaction for absorption and desorption processes, respectively. The equilibrium pressures during the absorption and desorption processes are obtained based on Equation 3.9 and Equation 3.11, respectively. The thermo-physical properties of hydrogen and Mg_2Ni are provided in Table 3.1.

Table 3.1 Thermo-physical parameters of hydrogen and metal hydride in model equations (Wu et al., 2014; Wu et al., 2016; Ardahaie et al., 2021)

Parameters	Symbols	Values
Molecular weight of MH	M_{MH}	0.1073 kg mol^{-1}
Hydride specific heat	$C_{p,MH}$	1,414 J kg^{-1} K^{-1}
Density of MH	ρ_{MH}	3,200 kg m^{-3}
Density of saturated MH	$\rho_{ss,MH}$	3,319.32 kg m^{-3}
Reaction enthalpy	ΔH	-6,3336 J mol^{-1}
Reaction entropy	ΔS	-120.84 J mol^{-1} K^{-1}
Reaction rate constant for absorption	C_a	175.07 s^{-1}
Reaction rate constant for desorption	C_d	2079 s^{-1}
Activation energy for absorption	E_a	49,674 J mol^{-1}
Activation energy for desorption	E_d	63,540 J mol^{-1}
Porosity	ε	0.5
Effective thermal conductivity of MH	k_{MH}	0.674 W m^{-1} K^{-1}
Maximum concentration of hydrogen in the MH	x_f	1.0
Initial concentration of hydrogen in the MH	x_0	0.043

Maximum mass content of hydrogen in the metal	wt	3.6 %
Permeability	K	1×10^{-8} m^2
Density of hydrogen	ρ_{H2}	0.32 kg m^{-3}
Thermal conductivity of hydrogen	λ_{H2}	0.167 W m^{-1} K^{-1}
Specific heat of hydrogen	$C_{p,H2}$	14,890 J kg^{-1} K^{-1}
Dynamic viscosity of hydrogen	μ_{H2}	8.41×10^{-6} Pa s
Molecular weight of hydrogen	M_{H2}	0.002 kg mol^{-1}

3.1.2 Phase Change Process

The study from Chapter 6 (Research Paper 3) employs the PCM as the external heat exchanger. The liquid PCM is considered as an incompressible Newtonian fluid without any viscous dissipation. The enthalpy-porosity technique is applied for the phase change process simulation.

The continuity equation is as follows:

$$\frac{\partial \rho}{\partial t} + \nabla \cdot \rho \vec{V} = 0 \tag{3.12}$$

The momentum and energy equations are as Equation 3.13 and Equation 3.14, respectively.

$$\frac{\rho \partial \vec{V}}{\partial t} + \rho\left(\vec{V} \cdot \nabla\right)\vec{V} = -\nabla \mathrm{P} + \mu\left(\nabla^2 \vec{V}\right) - \rho_{ref}\beta\left(T - T_{ref}\right)\vec{g} - \vec{S} \tag{3.13}$$

$$\frac{\rho C_p \partial T}{\partial t} + \nabla\left(\rho C_p \vec{V} T\right) = \nabla(\mathrm{k}\nabla \mathrm{T}) \tag{3.14}$$

The Darcy's law damping term is applied as the source term ($\vec{S}$) of momentum equation to represent the phase change effects of the convective heat transfer (Esapour et al., 2016; Pahamli et al., 2018).

$$\vec{S} = A_m \frac{(1-\lambda)^2}{\lambda^3 + 0.001}\vec{V} \tag{3.15}$$

The velocity of the mushy zone is defined by A_m, which is the mushy zone constant for the interface between solid and liquid phases, which is normally between 10^4 to 10^7 kg/m^{3}s. However, the present study uses 10^6 kg/m^{3}s, referring to the validation of the following studies; Askri et al. (2019); Mellouli et al. (2017); Hosseini et al. (2014).

The latent heat content (ΔH) is calculated as a function of material's latent heat (L_{PCM}) which varies from zero as a solid state to liquid state.

$$\Delta H = f L_{PCM} \tag{3.16}$$

where f is the liquid fraction which is zero at the solid state and 1 at the liquid state. The f can be obtained based on Equation 3.17.

$$f = \frac{\Delta H}{L_{PCM}} = \begin{Bmatrix} 0 \; if \; T < T_{Solidus} \\ 1 \; if \; T > T_{Liquidus} \\ \frac{T - T_{Solidus}}{T_{Liquidus} - T_{Solidus}} \; if \; T_{Solidus} < T < T_{Liquidus} \end{Bmatrix} \tag{3.17}$$

The required volume of the PCM jacket is calculated based on Equation 3.18. The required volume of the PCM is assumed to store all the heat released from the MH tank (Alqahtani et al., 2020a).

$$V_{PCM} = \frac{V_{MH} \times wt \times \Delta H_{MH} \times \rho_{MH} \times (1-\varepsilon)}{M_{H_2} \times \rho_{PCM} \times L_{PCM}} \quad (3.18)$$

where V_{MH} is the volume of MH. ρ_{MH} and ρ_{PCM} are the density of MH and PCM, respectively. L_{PCM} is the latent heat of PCM. Thermo-physical properties of PCM are provided in Table 3.2. The effect of the sensible enthalpy is negligible and not included to calculate the required amount of PCM (Alqahtani et al., 2020a).

Table 3.2 Thermo-physical properties of PCM ($NaNO_3$) (Ardahaie et al., 2021;Alqahtani et al., 2020a;Nunes et al., 2006)

Parameters	**Symbols**	**Values**
Solidus temperature	T_s	579 K
Liquids temperature	T_l	580 K
Solid density	ρ_s	2,260 kg m^{-3}
Liquid density	ρ_l	1,900 kg m^{-3}
Solidus specific heat capacity	$c_{p,s}$	1,820 J kg^{-1} K^{-1}
Liquids specific heat capacity	$c_{p,l}$	1,800 J kg^{-1} K^{-1}
Thermal conductivity	k	0.48 W m^{-1} K^{-1}
Dynamic viscosity	μ	0.003 Pa s
Thermal expansion coefficient	β	4e-5 (K^{-1})
Latent heat capacity	L_{PCM}	174,000 J kg^{-1}

3.1.3 Heat Transfer Fluid

The governing equations of the heat transfer and turbulent flow for the HTF are presented as the following equations (Ardahaie et al., 2021; Kumar et al., 2006). This method is applied only for the studies from Chapter 4 to Chapter 6 (the first three research papers).

Continuity:

$$\frac{\partial U_i}{\partial x_i} = 0 \quad (3.19)$$

Momentum:

$$\rho \frac{\partial U_i}{\partial t} + \rho U_i \frac{\partial U_i}{\partial x_i} = -\frac{\partial P}{\partial x_j} + \frac{\partial}{\partial x_i}\left[\mu\left(\frac{\partial U_i}{\partial x_j} + \frac{\partial U_j}{\partial x_i}\right) - \overline{\rho u_i' u_j'}\right] \quad (3.20)$$

Energy:

$$\rho C_p \frac{\partial T}{\partial t} + \rho C_p U_i \frac{\partial T}{\partial x_i} = \frac{\partial}{\partial x_i}\left[\lambda \frac{\partial T}{\partial x_j} - \rho C_p \overline{u_i' T'}\right] \quad (3.21)$$

where U_i and T are the time-averaged velocity and temperature. The average Reynolds stresses and turbulent heat fluxes are defined as $\overline{\rho u_i' u_j'}$ and $\rho C_p \overline{u_i' T'}$, respectively.

The kinetic energy equation is expressed as:

$$\frac{\partial}{\partial t}(\rho k_t) + \frac{\partial}{\partial x_j}(\rho k_t u_j) = \frac{\partial}{\partial x_j}\left[\left(\mu + \frac{\mu_t}{\sigma_{k_t}}\right)\frac{\partial k_t}{\partial x_j}\right] + G_{k_t} + G_b - \rho\varepsilon_t - Y_M + S_{k_t} \quad (3.22)$$

The dissipation rate of the turbulent kinetic energy equation is defined as:

$$\frac{\partial}{\partial t}(\rho\varepsilon_t) + \frac{\partial}{\partial x_j}(\rho\varepsilon_t u_j) = \frac{\partial}{\partial x_j}\left[\left(\mu + \frac{\mu_t}{\sigma_{\varepsilon_t}}\right)\frac{\partial \varepsilon_t}{\partial x_j}\right] + \rho C_1 S\varepsilon_t - \rho C_2 \frac{\varepsilon_t^2}{k_t + \sqrt{\nu\varepsilon_t}} + C_{1,\varepsilon_t}\frac{\varepsilon_t}{k_t}C_{3,\varepsilon_t}G_b + S_{\varepsilon_t} \quad (3.23)$$

where the constant coefficients can be defined as $C_1 = 1.47$, $C_2 = 1.92$, $\sigma_{k_t} = 1.0$, and $\sigma_{\varepsilon_t} = 1.3$. The turbulence kinetic energy productions which induced by mean velocity gradients and buoyancy are G_{k_t} and G_b, respectively. Y_M is the contribution of the fluctuating dilatation in the incompressible turbulence to the overall dissipation rate. The turbulent viscosity is defined as $\mu_t = \rho C_\mu \frac{{k_t}^2}{\varepsilon_t}$. The turbulent intensity is calculated based on the average Reynolds number at inlets by $I = 0.16\left(Re_{D_h}\right)^{-0.125}$.

3.1.4 Heat Transfer Fluid and Fins

The following governing equations are applied only for Chapter 7 (Research Paper 4) as the main objective of this chapter is to study the effect of the new fin design on the heat transfer performance.

The governing equations for the heat transfer fluid are as the following equation (Eisapour et al., 2021a):

$$\nabla\vec{v}_f = 0, \frac{\partial T_f}{\partial t} = 0 \quad (3.24)$$

The heat transfer coefficient (h_f) between the heat transfer fluid and MH bed is calculated based on Equation 3.25

$$h_f = \frac{\lambda_f}{d} Nu_f \quad (3.25)$$

In this study, various values of the heat transfer coefficient (h_f) between the HTF and MH bed are selected and applied to analyse the effect of this parameter on the heat transfer efficiency of the heat exchanger. This can be found under the parametric study section. The Nusselt number (Nu_f) for the internal straight tube, which is used for heat transfer fluid, can be calculated based on turbulent flow (Equation 3.26) (Yang & Tao 1998; Wu et al., 2016).

$$Nu_f = 0.012\left(Re_f^{0.87} - 280\right)Pr_f^{0.4}\left[1 + (d/L)^{2/3}\right]\left(Pr_f/Pr_m\right)^{0.11} \quad (3.26)$$

where Re_f is the Reynolds number and Pr_f is Prandtl number. These two parameters can be obtained based on the following equation:

$$Re_f = \frac{\rho_f d v_f}{\mu_f}, Pr_f = \frac{\mu_f C_{p_f}}{\lambda_f} \quad (3.27)$$

For copper fins, the energy equation for the heat conduction is expressed as:

$$\left(\rho C_p\right)_{fin}\frac{\partial T}{\partial t} = \lambda_{fin}\nabla^2 T \quad (3.28)$$

where $\left(\rho C_p\right)_{fin}$ is the heat capacity of copper fins.

It should be noted that conditions from above mentioned are applied for all simulations, except the effect of pressure losses due to the heat exchanger structures. Under the study of pressure variation

along the heat exchanger tubes, the turbulent HTF flow is selected under the realizable k-ε turbulence model with a velocity at 76.86 m s^{-1} and a Reynolds number of 9000. Air is selected as the HTF for this study.

3.2 Initial and Boundary Conditions

The initial and boundary conditions can be found separately under each main chapter (Chapter 4 to Chapter 7). This is due to the different storage system configurations and selected parameters from each chapter.

3.3 Model Validation and Numerical Schemes

3.3.1 Model Validation

Various model validations are performed to compare the results between the use of CFD simulation and the experimental work from the available literature. These include the model validations of utilised codes during hydrogen absorption/desorption, the phase change process, and the selected turbulence model for the CFD simulation.

- *Validation for the Absorption Process and Desorption Process of Metal Hydride Storage System*

To perform the CFD simulation, the utilised code is performed and applied for the hydrogen kinetic reaction during the absorption process as the energy source term. This absorption kinetic reaction is provided in Equation 3.6. The model validation for the use of a metal hydride storage system during the absorption process is performed and presented in Figure 3.1. The purpose of this model validation is to compare the results between the utilised code from Equation 3.6, experimental work, as well as numerical work from the available literature. As mentioned earlier, the use of Equation 3.6 is only for the studies in Chapter 4 and Chapter 5 (the first two research papers). From Figure 3.1a, the utilised code for the absorption process of the magnesium-based MH tank from the current study is investigated and compared to the experimental study by Muthukumar et al. (2008). This experimental study used the Mg_2Ni alloy as the MH material, which was filled in the stainless-steel tube with inner copper fins. The initial temperature of the tank was 473 K with loading pressure at 2.0 MPa. From this figure, the average bed temperature from these two studies is similar and in the same trend. Moreover, the utilised code for the absorption process is also validated against the numerical study by Wu et al. (2014). This study also used the Mg_2Ni alloy as the MH material and the helical coil as the heat exchanger for the hydrogen absorption process. The initial temperature of the storage system was 573 K with the loading pressure at 1.8 MPa and the same initial boundary conditions. The average bed temperature of the storage system between this study and the present study is compared and presented in Figure 3.1b. From this figure, it is obvious that the average bed temperature from the present study follows the same trend as this reference. Therefore, the utilise code based on Equation 3.6 is applied for the CFD simulation of this study from Chapter 4 to Chapter 5.

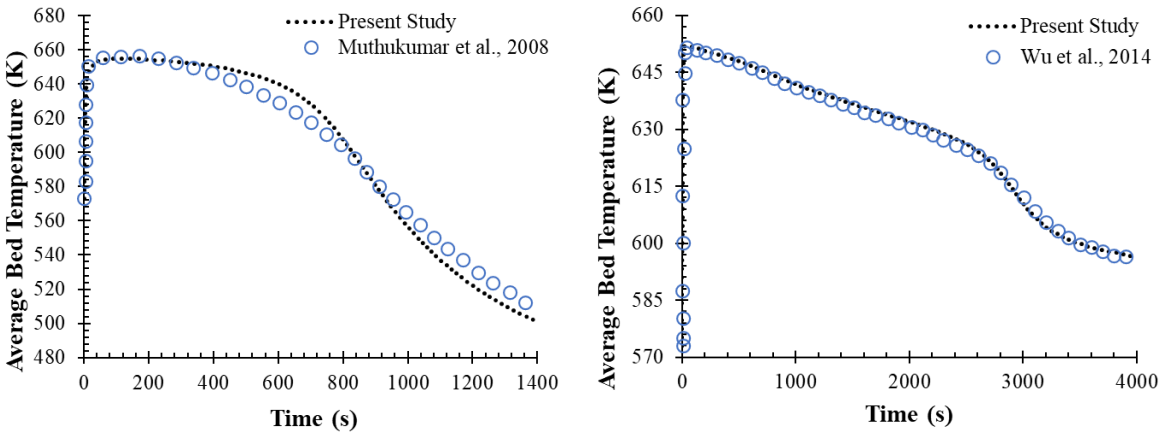

(a) **(b)**

Figure 3.1 The validation of utilised code for the hydrogen absorption process of the Mg_2Ni-based reactor. (a) average bed temperature between experimental results (Muthukumar et al., 2008) and numerical results from present study and (b) average bed temperature between the numerical results from Wu et al. (2014) and numerical results from present study.

As mentioned earlier, the works from Chapter 6 (Research Paper 3) and Chapter 7 (Research Paper 4) are performed based on the hydrogen kinetic reactions from Equation 3.8 (for absorption) and Equation 3.10 (for desorption). The utilised codes from absorption and desorption processes are performed under these two equations as the energy source terms for the present CFD simulations. Figure 3.2 presents the model validation results during both absorption and desorption processes between the current study (based on utilised codes), the experimental work, as well as the numerical work from the available literature. The validation is still based on the MHHS during absorption and desorption processes under the use of a magnesium-nickel alloy based on Mg_2Ni. The model validations under these uitilised codes are based on the experimental study from Muthukumar et al., (2008) and numerical study from Wu et al., (2014) for the hydrogen absorption. For the hydrogen desorption, the utilised code is validated based on the study from Wu et al., (2016). For hydrogen absorption (Figure 3.2a, 3.2b), the experiment study from Muthukumar et al. (2008) employed Mg_2Ni as the MH powder with internal copper fins to improve the hydrogen kinetic reaction. The initial storage temperature was 473 K with hydrogen pressure at 2.0 MPa. Furthermore, the utilised codes for hydrogen absorption are also validated against the numerical study from Wu et al. (2014). This study also used the MHHS based on Mg_2Ni alloy. The initial storage temperature and loading pressure were set at 573 K and 1.8 MPa, respectively. For the hydrogen desorption (Figure 3.2c), the code validation for the MHHS is performed and compared with the numerical study from Wu et al. (2016). This study used the same Mg_2Ni powder with an initial storage temperature of 573 K, a hydrogen pressure of 1.6 atm, and the same initial boundary conditions. From these comparisons, it is obvious that there are good agreements on the average bed temperature in both absorption and desorption between these studies. The average bed temperature from these studies is similar and follows the same trend. Therefore, the utilised codes based on Equation 3.8 and 3.10 are applied for the present CFD simulations in Chapter 6 and Chapter 7.

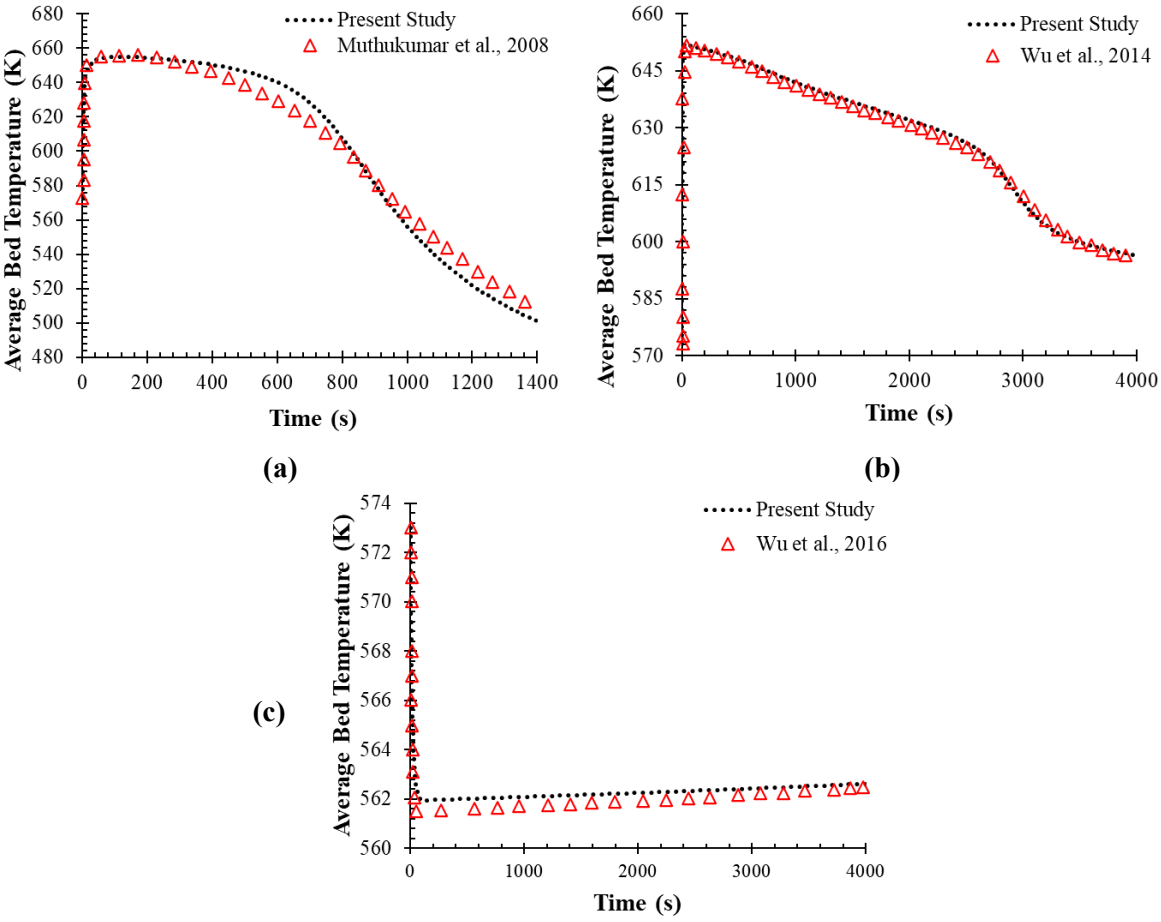

Figure 3.2 The comparison of average bed temperature between numerical results and experimental results from available literature. (a) hydrogen absorption (Muthukumar et al., 2008) and (b) hydrogen absorption (Wu et al., 2014), and (c) hydrogen desorption (Wu et al., 2016).

- *Validation for Phase Change Process*

The current study under Chapter 6 (Research Paper 3) is based on the combination of internal and external heat exchangers. This is to further enhance the heat transfer efficiency, resulting in the improvement of the overall storage performance. Phase change material (PCM) is employed as the external heat exchanger for this purpose. Therefore, the validation for the phase change process is performed and presented in Figure 3.3. To validate the phase change process, the experimental study of thermal energy storage from Sodhi et al. (2021) is used to validate the numerical model used for the PCM subdomain of the present study (see Figure 3.3a). The $NaNO_3$ PCM was filled in the stainless-steel capsule with air as the HTF. The initial temperature of the storage was 323 K and the inlet temperature of the HTF was 633 K. The average PCM temperatures between the present study and this study follow the same trend from this figure. Moreover, the average PCM temperature during the absorption and desorption of the MH storage from the present numerical model is also validated against the numerical study from Alqahtani et al. (2020a). The results of this comparison are presented in Figure 3.3b. This study used Mg_2Ni as MH material and $NaNO_3$ as the PCM jacket and PCM sandwich. However, only the result from the PCM jacket is selected for the comparison as the present study only focuses on the use of the PCM jacket. The average PCM temperatures of these studies follow the same trend for both absorption and desorption. It should be noted that these two studies are selected for verification due to having the same PCM material that is used for the present study. Therefore, the CFD simulations with the use of PCM are performed under this phase change process condition.

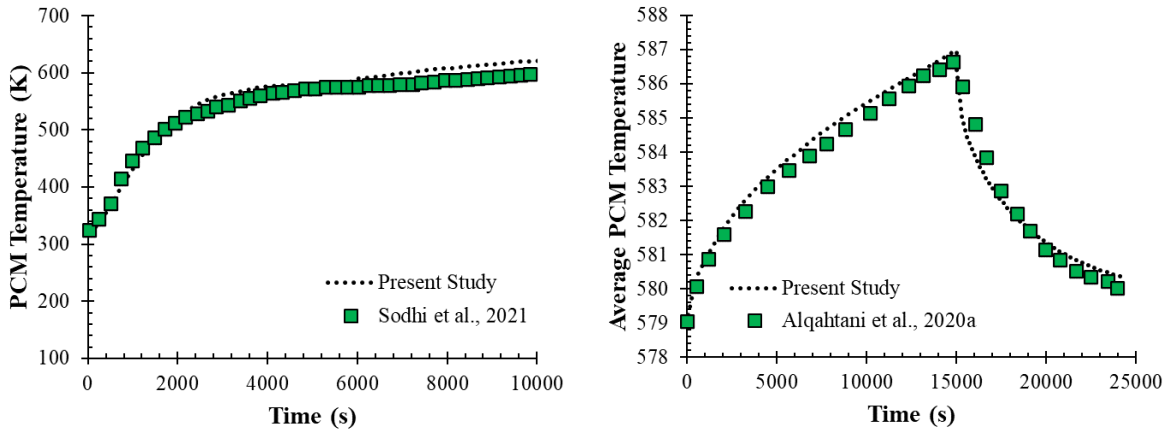

(a) **(b)**

Figure 3.3 The comparison of average bed temperature of phase change material between the present study and experimental studies. (a) phase change material for thermal energy storage system (Sodhi et al., 2021) and (b) phase change material for metal hydride storage system (Alqahtani et al., 2020a).

- *Validation for Turbulence Model*

To validate the turbulence model which is mainly used for the flow simulation under Chapter 4 to Chapter 6 (the first three research papers), the results from this present study are compared with the experimental results from Kumar et al. (2006) in order to validate the selected turbulence model. Kumar et al. (2006) studied the turbulent flow in a tube-in-tube helical heat exchanger. Water was employed as both hot and cold fluids which were injected from opposite directions. The hot and cold fluids temperature was 323 K and 300 K, respectively. The Reynolds number for the hot fluid varied from 3100 to 5700, and 21000 to 35000 for the cold fluid. The Dean number for the hot fluid was 550-1000, and 3600-6000 for the cold fluid. The diameter of the inner tube (for hot fluid) and outer tube (for cold fluid) were 0.0254 m and 0.0508 m, respectively. The helical coil diameter and pitch were 0.762 m, and 0.100 m. Figure 3.4 shows the comparison of the experimental and present results in terms of various Nusselt numbers and Dean numbers for hot fluid in the inner tube. Three different turbulent models are performed and compared with experimental results based on the same boundary conditions with Kumar et al. (2006). As shown in Figure 3.4, the results from the realizable k-ε turbulence model obtain a good agreement with experimental data. Therefore, this model is selected for this present study.

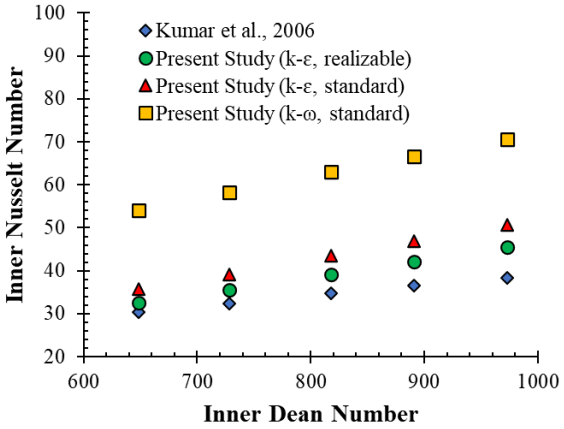

Figure 3.4 Validation study of the turbulence model in helical tube by the comparison of present study and Kumar et al. (2006).

It should be noted that in some applications, the k-ε turbulence model provides better results than the k-ω turbulence model. Refer to Kumar et al. (2006), for complex flow, the k-ε turbulence model has

long been popular since the five turbulence parameters are not very sensitive to flow conditions and the default values can usually be used to make reasonable predictions. Turbulent flow is characterised by five parameters, including a disorder in the movement of fluid particles, irregular eddy patterns, an overall irreproducible behaviour, and the manifestation of multiple space and time scales. Compared with the other models reported in the literature (such as k-ε RNG, k-ω, and SST k-ω) the wide range of applicability of the turbulence parameters is the main advantage of the k-ε turbulence model. The standard k-ε turbulence model is widely used in industrial flows and heat transfer problems because of its economy and accuracy. It also takes less time and memory during the simulations as compared to other models reported in the literature. However, comparing between the standard k-ε turbulence model and realizable k-ε turbulence model, the realizable k-ε turbulence model offers further improvement, especially in near-wall regions and more complex flow conditions.

- *Selection of time step size for the simulations*

The selection of the time step size for the simulation is performed under the different time step sizes by using the new heat exchanger, namely a semi-cylindrical coil heat exchanger. The time step sizes include 1s, 0.5s, 0.25s, 0.1s, and 0.05s. The results are compared and provided in Figure 3.5 and Table 3.3

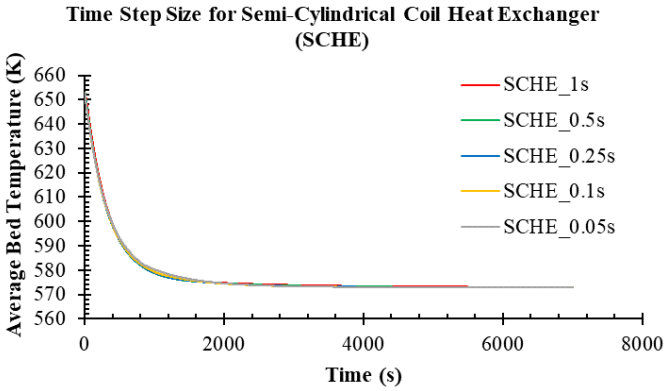

Figure 3.5 Selection of time step sizes for semi-cylindrical coil heat exchanger.

Table 3.3 The average bed temperature at the end of the absorption process at 6215s based on 1s of time step size.

At 6215 s	Time Step Size for SCHE				
	1 s	**0.5 s**	**0.25 s**	**0.1 s**	**0.05 s**
Average Bed Temperature (K)	573.082	573.022	573.007	573.003	573.002

Based on the above figure and above table, it is obvious that the average bed temperature from all time step sizes obtains a similar trend. At 6215s (the end of absorption process for 1s time step for SCHE case), the difference in average bed temperatures from all time step sizes is around not over than 0.08 K. Therefore, to save computational time, the 1s time step size was selected for all simulation cases.

3.3.2 Numerical Schemes

The simulations in the present study are performed by using ANSYS Fluent. The energy source terms for hydrogen kinetic reactions are applied for hydrogen absorption and desorption (Equation 3.6, Equation 3.8, and Equation 3.10). The PISO scheme and PRESTO method are chosen for pressure variables (Versteeg & Malalasekera 2007). All related equations are solved by the second-order upwind scheme. The relaxation factors are set as 0.5 for pressure, 0.7 for energy and all velocity components, and 0.9 for liquid fraction. The standard wall function of the heat exchanger is chosen for the turbulence

model of the HTF. The convergence criteria for all parameters is set as 10^{-6} under the transient simulation.

To clarify the initial parameters and boundary conditions, section “8.4 Selection of input parameters for the proposed designs on the realistic and practical applications” is separately provide under the conclusion section.

Chapter 4 – Design Optimisation of a Magnesium-based Metal Hydride Hydrogen Energy Storage System

Research Paper: **Larpruenrudee, P.,** Bennett, N.S., Gu, Y., Fitch, R., & Islam, M.S., (2022). Design Optimization of a magnesium-based metal hydride hydrogen energy storage system. **Scientific Reports** 12, 13436. https://doi.org/10.1038/s41598-022-17120-3. **SJR: 0.973 [Q1], IF: 4.997**

Conference Paper: **Larpruenrudee, P.,** Bennett, N.S., Hossain, M.J., Fitch, R., Islam, M.S. Hydrogen energy storage system: how does the semi-cylindrical helical coil heat exchanger affect metal hydride beds' thermal conductivity?. In Proceeding of the 23rd Australasian Fluid Mechanics Conference., eds C. Lei, B. Thornber, and S. Armfield. Sydney, Australia, 5-8 December 2022, 421.

4.1 Summary

Objectives to achieve the aim of this study:

- Propose the new design of an internal heat exchanger to enhance the storage thermal performance
- Identify an appropriate initial value of each operating parameter under the new storage configuration and heat exchanger

Achievements and innovations in this chapter:

- Propose the new internal heat exchanger design, namely a semi-cylindrical coil heat exchanger, which is developed from a conventional helical coil heat exchanger
- Optimise the design of this new heat exchanger configuration based on the effect of coil pitch on the hydrogen absorption and metal hydride volume
- Investigate the initial value of the metal hydride bed storage system and heat transfer fluid, including; the initial temperature and loading pressure of the storage system, initial flow velocity of the heat transfer fluid, and heat transfer fluid temperature

4.2 Abstract

Metal hydrides (MH) are known as one of the most suitable material groups for hydrogen energy storage because of their large hydrogen storage capacity, low operating pressure, and high safety. However, their slow hydrogen absorption kinetics significantly decreases storage performance. Faster heat removal from MH storage can play an essential role to enhance its hydrogen absorption rate, resulting in better storage performance. In this regard, the present study aims to improve heat transfer performance to positively impact the hydrogen absorption rate of MH storage systems. A novel semi-cylindrical coil is first designed and optimized for hydrogen storage and embedded as an internal heat exchanger with air as the heat transfer fluid (HTF). The effect of novel heat exchanger configurations is analyzed and compared with normal helical coil geometry, based on various pitch sizes. Furthermore, the operating parameters of MH storage and HTF are numerically investigated to obtain optimal values. ANSYS Fluent 2020 R2 is utilized for the numerical simulations. Results from this study demonstrate that MH storage performance is significantly improved by using a semi-cylindrical coil heat exchanger (SCHE). The hydrogen absorption duration reduces by 59% compared to a normal helical coil heat exchanger. The lowest coil pitch from SCHE leads to a 61% reduction of the absorption time. In terms of operating parameters for the MH storage with SCHE, all selected parameters provide a major improvement in the hydrogen absorption process, especially the inlet temperature of the HTF.

Keywords: Hydrogen absorption, Magnesium based metal hydride reactor, Helical coil heat exchanger, Sensitivity analysis, Novel heat exchanger

4.2.1 Graphical Abstract

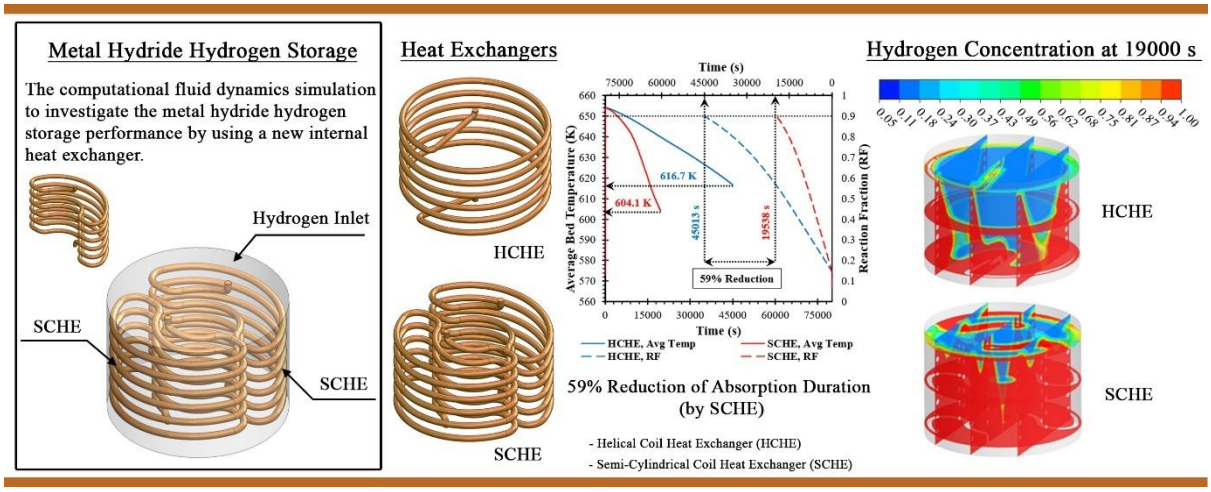

Figure 4.1 Graphical abstract for the first research paper

4.3 Introduction

A move away from fossil fuel-based energy resources towards renewable forms of energy is underway at a global scale. Since many forms of renewable energy provide electricity in a dynamic way, energy storage is required to balance load. Hydrogen-based energy storage is receiving much attention for this purpose, not least because hydrogen can be employed as a 'green' alternative fuel and energy storage medium, because of its characteristics and portability (Tange et al., 2011). Furthermore, hydrogen also offers a higher energy capacity per mass compared to fossil fuels (Harries et al., 2012). There are four main types of hydrogen energy storage: compressed gas, underground storage, liquid storage, and solid storage. Compressed hydrogen gas is the main type that has been used in fuel-cell vehicles such as buses and forklifts. However, this storage provides a low volumetric hydrogen density (around 0.089 kg/m^3) and presents safety concerns regarding high operating pressure (Abe et al., 2019). Liquid storage will store hydrogen in liquid form, based on the converting process with a low temperature and ambient pressure. However, there is around 40% energy loss during the liquefaction process. Moreover, this technique is also known for higher energy consumption as well as being time-consuming compared to the solid storage technique (Colozza 2002). Solid storage is a feasible option for the hydrogen economy that stores hydrogen by combining it within solid materials through absorption and releasing hydrogen through desorption (Yue et al., 2021). Metal hydride (MH) is one of the solid material storage technologies that has recently attracted significant interest in fuel cell applications because of having a high hydrogen capacity, low operating pressure, and low cost compared to liquid storage, for both stationary and mobile applications (Sakintuna et al., 2007; Jain et al., 2010). Moreover, MH materials also offer safe performance as high-volume efficiency storage (Rusman & Dahari 2016). However, there is one problem that limits MH performance: MH reactors suffer from low thermal conductivity (Zhao et al., 2020), resulting in slow hydrogen absorption and desorption.

Appropriately transferring heat during the exothermic and endothermic reactions is the key to improving MH reactor performance. For the hydrogen charging process, the generated heat must be removed from the reactor in order to control the hydrogen charging flow at the desired rate with the maximum storage capacity (Nguyen & Shabani 2021). In contrast, heat is required to improve the hydrogen release rate during the discharging process. To improve the heat and mass transfer performances, many researchers have studied the design and optimization based on several factors including operating parameters, MH structure, and MH optimization (Yehui et al., 2022). MH optimization can be done by adding high thermal conductivity materials such as the metal foams into the MH bed (Laurencelle & Goyette 2007; Ferekh et al., 2015). By this method, the effective thermal conductivity can be increased from 0.1 W/mK up to 2 W/mK (Nguyen & Shabani 2021). However, adding solid material significantly reduces the MH reactor capacity. For the operating parameters, improvements can be achieved by optimization of the initial operating conditions of the MH bed and heat transfer fluid (HTF). The MH structure can be optimized by the reactor's geometry and the arrangement of heat exchanger designs (Cui et al., 2022). In terms of heat exchanger configuration of the MH reactor, approaches can be classified into two types. These are an internal heat exchanger, which is embedded in the MH bed, and an external heat exchanger such as fins, cooling jacket and water bath that cover the MH bed (Mazzucco et al., 2014). For external heat exchanger, Kaplan (2009) analyzed the performance of a MH reactor by employing cooling water as a jacket to reduce the temperature inside the reactor. The results were compared to a reactor with 22 circular fins and another reactor that cools by natural convection. They claimed that having a cooling jacket significantly reduced MH temperature resulting in a better absorption rate. The numerical study of the MH reactor with water jacket from Patil & Gopal (2013) indicated that the hydrogen supply pressure and temperature of HTF are the key parameters to affect the hydrogen absorption and desorption rates.

Increasing heat transfer area by adding fins and heat exchangers embedded inside MH are key for improving heat and mass transfer characteristics that lead to the enhancement of MH storage performance (Wu et al., 2016). Several internal heat exchanger configurations (straight tube and helical coil tube) have been developed in order to circulate cooling fluid throughout the MH reactor (Mohan et al., 2007; Hardy & Anton 2009; Mellouli et al., 2007; Dhaou et al., 2010; Visaria & Mudawar 2012a, 2012b; Wu et al., 2014; Raju & Kumar 2012). With an internal heat exchanger, the cooling or heating fluid will transfer local heat inside the MH reactor during the hydrogen sorption processes. Raju & Kumar (2011) employed several straight tubes as heat exchangers to improve MH performance. Their results indicated that the absorption time was reduced when using straight tubes as heat exchangers. Similarly, using a straight tube also reduced the hydrogen desorption time (Chung & Lin 2009). A higher flow rate of cooling fluid increases hydrogen charging and discharging rates (Singh et al., 2015). However, increasing the number of cooling tubes positively affects MH performance rather than the flow rate of cooling fluid (Kumar et al., 2019; Raju et al., 2019b). Raju et al. (2019a) investigated the performance of multi-tube heat exchangers inside the reactor by using $LaMi_{4.7}Al_{0.3}$ as MH materials. They reported that the operating parameters significantly affect the absorption process, especially supply pressure, followed by HTF flow rate. However, the absorption temperature was found to be less significant.

The performance of MH reactors was further improved by utilizing a helical coil heat exchanger, as it enhances the heat transfer compared to straight tubes. This is because of secondary circulations that result in better heat removal from the reactor (Wu et al., 2024). Moreover, the helical tube provides more surface area for heat removal from the MH bed to the cooling fluid. This method also produces a more uniform distribution of the heat transfer tubes when it is embedded inside the reactor (Fernandez-Seara et al., 2014). Wang et al. (2012) studied the effect of hydrogen absorption duration by adding a helical coil in the MH reactor. Their results indicated that the absorption time decreased when increasing the heat transfer coefficient of the heat transfer fluid. Wu et al. (2014), studied the performance of a MH reactor based on Mg_2Ni and helical coil heat exchanger. Their numerical study showed a reduction in the reaction time. The enhancement of the heat transfer mechanism in a MH reactor is based on a smaller ratio of helical pitch to the helical diameter and non-dimensional pitch. The experimental study of using a helical coil as an internal heat exchanger by Mellouli et al. (2007) proved that the initial temperature of HTF significantly affects the improvement of hydrogen absorption and desorption times. The combination of various internal heat exchangers has been made by several studies. Eisapour et al. (2021a) studied MH storage by employing a helical coil heat exchanger along with a central return tube in order to improve the hydrogen absorption process. Their results indicated that a helical tube along with a central return tube significantly improved heat exchanged between cooling fluid and MH. A lower pitch of the helical tube and a higher tube diameter increased the heat and mass transfer rate. Ardahaie et al. (2021) employed flat spiral tube planes as a heat exchanger for heat transfer enhancement inside a reactor. They reported that the absorption duration was reduced by increasing the number of flat spiral tube planes. The combination of various internal heat exchangers has been made by several studies. Dhaou et al. (2011) improved the MH performance by employing both helical coil heat exchanger and fins. Their results showed that this technique reduces hydrogen refilling time which is a 2 times reduction comparing to without fins. The annular fin was incorporated with the cooling tube and embedded inside the MH reactor (Lin et al., 2021). The results from this study showed that this combination technique obtains more uniform heat transfer compared to the MH reactor without using fin. However, combining various heat exchangers will negatively affect the gravimetric and volumetric of the MH reactor. A comparison of different heat exchanger configurations was made by Wu et al. (2016). These included a straight tube, fins, and helical coil. The authors reported that the helical coil has the best effects on the heat and mass transfer improvements. Similarly, a double coiled tube has a

better effect on the heat transfer enhancement compared to a straight tube, spiral tube, and straight tube incorporating with spiral tube (Tong et al., 2019a). The study from Sekhar et al. (2015) proved that using a helical coil as an internal heat exchanger and an external cooling jacket with fins obtained a similar improvement in hydrogen absorption.

From the above mentioned example, using a helical coil as an internal heat exchanger offers a better heat and mass transfer improvement compared to other heat exchangers, especially straight tube and fin. Therefore, the aim of this study is to further develop a helical coil to increase heat transfer performance. A novel semi-cylindrical coil has been firstly developed from the traditional helical coil for MH storage. The expectation from this study is to enhance hydrogen storage performance due to the structure of a novel heat exchanger that provides a better heat transfer area arrangement by considering the constant volume of the MH bed and HTF tube. The storage performance of this novel heat exchanger is then compared with a normal helical coil heat exchanger based on various coil pitches. From the available literature, the operating conditions and coil pitch are the main factors that affect the MH reactor's performance. To optimize the design of this novel heat exchanger, the effect of coil pitch on the hydrogen absorption time and the MH volume is investigated. Furthermore, to understand the relationship between a novel semi-cylindrical coil and the operating conditions, the secondary aims of this present study are to investigate the reactor's performance based on various operating parameter ranges and identify an appropriate value for each operating parameter.

4.4 System Description

The performance of hydrogen energy storage in this study is investigated based on two heat exchanger configurations (including a helical tube for case 1 to case 3 and a semi-cylindrical tube for case 4 to case 6), and sensitivity analysis on the operating parameters. The performance of a MH reactor is firstly examined based on the helical tube as a heat exchanger. Both HTF tube and the outer shell of the MH reactor are made of stainless steel. It should be noted that the size of MH reactor and the diameter of the HTF tube is constant for all cases, while the HTF pitch sizes vary. In this section, the impact of HTF coil pitch sizes is analyzed. The height and outer diameter of the reactor are 110 mm and 156 mm, respectively. The diameter of HTF tube is fixed as 6 mm. The detail regarding a schematic diagram of MH reactors with a helical tube and two semi-cylindrical tubes can be found in the **Appendices: A1**.

4.4.1 Metal Hydride Reactor with Helical Coil Heat Exchanger and Semi-Cylindrical Coil Heat Exchanger

Figure 4.2a presents the MH reactors with a helical tube and its dimensions. All geometrical parameters are provided in Table 4.1. The total helical tube volume and MH volume are approximately 100 cm^3 and 2000 cm^3, respectively. From this MH reactor, air as the HTF is injected from the bottom part into the porous MH reactor through a helical tube, while hydrogen is injected from the upper surface of the reactor.

In the second part, the performance of the MH reactor is then investigated based on the semi-cylindrical tubes as heat exchangers. Figure 4.2b shows the MH reactors with two semi-cylindrical tubes and their dimensions. Table 4.1 presents all geometrical parameters for a semi-cylindrical tube that are kept constant except the pitch sizes. It should be noted that the semi-cylindrical tube from case 4 was designed by considering the constant volume of HTF tube and MH alloys from the helical tube (case 3). Regarding Figure 4.2b, air is also injected from the bottom part for both HTF semi-cylindrical tubes, whereas hydrogen is injected from the opposite direction of MH reactor.

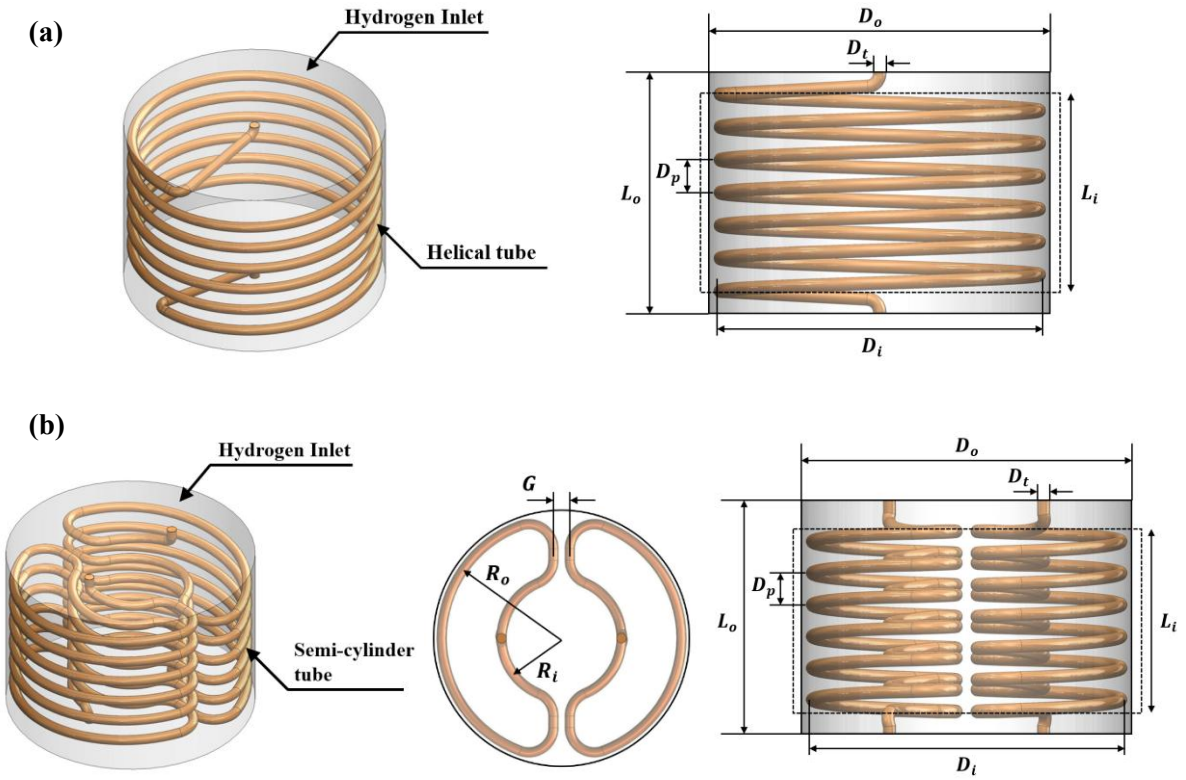

Figure 4.2 Characteristics of selected geometries for metal hydride reactors. (a) With helical tube heat exchanger, and (b) With semi-cylindrical tube heat exchanger

Table 4.1 Geometrical characteristics of MH reactors for the helical tube (case 1 to case 3) and the semi-cylindrical tube (case 4 to case 6)

Case No.	D_i **(mm)**	D_o **(mm)**	D_p **(mm)**	D_t **(mm)**	G **(mm)**	L_i **(mm)**	L_o **(mm)**	R_o **(mm)**	R_i **(mm)**
Case 1	Equal: 146	Equal: 156	15	Equal: 6	-	Equal: 90	Equal: 110	-	-
Case 2			12.86		-			-	-
Case 3			10		-			-	-
Case 4			15		Equal: 10			Equal: 73	Equal: 36.5
Case 5			12.86						
Case 6			10						

4.4.2 Sensitivity Analysis

Due to the new design of the heat exchanger, the objective of this section is to identify appropriate initial values for the operating parameters of the MH reactor that is incorporated with SCHE. For all cases, air is employed as the HTF to remove the heat from the reactor. Among HTFs, air and water are commonly selected as the HTF for the MH reactor due to having a low cost and less environmental impact. Due to a high operating temperature range of magnesium-based alloy, air is selected as the HTF for the present study. Moreover, it also has better flow characteristics compared to other liquid metals and molten salt (Aoyagi et al., 1995). Table 4.2 represents the properties of air at 573 K. For sensitivity analysis, only the best configuration of MH-SCHE performance case (among case 4 to case 6) is then

applied to this section. This section is evaluated based on various operating parameters, including an initial temperature of the MH reactor, loading pressure of hydrogen, inlet temperature of HTF, and the Reynolds number, which is calculated by changing the velocity of the HTF. All operating parameters for sensitivity analysis are included in Table 4.3.

Table 4.2 Thermo-physical properties of air at 573 K (Eisapour et al., 2021a)

Parameters	**Symbols**	**Values**
Density	ρ_f	0.60875 kg m^{-3}
Specific heat	$C_{p,f}$	1,045 J kg^{-1} K^{-1}
Thermal conductivity	λ_f	0.045 W m^{-1} K^{-1}
Dynamic viscosity	μ_f	2.061 × 10^{-5} Pa s

Table 4.3 Operating conditions for sensitivity analysis

Operating parameters	**Base value**	**Sensitivity value**
Initial temperature of MH reactor (K)	573	473, 523, 623
Loading pressure of hydrogen (MPa)	1.8	1.2, 2.4, 3.0
Inlet temperature of HTF (K)	573	373, 473, 673
Reynolds number of HTF	14000	10000, 18000, 22000

4.5 Mathematical Model

This section describes all the necessary governing equations for the hydrogen absorption process, turbulent flow and heat transfer of the heat transfer fluid. The initial and boundary conditions, numerical schemes, grid independency, and model validation are also included in this section.

4.5.1 Governing Equations

The appropriate selection of MH material for the use of this thesis are provided in "Chapter 3 – Methodology" section. The governing equations regarding the absorption process as well as the heat transfer fluid can be found in the same chapter as "Chapter 3 – Methodology". For the absorption process, the governing equations are provided in 3.1.1 Absorption Process and Desorption Process. The governing equations of heat transfer fluid can be found in "3.1.3 Heat Transfer Fluid".

The fluid flow is considered as turbulent due to its velocity and the Reynolds number (Re), which are 78.75 m s^{-1} and 14000, respectively. The realizable k-ε turbulence model is selected in this present study. It was observed that this method provides more accuracy when compared with other k-ε methods and also provides less computational time than the RNG k-ε method (Lewis & Chippar 2020; Darzi et al., 2013).

4.5.2 Initial and Boundary Conditions

At the initial time, uniform conditions are applied for the temperature inside the MH reactor with the average concentration of hydrogen as 0.043. The outer boundary of the MH reactor is assumed to be well insulated. The magnesium-based alloys usually require a high operating temperature for the reaction to store and release the hydrogen from the reactor. For the Mg_2Ni, this alloy requires the temperature range of 523-603 K to achieve the maximum absorption and the temperature range of 573-603 K to complete the desorption (Vijay et al., 2005). However, the experimental study by Muthukumar et al. (2008) proved that using the operating temperature at 573 K could achieve the maximum hydrogen

storage capacity of the Mg_2Ni storage which is equal to its theoretical capacity. Therefore, the temperature at 573 K is selected for the initial temperature of the MH reactor in the present study.

$$T_{MH} = T_0 = 573\ K, P_0 = 1.8\ MPa, x_0 = 0.043 \tag{4.1}$$

1) At the shell of the reactor:

$$\frac{\partial T_{MH}}{\partial \vec{n}} = 0\ , \tag{14}$$

2) At the heat transfer fluid inlet

$$u_x = u_z = 0, u_y = u_{in}, T = T_{in}\ , \tag{15}$$

3) At the heat transfer fluid outlet

$$p = p_s = p_a \quad . \tag{16}$$

4.5.3 Numerical Schemes, Grid Independency, and Model Validation

- Numerical Schemes and Grid Independency

Due to the similar setup conditions for the pre-processing process, the numerical schemes for all chapters are summarised and provided in "3.3.2 Numerical Schemes" under "Chapter 3 – Methodology section". Various grid sizes are established in order to verify and achieve reliable results. The average temperature at selected locations for the hydrogen absorption process from four different element numbers are provide in Figure 4.3. It is worth mentioning that only one case for each configuration is selected for grid independency checks due to having similar geometries. The same meshing methods are applied to other cases. Therefore, case 1 for the helical tube and case 4 for the semi-cylindrical tube are chosen. Figure 4.3a, b demonstrates the average temperature in the reactor from case 1 and case 4, respectively. The three selected locations represent the bed temperature contour at the top, middle, and bottom parts of the reactor. From temperature contours at the selected locations, the average temperature becomes stable and shows minor changes at the element numbers of 428891 and 430599 for case 1 and case 4, respectively. Therefore, these grid sizes are selected for further computational calculations. The details about the average bed temperature for the hydrogen absorption process for various mesh size and the successively refined grids for these two cases can be found in the "Appendices: A1".

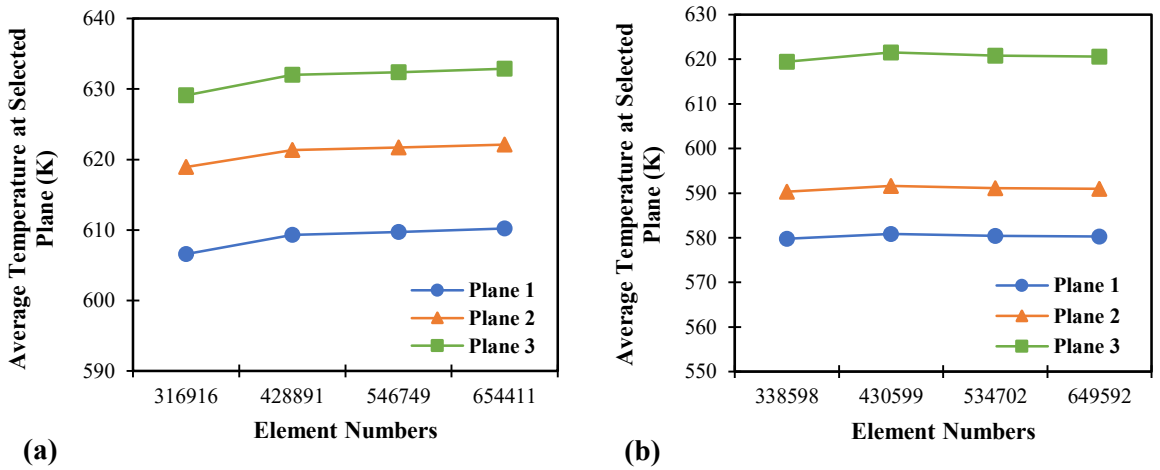

Figure 4.3 Average bed temperature at selected location for the hydrogen absorption process in the metal hydride reactor under various grid numbers. (a) Average temperature at selection location for case 1, and (b) Average temperature at selection location for case 4

- *Model Validation*

The model validations for the use of metal hydride storage system based on Mg_2Ni as well as the selection of turbulence model for the HTF are provided in "3.3.1 Model Validation" under "Chapter 3 – Methodology" section.

4.6 Results and Discussion

This section provides the results of numerical simulation of the heat transfer improvement inside the MH reactor by using a helical coil heat exchanger (HCHE) and semi-cylindrical coil heat exchanger (SCHE) for the hydrogen absorption process. The effect of the HTF pitch on the reactor bed temperature and absorption duration is analyzed. The critical operating parameters for the absorption process are investigated and presented in the sensitivity analysis section.

4.6.1 Geometrical Parameters

- *Effect of Helical Coil Pitch*

Three heat exchanger configurations with different pitches were examined in order to study the effect of coil pitch on the heat transfer in the MH reactor. Three different pitches of 15 mm, 12.86 mm, and 10 mm are assigned as case 1, case 2, and case 3, respectively. It should be noted that the tube diameter is fixed as 6 mm under the initial temperature of 573 K and loading pressure of 1.8 MPa for all cases**.** Figure 4.4 presents the average bed temperature and hydrogen concentration of the MH bed during the hydrogen absorption process for case 1 to case 3. In general, the reaction between metal hydride and hydrogen is exothermic for the absorption process. Consequently, the bed temperature rapidly increases due to the initial moments when hydrogen is first injected into the reactor. The bed temperature is continually increasing until reaching the maximum value and gradually decreasing because the heat is removed by the HTF, which has a lower temperature and acts as a cooling fluid. As shown in Figure 4.4a, the bed temperature rapidly increases and continually decreases due to the previous explanation. The hydrogen concentration for the absorption process is usually based on the bed temperature of the MH reactor. When the average bed temperature decreases to certain temperatures, the metal surface will absorb the hydrogen. This is because of the acceleration of physisorption, chemisorption, diffusion of hydrogen and its hydride formation in the reactor (Ardahaie et al., 2021). It can be seen in Figure 4.4b, the rate of hydrogen absorption from case 3 is lower than other cases due to having a lower pitch value of the coil heat exchanger. This results in higher tube length in total and higher heat transfer area of HTF tube. The absorption time from case 1 is 46276 s for the average hydrogen concentration as 90%. Comparing to the absorption duration from case 1, the absorption duration for case 2 and case 3 decreases 724 s and 1263 s, respectively. The temperature contours and hydrogen concentration contours at selected locations of the HCHE-MH bed are provided in the "Appendices: A1".

- *Effect of Semi-Cylindrical Coil Pitch*

To improve the heat transfer performance of the MH reactor, two SCHEs are designed under a constant volume of MH (2000 cm^3) and helical coil heat exchanger (100 cm^3) from case 3. This section also considers the effect of coil pitch as 15 mm for case 4, 12.86 mm for case 5, and 10 mm for case 6. Figure 4.4c, d presents the average bed temperature and concentration for the hydrogen absorption process based on initial temperature at 573 K and loading pressure at 1.8 MPa. According to the average bed temperature from Figure 4.4c, a lower coil pitch from case 6 significantly results in lower temperature compared to the other two cases. The lower bed temperature leads to higher hydrogen concentrations (see Figure 4.4d) for case 6. The hydrogen absorption time for case 4 is 19542 s which is over 2-times lower than using HCHE as case 1-3. In addition, the absorption time with lower pitch values from case 5 and case 6 also reduces 378 s and 1515 s compared to case 4. The temperature

contours and hydrogen concentration contours at selected locations of the SCHE-MH bed are provided in the “Appendices: A1”.

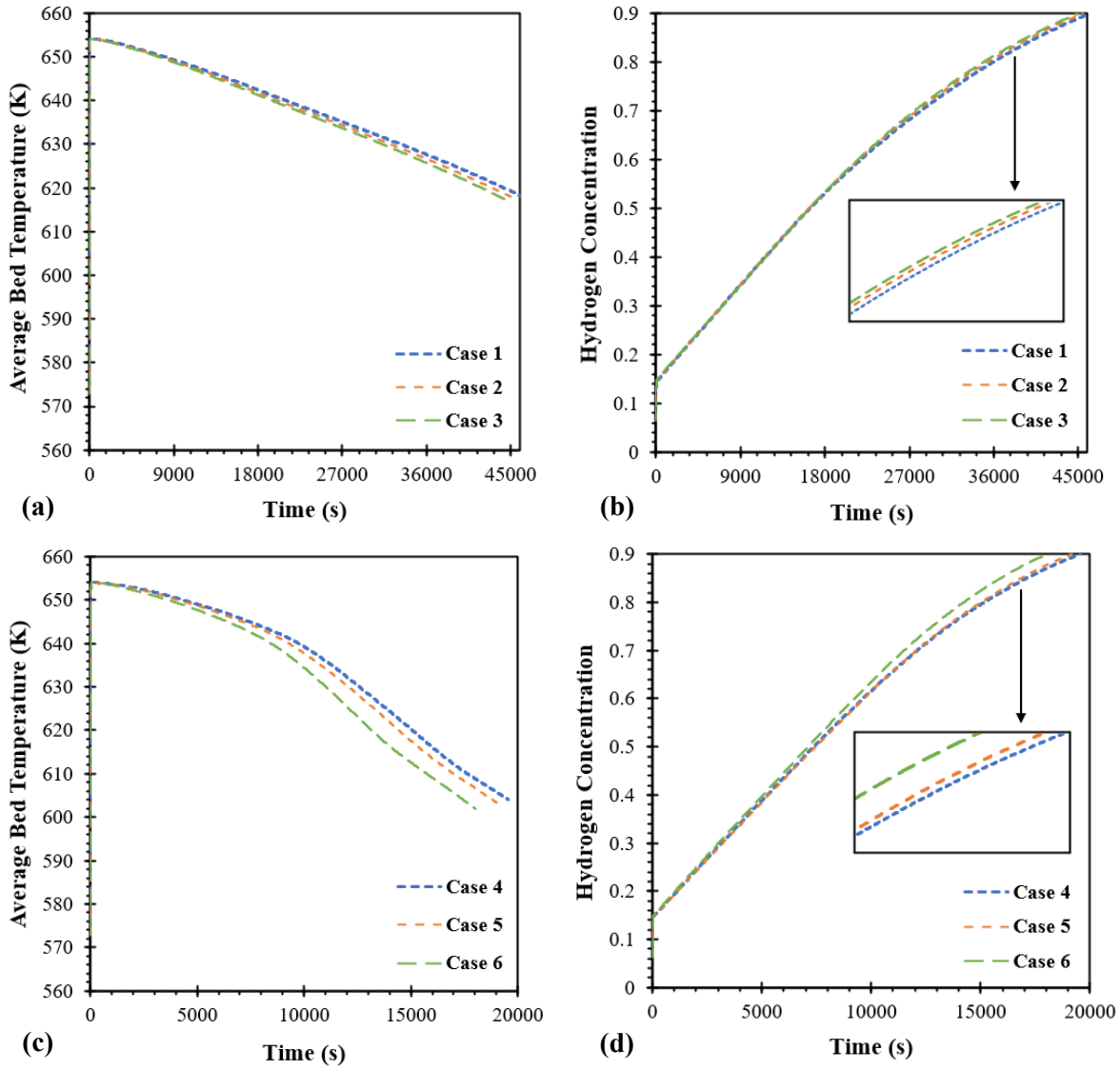

Figure 4.4 Effect of coil pitch on average bed temperature and hydrogen concentration. (a) Average bed temperature for helical coil pitch, (b) Hydrogen concentration for helical coil pitch, (c) Average bed temperature for semi-cylindrical pitch, and (d) Hydrogen concentration for semi-cylindrical pitch

- Performance comparisons between the MH Reactors with Helical Coil Heat Exchanger and Semi-Cylindrical Coil Heat Exchanger

To study the performance of two heat exchanger configurations, the temperature profiles at three selected locations are made and presented in this section. The MH reactor with HCHE from case 3 is selected to compare with the MH reactor incorporated SCHE from case 4 as having constant MH volume and tube volume. Operating conditions for this comparison are 573 K as an initial temperature and 1.8 MPa as loading pressure. Figure 4.5a, b presents all three selected locations for temperature profiles from case 3 and case 4, respectively. Figure 4.5c represents temperature profiles and bed concentration after 20000 s of the hydrogen absorption process. According to Line 1 from Figure 4.5c, the temperature around HTF from case 3 and case 4 reduces because of having convective heat transfer from the cooling fluid. This leads to a higher hydrogen concentration around this area. However, using two SCHEs results in higher bed concentration. A more rapid kinetic reaction was found around the

HTF area for case 4. Furthermore, a maximum concentration of 100% was also found around this area. From Line 2, located at the middle part of the reactor, the temperature from case 4 is significantly lower than for case 3 for all locations except at the center of the reactor. This leads to the maximum amount of hydrogen concentration for case 4 excepted around the center of the reactor where it is far away from the HTF. However, the concentration for case 3 is insignificantly changed. The huge difference in temperature and bed concentration was observed at Line 3, which is near the HTF inlet. The bed temperature from case 4 significantly reduces, resulting in full hydrogen concentration at this area, while the concentration line from case 3 still fluctuates. This is due to the heat transfer acceleration from SCHEs. The details and discussion regarding the comparison of the average temperature of the MH bed and the HTF tube between case 3 and case 4 are provide in the “Appendices: A1”.

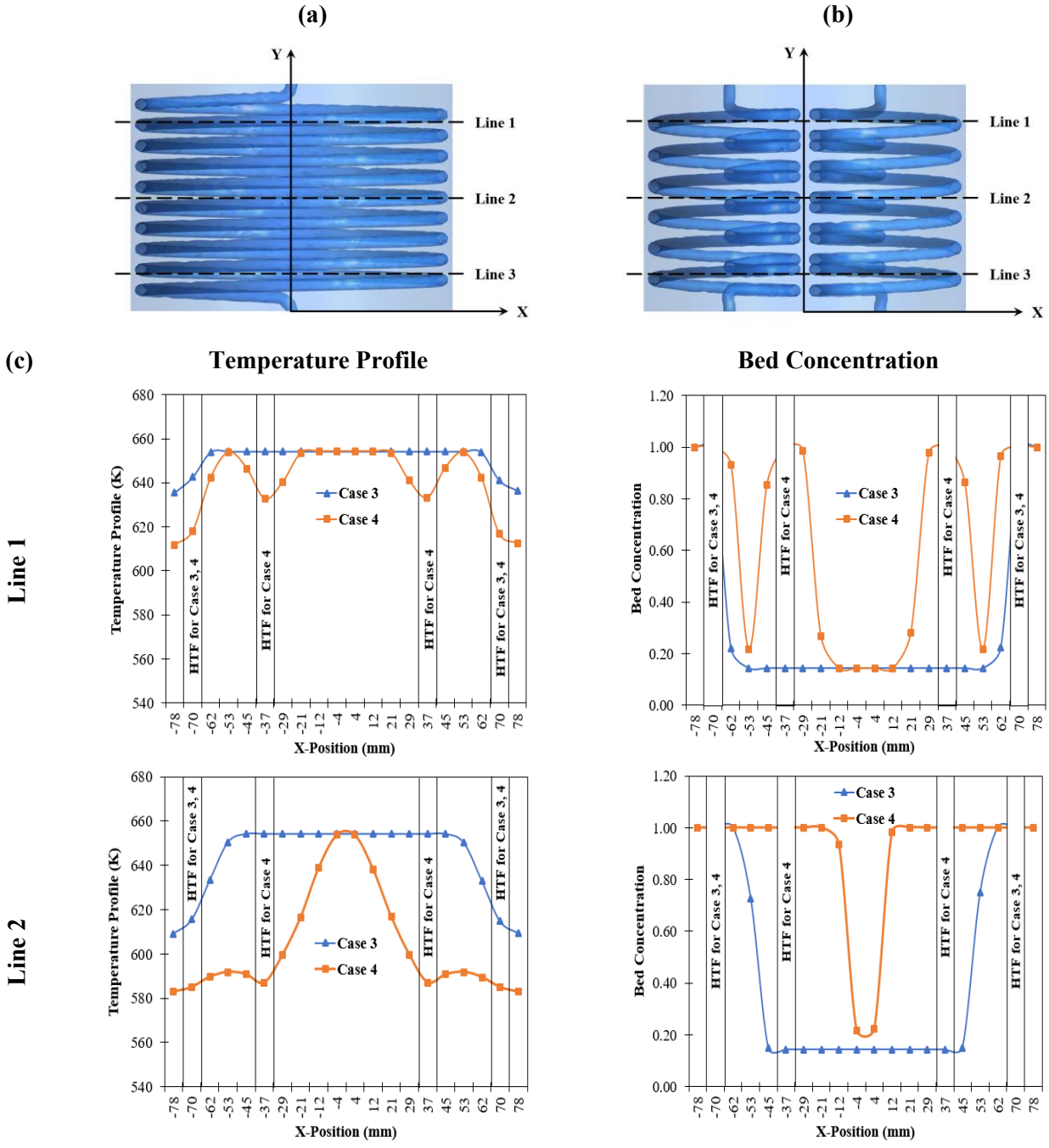

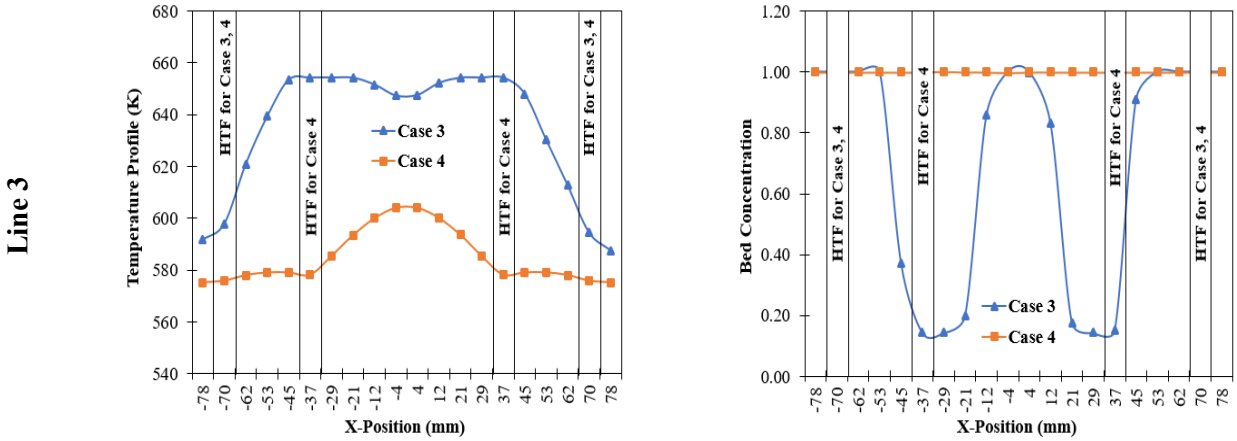

Figure 4.5 Temperature profiles and bed concentration at selected locations of the metal hydride reactor. (a) Selected locations for case 3, (b) Selected locations for case 4, and (c) Temperature profiles and bed concentration at selected locations after 20000 s of hydrogen absorption process for case 3 and case 4

Figure 4.6 displays the comparison of average bed temperatures (see Figure 4.6a) and hydrogen concentrations (see Figure 4.6b) during the absorption process between HCHE and SCHE. From this figure, it is evident that the MH bed temperature significantly reduces because of an increasing of heat transfer area. Having more heat removal rate from the reactor leads to a faster hydrogen absorption rate. Although both heat exchanger configurations have a similar volume, the hydrogen absorption time based on SCHE as case 4 significantly reduces at 59% compared to using HCHE as case 3. For more analysis, the hydrogen concentrations from both heat exchanger configurations are displayed as contours in Figure 4.7. This figure shows that the hydrogen starts to be absorbed in the bottom part around the HTF inlet for both cases. A higher concentration was found at HTF areas, while a lower concentration was observed at the center of the MH reactor due to being far away from the heat exchangers. At 10000 s, the hydrogen concentration from case 4 is significantly higher than case 3. At 20000 s, the average hydrogen concentration inside the reactor rises to 90% for case 4, while there is only 50% hydrogen for case 3. This can be explained by the reason that incorporating two SCHEs have a higher effective heat removal which leads to having lower temperature inside the MH bed. Thus, more equilibrium pressure declines inside the MH bed and then causes faster hydrogen absorption.

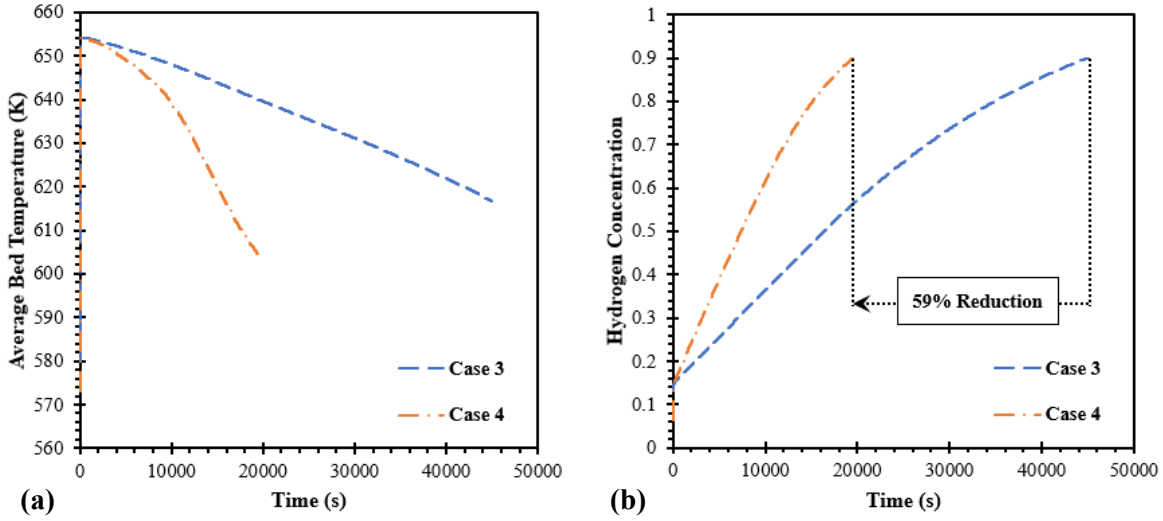

Figure 4.6 Comparison of average bed temperature and hydrogen concentrations between two heat exchanger configurations as case 3 and case 4

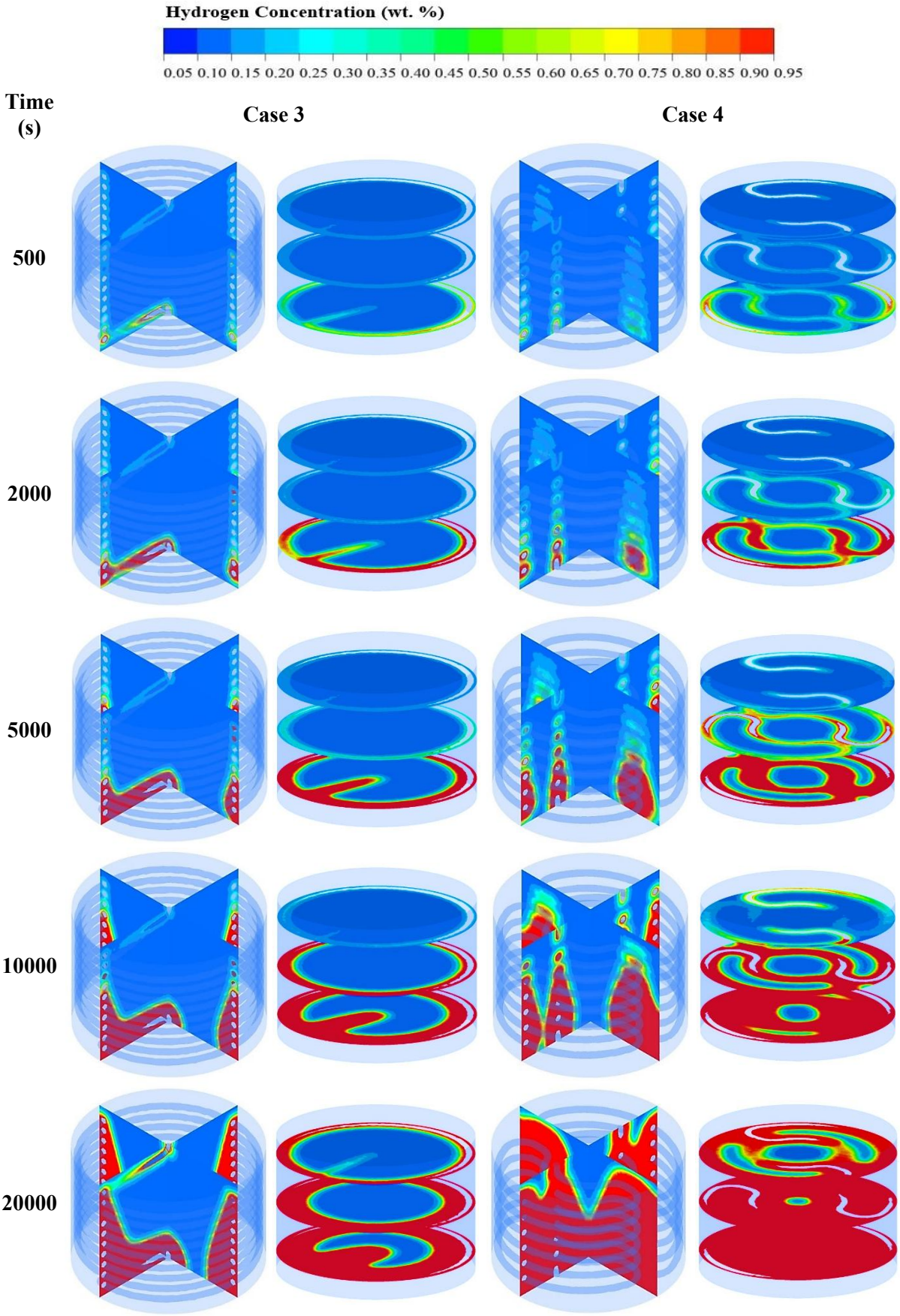

Figure 4.7 Comparison of hydrogen concentrations at 500 s, 2000 s, 5000 s, 10000 s, and 20000 s after the start of the hydrogen absorption process between case 3 and case 4

Table 4.4 summarizes the hydrogen absorption durations for all cases. Moreover, the hydrogen absorption time in percentage is also presented in this table. The percentage is calculated based on the absorption time from case 1. From this table, the absorption time from the MH reactor with HCHE is around 45000 s to 46000 s, while the absorption time incorporating SCHE is around 18000 s to 19000 s. When compared to case 1, the absorption time from case 2 and case 3 reduces only 1.6% and 2.7%, respectively. By employing SCHE instead of HCHE, the absorption time significantly reduces by 58% to 61% from case 4 to case 6. It is evident that incorporating SCHE inside the MH reactor significantly enhances the hydrogen absorption process and MH reactor performance. Although inserting the heat exchanger inside the MH reactor will reduce the storage capacity, this technique obtains a significant heat transfer improvement compared to other techniques. Moreover, the reduction of pitch values will increase the SCHE volume which leads to reducing the MH volume. In case 6, which has the highest SCHE volume, there is only a 5% reduction in the MH volume capacity compared to case 1, which has the lowest HCHE volume. Furthermore, during the absorption process, case 6 indicates faster and better performances with a reduction of 61% in absorption duration. Therefore, case 6 is selected to further investigation regarding sensitivity analysis. It should be noted that the long hydrogen absorption time is due to the storage capacity which contains the MH volume at around 2000 cm^3.

Table 4.4 Summary of hydrogen absorption times for all six cases. (The percentage of hydrogen absorption duration is calculated based on the absorption time from case 1)

Case	Absorption Time (s)	Absorption Duration (%)
1	46276	100
2	45552	98.4
3	45013	97.3
4	19542	41.4
5	19164	41.3
6	18027	38.9

4.6.2 Sensitivity Analysis of Operating Conditions

The operating parameters during the reaction process are essential factors that can be positively or negatively impact the performance of MH reactor in actual utilization. The sensitivity analysis is considered in this study to identify appropriate initial values of operating parameters for the MH reactor that is incorporated with SCHE, this section investigates four main operating parameters based on the best reactor configuration from case 6. The results from all operating conditions are presented in Figure 4.8.

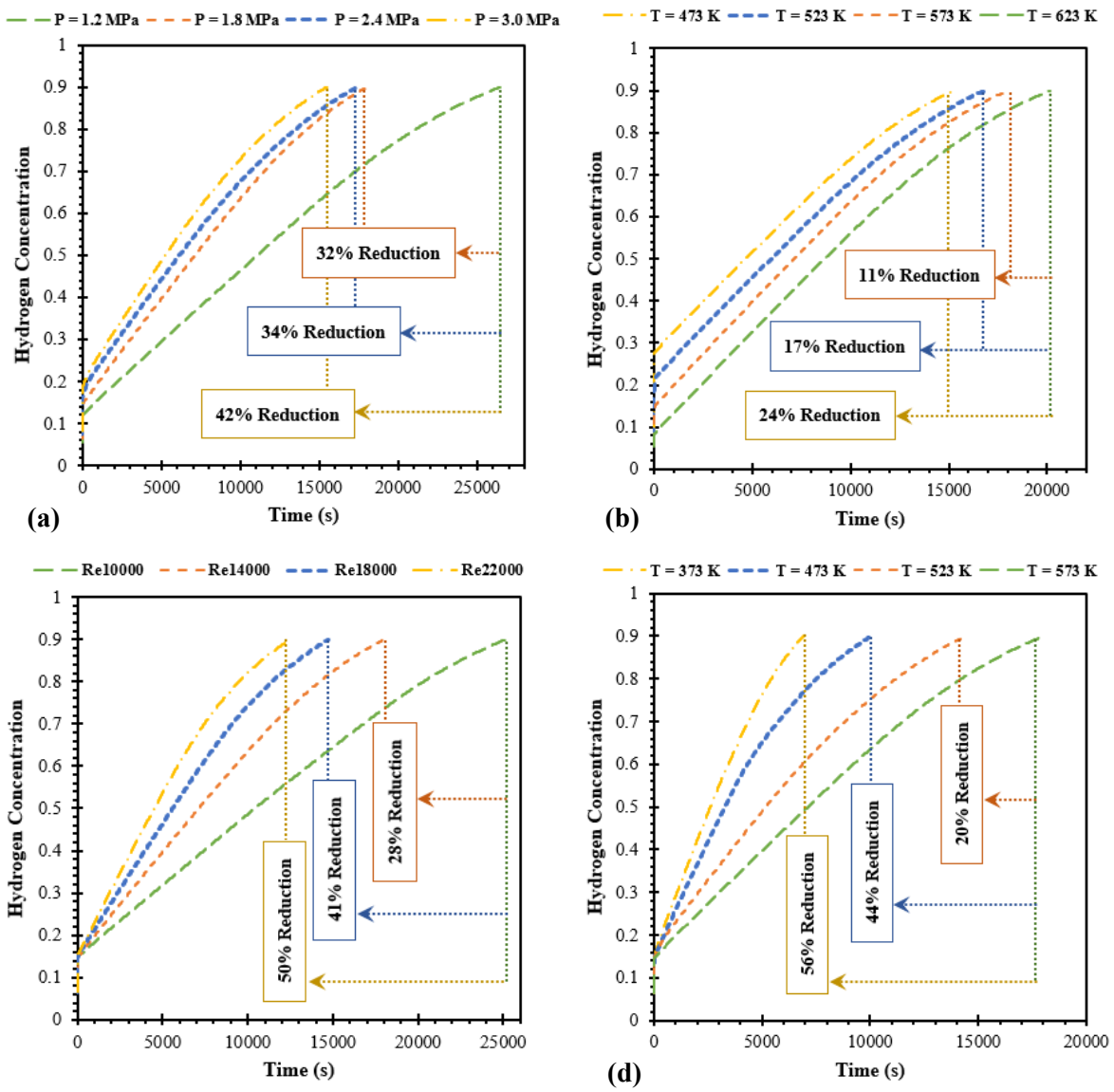

Figure 4. 8 Hydrogen concentration diagram for various operating conditions in the use with the semi-cylindrical coil heat exchanger. (a) Loading pressures, (b) Initial bed temperatures, (c) Reynolds numbers of heat transfer fluid, and (d) Inlet temperatures of heat transfer fluid

- *Effect of the Loading Pressure on the Hydrogen Absorption Process*

Four different loading pressures of 1.2 MPa, 1.8 MPa, 2.4 MPa, and 3.0 MPa were chosen based on the constant initial temperature at 573 K and HTF flow velocity at 14000 of Reynolds number. Figure 4.8a reveals the effect of loading pressure and the SCHE on the hydrogen concentration with respect to time. The absorption time is reduced by an increment of loading pressure. Employing exerted hydrogen pressure with 1.2 MPa is the worst case for the hydrogen absorption process with the absorption duration over than 26000 s for achieving 90% of hydrogen absorption. However, higher loading pressure results in the reduction of absorption times by 32% to 42% from 1.8 MPa to 3.0 MPa. This is due to higher initial hydrogen pressure causing a larger difference between the equilibrium pressure and exerted pressure. Thus, this generates a greater driving force for hydrogen absorption kinetic (Wu et al., 2014). At the initial moment, the hydrogen is rapidly absorbed because of the greater difference between the equilibrium pressure and exerted pressure (Afzal & Sharma 2021a). With loading pressure at 3.0 MPa, 18% of the hydrogen is rapidly stored within the first 10 s. The hydrogen is stored at 90% of the reactor at the final stage with 15460 s. However, the absorption time is significantly reduced by 32% from the

loading pressure at 1.2 MPa to 1.8 MPa. Other higher pressures have less effect on the improvement of the absorption time. Consequently, the loading pressure at 1.8 MPa is recommended for the MH-SCHE reactor. The hydrogen concentration contours for various loading pressures at 15500 s are provided in the "Appendices: A1".

- *Effect of the Initial Temperature on the Hydrogen Absorption Process*

Selecting the appropriate initial temperature of the MH reactor is one of the main factors that influence the hydrogen sorption process, as it will affect the driving force of the hydride-producing reaction. To study the effect of SCHE on the initial temperature of the MH reactor, four different temperatures were chosen under constant loading pressure at 1.8 MPa and Reynolds number at 14000 of HTF. Figure 4.8b presents the comparison of various initial temperatures, including 473 K, 523 K, 573 K, and 623 K. In fact, the Mg_2Ni alloy will have effective performance for the hydrogen absorption process when the temperature is above 230 ℃ or 503 K (Reiser et al., 2000). However, the temperature will rapidly increase at the initial moment when hydrogen is injected. Thus, the MH bed temperature will be over 523 K. For this reason, hydride formation is then promoted due to the absorption rate enhancement (Muthukumar et al., 2008). From Figure 4.8b, the hydrogen is absorbed faster when the initial temperature of the MH bed is reduced. When having a lower initial temperature, it leads to generating lower equilibrium pressure. The larger different pressures between equilibrium pressure and exerted pressure cause a faster hydrogen absorption process. By 473 K initial temperature, the hydrogen is rapidly absorbed to 27% within the first 18 s. Moreover, the absorption time from lower initial temperatures is also reduced from 11% to 24% compared to the initial temperature at 623 K. The absorption time with the lowest initial temperature at 473 K is 15247 s which is similar to the best case of loading pressure. However, reducing initial reactor temperature results in lower hydrogen storage capacity. The initial temperature of MH reactor should not be less than 503 K (Muthukumar et al., 2008). Furthermore, the maximum hydrogen storage capacity of 3.6 wt% can be achieved by using the initial temperature of 573 K (Muthukumar et al., 2008). Focusing on the hydrogen storage capacity and the duration of the absorption, there is only a 6% time reduction by the temperature between 523 K and 573 K. Therefore, the temperature at 573 K is recommended for the initial temperature of the MH-SCHE reactor. However, the effect of initial temperature on the absorption process is less significant compared to loading pressure. The hydrogen concentration contours for various initial temperatures at 15500 s are provided in the "Appendices: A1".

- *Effect of the Reynold's Number of the Heat Transfer Fluid on the Hydrogen Absorption Process*

The flow velocity is one of the essential parameters for both hydrogeneration and dehydrogenation because of its ability that affect the turbulence and heat removal or heat supplying regarding hydriding and dehydriding processes (Wang et al., 2021). A large flow velocity will generate a turbulent stage and cause faster fluid flow through the HTF tube. This reaction will result in faster heat transfer. Various inlet velocities of HTF are calculated based on the Reynolds number as 10000, 14000, 18000, and 22000. The initial temperature of MH bed is fixed at 573 K with the loading pressure at 1.8 MPa. The result from Figure 4.8c proves that utilizing a higher Reynolds number incorporated with the SCHE leads to a faster absorption rate. With the increase of the Reynolds number from 10000 to 22000, the absorption time reduces approximately 28% to 50%. The absorption time from the Reynolds number at 22000 is 12505 s which is lower than the absorption time based on various initial temperatures and loading pressures. The hydrogen concentration contours for various Reynolds numbers of the HTF at 12500 s are presented in the "Appendices: A1".

- *Effect of the Initial Temperature of the Heat Transfer Fluid on the Hydrogen Absorption Process*

The effect of the SCHE on the initial HTF temperature is analyzed and displayed in Figure 4.8d. Four initial temperatures of 373 K, 473 K, 523 K, and 573 K are chosen for this analysis under the initial

MH temperature at 573 K and loading pressure of hydrogen at 1.8 MPa. Figure 4.8d indicates that the decrease in inlet HTF temperature leads to a shorter absorption time. Compared to the base case with inlet temperature at 573 K, the absorption time reduces around 20%, 44% and 56% for inlet temperature of 523 K, 473 K, and 373 K, respectively. At 6917 s with the initial temperature of the HTF at 373 K, there is a 90% of hydrogen concentration inside the reactor. This can be explained by the enhancement of convective heat transfer between the MH bed and the HTF. A lower HTF temperature will increase the heat removal rate and result in an improvement of the hydrogen absorption rate. Among all operating parameters, improving the MH-SCHE reactor's performance by increasing the inlet temperature of the HTF is the most suitable method as the end of the absorption process is lower than 7000 s while the minimum absorption time from other methods is greater than 10000 s. The hydrogen concentration contours for various initial temperature of the HTF at 7000 s are presented in the "Appendices: A1".

4.7 Conclusion

The present study first introduces a novel semi-cylindrical coil heat exchanger embedded inside the metal hydride storage unit. The hydrogen absorption capacity of the proposed system is investigated under different heat exchanger configurations. The effect of operating parameters between the metal hydride bed and heat transfer fluid on the heat exchanged are examined, in order to find optimal conditions for the metal hydride storage with a novel heat exchanger. The key findings from this study are summarized as follows:

- Using a semi-cylindrical coil heat exchanger, heat transfer performance is improved as it has more uniform heat distribution in the magnesium bed reactor resulting in a better hydrogen absorption rate. Under the constant volume of the heat exchanger tube and metal hydride, the absorption reaction time is significantly reduced by 59% compared to a normal helical coil heat exchanger.
- Reducing the pitch size of coil heat exchangers positively affects the absorption duration because of having more heat transfer area. Among other pitch values, there is a 61% reduction of hydrogen absorption time when using semi-cylindrical coil heat exchangers with a pitch size of 10 mm. With this size, there is around a 5% reduction in the metal hydride volume capacity compared to the highest pitch size. Therefore, using a semi-cylindrical coil heat exchanger with 10 mm pitch size is recommended.
- Increasing the loading pressure of hydrogen injection leads to a lower hydrogen absorption time. The absorption duration significantly reduces, by 32%, with loading pressure at 1.8 MPa compared to 1.2 MPa. However, other higher values have less effect on the absorption duration. Therefore, the loading pressure at 1.8 MPa is recommended for the storage with a new heat exchanger.
- The lower initial temperature of the metal hydride bed results in a faster hydrogen absorption rate. However, to maintain the storage capacity with a Mg_2Ni-based alloy, the initial temperature should not be less than 503 K. Considering the storage capacity and the absorption duration, the initial temperature at 573 K is recommended for the storage with a semi-cylindrical coil heat exchanger.
- The initial conditions of heat transfer fluid are the main parameters that significantly affect the improvement of storage performance with a novel heat exchanger. Higher Reynolds number of the heat transfer fluid positively influences hydrogen absorption duration because of having higher fluid flow velocity. Furthermore, a lower inlet temperature of heat transfer fluid also improves the convective heat transfer between the bed and the cooling fluid. By these two parameters, the absorption duration is significantly reduced by 50-56%.

The results from this study provide a heat transfer improvement regarding the absorption process of magnesium-based hydrogen energy storage under a novel heat exchanger configuration with optimized

operating conditions. The comprehensive study on this proposed system could be beneficial for industrial applications. To improve the hydrogen absorption duration, the metal hydride storage with a novel semi-cylindrical coil heat exchanger will be further incorporated with other heat exchangers in the next study. Furthermore, the effect of using a novel heat exchanger on the hydrogen desorption process will be further considered. It should be noted that this study only considers the heat transfer enhancement based on the different heat exchanger structures. The well-arrangement of the new heat exchanger design significantly indicates good performance. The heat transfer surface area as well as the heat exchanger volume are constant between both heat exchangers.

Chapter 5 – A Novel Design for Faster Hydrogen Storage: A Combined Semi-Cylindrical and Central Return Tube Heat Exchanger

Research Paper: **Larpruenrudee, P.,** Bennett, N.S., Luo, Z., Fitch, R., Sauret, E., & Islam, M.S., (2023). A novel design for faster hydrogen storage: a combined semi-cylindrical and central return tube heat exchanger. **Journal of Energy Storage** 71, 108018. https://doi.org/10.1016/j.est.2023.108018. **SJR: 1.456 [Q1], IF: 9.4**

5.1 Summary

Objectives to achieve the aim of this study:

- Further enhance the thermal performance of the storage and heat exchanger by further developing the new internal heat exchanger structure from Chapter 4 (Research Paper 1)
- Further enhance the thermal performance of the storage and heat exchanger by combining developed internal heat exchanger with external heat exchanger under active thermal management technique
- Identify an appropriate initial value of each operating parameter under the new storage configuration and heat exchanger

Achievements and innovations in this chapter:

- Further enhance the thermal performance of the semi-cylindrical coil heat exchanger by combining itself with the central return tube
- Optimise the design of this new heat exchanger configuration based on the effect of heat exchanger tube diameter on the hydrogen absorption and metal hydride volume
- Further enhance the thermal performance of the storage system and heat exchanger by combining this new heat exchanger with a cooling jacket as an external heat exchanger
- Investigate the initial value of the heat transfer fluid's parameter based on the new storage configuration, including; the initial flow velocity and temperature of the heat transfer fluid, and the heat transfer coefficient between the storage and heat transfer fluid

5.2 Abstract

Metal hydrides (MH) have recently attracted significant interest for hydrogen storage as they provide large storage capacity and a high degree of safety. The main disadvantage, however, is that storage speed is compromised by their low rate of hydrogen absorption. One possible way to accelerate the absorption reaction, and thus improve storage performance regarding incoming hydrogen transfer speed, is to increase the heat transfer rate inside the storage system. Among internal heat exchangers, using helical coil and semi-cylindrical coil heat exchangers significantly improves the heat transfer performance inside the storage system because of the secondary circulation. However, the central area of the storage system still has a lower heat transfer rate as this area is far away from the heat transfer fluid. For this purpose, the development of a heat exchanger structure is considered for the new achievement of this study. A semi-cylindrical coil heat exchanger incorporating a central return tube (SCHE-CR) is first developed from a semi-cylindrical coil heat exchanger (SCHE) to improve heat exchange rate at the MH central area. The tube size's effect on absorption is analysed. Further, a combination of internal and external heat exchangers is considered for further improvement of MH storage performance. The operating parameters of the heat transfer fluid for various heat exchanger configurations are investigated to determine optimal values. Results from numerical simulations indicate that absorption duration reduces by 30% in the SCHE-CR case compared to the SCHE. Increasing the tube diameter of SCHE-CR results in a 40% faster absorption reaction. Using SCHE-CR with a cooling jacket reduces the absorption duration by 51% compared to the SCHE-CR. Among other operating conditions, the operating temperature of the cooling fluid is found to significantly affect the hydrogen absorption reaction with up to a 36% enhancement of the absorption rate. However, the heat transfer coefficient between cooling fluid and MH, is not found to have a significant effect, as the improvement of the absorption rate is only 8%. The new MH reactor configuration would be beneficial to improve heat exchange in MH storage applications

Keywords: Hydrogen absorption, Semi-cylindrical coil, Reaction time, Faster hydrogen storage, Sensitivity analysis.

5.2.1 Graphical Abstract

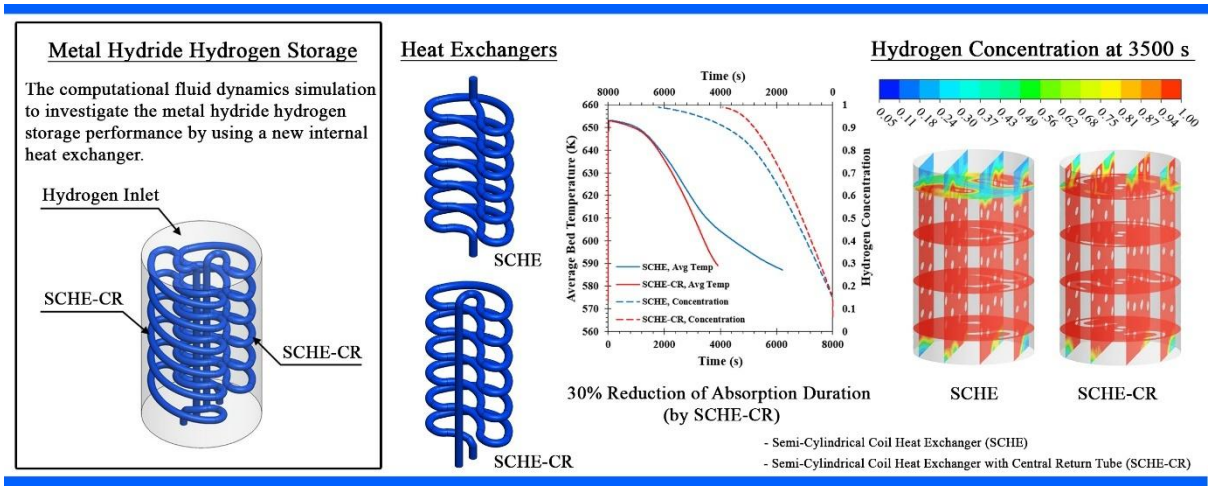

Figure 5.1 Graphical abstract for the second research paper

5.3 Introduction

The environmental crisis around the world has demonstrated the need for alternative energies like renewable energy. Hydrogen is one of the alternative fuels and energy storage mediums that has been widely proposed because of its characteristics and portability, as it is well known as the lightest gas and a good energy carrier (Tang et al., 2011; Urunkar & Patil 2021). The energy storage capacity per unit mass from hydrogen is also higher when compared to fossil fuels (Harries et al., 2012). Hydrogen storage in the form of metal hydride (MH) has been recently used for fuel cell applications, as it provides low cost, a high hydrogen capacity, as well as high safety due to a low operating pressure, compared to other techniques (Sakintuna et al., 2007; Jain et al., 2010). In general, for solid storage, hydrogen will be combined with the solid material to be stored inside the reactor by absorption and released from the reactor by the desorption process (Yue et al., 2021). However, having a low thermal conductivity is the main disadvantage of MH materials (Zhao et al., 2020). This problem significantly causes slow hydrogen absorption and desorption. To solve this problem, enhancing the heat transfer inside the storage system is required. To control the desired charging rate during absorption, generated heat is required to be released from a system, while heat is required for the hydrogen discharging process (Nguyen & Shabani 2021). Consequently, faster heat removal from the storage system will result in faster absorption, while the opposite is required for the desorption process.

There are several heat exchanger configurations that have been designed for MH reactors. For example, cooling/heating jackets were designed to cover around the storage system as an external heat exchanger. Based on this technique, the experimental study of Kaplan (2009) proved that using a cooling jacket positively affected the heat transfer in the storage system as a MH bed temperature from a case with the cooling jacket was around 60% lower than the case without the cooling jacket. The supply pressure of hydrogen injection as well as the operating temperature of the heat transfer fluid (HTF) were the key factors that improved the MH storage performance. Similarly, the study by Valizadeh et al. (2016) reported that initial HTF temperature was the key parameter for the desorption. From this technique, there is the heat transfer at the outer wall of the MH bed, which contact with the cooling/heating jacket. In contrast, there is heat transfer inside the MH bed when using the internal heat exchangers. Therefore, the development of several internal heat exchangers has been proposed to circulate the HTF throughout the storage system during the hydrogen sorption (Wu et al., 2016). These include straight tubes, helical coils, as well as the semi-cylindrical coil.

The straight tube was located inside the MH reactor, which contained aluminium foam and $LaNi_5$ as MH alloy (Mellouli et al., 2009). The results from this study demonstrated that the absorption duration significantly reduced by 60% when combining a straight tube with metal foam compared to the normal case. However, adding metal foam resulted in the reduction of hydrogen storage capacity. Several inner straight tubes were used by Raju & Kumar (2011). Their results indicated that using several straight tubes reduced the hydrogen absorption time. A multi-zone configuration of the HTF was designed and incorporated with the MH reactor by Eisapour et al. (2021b). Their numerical results highlighted that increasing the number of air passages significantly improves the hydrogen charging time. Furthermore, increasing the pressure of hydrogen injection and the Reynolds number of the HTF also improved the absorption reaction rate.

The helical coil heat exchanger (HCHE) was designed for the purpose of increasing in heat and mass transfer performance inside storage systems. Because of the secondary circulations of this heat exchanger, which provided more heat transfer surface area in the storage, the heat exchange rate significantly improved compared to using a straight tube (Wu et al., 2014). Also, several heat exchanger configurations were proposed and compared (Wu et al., 2016; Tong et al., 2019a). Among different

heat exchanger configurations, using the HCHE provided higher heat and mass transfer rates in comparison to other types, including fins and straight tubes. The study by Wang et al. (2012) demonstrated that a higher heat transfer coefficient of the HTF also decreased the hydrogen absorption duration. Mellouli et al. (2007) designed a new spiral tube that had the same direction as the HTF inlet and outlet to increase the heat transfer surface area for their experimental study. The authors stated that the HTF temperature was the main parameter that significantly decreased hydrogen sorption duration compared to other parameters, including operating pressure, the volume and temperature of the storage. Similarly, Visaria & Mudawar (2012a, b) also reported that reducing the HTF temperature for coil tube resulted in faster hydrogen absorption duration for the MH reactor based on $Ti_{1.1}CrMn$ alloy. The absorption duration was reduced from 20.9 minutes to 12.2 minutes when reduced the HTF temperature from 21 ℃ to 2.5 ℃. The magnesium-based Mg_2Ni reactor was combined with the HCHE in the numerical simulation (Wu et al., 2014). The authors summarised that lower ratios of coil pitch to diameter, as well as a non-dimensional pitch, positively affected the heat transfer inside a storage system. A flat spiral tube was designed to be used with the MH reactor based on Mg_2Ni material (Ardahaie et al., 2021). This study observed a faster absorption with a higher number of spiral tubes. A new helical coil with a centrally-located return pipe was designed to enhance heat transfer, especially in the central area of the MH storage system (Eisapour et al., 2021a). Moreover, this study indicated that using this new heat exchanger significantly reduced the absorption duration. Furthermore, a lower pitch and higher diameter of the helical coil positively affected the rates of heat and mass transfers. The semi-cylindrical coil heat exchanger (SCHE) was developed from a HCHE and located inside the MH storage system (Larpruenrudee et al., 2022a). This study proved that using this heat exchanger significantly reduced hydrogen absorption duration by 59% in comparison to the HCHE type. Improving in surface area arrangement of the semi-cylindrical coil, the hydrogen storage performance was also significantly enhanced. However, the centre of the MH bed, which was distant from the HTF area, still had a higher temperature which resulted in lower hydrogen concentration in this area. Several heat exchanger techniques were combined to improve the MH reactor's performance. Raju & Kumar (2012) proposed various MH reactor configurations that were equipped with several types of heat exchangers including; (1) cooling jacket with inner straight tubes and fins, (2) cooling jacket with inner helical coil tubes, and (3) cooling jacket with straight tubes that were placed in horizontal. The authors stated that the MH storage system with a cooling jacket and HCHE obtained better gravimetric and volumetric densities when compared to other heat exchanger types. Combining the outer cooling jacket and inner cooling tubes significantly improved the kinetic reaction rate, which resulted in faster hydrogen sorption (Freni et al., 2009; Karmakar et al., 2021; Afzal & Sharma 2018).

From the above examples, combining inner and outer heat exchangers significantly improves the heat transfer rate. Using HCHE, especially with a centrally-mounted tube, considerably improves heat and mass transfer mechanisms. Although using a SCHE obtains the better heat transfer enhancement in comparison to a HCHE, the centre of the MH bed still has a less conductive heat transfer rate. Based on the structure of a SCHE, there is no contact area between the MH and the cooling fluid in this area. For this reason, the present work aims to further develop a SCHE. The SCHE incorporating a central return tube (SCHE-CR) is introduced for the first time for the improvement of the heat transfer at central areas. The work from present study is expected to increase the storage system performance by focusing on improving the heat exchange rate, especially at the central area in the storage system based on the new heat exchanger type. Moreover, the new heat exchanger is then combined with the cooling jacket to further improve the heat transfer inside the MH system. To verify this hypothesis, a comprehensive investigation of storage performance is performed by comparing the temperature variation and hydrogen absorption duration along the absorption process using the new heat exchanger configurations. In addition, the operating conditions and tube diameter of the HTF significantly affect

the improvement of the MH reactor's performance. To investigate the new heat exchanger's performance, the relationship between the tube diameter, MH volume, and hydrogen absorption duration are considered in this study. Furthermore, determining a suitable value for each operating parameter of the HTF is the secondary objective.

5.4 System Description

The present study proposes a new design of the internal heat exchanger that was developed from SCHE. The MH reactor's performance is analysed based on the different heat exchanger configurations between SCHE and SCHE-CR, and sensitivity analysis under various operating conditions. Stainless steel is chosen as the material used for the HTF tube and the MH tank with a constant size of MH reactor for all cases. The outer diameter and total height of the tank are 50 mm and 80 mm with reference to Wu et al. [15]. The coil pitch of SCHE is 10 mm, while it is 11.67 mm for SCHE-CR. It should be noted that the coil pitch of 10 mm of SCHE is selected based on the recommendation from the study of Eisapour et al. (2021a). The HTF tube diameter is considered as the main parameter of the heat transfer enhancement and is presented under the geometrical parameters under the results and discussion. **Figure 5.2a** presents the single HTF tube for SCHE and SCHE-CR.

5.4.1 Storage System with Semi-Cylindrical Coil

A schematic diagram of the MH storage system with SCHEs, and geometrical parameters are provided in Figure 5.2b and Table 5.1. From Table 5.1, case 1 and case 2 refer to the SCHEs with a 3 mm and 4 mm of tube diameter, respectively. From the SCHE case, the air is set to be injected from the bottom part of the system through the SCHE, whereas it is in the opposite direction of the hydrogen injection (top surface).

5.4.2 Storage System with Semi-Cylindrical Coil and Central Return Tube

Figure 5.2c demonstrates the schematic diagram of a MH tank with SCHE-CRs. In this case, the HTF inlet and outlet are designed to be in the same direction because of the new heat exchanger configuration, which includes the central return tube. Based on this, the direction of the hydrogen injection is still the same. All geometrical parameters for SCHE-CR can be found in **Table 5.1**. From this table, case 3 and case 4 are the SCHE-CRs with 3 mm and 4 mm of tube diameter, respectively.

5.4.3 Storage System with Internal and External Heat Exchanger

To improve the reactor's performance, a cooling jacket (3 mm thickness) is employed as an external heat exchanger, which will be further incorporated with the best MH reactor configuration case (selected from case 1 to case 4). It is important to highlight that this study only focuses on the analysis of the thermal performance of the SCHE and SCHE-CR under the variation of tube sizes. The effect of the various thicknesses of a cooling jacket on thermal performance is not considered in this study. This parameter will be further analysed in the next study.

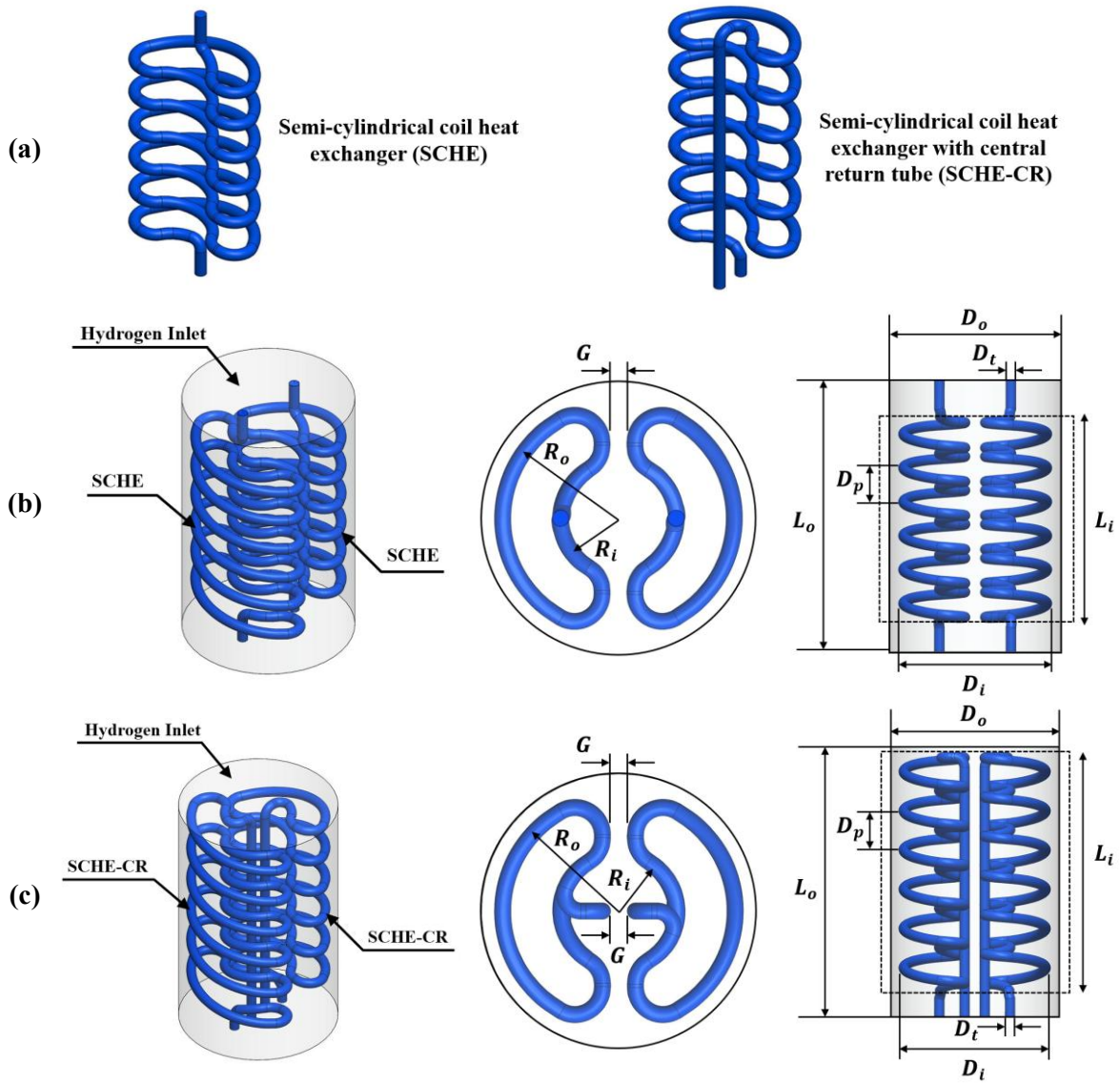

Figure 5.2 Schematic diagram of storage tanks with two heat exchangers. (a) single HTF tube from SCHE and SCHE-CR, (b) characteristics of MH reactor with SCHEs, and (c) characteristics of MH reactor with SCHE-CRs

Table 5.1 Characteristic of MH tanks for the SCHE (case 1, 2) and SCHE-CR (case 3, 4)

Case No.	D_i (mm)	D_o (mm)	D_p (mm)	D_t (mm)	G (mm)	L_i (mm)	L_o (mm)	R_o (mm)	R_i (mm)
1	Equal: 42	Equal: 50	Equal: 10	3	Equal: 6	Equal: 60	Equal: 80	-	-
2				4				-	-
3			Equal: 11.67	3		Equal: 70		Equal: 21	Equal: 10.5
4				4					

5.4.4 Sensitivity Analysis for Operating Conditions

To determine appropriate values of initial operating parameters of the HTF with the new heat exchanger design, the best configuration case (case 1 to case 4) is selected for further analysis. To identify the best case, the reduction of the MH bed volume, as well as the HTF tube and absorption duration are considered as the main parameters. The HTF operating conditions include the Reynolds number (Re) and HTF inlet temperature. Furthermore, the effect of various selected values of the Re on the HTF tube is examined in this section. Referring to available literature, most recent studies only focus on investigating the effect of the heat transfer coefficient (HTC) by using several heat exchangers. A comprehensive analysis of the effects of various flow velocities on the turbulence intensity of the HTF tube is still not available in the literature. Therefore, the level of turbulence intensity of the HTF under the different values of the Re is considered in the present study. It should be noted that these two parameters are analysed to optimise the appropriate values for the internal heat exchanger only. The sensitivity analysis for the outer cooling jacket (considered as an external heat exchanger) is investigated based on the HTC between the MH and HTF of the cooling jacket. The HTF operating conditions can be found in Table 5.2. It is important to mention that air is considered to be the HTF for all cases as it has a less environmental impact and low cost compared to other HTFs.

Table 5.2 Operating values for the HTF

Parameters	**Base value**	**Sensitivity value**
HTF Inlet temperature (K)	573	423, 473, 523
Reynolds number of HTF	9000	6400, 11700, 14500
Heat transfer coefficient of a cooling jacket (W m^{-2} K^{-1})	250	500, 750, 1000

5.5 Mathematical Model

The all related equations regarding the governing equations for the hydrogen absorption and heat transfer fluid are provided in this section. The initial and boundary conditions, numerical schemes, grid independency, and model validation are also included in this section.

5.5.1 Governing Equations

The appropriate selection of MH material for the use of this thesis are provided in "Chapter 3 – Methodology" section. The governing equations regarding the absorption process as well as the heat transfer fluid can be found in the same chapter as "Chapter 3 – Methodology". For the absorption processes, the governing equations are provided in 3.1.1 Absorption Process and Desorption Process. The governing equations of heat transfer fluid can be found in "3.1.3 Heat Transfer Fluid".

The turbulent condition is applied under the realizable k-ε turbulence model for the fluid flow in the present study with the inlet velocity of 76.86 m s^{-1} corresponding to the Re of 9000. The average y+ ≈ 30 for the present study. Among k-ε methods, the realizable k-ε turbulence model provides more accuracy and less computational time (Ardahaie et al., 2021; Kumar et al., 2006). The validation of the selected turbulence model was performed from the previous study (Larpruenrudee et al., 2022a), which was compared with the experimental results (Kumar et al., 2006).

5.5.2 Initial and Boundary Conditions

In general, a high operating temperature is required to activate the MH storage system for hydrogen sorption, especially magnesium-based alloys. To obtain the maximum absorption for Mg_2Ni alloy, the experimental results from Muthukumar et al. (2008) demonstrated that the maximum hydrogen storage capacity ofMg_2Ni storage could be obtained by using an operating temperature of 573 K. Consequently, the initial temperature of the MH storage system ($T_{MH} = T_0$) is set as 573 K. Furthermore, the previous study from Larpruenrudee et al. (2022a) also showed that using a 1.8 MPa of loading pressure (P_0)

obtains better hydrogen absorption performance compared to other values. Therefore, this value is chosen as hydrogen loading pressure. The boundary condition is set as the inlet velocity for the heat transfer fluid injection from the bottom part through the heat exchanger tube in the y-axis direction to the heat exchanger outlet. The zero-gauge pressure condition is applied for the outlet of the HTF. The standard wall function was used as the near-wall model for the realizable k-ε turbulence model, appropriate for the wall y+ values (≈30) in these simulations. The no-slip velocity and constant temperature conditions were applied at the heat exchanger wall.

5.5.3 Numerical Schemes, Grid Independency, and Model Validation

- Numerical Schemes and Grid Independency

Due to the similar setup conditions for the pre-processing process, the numerical schemes for all chapters are summarised and provided in "3.3.2 Numerical Schemes" under "Chapter 3 – Methodology section". Different grid sizes are performed for the grid refinement test to obtain accurate results. Figure 5.3 illustrates the average bed temperature during the absorption under different selected element numbers for each reactor configuration. It is important to highlight that the same meshing techniques are applied to all cases under the same structure of the HTF tube. Therefore, only two base cases for each HTF tube are chosen for the grid refinement test. The average temperature at three locations, including the reactor's top, middle, and bottom parts, is obtained to compare the results. The grid refinement test regarding the average temperature is provided in Figure 4.3a for the SCHE (case 1) and in Figure 4.3b for the SCHE-CR (case 3). From three selected locations, the average temperature is more stable and has minor change at 256,189 (for case 1) and 272,449 (for case 3) of the element numbers. Therefore, these grid sizes are chosen for further numerical simulations.

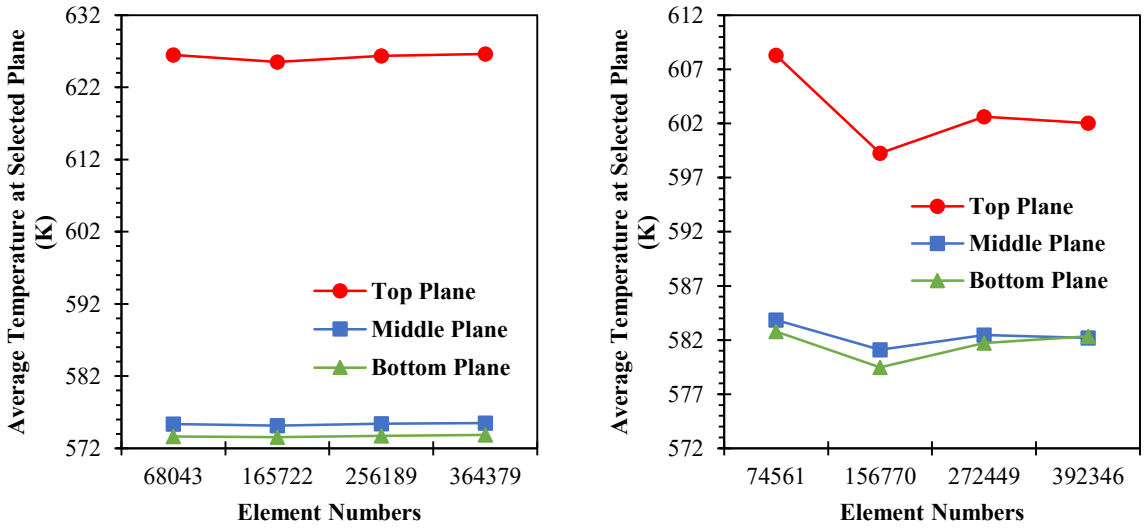

Figure 5.3 Average temperature for the hydrogen absorption in the MH storage system from different grid sizes. (a) average temperature at three selected planes for SCHE case and (b) average temperature at three selected planes for SCHE-CR case

- Model Validation

The model validations for the use of metal hydride storage system based on Mg_2Ni as well as the selection of turbulence model for the HTF are provided in "3.3.1 Model Validation" under "Chapter 3 – Methodology" section.

5.6 Results and Discussion

The numerical results for the heat transfer enhancement inside the storage system based on heat exchanger configuration designs are provided in this section. These also include the analysis of the effect of a tube diameter for a semi-cylindrical coil heat exchanger (SCHE) and a semi-cylindrical coil heat exchanger with a central return tube (SCHE-CR) on improving in heat transfer performance. The performance of SCHE and SCHE-CR is compared and presented as the absorption duration and the bed temperature inside the reactor. The best internal heat exchanger configuration case is then combined with a cooling jacket as an external heat exchanger for further heat transfer enhancement of the reactor. The operating conditions for the HTF with the best heat exchanger case are finally analysed and provided in the sensitivity analysis.

5.6.1 Geometrical Parameters

- Effect of Heat Exchanger Tube Diameter

The performance for SCHE and SCHE-CR is analysed based on two sizes of the HTF tube diameter. It is worth mentioning that the present study only focuses on the tube diameter at 3 mm and 4 mm. Greater tube diameter will reduce the MH volume, which is over 10% of volume reduction. The average bed temperature of a MH as well as hydrogen concentration during absorption process from SCHE and SCHE-CR are demonstrated in Figure 5.4. Figure 5.4a presents the average bed temperature (solid lines) and hydrogen concentration (dashed lines) for the SCHE and SCHE-CR based on the tube diameter at 3 mm, while Figure 5.4b is for the tube diameter at 4 mm. Case 1 and case 2 refer to SCHE with 3 mm and 4 mm of the tube diameter, respectively. Case 3 and case 4 are for SCHE-CR with 3 mm and 4 mm of tube diameter, respectively. The numerical simulation for these four cases was done based on a 573 K as the operating temperature of the system and 1.8 MPa as the hydrogen pressure. Initially, after the hydrogen firstly injected into the storage system, the temperature of the MH bed rapidly increases because of the interaction between the metal alloy and hydrogen, which is classified as an exothermic absorption process. The MH temperature slowly increases until reaching the maximum value. When the cooling fluid temperature becomes lower than MH bed temperature, the heat is then transferred from the MH bed to the cooling fluid. As a result, the MH bed temperature is then gradually decreased. The average bed temperature inside the storage system (refer to solid lines from Figure 5.4a, b) also supports this fact, as the bed temperature for all cases rapidly increases and continually decreases. It is important to highlight that the average bed temperature inside the system from this present study is calculated based on the area-weighted average temperature across the geometrical model. Comparing to the SCHE (case 1 and case 2), the average bed temperature from SCHE-CR (case 3 and 4) decreases faster than SCHE, especially from the case with 4 mm of the tube diameter. It is obvious that the cases with a 4 mm tube diameter obtain better heat transfer improvements in the system. This can be because increasing the tube diameter leads to having more HTF flowing throughout the heat exchanger tube. As a result, the heat exchange rate between cooling fluid and MH bed is improved.

For the hydrogen concentration, the amount of hydrogen absorption is always related to the MH bed temperature, as the surface of the metal alloy starts to absorb the hydrogen when the temperature of the MH reduces until reaching a certain temperature. This is due to the chemisorption, acceleration of physisorption, hydride formation in the system, and diffusion of hydrogen (Ardahaie et al., 2021). The effect of MH bed temperature on the hydrogen concentration is provided in Figure 5.4a for 3mm of tube diameter and Figure 5.4b for tube diameter at 4 mm. From this figure, faster hydrogen absorption is usually found in cases with a lower average bed temperature. A higher tube diameter of the HTF results in faster hydrogen absorption, as a larger tube diameter will obtain more heat transfer surface areas. From the cases with 3 mm of tube diameter, the absorption duration for SCHE (case 1) is 9481 s, while it is 6625 s for SCHE-CR (case 3). At 6625 s, the average bed temperature from SCHE-CR (case 3) is

586.19 K, while it is 596.97 K for SCHE (case 1). From the cases with 4 mm of tube diameter, the absorption duration for SCHE (case 2) is 6215 s, while there are 3910 s of the absorption duration from SCHE-CR (case 4). At 3910 s, the average bed temperature from SCHE-CR (case 4) is 589.58 K, while the average bed temperature from SCHE (case 2) is still 605.13 K.

Compared to a 3 mm tube diameter, the absorption duration for a 4 mm tube diameter decreases by 34% and 41% for SCHE and SCHE-CR, respectively. Furthermore, it can be seen that the absorption time greatly decreases in the SCHE-CR case compared to the SCHE case. For a tube diameter of 3 mm, the absorption duration reduces by 30% when using SCHE-CR (case 3) compared to SCHE (case 1). For a tube diameter of 4 mm, using SCHE-CR (case 4) as a heat exchanger results in a 37% reduction of absorption duration compared to SCHE (case 2).

Figure 5.4, shows that using SCHE-CR as an internal heat exchanger improves heat transfer inside the MH storage system compared to using SCHE. The faster the heat is removed from the storage system enables the faster hydrogen absorption, especially with the tube diameter at 4 mm of the HTF. Therefore, the cases with 4 mm of the HTF tube are considered for further analysis. These include case 2 for SCHE and case 4 for SCHE-CR.

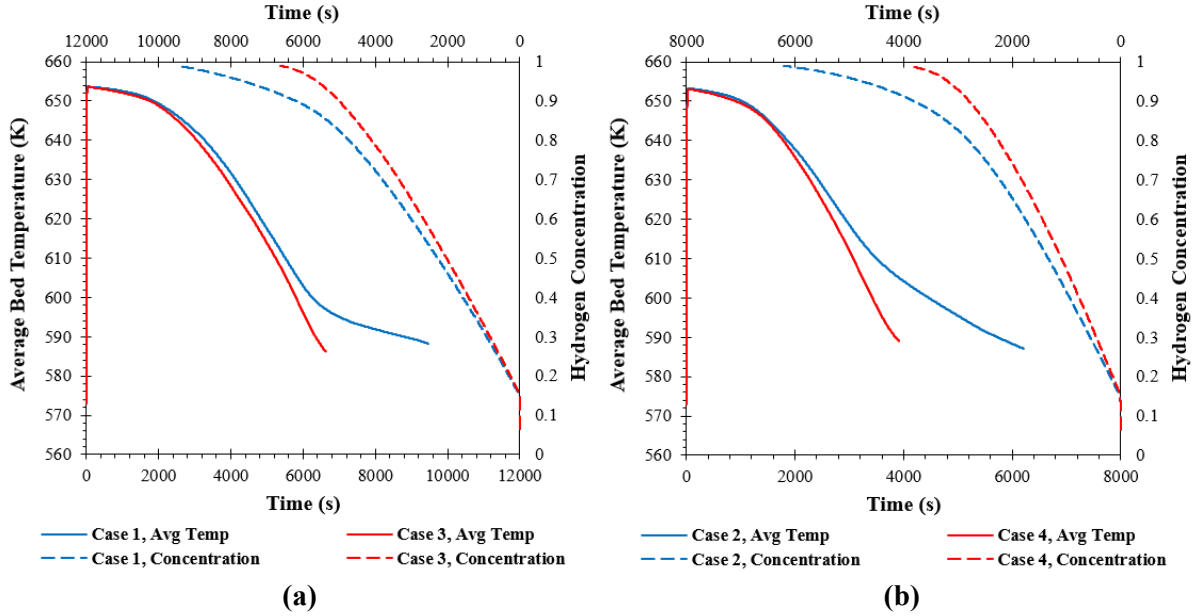

Figure 5.4 Average bed temperature and hydrogen concentration based on the variation of HTF tube diameters; (a) a 3 mm of tube diameter and (b) a 4 mm of tube diameter. (Blue colour refers to the SCHE case, while red colour refers to the SCHE-CR case; the solid line is for average bed temperature and the dashed line is for hydrogen concentration)

- Storage Performance Comparisons between Semi-Cylindrical Coil with and without Central Return Tube

The average temperature of the MH in a storage system and heat exchanger tube from SCHE and SCHE-CR is compared and presented in Figure 5.5. Only the cases with a 4 mm HTF tube diameter are selected in this section as this size obtains a better heat transfer performance when comparing to the cases with a 3 mm tube diameter. Case 2 refers to the reactor with SCHE, while case 4 refers to the reactor with SCHE-CR. The five selected times after starting the absorption process (250 s to 3500 s) are illustrated as the temperature contour. For SCHE (case 2), the HTF starts flowing from the bottom part and circulates through the tube to the outlet at the top of the storage system. The HTF starts flowing from the same location for SCHE-CR (case 4). However, due to the central return tube, both inlet and outlet of the HTF are in the same direction instead.

From Figure 5.5, it is obvious that the HTF temperature around the bottom part is always lower than the upper part because this part is first exposed to the reaction of the generated heat during the absorption process from the top surface of the storage system. In the beginning, the MH bed temperature rapidly increases when the hydrogen is first injected and is significantly higher than the HTF temperature because of the exothermic behaviour of hydrogen absorption. A high heat transfer rate is then generated due to this phenomenon. Therefore, the HTF temperature first increases and then gradually decreases, which leads to having conductive heat transfer between cooling fluid and MH. In addition, the lower MH bed area usually has a lower temperature because this part is close to the inlet area of the HTF. The temperature of the MH bed from both cases is found to be similar between times of 250 s and 1500 s. However, the temperature at the upper part of case 4 (SCHE-CR) is found to be lower than case 2 (SCHE) after 2500 s. Moreover, the bed temperature at the central area from SCHE-CR is lower than the SCHE after 2500 s. The difference in heat transfer performance between SCHE and SCHE-CR is because the central return tube from case 4 reduces the space between the MH and HTF. This leads to having more uniform temperature distribution and lower thermal resistance inside the storage system, especially at the centre of the MH bed.

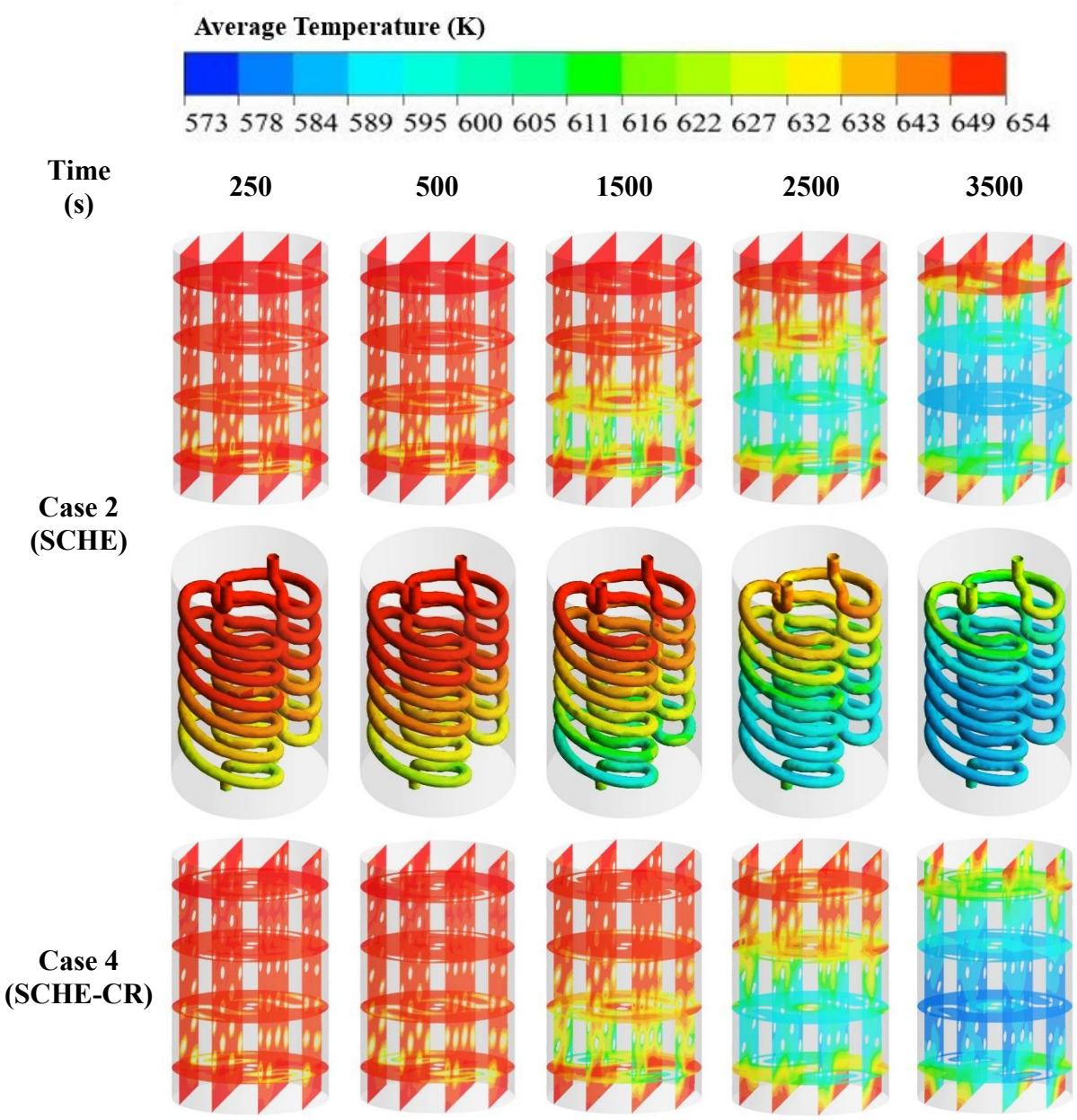

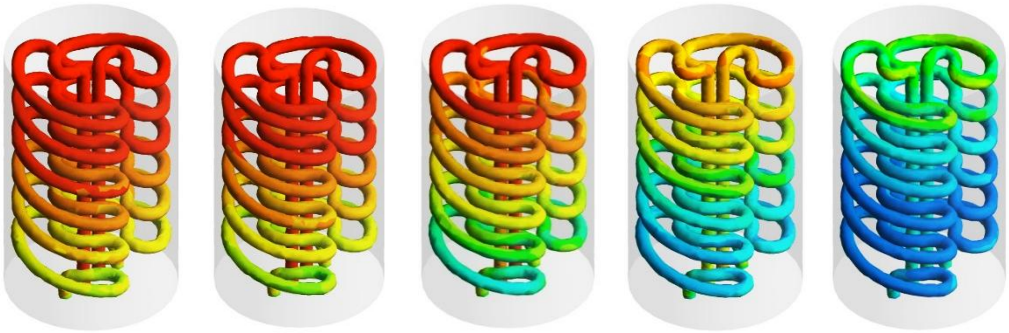

Figure 5.5 Average temperature of MH bed and heat exchanger tube at 250 s, 500 s, 1000 s, 2000 s, and 4000 s after starting hydrogen absorption process between SCHE and SCHE-CR

For more analysis, the heat transfer coefficient (HTC) and turbulence intensity on the surface of the HTF tube for both SCHE (case 2) and SCHE-CR (case 4) are compared and presented in Figure 5.6. Figure 5.6a demonstrates the HTC for both cases during the hydrogen absorption process. In general, the convective HTC refers to the heat transfer rate between a solid surface and a fluid per unit surface area per unit temperature difference (Bergman et al., 2011). A higher HTC means a higher heat transfer occurring. The complex HTF tube's structure is one of the key parameters to generate turbulent flow inside the HTF tube which results in the improvement of the heat transfer rate. In both cases, a higher HTC usually occurs at the curve of the HTF tube. Referring to Figure 5.6a, the HTC for both SCHE and SCHE-CR cases is similar (less than 423 W/m^2K). However, the higher HTC (423-504 W/m^2K) is found at the top area of the central return tube from SCHE-CR. The structure of the HTF tube from SCHE-CR can be one of the primary reasons causing the difference in heat transfer performance as well as temperature magnitude, especially at the central area and the top of MHHS (refer to Figure 5.5).

To clarify this point, the turbulence intensity on the HTF tube is performed and presented in Figure 5.6b. Turbulence intensity refers to the level of turbulent flow during inside the HTF tube. In general, a high-velocity magnitude will generate a turbulent flow which can be classified by the Reynolds number (Re). If the Re of the internal flow is higher than 4000, the fluid flow will be turbulent (Jin et al., 2013). As mentioned earlier in the mathematical model, the Re of the HTF velocity at the inlet for all cases is over 9000. The fluid flow inside the HTF tube is turbulent because of having the same tube diameter. Due to the new design of the SCHE-CR (case 4), which has the central return tube, the highest turbulence intensity at 11.89% (with the maximum velocity at 93.38 m/s) is found at the top of the return tube, which is the most complex part, while other parts are around 6.01-9.68%. However, the highest turbulence intensity from the SCHE (case 2) is found at 9.66% (with the maximum velocity at 83.68 m/s) only. When having a higher velocity, resulting in higher turbulence, the heat inside the MH bed will be transferred faster. This leads to a lower MH bed temperature (refer to Figure 5.5) at the upper part of the reactor for SCHE-CR (case 4) compared to SCHE (case 2).

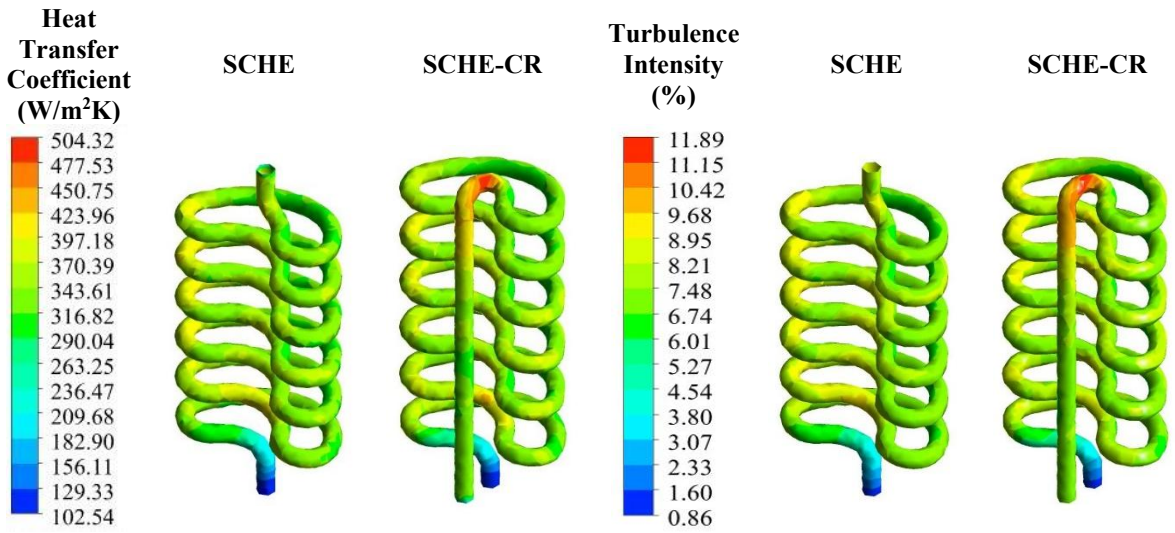

Figure 5.6 Comparison of the heat exchanger performance between the SCHE and SCHE-CR. (a) heat transfer coefficient at the surface of the HTF tube and (b) turbulence intensity on the HTF tube

The hydrogen concentration contours are displayed in Figure 5.7, which illustrates that hydrogen usually starts to be absorbed in the lower section of the reactor, which is close to the inlet area of the HTF. Furthermore, a higher hydrogen concentration is usually found around the HTF area. A lower hydrogen concentration is found at the centre of the MH bed from case 2 (SCHE), as this area is far away from the HTF. In contrast, having a central return tube for case 4 (SCHE-CR) results in higher hydrogen concentration at the central area, which is clearly seen after 2500 s. At 3500 s, the average hydrogen concentration rises up to 94% in most areas of the MH bed for both cases, except at the upper part of the reactor. Focusing on the upper part, the average concentration for case 4 (SCHE-CR) is totally higher than case 2 (SCHE). This can be explained by the reason that combining the SCHE with central return tube causes better heat transfer improvement at the central area, especially at the top part of central area. Due to lower MH bed temperature from SCHE-CR, the equilibrium pressure inside the MH bed is more declined, leading to faster hydrogen absorption.

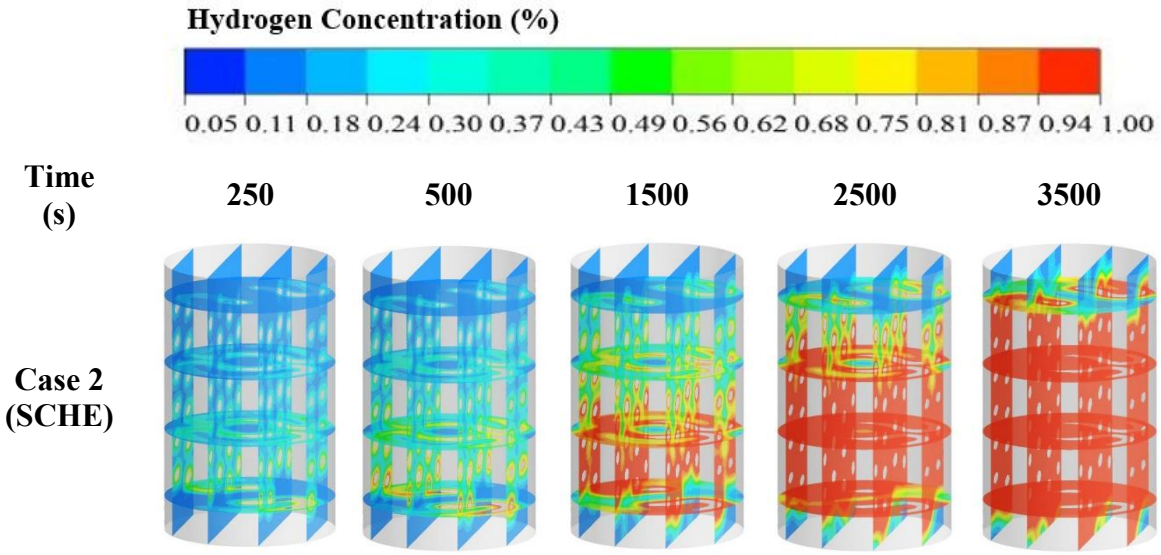

Case 4 (SCHE-CR)

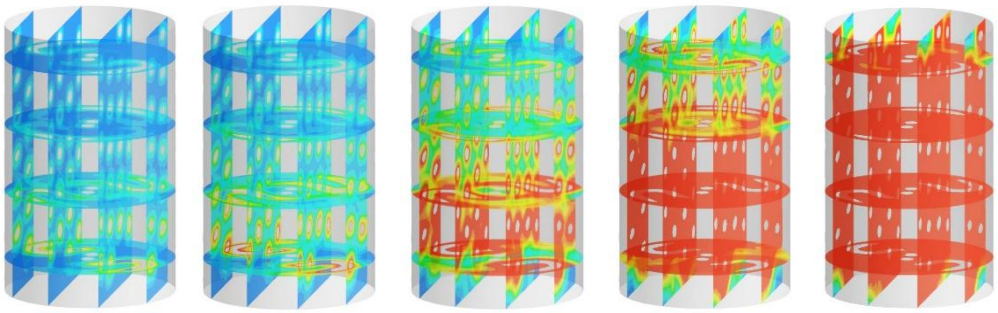

Figure 5.7 Hydrogen concentration at 250 s, 500 s, 1500 s, 2500 s, and 3500 s after starting hydrogen absorption between SCHE and SCHE-CR

The observation of MH volume and HTF tube volume based on various heat exchanger configurations corresponding to absorption duration is presented in Figure 5.8. From Figure 5.8a, the MH and HTF tube volumes from SCHE with 3 mm of tube diameter (case 1) are 148.44 cm^3 and 8.64 cm^3, respectively. When having a central return tube (SCHE-CR, case 3), the MH volume decreases only 0.67% (147.44 cm^3). However, when increasing the tube diameter from 3 mm to 4 mm (case 2 for SCHE and case 4 for SCHE-CR), the MH volume decreases by around 4.51% for the SCHE (from 148.44 cm^3 to 141.74 cm^3) and around 5.72% for the SCHE-CR (from 148.44 cm^3 to 139.36 cm^3). Focussing on the surface area of the HTF tube in Figure 5.8b, SCHE with 3 mm of the tube diameter (case 1) has a surface area of only 11539.28 mm^2, while having a central return tube (SCHE-CR, case 3) results in increasing in surface area to 12880.52 mm^2. When increasing the tube diameter from 3 mm to 4 mm (case 2 for SCHE and case 4 for SCHE-CR), the HTF tube surface area increases by around 25-33% for both heat exchangers (from 11539.28 mm^2 to 15398.76 mm^2 for SCHE and from 12880.52 mm^2 to 17184.78 mm^2 for SCHE-CR). It is obvious that a greater HTF tube surface area obtains a greater heat transfer surface area. Furthermore, the absorption duration for all cases is summarised as the percentage and provided in Figure 5.8c. The percentage calculation in this figure is performed based on the absorption duration from SCHE with a 3 mm tube diameter (case 1). From this figure, the absorption duration significantly reduces, corresponding to an increase in the surface area of the HTF. For the tube diameter at 3 mm, the absorption duration is reduced by 30.12%, with the central return tube (SCHE-CR, case 3) in comparison to the SCHE case (considered as the base case). With the tube diameter at 4 mm (case 2 for SCHE and case 4 for SCHE-CR), the absorption duration reduces by 34.45% for SCHE and 58.76% for SCHE-CR in comparison to the base case (SCHE with 3 mm tube diameter). It is obvious that SCHE-CR, with a tube diameter of 4 mm (case 4), obtains the best performance with a reduction of 58.76% in absorption duration by reducing the MH volume by 5.72% only. Therefore, this heat exchanger configuration (case 4) is selected for further investigation regarding the combination of two heat exchanger techniques and sensitivity analysis. It is important to highlight that increasing in tube diameter of the HTF, which is greater than 4 mm, will reduce the MH volume that will be over 10%. To clarify, if the tube diameter of the HTF is 5 mm, the tube volume will be 24 cm^3 and 27.42 cm^2 for SCHE and SCHE-CR, respectively. This leads to the reduction of the MH volume from 148.44 cm^3 (based on the tube diameter at 3 mm for the SCHE case) to 124.44 cm^3 and 121.02 cm^3 for the tube diameter at 5 mm of SCHE and SCHE-CR, respectively. This results in having around 17-19% reduction of MH volume. Therefore, the other higher sizes of the HTF tube diameter are not considered in the present study.

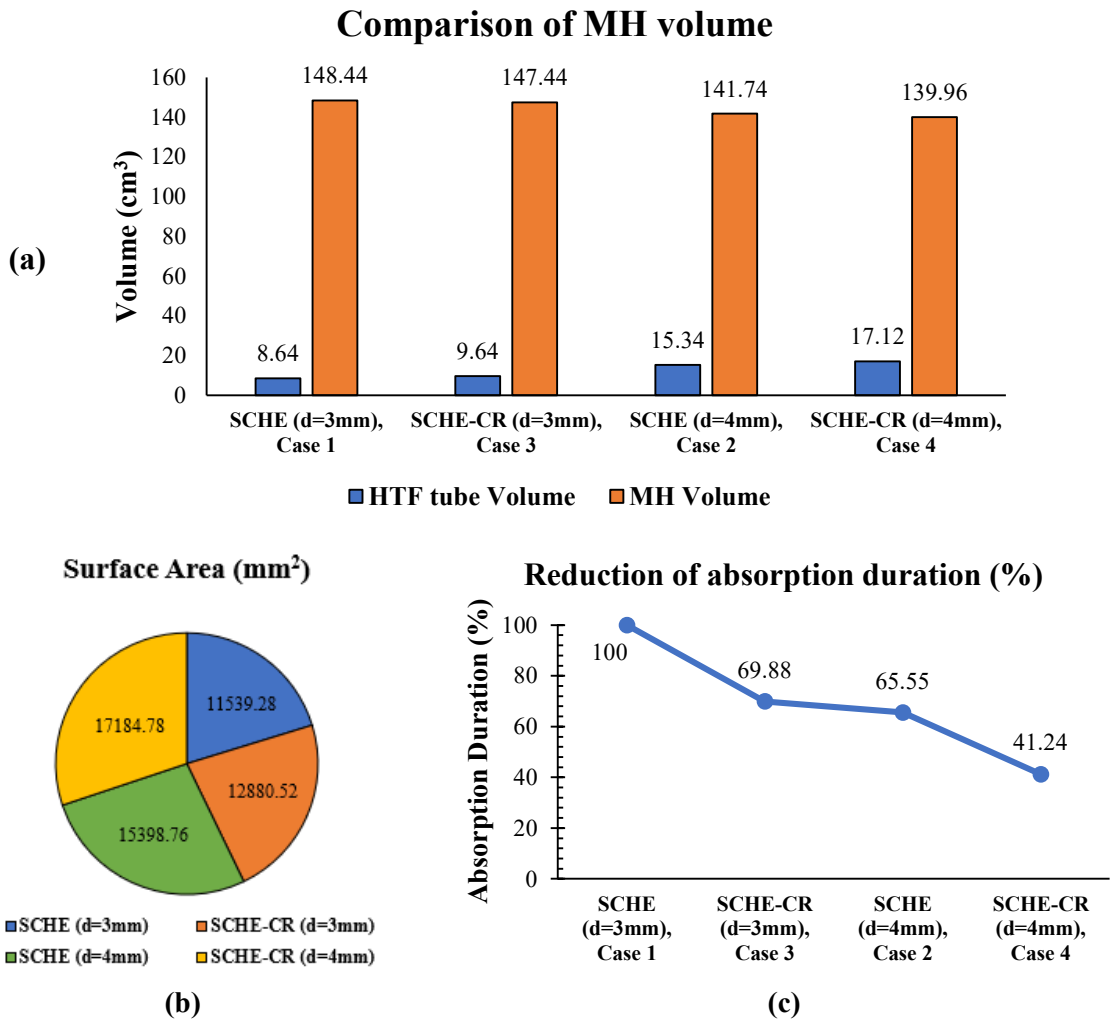

Figure 5.8 Comparison of MH and HTF tube volume on the hydrogen absorption duration for all four cases. (a) comparison of MH volume, (b) surface area of the HTF tube, and (c) reduction of absorption duration

- *Combination of Internal and External Heat Exchangers*

To improve the MH reactor performance, an outer cooling jacket is used and incorporated with the inner SCHE-CR. The proposed MH reactor configuration was performed under a 573 K as the operating temperature of the system and a 1.8 MPa as the hydrogen pressure. The HTC between the MH and cooling fluid of the cooling jacket was 250 W/m^{2}K. The schematic diagram of the proposed MH storage system with SCHE-CR and the cooling jacket is presented in Figure 5.9a. The MH reactor's performance for SCHE-CR with the cooling jacket is compared to SCHE (case 2) and SCHE-CR (case 4) based on the HTF tube diameter of 4 mm. Furthermore, the additional case with helical coil heat exchanger (HCHE) is also performed for the comparison of the MH reactor performance. It is worth mentioning that the HTF tube diameter of the HCHE case is fixed at 4 mm with the constant of the tube volume. From Figure 5.9b, the average bed temperature from this figure indicates that using a cooling jacket with SCHE-CR significantly improves the heat transfer performance as the average bed temperature significantly reduces faster than in the other cases, especially for the case with HCHE. Faster temperature reduction of the MH bed leads to faster absorption reaction (Figure 5.9c). The average bed temperature from the case with HCHE is still higher than 600 K at 6000 s, while the average bed temperature from the other cases is lower than 590 K with less charging time. This leads to slower hydrogen absorption as there is only around 86% of the hydrogen concentration at 6000 s for the reactor with HCHE. Compared to the reactor with SCHE, the case with a central return tube (SCHE-CR) has

better heat transfer improvement, which results in a 37% reduction in absorption duration. The absorption duration reduces from 6215 s to 3910 s in the SCHE-CR case. However, using SCHE-CR with a cooling jacket results in a 51% reduction of absorption duration compared to SCHE-CR only. The absorption duration reduces from 3910 s to 1928 s. It should be noted that the absorption duration for the SCHE with the cooling jacket is 2692 s which is still higher than 2000 s. Therefore, it is evident that using SCHE-CR incorporating a cooling jacket significantly enhances the MH reactor performance for an absorption time that is lower than 2000 s. The effect of the HTC of the outer cooling jacket on the MH reactor performance is then further investigated in the sensitivity analysis section.

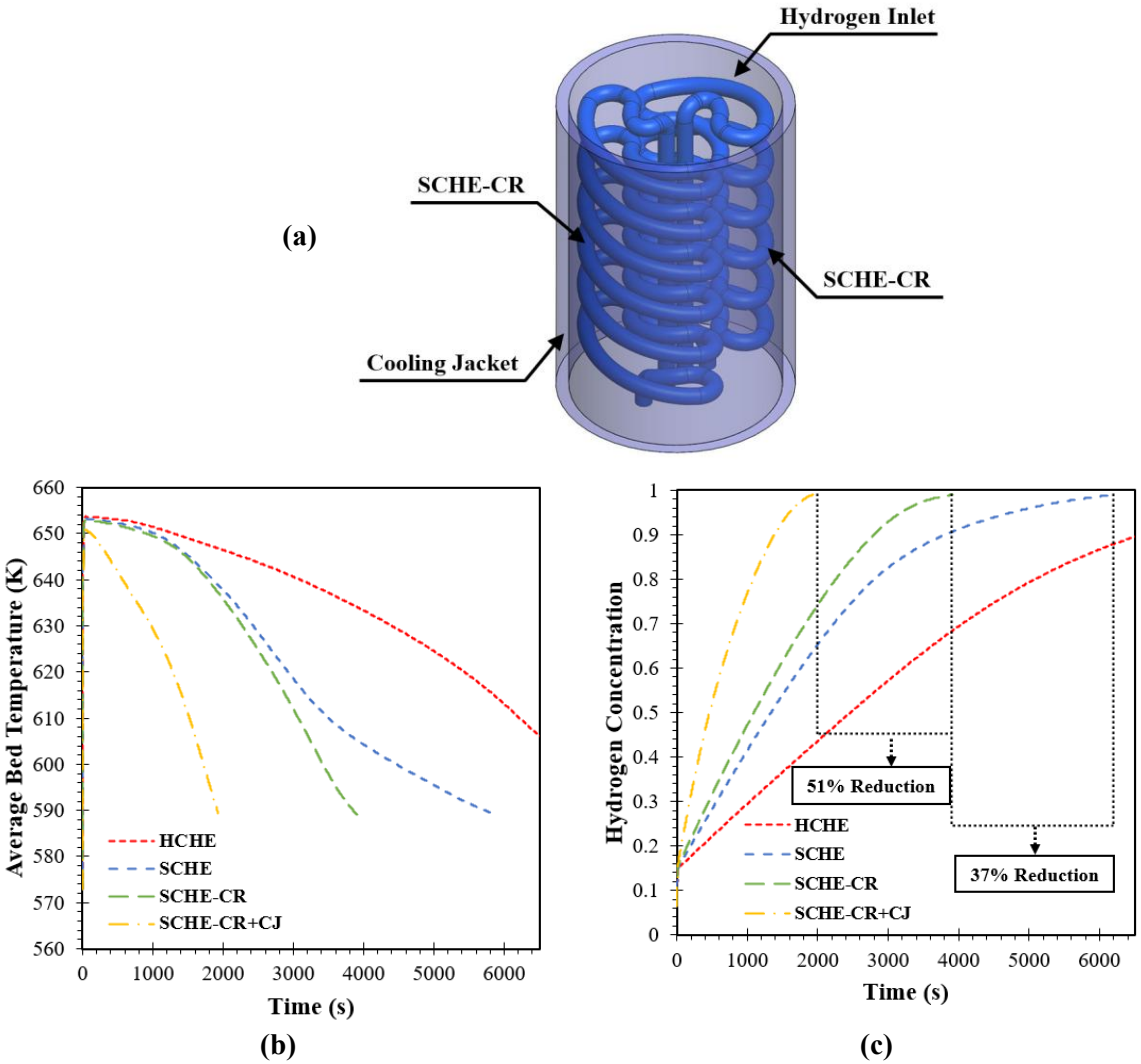

Figure 5.9 Comparison of hydrogen concentration from different hydrogen reactor configurations. (a) characteristic of MH reactors with SCHE-CR + cooling jacket (SCHE-CR+CJ), (b) average bed temperature, and (c) hydrogen concentration

5.6.2 Sensitivity Analysis

The operating conditions are the key factors that might positively or negatively affect the MHHS performance during the reaction process. To determine appropriate values of operating conditions of the HTF with the new heat exchanger that can be used with the MH reactor, the sensitivity analysis in this section is investigated by using the best configuration case from SCHE-CR with a 4 mm tube diameter. This looks at the absorption performance by considering the Re and HTF inlet temperature. For more analysis, the effect of the Re of the HTF on the turbulence intensity, turbulence kinetic energy and the HTC of the HTF tube is investigated. The effect of the HTC on the absorption performance is considered for the cooling jacket case only.

- *Operating Conditions of the Heat Transfer Fluid for Semi-Cylindrical Coil with Central Return Tube*

The HTF velocity can be considered as one of the main parameters for the hydrogen absorption/desorption process, as it can impact the turbulence and heat removal during the absorption/desorption process (Wang et al., 2021). A turbulent stage can be generated from a high-velocity flow rate, resulting in a faster HTF flow during circulating inside the HTF tube. Therefore, a faster heat transfer rate will occur due to this reaction. Four inlet velocities of the HTF from this study are obtained under the four selected values of the Re at 6400, 9000, 11700, and 14500. The operating temperature of the HTF and storage system is set at 573 K with a supply pressure of 1.8 MPa. The results of the hydrogen absorption duration from various selected values of the Re are presented in Figure 5.10a. From this figure, it is obvious that higher Re results in faster hydrogen absorption duration. At the end of the absorption process (100% absorption), the absorption duration from the Re at 6400 is 5146 s, while it is 3910 s for the absorption duration with the Re at 9000. The durations are 3262 s and 2873 s for the absorption with the Re at 11700 and 14500, respectively. There is a 24% reduction in the absorption duration when increases the Re from 6400 to 9000. However, there are only 17% and 12% reductions in the absorption duration when increasing the Re from 9000 to 11700 and from 11700 to 14500, respectively.

The operating temperature of the HTF also plays an essential role in reducing absorption duration, as during the absorption, a higher heat removal rate will be occurred with a lower HTF temperature. The greater the temperature difference between the MH bed and cooling fluid leads to the greater the convective heat transfer rate. In other words, a large temperature difference will lead to a large amount of heat energy, which will transfer from the MH bed to HTF. Four initial temperatures of the HTF are selected to study the heat transfer improvement for the new heat exchanger (SCHE-CR) under the constant initial conditions with a 573 K as the MH temperature and a 1.8 MPa as the hydrogen pressure. All results of the hydrogen absorption duration from several initial temperatures of the HTF (varying from 423 K to 573 K) are presented in Figure 5.10b. Referring to Figure 5.10b, it is obvious that the reduction of HTF temperature leads to the reduction of hydrogen absorption time. The final time at the end of the hydrogen absorption process by using 573 K as the HTF temperature is 3910 s, while it is 2503 s for the case with 523 K as the HTF temperature. There is a 36% reduction in the hydrogen absorption duration in these two cases. The absorption time at the final process for 473 K and 423 K HTF temperature is 1882 s and 1531 s, respectively. Therefore, when reducing the HTF temperature from 523 K to 473 K and from 473 K to 423 K, there are 25% and 19% reductions in the absorption time, respectively. It is evident that the temperature of a cooling fluid has a greater effect on the absorption reaction rather than the Re.

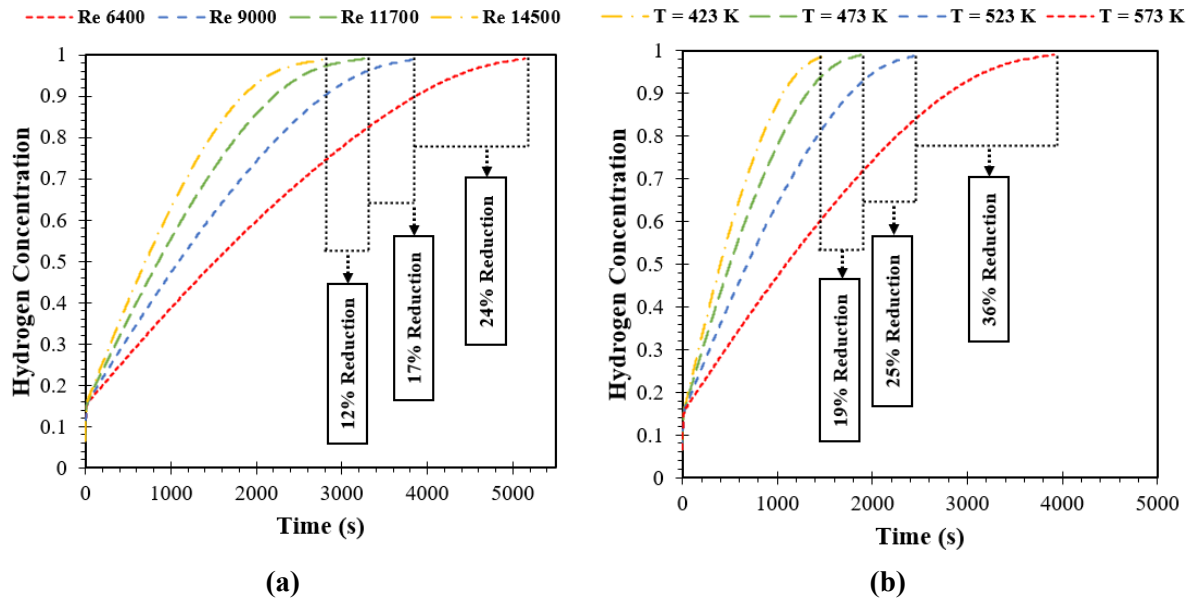

Figure 5.10 Hydrogen concentration for different operating conditions of the HTF in the case with SCHE-CR. (a) Reynolds numbers and (b) initial temperatures of the HTF

The velocity magnitude along the HTF tube for different values of the Re on the z-axis is presented in Figure 5.11. Referring to this figure, a higher velocity generally locates at the curve area of the heat exchanger tube for all four cases. Due to the complex structure at the top area of the central return tube, the maximum velocity magnitude for each Re case is found around this area. A higher Re significantly generates a higher flow velocity in this area. The maximum velocity at this area for the Re at 6400 and 9000 is 50.32 m/s and 70.52 m/s, respectively. For the cases with the selected values of the Re at 11700 and 14500, the maximum velocity at this area is 91.62 m/s and 113.53 m/s, respectively. This is the reason for the higher turbulence intensity that is usually observed in this area.

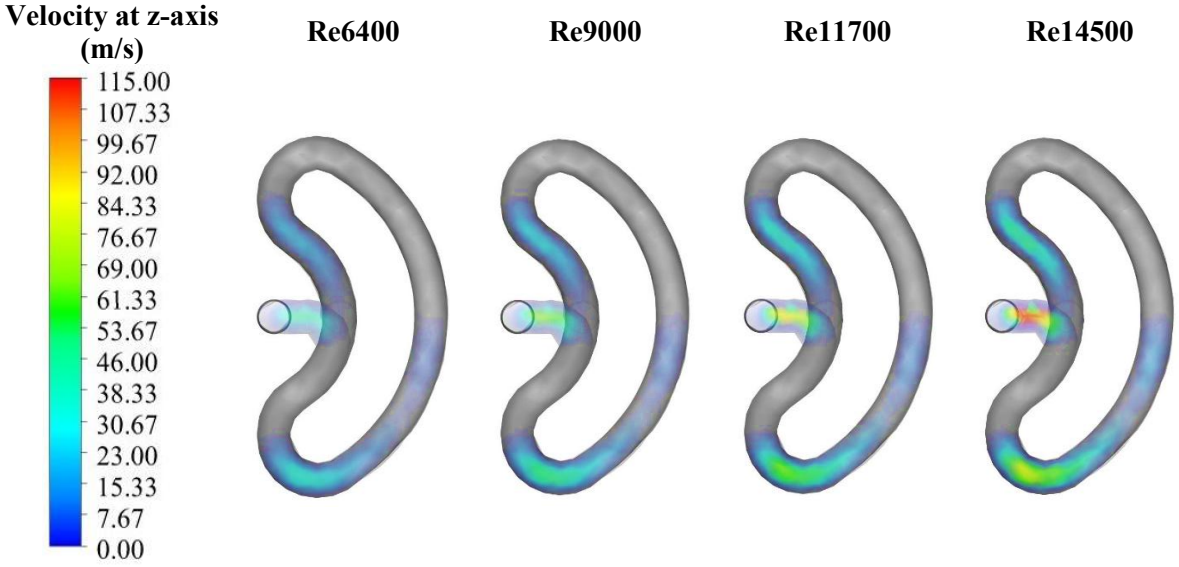

Figure 5.11 Velocity flow in the HTF tube at z-axis (top view) for different Reynolds numbers of HTF

The level of turbulence is usually presented as turbulence intensity which can be measured by the intensity of the flow fluctuations. To understand the relationship between the fluid flow and turbulent intensity of the new heat exchanger (SCHE-CR), turbulence intensity based on various flow velocities is presented as the contours in Figure 5.12 According to this figure, a higher Re causes higher turbulence intensity of the HTF tube, especially at the central return tube area. Turbulence intensity is usually lower

at the inlet area of the HTF tube in all cases. Higher turbulence intensity is usually found at the top area of the return tube, which is considered as the most complex part of the SCHE-CR structure for all cases.

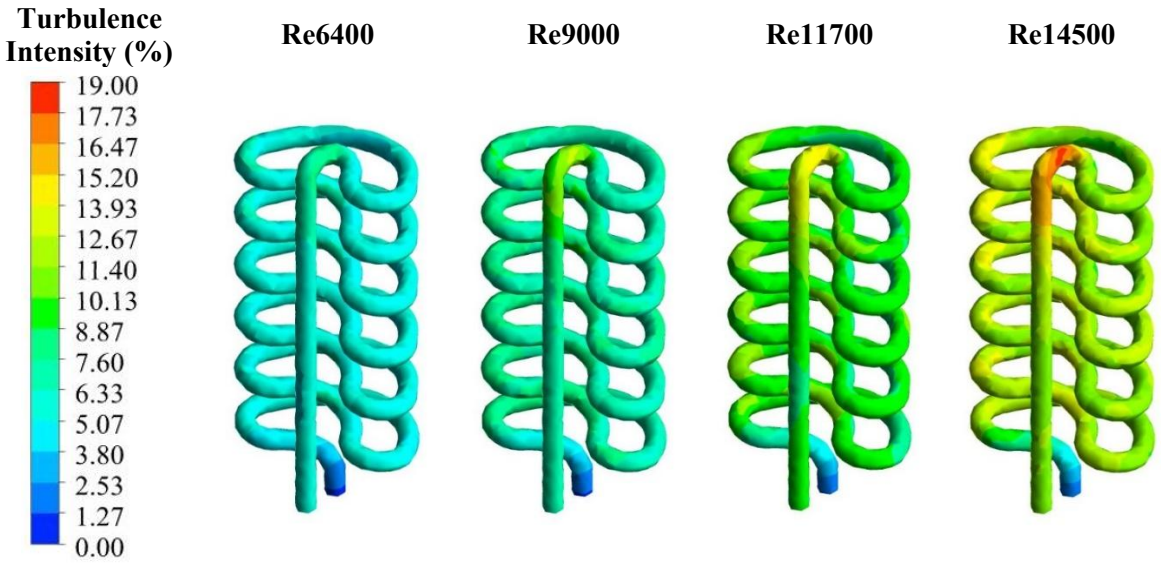

Figure 5.12 Turbulence intensity on the HTF tube for different Reynolds numbers

It should be noted that the turbulence intensity shown near the wall in Figure 5.6 (b) and Figure 5.12 reflects the near-wall region, not the exact wall surface. These values result from post-processing based on turbulent kinetic energy and local velocity in the first adjacent cell. The elevated turbulence intensity is due to physical boundary layer interactions and numerical representation, particularly in regions with strong turbulence near the wall.

The average turbulent kinetic energy across the flow domain and average HTC on the surface of the HTF tube are collected under various selected values of the Re and presented in Figure 5.13. The turbulent kinetic energy refers to the mean kinetic energy per unit mass for a turbulent flow. It is normally used to measure the intensity of turbulence in a flow. Focussing on the average turbulent kinetic energy from Figure 5.13a, the case with Re at 6400 generates the average turbulent kinetic energy at 47.43 m^2/s^2, while it is 87.28 m^2/s^2 when increases the Re from 6400 to 9000. The average turbulent kinetic energy from Re at 11700 and Re at 14500 is 140.64 m^2/s^2 and 208.00 m^2/s^2, respectively. It can be seen that the average turbulent kinetic energy increases by 46% when increases the Re from 6400 to 9000. However, there are around 37% and 32% improvements in average turbulent kinetic energy when increases the Re from 9000 to 11700 and from 11700 to 14500, respectively. In some cases, there could be oscillations due to the high-speed flow of the HTF and the design of the HTF tube. In general, the oscillations can influence the heat and mass transfer characteristics (Schlichting 1979; Claman & Minton 1977). Increasing the pitch and curvature ratio of the helical coil, as well as the Re result in an increase in the oscillation phenomenon (Lin & Ebadian 1997). Therefore, the change of oscillations can increase the heat and mass transfer rates (Schlichting 1979; Claman & Minton 1977). However, in some cases, these changes can also induce flow instabilities in equipment due to the fluctuation flow and pressure drop (Pendyala et al., 2008).

The average HTC on the surface of the HTF is presented in Figure 5.13b to support the discussion of the effect of Re on the heat transfer improvement. As mentioned earlier, a higher turbulent level of fluid flow results in a higher heat transfer rate which leads to a higher HTC. The average HTC from the Re at 6400 is 265.65 W/m^2K, while it is 336.40 for the Re at 9000. The average HTC from the cases with Re at 11700 and 14500 is 405.85 W/m^2K and 474.31 W/m^2K, respectively. There is a 21% improvement

in average HTC when increases the Re from 6400 to 9000. However, there are around 17% and 14% improvements when increasing the Re from 9000 to 11700 and from 11700 to 14500, respectively.

From Figure 5.13, it is obvious that there is a 46% improvement in average turbulent kinetic energy and a 21% improvement in average HTC on the surface of the HTF tube when increasing the Re from 6400 to 9000. However, there is less than a 38% improvement in average turbulent kinetic energy and a 18% improvement in average HTC when using other higher values of Re. This leads to the reduction of hydrogen absorption duration (refer to Figure 5.10a), which is around 24% reduction when increases the Re from 6400 to 9000. The reduction of absorption durations from other higher values of Re is less than 18%. Therefore, using the Re at 9000 for the HTF is recommended for the present storage system with SCHE-CR.

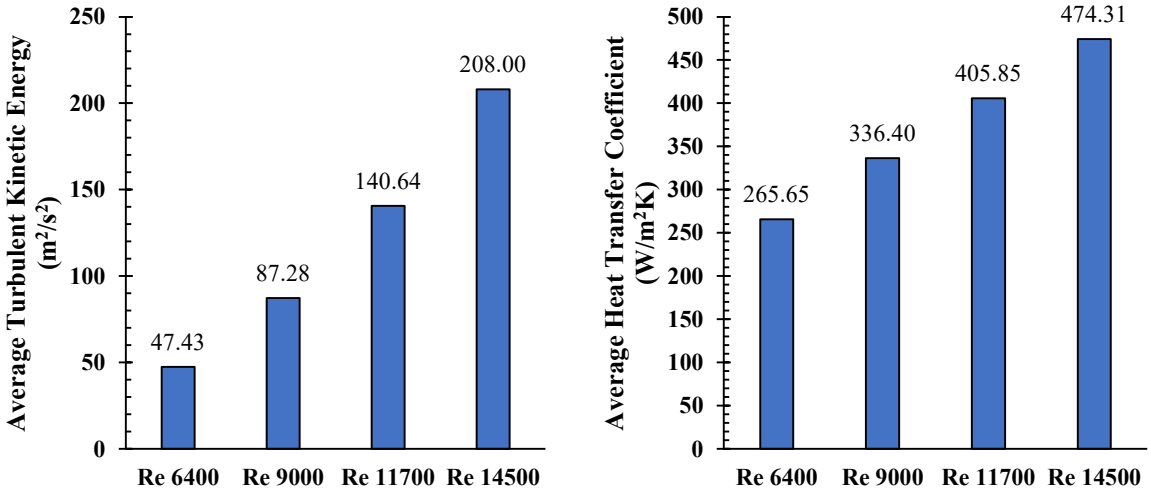

Figure 5.13 Effect of Reynolds number on; (a) average turbulent kinetic energy and (b) average heat transfer coefficient on the surface of the HTF tube

- *Heat Transfer Coefficient of the Cooling Jacket on the Hydrogen Absorption Process*

The relationship between both MH bed and fluid for heat transfer efficiency can be determined directly through the convection HTC (Corre et al., 1998). Thus, four different HTCs, including 250, 500, 750, and 1000 W/m^{2}K are selected to investigate the cooling jacket performance (with the storage system incorporating SCHE-CR as the inner heat exchanger). The calculation is performed under the constant operating temperature of 573 K for the MH bed and HTF with 1.8 MPa as hydrogen loading pressure. The results from these four cases are provided in Figure 5.14 as the hydrogen concentration (Figure 5.14a) and absorption duration (Figure 5.14b). The percentage from Figure 5.14b is obtained by the hydrogen absorption duration from the case with the HTC at 250 W/m^{2}K. From Figure 5.14a, b, it is clear that increasing the HTC from 250 W/m^{2}K to 500 W/m^{2}K reduces the hydrogen absorption time by approximately 8%. However, the larger value of HTC (over 500 W/m^{2}K) has less effect on the absorption duration. There are only 3% and 1% reductions in hydrogen absorption duration when using the HTC of 750 W/m^{2}K and 1000 W/m^{2}K, respectively. Therefore, using the HTC between the cooling jacket and the MH bed (with SCHE-CR) at 500 W/m^{2}K is recommended in the present study.

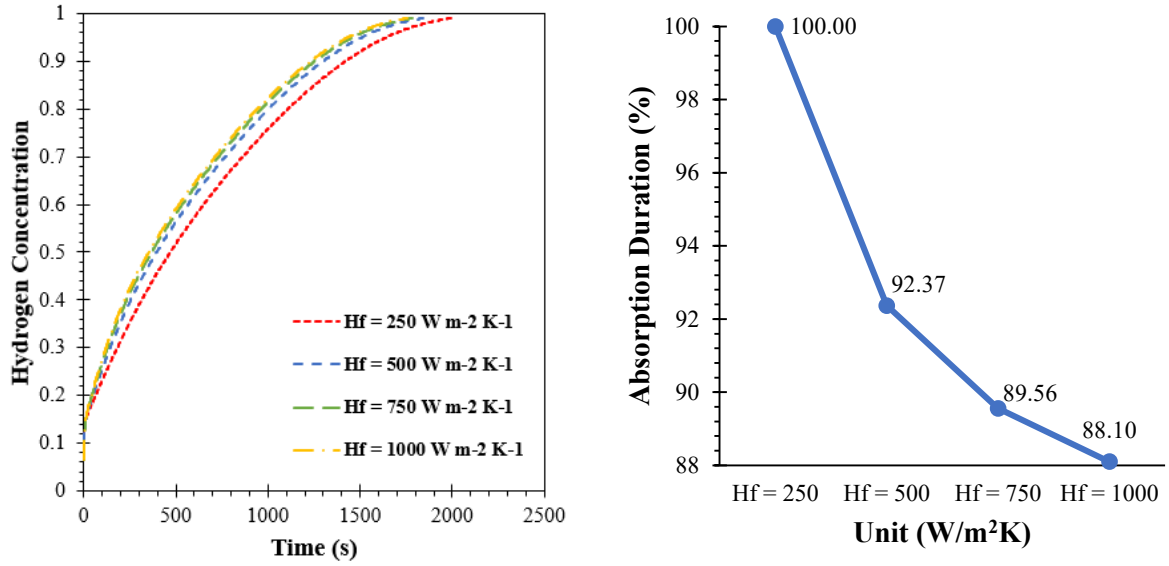

(a) **(b)**

Figure 5.14 Hydrogen concentration diagram at different heat transfer coefficients of the cooling jacket. (a) hydrogen concentration, and (b) absorption duration

5.7 Conclusion

A novel semi-cylindrical coil with a return tube is designed and evaluated to improve the storage performance, especially in the central area of the storage system. This new heat exchanger configuration is developed from the semi-cylindrical coil for using with the metal hydride storage system. Under the new proposed storage system, the tube diameters and operating conditions of the heat exchanger are analysed by considering the absorption reaction performance. The following points are the key findings:

- The heat transfer performance inside the storage system is improved when utilising a semi-cylindrical coil incorporating a central return tube as this obtains more uniform heat distribution in the metal hydride system, especially in the central area of the upper part of the reactor. The duration of the absorption reaction is decreased by 30% with a return tube compared to without having a return tube.
- Using a larger tube size of the heat exchanger significantly reduces the hydrogen absorption duration due to having more heat transfer surface area. The absorption time for the case with a return tube is reduced by 40% when increasing the tube diameter from 3 mm to 4 mm.
- Incorporating the new inner heat exchanger with an outer cooling jacket reduces the absorption time by 51% in comparison to the reactor with a return tube only.
- The operating conditions of the heat transfer fluid for this new heat exchanger are the key factors that significantly influence the metal hydride storage system performance. Considering the effect of average turbulence kinetic energy and average heat transfer coefficient of the new heat exchanger, as well as the absorption reaction (24% of reduction), the Reynolds number of heat transfer fluid at 9000 is recommended for the present study. The absorption time is decreased by 19-36% when changing the cooling fluid temperature between 523 K and 423 K.
- The heat transfer coefficient between the cooling jacket and metal hydride has less effect on the absorption reaction. There is only an 8% improvement in the absorption reaction when increasing the heat transfer coefficient from 250 W/m^{2}K to 500 W/m^{2}K. Other higher values improve the absorption reaction by only 1-3%.

The comprehensive numerical simulation from this study provides a better understanding of heat transfer enhancement for accelerating the absorption reaction of a hydrogen storage system that is

incorporated with the new heat exchanger configuration under the selection of appropriate operating conditions. The results from this study prove that using the new heat exchanger, improves the storage performance regarding the heat transfer performance and hydrogen absorption reaction. Moreover, combining the new heat exchanger type with the cooling jacket as an external heat exchanger significantly improves the storage performance. Further studies will be focused on the effect of this new heat exchanger configuration on the desorption process as well as the effect of this heat exchanger on the oscillations. Furthermore, the next study will also consider the combination of other heat exchanger techniques with the present heat exchanger configuration to improve the performance of metal hydride storage systems. Further experimental work will be performed to support the numerical results of the present study.

Chapter 6 – Investigation of Metal Hydride Hydrogen Storage Performance using Phase Change Materials

Research Paper: **Larpruenrudee, P.,** Bennett, N.S., Fitch, R., Sauret, E., Gu, Y., & Islam, M.S., (2024). Investigation of metal hydride hydrogen storage performance using phase change materials. **International Journal of Hydrogen Energy**, 60, 996-1019. https://doi.org/10.1016/j.ijhydene.2024.02.057. **SJR:1.318 [Q1], IF: 7.2**

6.1 Summary

Objectives to achieve the aim of this study:

- Further enhance the thermal performance of the storage and heat exchanger by combining the new internal heat exchanger from Chapter 5 (Research Paper 2) with the external heat exchanger under a passive thermal management technique
- Identify an appropriate initial value of each operating parameter under the new storage configuration and heat exchanger

Achievements and innovations in this chapter:

- Investigate the previous heat exchanger performances from first two chapters (Chapter 4 and Chapter 5) on the hydrogen desorption process, and one complete hydrogen absorption-desorption cycle
- further enhance the thermal performance of the storage and heat exchanger by considering the design of the new storage configuration from the combination of various heat exchanger types, including internal heat exchanger and phase change material as the external heat exchanger.
- Analyse the effect of storage weight from phase change materials on the heat recovery
- Investigate the initial temperature of the heat transfer fluid based on the new storage configuration and heat exchanger for both hydrogen absorption and desorption processes

6.2 Abstract

Metal hydride storage system (MHHS) has been widely used mostly because of its large storage capacity and high degree of safety. The improvement of the heat transfer performance is one of possible techniques to enhance the overall MHHS performance. The well arrangement of the heat exchanger structure from a semi-cylindrical coil heat exchanger with central return tube (SCHE-CR) significantly reduces the hydrogen absorption duration. However, the modelling of the thermal behaviour for the SCHE-CR during desorption process is missing in the literature. Therefore, this study aims to develop a model for both hydrogen absorption and desorption processes and analyse the thermal performance during the cycle. Phase change material (PCM) is incorporated with the heat exchanger for further improvement of the MHHS performance. The storage is designed under three different PCM configurations, including PCM jacket, pool bed, and capsule. The numerical results report that the duration of the absorption-desorption cycle is reduced by over 50% when using SCHE-CR instead of a helical coil. The PCM configurations, especially the PCM capsule, increase the MHHS performance, especially during the absorption. The duration of one cycle is decreased by at least 39% when combining the SCHE-CR with PCM. The HTF temperature significantly affects the MHHS performance, especially during the desorption. Reduction in HTF temperature reduces the absorption duration by at least 15%, while increasing the HTF temperature reduces the desorption duration by at least 25%. The new MHHS configuration would be beneficial to enhance the heat exchange during the absorption-desorption cycle of industrial MHHS applications.

Keywords: Hydrogen absorption, Hydrogen desorption, Semi-cylindrical coil, Reaction time, Phase change materials.

6.2.1 Graphical Abstract

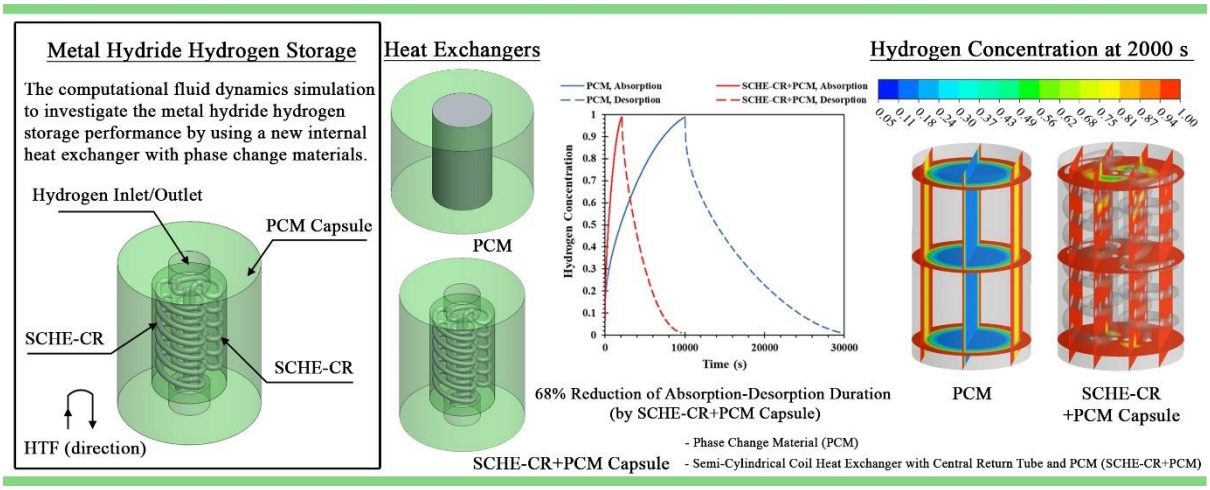

Figure 6.1 Graphical abstract for the third research paper

6.3 Introduction

Renewable energies have been used instead of fossil fuels to reduce global warming and large-scale shifts in weather patterns (Musharavati & Khanmohammadi 2022). Hydrogen energy is one of the renewable energies which has been applied in several fields. Basically, hydrogen can be produced by hydrocarbon reforming (Luts et al., 2004; Koroneos et al., 2004). However, the production processes based on this technique are not environmentally friendly. One of the alternative ways to produce hydrogen is to be produced from the water by virtue of electrolysis (Ni et al., 2008). In general, the hydrogen can be produced from the electrolyser based on given inputs. The metal hydride storage is then stored the hydrogen from this electrolyser. The only one input of the fuel cell to generate the electricity is the hydrogen from the metal hydride storage (Bhogilla et al., 2024). Among fuel cells, PEM fuel cell has been widely used for both mobile and stationary power generation applications. This is due to its advantages that offer low operating temperature, higher efficiency, low start-up time, longer life, and high power density (Bhogilla et al., 2024). Several studies have recently focused on the possibility and efficiency improvement when integrating the PEM fuel cells with metal hydride storage (Omrani et al., 2020; Førde et al., 2009; Khaitan & Raju 2012).

For the metal hydride storage system (MHHS), it is known as one of the cost-effective hydrogen storage systems which has been applied to several applications, including fuel cells (Yao et al., 2020b; Gambini et al., 2019), concentrating solar thermal power or CSP (Paskevicius et al., 2015; Malleswararao et al., 2020; Corgnale et al., 2014), and water pumping systems (Askri et al., 2019; Miled et al., 2017). However, one of the main problems of MHHS is that the metal hydride (MH) materials usually have a low thermal conductivity which leads to slow hydrogen kinetic reaction. Therefore, several thermal management methods have been used to solve this problem. Employing the external/internal heat exchanger is one of active thermal management methods that require the heat transfer fluid (HTF) to transfer the heat. These include internal straight tube (Raju & Kumar 2011; Bhouri et al., 2015; Kumar et al., 2019), helical/spiral coil tube (Wang et al., 2012; Mellouli et al., 2007; Dong et al., 2017; Eisapour et al., 2021a; Wang et al., 2020), and semi-cylindrical coil tube (Larpruenrudee et al., 2022a, b). Among internal heat exchangers, using helical/spiral coil tube obtains better heat transfer improvement than other types due to increasing heat transfer surface area from the secondary circulation (Wu et al., 2014; Fernández et al., 2018). The study from Wu et al. (2016) indicated that the average reaction conversion from the MHHS with helical coil tube reached 40% within 4000 s, while the average reaction conversion from the case with straight tube was still less than 40% at 10000s. Semi-cylindrical coil tube shows more heat transfer improvement, resulting in a 59% reduction of hydrogen absorption duration, compared to helical coil tube (Larpruenrudee et al., 2022a, b). This is because the well arrangement of HTF tube's structure provides more uniform temperature distribution as well as higher turbulence level of the HTF. The semi-cylindrical coil tube was then developed to improve the heat transfer at the centre of the MH bed by incorporating with the central return tube (Larpruenrudee et al., 2023). The comparison between the semi-cylindrical coil tube with and without central return tube indicated that having a central return tube increase the heat transfer mechanism inside the MH bed, especially at the centre of the MH bed, resulting in a 30% reduction of the hydrogen absorption duration for 3 mm of the tube diameter and a 37% reduction of absorption duration for 4 mm of the tube diameter.

The use of phase change materials (PCMs) is well known as one of the passive thermal management techniques that do not require additional energy (i.e. HTF) to cool down or heat up the system. The main advantages of PCMs are their ability to offer a high storage density, constant temperature during the phase change, as well as low pressure drop during heat recovery (Ardahaie et al., 2021). PCMs have been widely used for several thermal energy storage applications for both sensible and latent heat storages such as ventilation systems, hot water tanks, and net zero energy buildings. Furthermore, PCMs

are also applied for MHHS to recover the waste heat during the hydrogen sorption. In general, PCMs will absorb the generated heat during the hydrogen absorption and release it as the supply heat during the hydrogen desorption (Cui et al., 2022). These processes will result in the improvement of hydrogen kinetic reaction and finally lead to the reduction of hydrogen absorption and desorption duration. Therefore, several PCM configurations have been designed and proposed recently, including pool bed PCM (Garrier et al., 2013; Yao et al., 2020a; Darzi et al., 2016; Mellouli et al., 2016), jacket bed PCM (Nguyen & Shabani 2020; Lewis & Chippar 2021), and sandwich bed PCM (Alqahtani et al., 2020a, b; Ye et al., 2020; Ye et al., 2021a). Yao et al. (2020a) performed the experimental and numerical studies of the $LaNi_5$-based storage system that was incorporated with paraffin as the pool bed PCM and expanded graphite. This study proved that incorporating the PCM with the MHHS improved the storage efficiency by 47% compared to the case without PCM. However, the study from Alqahtani et al. (2020a) indicated that using sandwich bed PCM obtained the better heat transfer performance, compared to the jacket bed PCM under the same PCM volumes. The MH bed was designed and placed in the middle between PCM beds unlike the pool bed or jacket bed that only covered the MH bed. Similarly, the study from Ye et al. (2021a) also supported that the hydrogen desorption duration was improved by 21.8% when using the sandwich bed PCM, compared to the case with jacket bed PCM. This is due to a larger heat transfer surface area of the sandwich bed PCM (Ye et al., 2020). However, the studies of Alqahtani et al. (2020a, b) were analysed by adding the aluminium foam to the MH bed, resulting in an increasing in the effective thermal conductivity of the Mg_2Ni material from 0.674 W/mK to 1.33 W/mK. Increasing the effective thermal conductivity by adding the metal foam is also another technique that improved the MH performance. The study from Mellouli et al. (2009) indicated that adding the aluminium foam to the MH bed significantly reduced the hydrogen absorption time by 66%, compared to the case without metal foam. However, adding the metal foam significantly increases the overall weight of MHHS and reduces the hydrogen storage capacity. Furthermore, the disintegration of itself during the hydrogen absorption/desorption is also the main problem of this technique (Nguyen & Shabani 2021).

The combination between internal heat exchanger tubes and external PCM also greatly improves the heat transfer performance (Ardahaie et al., 2021; Ye et al., 2021a; Mellouli et al., 2017). The hydrogen absorption and desorption duration reduced by 44% and 20% when using the $NaNO_3$-based PCM jacket with inner spiral coil tube for the Mg_2Ni-based storage system, compared to the case without PCM jacket (Ardahaie et al., 2021). Under the same MH materials and PCM, using several internal cooling tubes and PCM jacket also reduced the hydrogen absorption by 94%, compared to the case with PCM jacket only (Mellouli et al., 2017). The combination of internal straight tube with fin and $LiNO_3$-$3H_2O$-based PCM jacket also increased the hydrogen kinetic reaction rate of the $LaNi_5$-based storage, resulting in a 50% reduction of hydrogen sorption duration, compared to the case without PCM jacket (Ye et al., 2021a).

From our previous study (Larpruenrudee et al., 2023), using semi-cylindrical coil tube with central return tube enhanced heat transfer compared to the case without central return tube and helical coil tube. However, our previous work only analysed the MHHS performance with this heat exchanger for the absorption process. Therefore, the aim of this present study is to analyse its performance during the desorption process to estimate the completion time of the whole absorption-desorption cycle. Furthermore, from the literature review, the combination between active and passive thermal management techniques, especially when combining the inner heat exchanger tube with outer PCM, significantly enhance storage performance for both hydrogen absorption and desorption processes. The PCM configuration also plays a significant role for the heat transfer improvement. Therefore, the secondary aim of this study is to enhance the MHHS performance by considering the combination of both active and passive heat transfer techniques under various storage configurations. The performance

of the storage system is analysed under the hydrogen absorption and desorption duration with the use of various PCM configurations incorporating semi-cylindrical coil tube. The volume of PCM and MH bed is constant to obtain the reasonable comparison between various configurations. Finally, appropriate selection of the initial HTF temperature is considered under the parametric study for the new MHHS with semi-cylindrical coil tube and PCM.

6.4 System Description

The results from our previous study proved that using semi-cylindrical coil heat exchanger (SCHE) and semi-cylindrical coil heat exchanger with central return tube (SCHE-CR) as the internal heat exchangers significantly improved the heat transfer mechanism inside the MHHS compared to the use of the original helical coil heat exchanger (HCHE) (Larpruenrudee et al., 2023). However, our previous work only focused on the performance of SCHE and SCHE-CR during the hydrogen absorption process. Therefore, the present study further analyses the heat transfer performance of these heat exchangers during hydrogen desorption. Moreover, the combination between the internal heat exchanger and PCM external heat exchanger is also included in this study to further enhance heat transfer rate. The effect of the initial temperature of the HTF during the hydrogen absorption and desorption is also considered under the parametric study section. For all cases, stainless steel is used as the material for the HTF tube and MHHS tank, as well as the outer tank of PCM.

6.4.1 Storage System Incorporating Internal Heat Exchanger (Semi-Cylindrical Coil with and without Central Return Tube)

The effect of the HTF tube size for both SCHE and SCHE-CR was previously analysed in our work (Larpruenrudee et al., 2023). The results from our previous study proved that the HTF tube diameter of 4 mm had a greater effect on heat transfer enhancement for both designs. There was a 40% reduction in hydrogen absorption duration when increasing the HTF tube size from 3 mm to 4 mm (Larpruenrudee et al., 2023). Therefore, the tube diameter as 4 mm of SCHE and SCHE-CR is used for the present study to investigate its performance during the desorption process. The purpose of this study is to estimate the duration of the absorption-desorption cycle. The total height and outer diameter of MHHS are 80 mm and 50 mm, respectively. This dimension is the same as our previous work. The schematic diagram and geometrical parameters of these two designs are presented in Figure 6.2. From this figure, the air HTF is injected from the bottom part throughout the outlet at the top part of MHHS for SCHE, while the outlet of SCHE-CR remains in the same direction as the inlet due to the central return tube. The hydrogen inlet and outlet are located at the top surface of the MHHS.

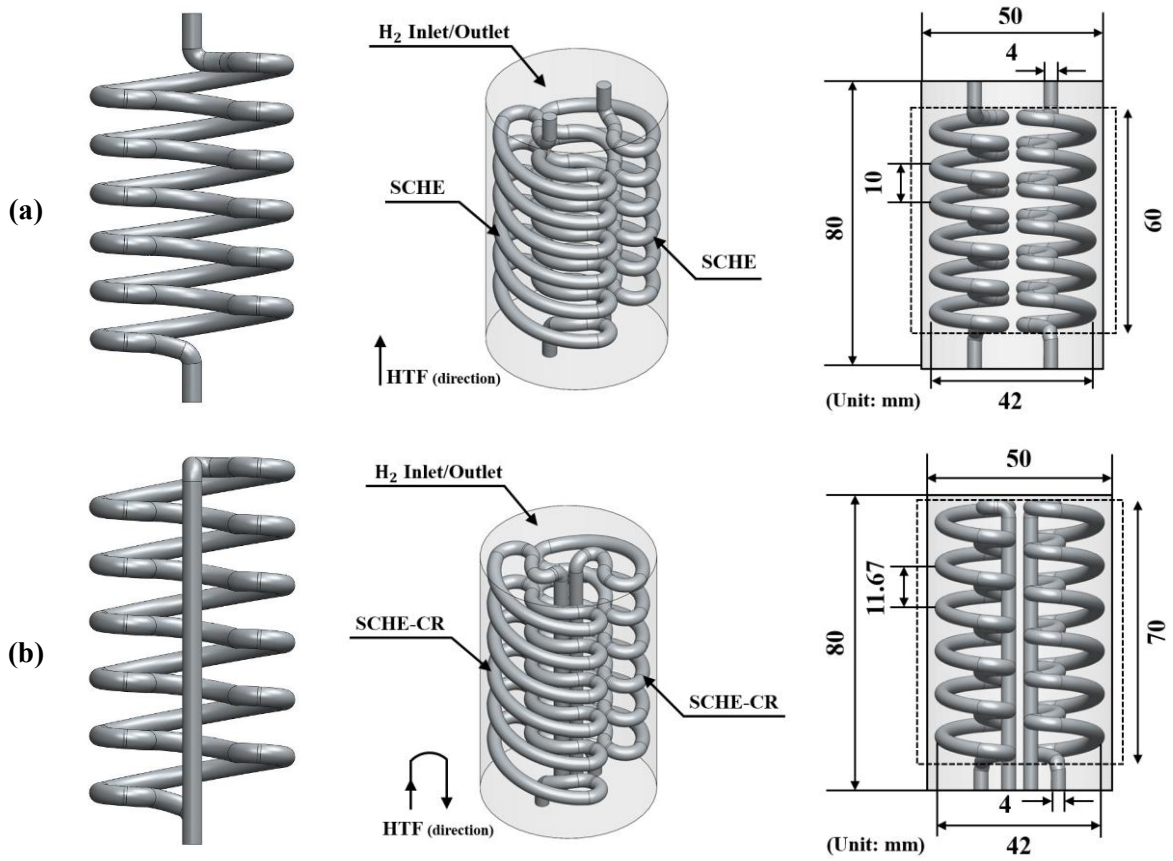

Figure 6.2 Schematic diagram of storage tanks with two heat exchangers. (a) characteristics of MH tank with SCHEs, and (b) characteristics of MH tank with SCHE-CRs

6.4.2 Storage System Incorporating Internal Heat Exchanger and External Heat Exchanger

The MHHS with SCHE-CR is combined with outer PCM to obtain further heat transfer improvement. The results from our previous work indicated that the absorption duration was significantly reduced by 37% when using SCHE-CR compared to the case with SCHE (Larpruenrudee et al., 2023). This comparison is between the cases with constant HTF tube diameter at 4 mm. Therefore, SCHE-CR is further used for this section. Figure 6.3 and Figure 6.4 present the schematic diagram and characteristics of MHHS with different designs. The MHHS with PCM jacket (case 1) and PCM pool bed (case 2) are included in this study to compare the performance of SCHE-CR when incorporated with outer PCM. Case 3 refers to the MHHS incorporating internal SCHE-CR and PCM jacket, while case 4 refers to the MHHS with SCHE-CR and PCM capsule. For the new design of the PCM capsule, the PCM container is designed to cover the MH bed including the top and bottom parts. The purpose of this design is to provide the additional heat transfer surface area at the top and bottom parts of MH bed. However, there is a hole left over the bottom and top parts for HTF inlet/outlet and hydrogen inlet/outlet purposes. The geometrical parameters of these cases are provided in Table 6.1. The MH volume is fixed at 140 cm^3, and the HTF tube volume is fixed at 17.12 cm^3 for case 3 and case 4. The MH volume for case 1 and case 2 also remains at 140 cm^3 for comparison purposes. To remains the similar of MH volume, the radius of MH section from case 1 and case 2 is 23.6 mm, which is only 47.2 mm of diameter in this section. However, the radius of MH section from case 3 and case 4 is 25 mm or it is 50 mm of diameter in this section. This is due to the effect of additional internal heat exchanger as SCHE-CR. It should be noted that the having the central return tube from SCHE-CR has only around 1 cm^3 reduction of the MH volume, compared to the case with SCHE only. Therefore, the MH volume from the cases with PCM only (case 1 and case 2) is considered as 140 cm^3 in this study. From the constant MH volume,

the mass of MH based Mg_2Ni with the density at 3200 kg m^{-3}, is about 0.45 kg for all cases. Furthermore, under the different PCM configurations, the PCM volume for all cases is fixed at 649 cm^2. The details for PCM selection and required PCM volume can be seen under the "Chapter 3 – Methodology" section.

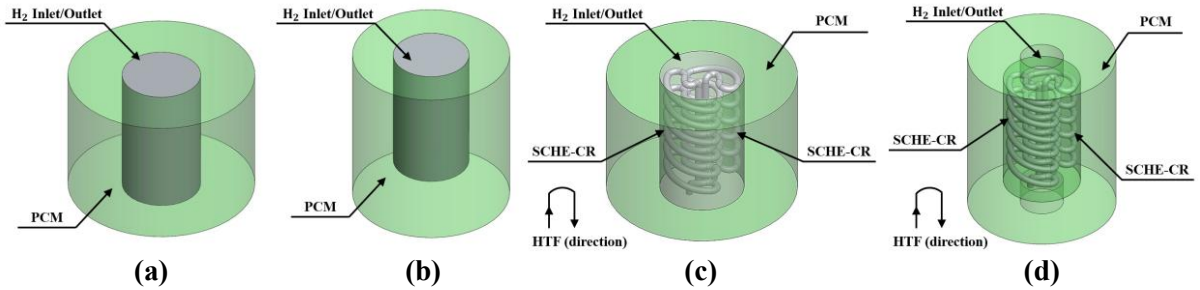

Figure 6.3 Schematic diagram of storage tanks with different heat exchangers. (a) MH tank with PCM jacket (case 1), (b) MH tank with PCM pool bed (case 2), (c) MH tank with SCHE-CRs incorporating PCM jacket (case 3), and (d) MH tank with SCHE-CRs incorporating PCM capsule (case 4).

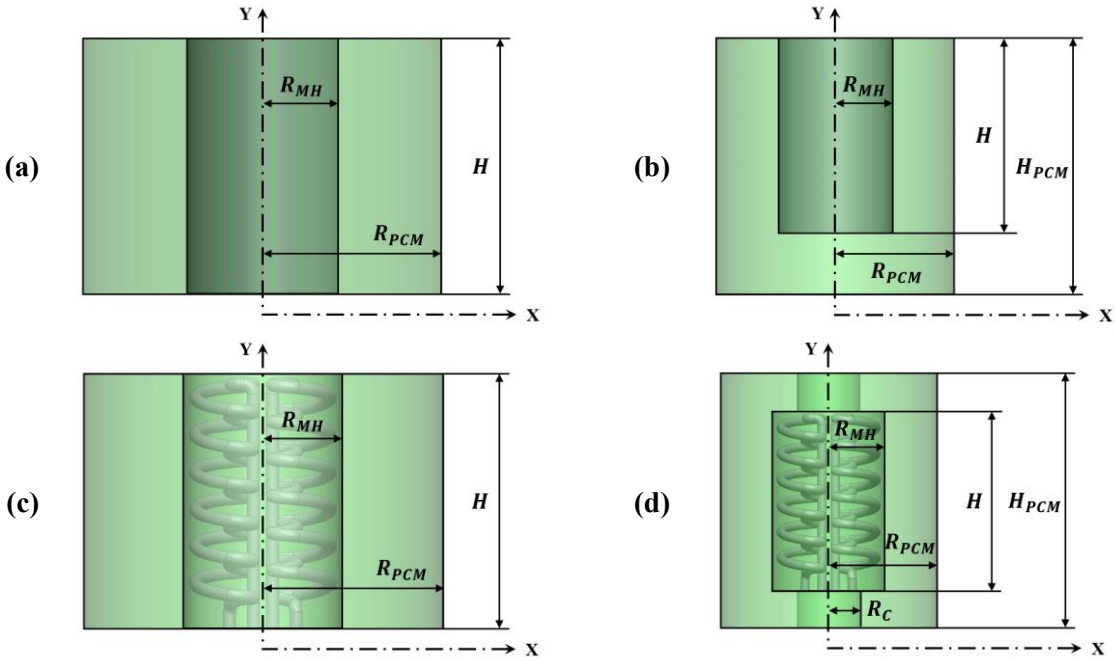

Figure 6.4 Characteristics of storage tanks with different heat exchangers. (a) MH tank with PCM jacket (case 1), (b) MH tank with PCM pool bed (case 2), (c) MH tank with SCHE-CRs incorporating PCM jacket (case 3), and (d) MH tank with SCHE-CRs incorporating PCM capsule (case 4).

Table 6.1 Characteristic of MH tanks with various heat exchanger designs; the PCM jacket (case 1), PCM pool bed (case 2), SCHE-CR incorporating PCM jacket (case 3), and SCHE-CR incorporating PCM capsule (case 4)

Case No.	H (mm)	H_{PCM} (mm)	R_{MH} (mm)	R_{PCM} (mm)	R_C (mm)	Total MH Volume (cm^3)	Total PCM Volume (cm^3)	Additional Heat Exchanger
1	Equal: 80	-	Equal: 23.6	56.1	-	Equal: 140	Equal: 649	-
2		105		48.9	-			-
3		-	Equal: 25	56.5	-			SCHE-CR
4		114.4		48	14			SCHE-CR

6.4.3 Parametric Study for Operating Conditions

The best MHHS performance among case 1 to case 4 is selected to further analyse the effect of the initial HTF temperature on the hydrogen absorption and desorption process. The HTF operating temperature is set as 573 K for the base case during both absorption and desorption. The HTF temperature values between 423 K to 523 K are selected for the absorption process, while the temperature values between 623 K to 723 K are for the desorption process. Table 6.2 provides all selected values of the HTF inlet temperature during these two states.

Table 6.2 Operating values for the HTF

HTF inlet temperature (K)	**Base value**	**Parametric value**
Absorption	573	423, 473, 523
Desorption	573	623, 673, 723

6.5 Mathematical Model

This section describes all necessary equations regarding the governing equations for the hydrogen absorption and desorption processes, turbulent flow and heat transfer of heat transfer fluid. Furthermore, all related equations for phase change process of phase change material are also included in this section. The initial and boundary conditions, numerical schemes, grid independency, and model validation are also included in this section.

5.5.1 Governing Equations

The appropriate selection of MH material, PCM, and HTF for the use of this thesis are provided in "Chapter 3 – Methodology" section. The governing equations regarding the absorption and desorption processes, phase change process, as well as the heat transfer fluid can be found in the same chapter as "Chapter 3 – Methodology". For the absorption and desorption processes, the governing equations are provided in 3.1.1 Absorption Process and Desorption Process. The governing equations for phase change process are provided in "3.1.2 Phase Change Process" section. The governing equations of heat transfer fluid can be found in "3.1.3 Heat Transfer Fluid" section.

The turbulent HTF flow is applied by using the realizable k-ε turbulence model in the present study with HTF flow velocity at 76.86 m s^{-1} (Reynolds number at 9000). The average y+ is about equal to 30 for this study. The model validation of selected turbulence model was performed from our previous study (Larpruenrudee et al., 2022a) against the experimental results from Kumar et al. (2006). All governing equations of the heat transfer and turbulent flow for the HTF can be found from our previous study (Larpruenrudee et al., 2023).

5.5.2 Initial and Boundary Conditions

The initial temperature of the storage system and PCM ($T_{MH,abs} = T_{PCM,abs} = T_{0,abs}$) is set as 573 K as this obtains the maximum hydrogen storage capacity of Mg_2Ni storage (Muthukumar et al., 2008). The loading pressure ($P_{0,abs}$) is set as 1.8 MPa for hydrogen absorption process as it obtains better absorption performance compared to other values (Larpruenrudee et al., 2022a). For the desorption process, the initial temperature of storage and PCM is set as the ultimate temperature of the absorption ($T_{MH,des} = T_{PCM,des} = T_{ultimate,abs} = T_{0,des}$). The pressure during the desorption ($P_{0,des}$) is set at 0.1 MPa as the ambient pressure (P_a) (Ardahaie et al., 2021). The initial temperature of HTF is 573 K for both absorption and desorption ($T_{HTF,abs} = T_{HTF,des}$). The inlet flow velocity and zero-gauge pressure at the outlet are applied as the boundary condition of the HTF. The HTF is injected from the bottom part throughout the outlet of the HTF tube in the y-axis direction.

5.5.3 Numerical Schemes, Grid Independency, and Model Validation

- Numerical Schemes and Grid Independency

Due to the similar setup conditions for the pre-processing process, the numerical schemes for all chapters are summarised and provided in "3.3.2 Numerical Schemes" under "Chapter 3 – Methodology section". The grid refinement test during the hydrogen absorption is performed under various different grid sizes to achieve accurate results and is presented in Figure 6.5. The grid refinement tests for the storage with SCHE and SCHE-CR were performed in our previous study (Larpruenrudee et al., 2023). Therefore, the grid refinement test of the present study is only for storage with PCM configuration. Only the case for the MHHS with PCM (case 1) and the case for MHHS with SCHE-CR and PCM (case 3) are selected for the grid refinement test. The same meshing techniques are used for the rest of other cases. The average temperature at the selected planes from case 1 is presented in Figure 6.5a, while Figure 6.5b is for case 3. It should be noted that there is only one selected plan from case 1 due to the effect of the PCM jacket, which obtains the constant temperature changes along the top and bottom parts of the MHHS. However, there are the two selected planes from the top and bottom parts of the MHHS for case 3, as this case has the internal SCHE-CR, which affects the temperature variations along the MHHS. From these two cases, the average temperature becomes stable and has a minor change at 134,608 of the element numbers for case 1 and at 630,782 of the element numbers for case 3. Therefore, these element numbers are selected for further simulations. The successively refined grids for these two cases are provided in the "Appendices: A2".

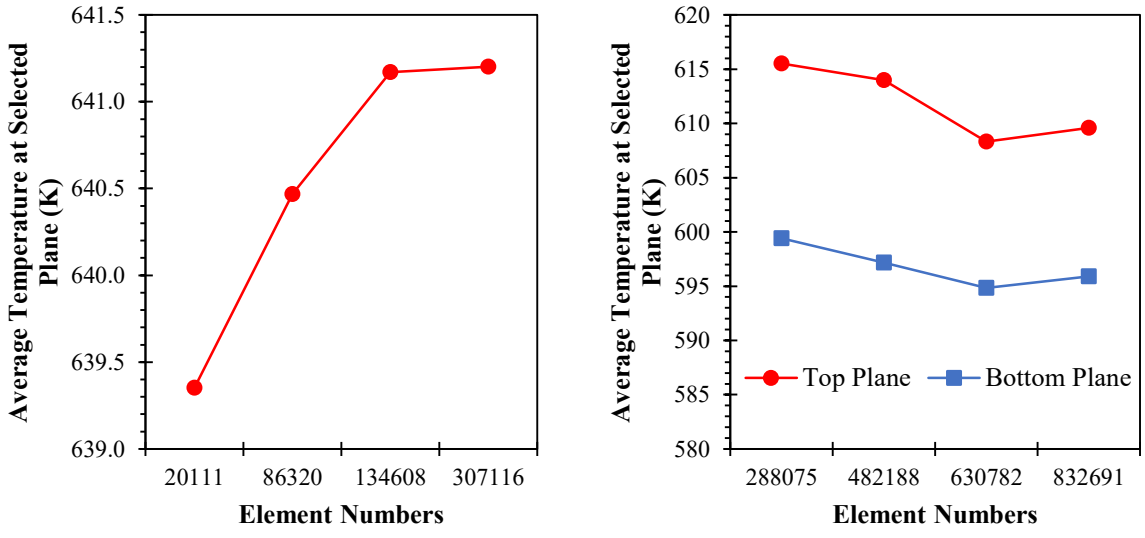

Figure 6.5 Average temperature for the hydrogen absorption in the MH storage system with different MHHS configurations from different grid sizes. (a) average temperature at selected plane for case 1 and (b) average temperature at two selected planes for case 3.

- Model Validation

The model validations for the use of metal hydride storage system based on Mg_2Ni, phase change process, as well as the selection of turbulence model for the HTF are provided in "3.3.1 Model Validation" under "Chapter 3 – Methodology" section.

6.6 Results and Discussion

This section provides the numerical results for hydrogen absorption and desorption of the metal hydride storage system (MHHS) incorporating various internal/external heat exchanger configurations. As mentioned earlier, our previous study (Larpruenrudee et al., 2023) focused on the performance of internal semi-cylindrical coil heat exchanger (SCHE) and semi-cylindrical coil heat exchanger with central return tube (SCHE-CR) during the hydrogen absorption process. The performance of these two heat exchanger designs is further investigated for the hydrogen desorption process by considering the desorption duration and average bed temperature inside the MHHS. The MHHS with SCHE-CR is then combined with outer phase changer material (PCM) to further enhance the MHHS performance. Finally, the best combination design is then analysed under the variation of initial HTF temperatures as the parametric study.

6.6.1 Storage System Incorporating Internal Heat Exchanger

The performance of three different heat exchanger designs, namely HCHE, SCHE, and SCHE-CR, is analysed and presented in Figure 6.6. It should be noted that the HCHE is designed to compare the performance of another two heat exchangers. The HCHE volume is the same as the SCHE volume for the comparison purpose. Figure 6.6a refers to the average bed temperature for the absorption-desorption cycle, while Figure 6.6b is for the hydrogen concentration for the absorption-desorption cycle. For all cases, the operating temperature of the storage system and HTF temperature is 573 K with loading pressure at 1.8 MPa for the absorption process. For the hydrogen absorption process, the MH bed temperature rapidly increases after the initial moment of hydrogen injection. This is due to the interaction between the metal alloy and hydrogen, which is also known as an exothermic absorption process. This phenomenon refers to the fact that the reaction rate (from Equation 3.8) reaches the maximum value when having the highest different pressure between the hydrogen pressure (constant at 1.8 MPa) and MH equilibrium pressure (from Equation 3.9). The reaction rate from Equation 3.8 is the source terms of the energy equation (Equation 3.2). This leads to the rapid increase in MH bed temperature. The MH bed temperature then slowly increases until reaching the maximum value and continually decreases due to the convective heat transfer from the HTF that removes the generated heat from the system. The faster MH bed temperature reduction means a greater heat transfer improvement for this stage. The average bed temperature of the MHHS from the SCHE-CR case is also reduced faster than the HCHE case and also faster than the SCHE case (Figure 6.6a). After the reduction of MH temperature to a certain point, the surface of the metal alloy starts to absorb the hydrogen. This is because of the chemisorption, acceleration of physisorption, hydride formation in the system, and hydrogen diffusion (Ardahaie et al., 2021). The hydrogen absorption is corresponding to the MH bed temperature as a faster MH bed temperature reduction results in faster hydrogen absorption. From Figure 6.6b, the duration of complete absorption for the case with SCHE is 6215 s, while there are only 3910 s of the hydrogen absorption duration when using the SCHE-CR. The absorption duration from the SCHE-CR case reduces by 37% compared to the SCHE case. At 3910 s, the hydrogen concentration from the SCHE and HCHE cases is only around 90% and 68%, respectively. More analysis and discussion regarding the SCHE and SCHE-CR effect on hydrogen absorption can be found in our previous study (Larpruenrudee et al., 2023).

The hydrogen desorption process is well known as the endothermic reaction process. For the present study, the operating temperature of the storage system for hydrogen desorption is the ultimate temperature of the absorption, while the HTF temperature remains at 573 K. The hydrogen pressure is set as 0.1 MPa. The MH temperature suddenly decreases after the initial moment of hydrogen desorption, which is opposite to the hydrogen absorption process. This leads to the system requirement for the supplied heat during the desorption. A faster MH bed temperature increases, resulting in faster

hydrogen desorption. The HTF inside the storage assists the storage system by providing heat to accelerate the hydrogen desorption from the metal surface. Therefore, there is a heat transfer between the HTF and MH bed. The average bed temperature (Figure 6.6a) of the MHHS from the SCHE-CR case increases faster than the SCHE and HCHE cases. This leads to faster hydrogen desorption from the SCHE-CR case compared to the SCHE and HCHE cases (Figure 6.6b). The completing desorption duration from the SCHE-CR case is 13369 s, while it takes 18936 s from the SCHE case. The desorption duration significantly reduces when using SCHE-CR compared to the case with SCHE only. The desorption duration from the SCHE-CR case reduces by 29% compared to the SCHE case. At 13369 s, the hydrogen concentration from SCHE case and HCHE case is still only 0.12% and 0.31%, respectively.

For more analysis of the hydrogen absorption-desorption cycle, the duration of the complete cycle from the HCHE case is over 35000 s. However, the duration significantly reduces when using SCHE and SCHE-CR as heat exchangers. The duration of complete cycle from SCHE and SCHE-CR is 25147 s and 17279 s, respectively. There is a 31% reduction in the duration for the complete cycle when using SCHE-CR instead of SCHE. There is over than a 50% reduction in the duration of the one complete cycle when changing the HCHE to SCHE-CR.

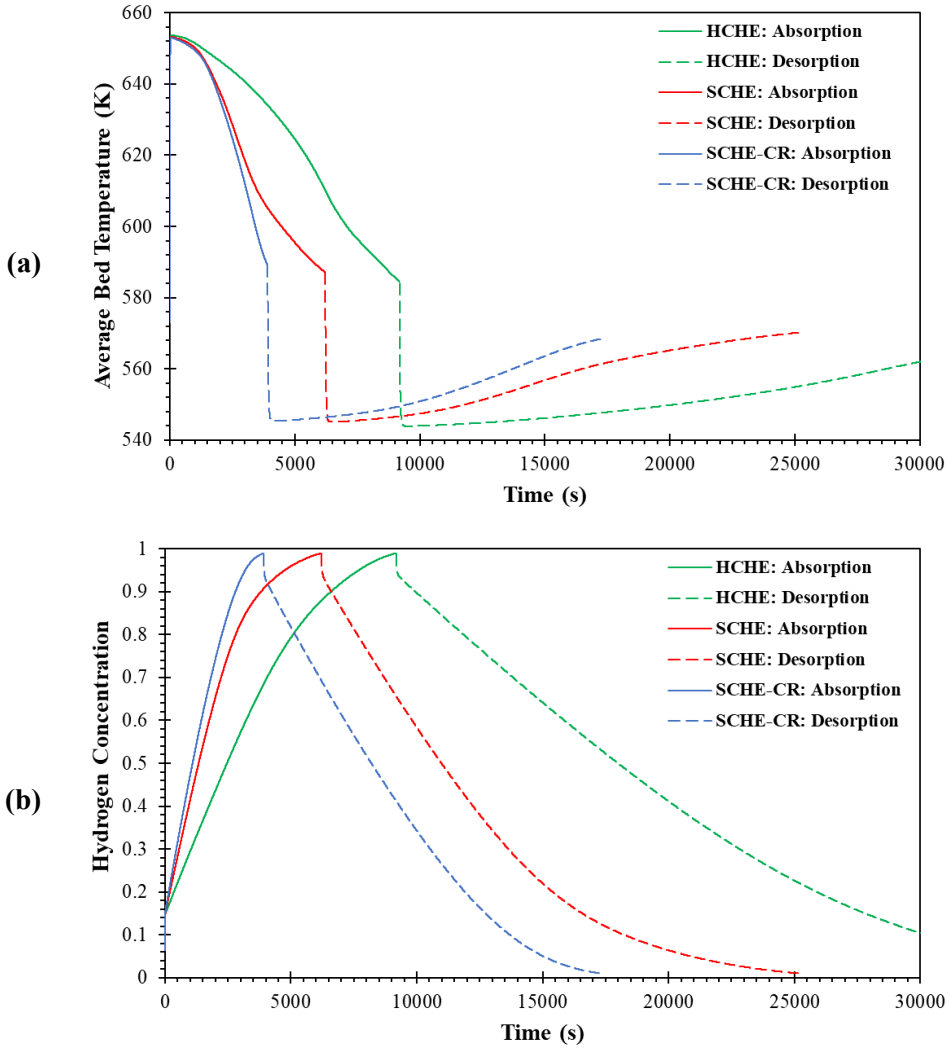

Figure 6.6 Average bed temperature and hydrogen concentration during the absorption-desorption cycle from storage system with different heat exchangers; (a) average bed temperature and (b) hydrogen concentration.

Figure 6.7 presents the temperature and hydrogen concentration during the desorption at selected points from the MHHS with HCE, SCHE and SCHE-CR. Figure 6.7a provides the location of four selected points inside the MHHS. P1 (25, 67, 0) and P2 (40, 73, 0) are located at the centre of the upper part and the side of the upper part, respectively. P3 and (25, 13, 0) and P4 (40, 13, 0) are placed at the centre of the lower part and the side of the lower part, respectively. Only half of MHHS (right side) is used to analyse in this section due to the symmetry of the heat exchanger designs. The bed temperature from Figure 6.7b, c significantly indicates that there is greater heat transfer enhancement inside the MHHS from SCHE-CR compared to SCHE and HCHE.

Separate comparison for each selected point, the bed temperature from SCHE increases faster than HCHE due to the well arrangement of the HTF tube structure, which leads to having more uniform temperature distribution inside the MHHS. However, the bed temperature from the centre points (P1 and P3) for SCHE-CR increases faster than the SCHE case. The temperature between SCHE-CR and SCHE is greater different at P1, while there is less difference in temperature at P2 and P4 from these two cases. This is because there are more heat transfers around the central area of the MHHS (P1) from the central return tube of SCHE-CR. There is the secondary circulation of the SCHE-CR at the top part due to the design of the central return tube, while there is the HTF outlet at the top part from SCHE. The same conditions also apply to the case of HCHE, which does not have the secondary circulation of the SCHE and central return tube from SCHE-CR. Consequently, the temperature from all four points for HCHE is significantly lower than in other cases. At P2, there is less temperature difference between SCHE and SCHE-CR due to the fact that this area is far away from the central return tube of SCHE-CR. However, there is still the secondary circulation of the SCHE-CR located higher than this point. This leads to a faster temperature increase from SCHE-CR compared to SCHE. At P3 and P4, the temperature from these two points increases faster than the temperature at P1 and P2 as P3 and P4 are located at the bottom part of MHHS. This phenomenon applies for all cases due to their locations of themselves, which are near the HTF inlet. There is a slight difference in temperature at P4 from SCHE and SCHE-CR because this area has similar heat transfer surface areas. The temperature at this point from SCHE and SCHE-CR is similar at the initial moment to 2500 s. After that, the temperature from SCHE-CR increases faster than SCHE due to the effect of the central return tube.

Therefore, the hydrogen desorption from SCHE-CR is faster than SCHE and HCHE for both P1, P2 (Figure 6.7d) and P3, P4 (Figure 6.7e). At the centre of the upper part (P1), the complete desorption duration from SCHE-CR is 12638 s, while there are 17093 s and 29060 s for the completion of desorption from SCHE and HCHE, respectively. At the side of the upper part (P2), the completion of desorption is 13410 s for SCHE-CR, 12177 s for SCHE, and 26526 s for HCHE. It is obvious that the desorption duration from P2 is shorter than P1 for all cases, except SCHE-CR. This is due to the effect of the central return tube from SCHE-CR. However, the complete desorption from the side of the lower part is shorter than the centre of the lower part for all cases. The completion of desorption at the centre of the lower part (P3) is 11699 s for SCHE-CR, 12177 s for SCHE, and 16829 s for HCHE, respectively. At the side of the lower part (P4), the completion of desorption is 9567 s for SCHE-CR, 10969 s for SCHE, and 14373 s for HCHE. In fact, the completion of desorption at P4 is faster than at P3 because this area is directly close to the HTF inlet. The heating HTF starts circulating from the inlet and goes to the outlet by passing the area around P4 first for the SCHE-CR case. The slower desorption at P3 from SCHE-CR is due to the effect of the HTF outlet which has a lower HTF temperature than the area at the HTF inlet and others. For SCHE and HCHE, there are no heat transfer surface areas near this point (P3), resulting in slower desorption compared to P4.

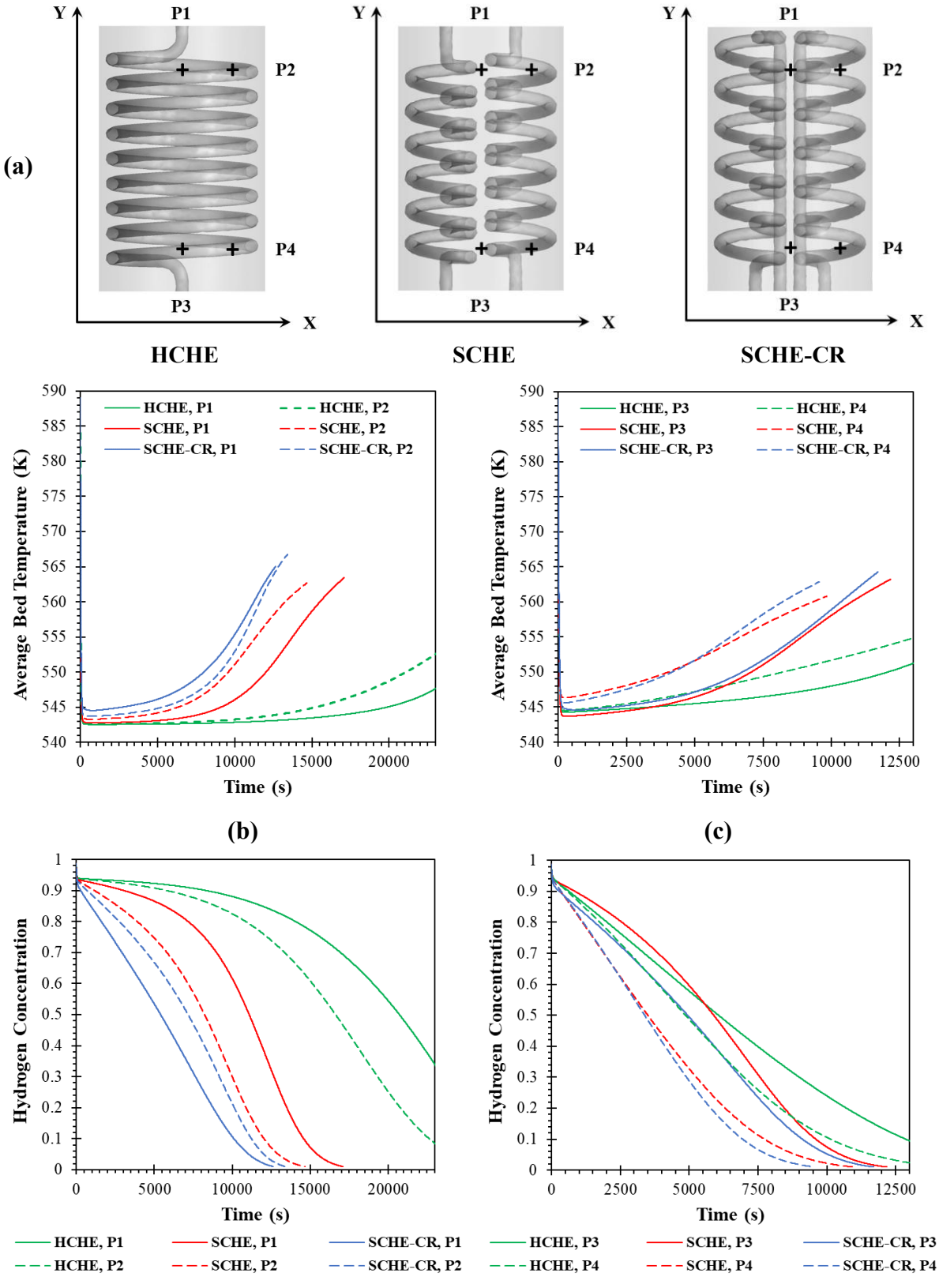

Figure 6.7 Temperature and hydrogen concentration at selected locations from the storage system with different heat exchangers; (a) position of selected points, (b) temperatures at the upper part, (c) temperatures at the lower part, (d) hydrogen concentrations at the upper part, and (e) hydrogen concentrations at the lower part.

The average temperature of MHHS with three different heat exchangers during the desorption is provided in Figure 6.8. This figure includes the temperature contours from five selected times after starting the desorption process. After starting the desorption process, the MH bed temperature significantly reduces to 543 K for all cases. The MH bed temperature at the bottom part is higher than other parts for cases at 250 s. This is because the bottom part is close to the HTF inlet area. However, the central area of MHHS from SCHE and SCHE-CR has a higher temperature than HCHE due to the well arrangement of the HTF tube structure. The MH bed temperature from the SCHE-CR case is also higher than the SCHE case. This is obvious at 5000 s, where the MH bed temperature at the top part from SCHE-CR is higher than SCHE. The significant difference in MH temperature variation from the top part between SCHE-CR and SCHE is found after 10000 s. The main reason is that the SCHE-CR has the secondary circulation of the coil and central return tube area at the top part, while SCHE and HCHE have only the HTF outlet at the top part. At 13250 s, the MH bed temperature around the middle part from SCHE-CR and SCHE is around 571 K, while the temperature from the HCHE case is still less than 567 K. However, the minimum temperature at the top part from HCHE and SCHE is still 543 K, while it is around 556 K from SCHE-CR. The average MH bed temperature at the top part from SCHE-CR is 565 K, while there are 547 K and 543 K from SCHE and HECHE, respectively. From all cases, the MH bed temperature from the bottom part is higher than other parts at the initial moment as it is close to the HTF inlet area. However, there are still some areas from the bottom part where it has a lower temperature than the middle part. This is because these areas do not have the secondary circulation of the coil. Therefore, there are fewer heat transfer surface areas around this part compared to the middle part. The overall temperature contour indicates that the case with SCHE-CR has more heat transfer improvement due to the structure of itself, resulting in having more uniform temperature distribution and lower thermal resistance inside the MH bed.

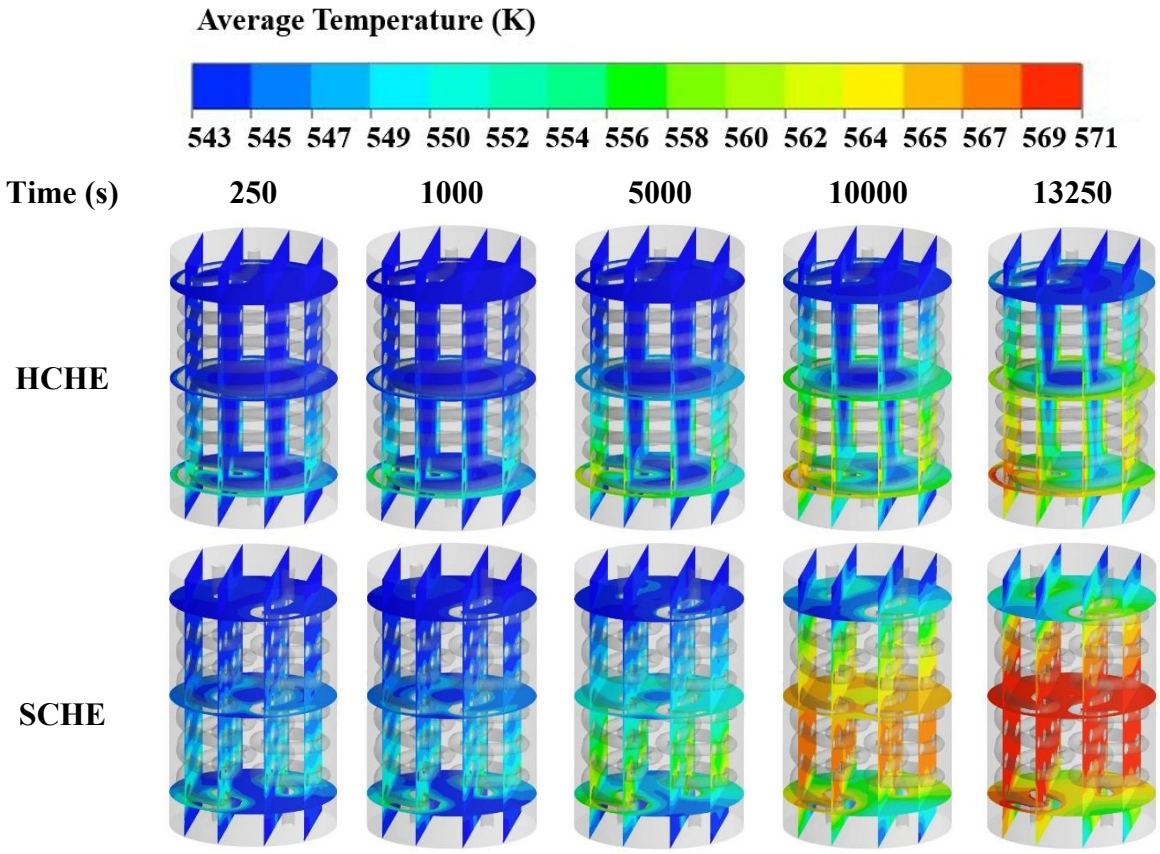

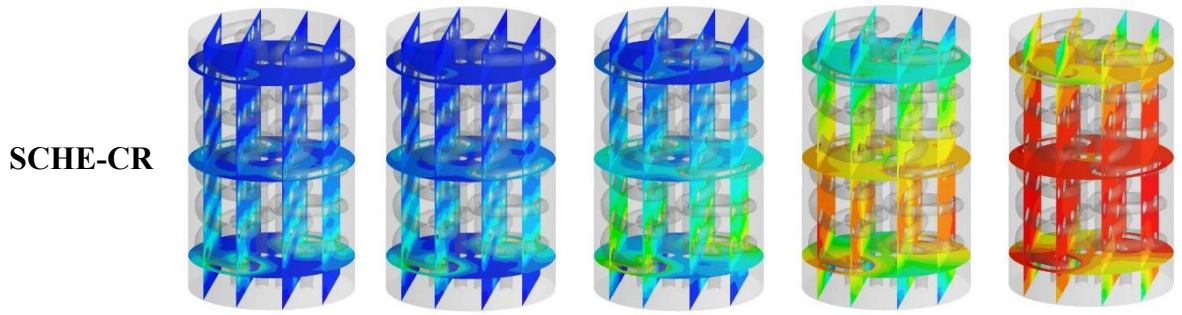

Figure 6.8 Average temperature of MH bed at 250 s, 1000 s, 5000 s, 10000 s, and 13250 s after starting hydrogen desorption process from HCHE, SCHE and SCHE-CR

Figure 6.9 presents the hydrogen concentration contours from three heat exchanger designs during the desorption process. The lower hydrogen concentration is usually observed around the HTF tube where it has a higher temperature compared to other areas. This is because the circulation of heating HTF inside the heat exchanger causes a higher temperature at the interface between the MH bed and the HTF tube. At 250 s, the hydrogen concentration from SCHE-CR is less than 94%, However, there is still a 100% of hydrogen concentration around some areas at the centre of HCHE and at the top of SCHE at 250 s and 1000 s. At 1000 s, the hydrogen concentration at the central area of the SCHE-CR case is less than the SCHE case due to the central return tube effect. After 5000 s, the hydrogen concentration at the top part of the MHHS from SCHE-CR is significantly lower than the top part from the case with SCHE. At 13250 s, the hydrogen concentration from the SCHE-CR case is almost around or less than 5%. In contrast, the hydrogen concentration is still around 24-75% at the top part of the SCHE case. However, more variation of hydrogen concentration is still found from the HCHE case at 13250 s. The hydrogen concentration at the bottom part is still 24% and the middle part is still 49-87%. The hydrogen concentration at the top part of this case still varies from 75% to 87%. It is obvious that the higher MH temperature results in a lower hydrogen concentration for all cases. The faster increase in MH temperature leads to faster hydrogen desorption which is found in the SCHE-CR case. The more uniform distribution of MH temperature causes more hydrogen desorption, especially at the top part and central area of the MHHS from SCHE-CR case compared to the cases with SCHE and HCHE. Therefore, the MHHS with SCHE-CR is then combined with the outer PCM to further enhance the heat transfer rate.

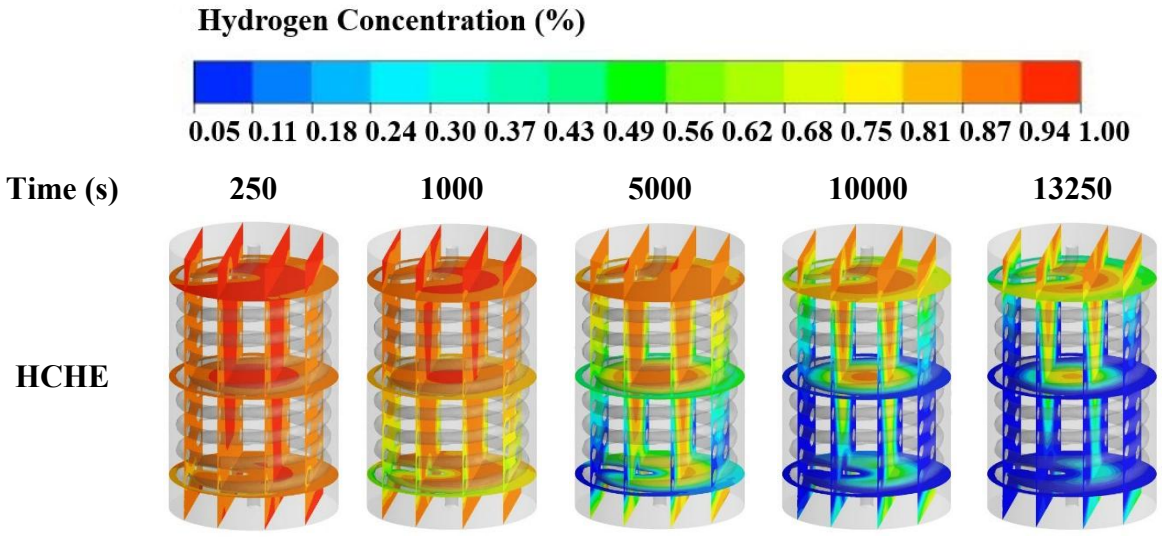

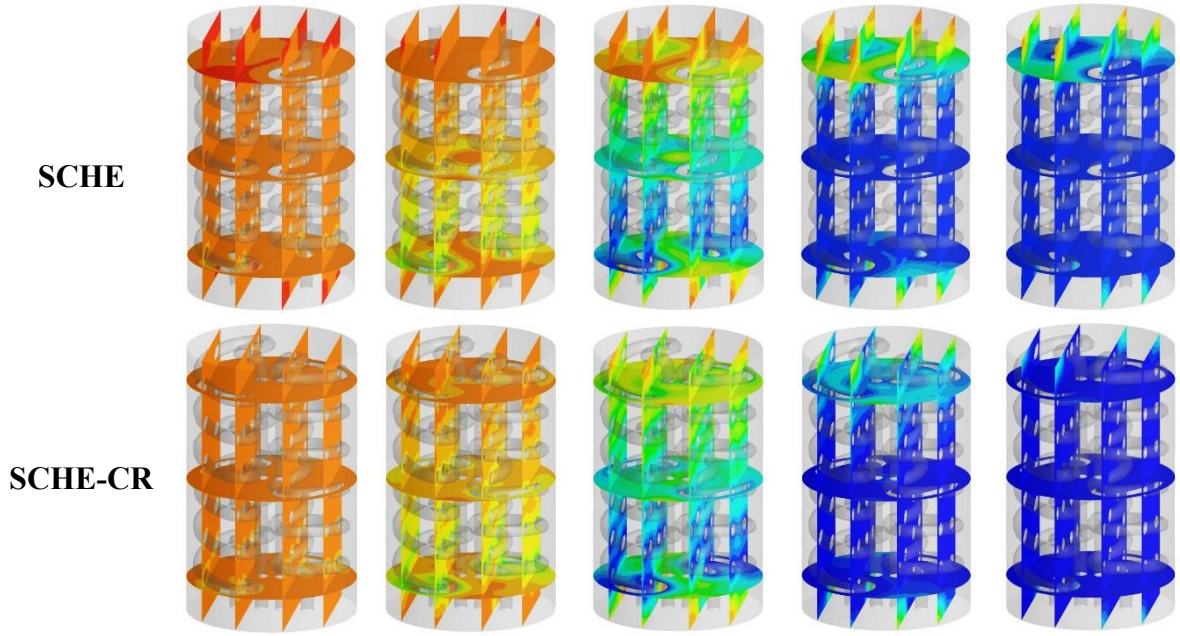

Figure 6.9 Hydrogen concentration at 250 s, 1000 s, 5000 s, 10000 s, and 13250 s after starting the hydrogen desorption process from HCHE, SCHE and SCHE-CR

6.6.2 Storage System Incorporating Internal Heat Exchanger and External Heat Exchanger

The combination between the internal SCHE-CR and external PCM is proposed to enhance the MHHS's performance. Four different MHHS configurations are designed under the use of external PCM. The volumes of MH and PCM are constant for all cases to propose a reasonable comparison. Case 1 and case 2 are the MHHS with only a PCM jacket and PCM pool bed, which act as the primary energy source in both absorption and desorption processes. Case 3 is for the MHHS with internal SCHE-CR and outer PCM jacket, while case 4 is for the MHHS with internal SCHE-CR and outer PCM capsule. For the hydrogen absorption, the initial temperature of the MHHS and PCM is set as 573 K and hydrogen pressure at 1.8 MPa. For hydrogen desorption, the initial temperature of the MHHS and PCM is the ultimate temperature from the absorption, while the hydrogen pressure is set at 0.1 MPa. These conditions are applied to all cases. For the HTF, the initial temperature of the HTF from case 3 and case 4 is 573 K, which is constant for both absorption and desorption. Figure 6.10 presents the average bed temperature of the MH and PCM during the absorption and desorption for all cases. Figure 6.10a refers to the results from case 1 and case 2, while Figure 6.10b refers to the results from case 3 and case 4.

As mentioned previously, the MH bed temperature suddenly increases after the initial moment of the hydrogen injection due to the exothermic effect of the hydrogen absorption process. The MH bed temperature from all cases suddenly increases. The MH bed temperature reaches up to around 652 K for case 1 and case 2, while it is around 650 K for case 3 and case 4. The MH bed temperature gradually decreases for all cases due to the outer PCM effect, which absorbs the generated heat from the MH bed. After absorbing the heat from the MH bed, the PCM starts to transform from solid phase to liquid phase. Therefore, the PCM bed temperature gradually increases during the absorption process. The PCM temperature raises up to around 586 K for case 1 and case 2. At the end of the absorption process, the MH bed temperature is 622 K for case 1 and 613 K for case 2. However, there is more heat transfer enhancement from case 2 (with PCM pool bed) compared to case 1 (with PCM jacket). The MH bed temperature from case 2 reduces faster than case 1. This is because of the PCM pool bed configuration, which absorbs the generated heat from MH on the side and bottom sections. The PCM jacket only absorbs the heat on the side only. However, the MHHS's performance is greatly enhanced when combining the outer PCM with the inner SCHE-CR. The MH bed temperature significantly faster

decreases from case 3 and case 4 due to the effect of HTF from SCHE-CR. The MH bed temperature at the end of absorption is less than 600 K for case 3 and case 4. The MH bed temperature from case 4 reduces faster than case 3 because of the PCM configuration's effect. Case 3 only combines with the PCM jacket, where there is a heat transferring from the side only. There are more heat transfers from the top and bottom parts of the MH bed due to the PCM capsule from case 4. This results in a higher PCM temperature from case 4 compared to case 3. The PCM temperature from the PCM capsule raises up to 581 K, while it is around 580 K from the PCM jacket.

For the desorption process, the MH bed temperature suddenly decreases due to the endothermic reaction. This phenomenon applies to all cases. The MH bed temperature from this process is less than 555 K for all cases. The MH bed temperature is lower than the melting temperature of the PCM, which is 580 K for $NaNO_3$. Then, the MH bed temperature continually increases when receiving the supply heat from the outer PCM, which previously stored the generated heat during the absorption. From this state, the PCM starts to release heat and transforms the phase from a liquid state to a solid state. Therefore, the MH bed receives the supply heat from the PCM to sustain the desorption process. The PCM temperature gradually decreases when changing the phase. At the end of the desorption process, the PCM temperature decreases to lower than the melting point for all cases. The PCM temperature range is between 576 K and 577 K. From the cases without SCHE-CR, the MH bed temperature from case 2 increases faster and higher than case 1 due to the PCM configuration's effect which releases the heat from the bottom part rather than only the side part. At the end of the desorption process, the MH bed temperature from case 1 is 563 K, while it is 565 K for case 2. However, the MH bed temperature from the cases with both SCHE-CR and PCM (case 3 and case 4) increases faster than the cases with PCM only (case 1 and case 2). At the end of desorption, the MH bed temperature from the cases with SCHE-CR and PCM is 568 K. Moreover, case 4 with PCM capsule obtains the faster MH bed temperature increase, compared to case 3 with PCM jacket. It is obvious that combining the SCHE-CR with the PCM capsule increases the heat transfer performance between the MH bed and heat exchanger sources.

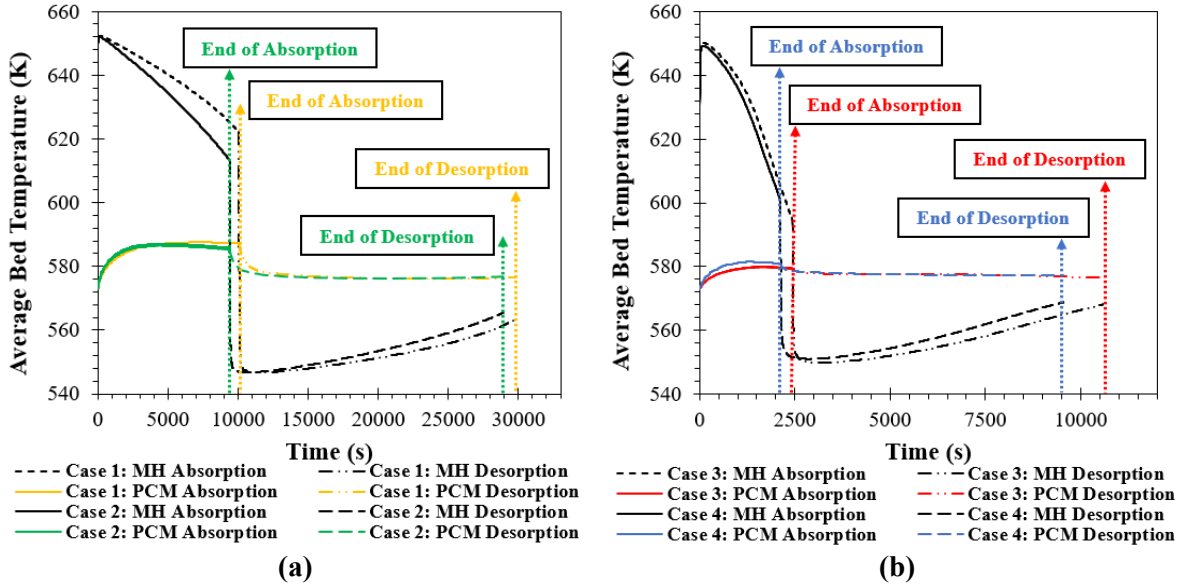

Figure 6.10 Average bed temperature of MH and PCM from storage systems during the absorption and desorption. (a) without SCHE-CR (case 1, 2) and (b) with SCHE-CR (case 3, 4)

The liquid fraction of the PCM for all cases is illustrated in Figure 6.11. During the absorption process, the PCM starts to change the phase from solid state to liquid state as it absorbs the generated heat from the MH. The PCM liquid fraction increases from 0 (fully solid state) to 0.63 from case 1 which means that there is a 63% of PCM changing the phase from solid state to liquid state during the absorption process. However, there is 0.68 of liquid fraction or a 68% of PCM liquidus from case 2. The overall liquid fraction from case 2 is higher than case 1 because there is additional PCM at the bottom part of MH bed from case 2, which absorbs more heat than case 1. Similarly, the PCM liquid fraction from the PCM capsule (case 4) is also higher than the case from the PCM jacket (case 3). However, the PCM liquid fraction from case 3 and case 4 is lower than case 1 and case 2. This is because of the internal SCHE-CR effect. The MH bed is faster cooled down from the cases with SCHE-CR compared to the case without SCHE-CR (case 1, 2). This leads to having less temperature differences between the MH bed and outer PCM from cases 3, 4. The less difference in temperature variation, results in the less heat transfer. Therefore, the liquid fraction for case 3 and case 4 is only 0.27 and 0.35, respectively. In other words, there is only 27% and 35% of PCM liquidus from case 3 and case 4. However, the PCM liquidus from case 4 is higher than case 3 due to the ability to absorb the heat from the top and bottom parts of the PCM capsule. After the completion of the absorption process, the MH bed rapidly decreases as the heat is stopped to generate. As mentioned earlier, the MH bed temperature is then lower than the PCM melting point for the desorption process. The PCM then starts to release the heat and transforms into a solid phase. Consequently, the PCM liquid fraction starts to reduce to reach 0 (at a fully solid-state) during the hydrogen desorption process.

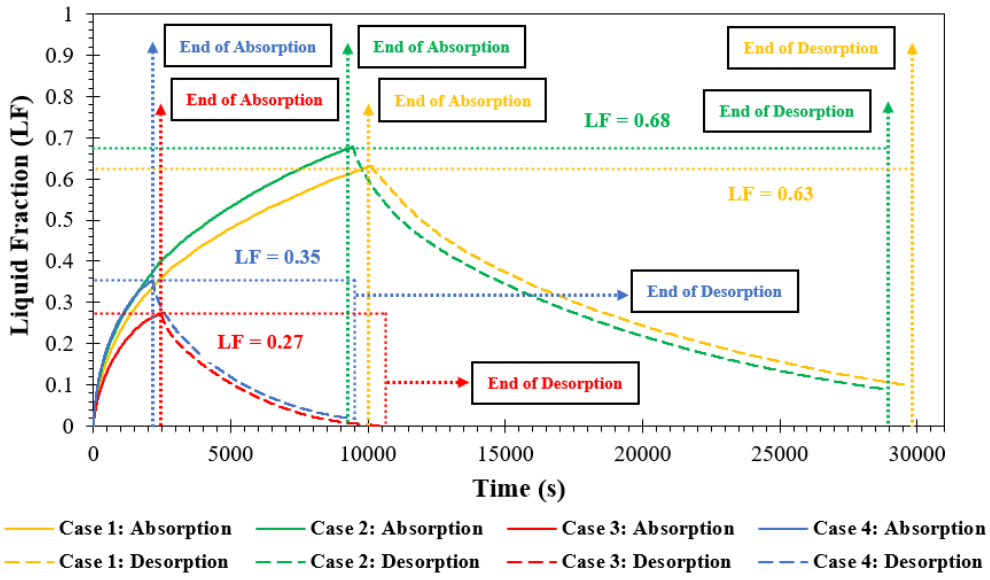

Figure 6.11 Liquid fraction from storage systems for case 1 to case 4 during the absorption and desorption

The faster heat removal from the MHHS results in faster hydrogen absorption, while a faster heat addition to the MHHS results in faster hydrogen desorption. The hydrogen concentration corresponding to the absorption and desorption times for all cases is presented in Figure 6.12. The complete absorption time for case 1 and case 2 is 10062 s and 9408 s, respectively. There is a 7% reduction in absorption duration when using a PCM pool bed instead of a PCM jacket. However, the complete absorption duration from case 3 is only 2435 s, which is a 74% reduction of absorption duration compared to case 2. It is obvious that incorporating the SCHE-CR inside the MH bed and PCM covering the MH bed significantly increases the heat transfer performance, resulting in faster hydrogen absorption.

Furthermore, the complete absorption duration from case 4 is 2121 s, which is shorter than case 3. There is a 13% reduction in hydrogen absorption duration when changing the PCM jacket to the PCM capsule. For the desorption process, the desorption duration from case 1 and case 2 is 19675 s and 19490, respectively. There is only a 1% reduction in desorption duration between these two cases. However, the desorption duration from case 3 and case 4 is 8152 s and 7425 s, respectively. There is a 58% reduction in desorption duration from case 3 compared to case 2. Moreover, the desorption duration is further decreased when using a PCM capsule (case 4) instead of a PCM jacket (case 3). The desorption duration reduces by 9% from case 4, compared to case 3.

For more analysis of the hydrogen absorption-desorption cycling process, case 1 and case 2 take time to complete the one cycling process at 29737 s and 28898 s, respectively. There is only a 3% reduction from case 2 compared to case 1. However, case 3 and case 4 take time only 10587 s and 9546 s to complete the one cycling process. There is a 63% reduction in the complete cycle from case 3 compared to case 2. Furthermore, the complete cycling duration is reduced by 10% from case 4 compared to case 3. It is obvious that the incorporation of SCHE-CR and PCM capsule (case 4) obtains better heat transfer performance compared to other cases. The consuming time from case 4 is less than 10000 s. From these results, it is obvious that incorporating SCHE-CR with outer PCM (case 3 and case 4) improves the MHHS performance compared to the MHHS with SCHE-CR only (refer to Figure 6.6 for the hydrogen absorption/desorption duration). The MHHS with SCHE-CR obtains the absorption and desorption durations at 3910 s and 13369 s, respectively. Therefore, the duration of the complete cycle from this case is 17279 s. The duration of the complete cycle is reduced by 39% from case 3 compared to the MHHS with SCHE-CR only, while there is a 45% reduction of duration for the complete cycle from case 4 compared to the same MHHS with SCHE-CR.

Under the constant volumes of MH and PCM, case 3 and case 4 obtain better heat transfer performance due to the effect of internal SCHE-CR. However, the PCM configuration also affects the MHHS's performance for both absorption and desorption. Without the SCHE-CR, the case with PCM pool bed (case 2) obtains better heat transfer performance rather than the case with PCM jacket (case 1). Focusing on the combination of both SCHE-CR and outer PCM, the case with PCM capsule (case 4) obtains better performance than the case with PCM jacket (case 3). The contours of some related parameters are created for all four cases to provide a better understanding of the heat transfer behaviour and its effect on the hydrogen concentration. These include the temperature contours, liquid fraction contours, and hydrogen concentration contours. It should be noted that only half of MHHS (right side) is used to analyse all contours (except for hydrogen concentration contours) due to the symmetry of the MHHS designs.

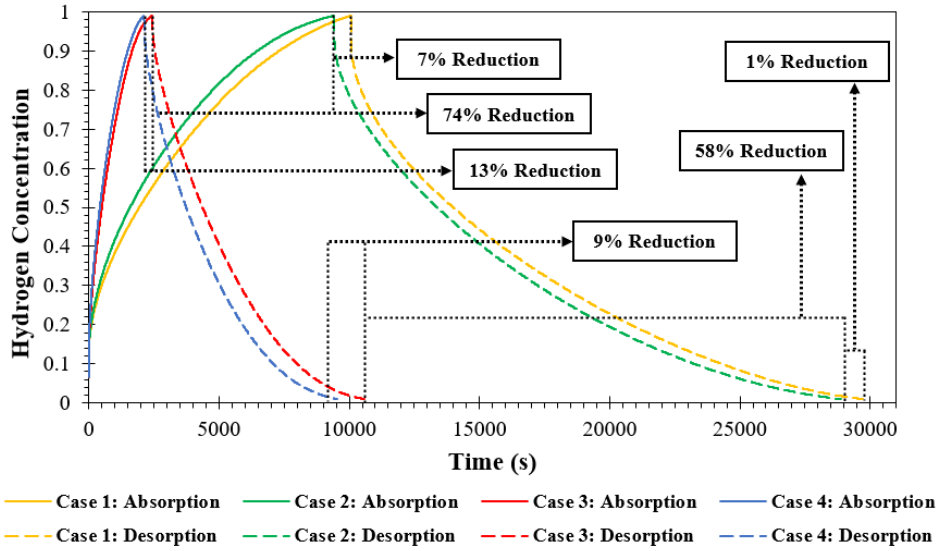

Figure 6.12 Hydrogen concentration from storage systems with different heat exchangers during the absorption and desorption

The temperature contours of the MH bed and outer PCM during the hydrogen absorption are illustrated in Figure 6.13. These contours present the selected time at 250 s and 2000 s after starting the absorption process and at the end of the absorption process for each case. At 250 s, the MH temperature near the interface between the MH and PCM is lower than in other areas due to the PCM effects. The PCM near the interface starts to absorb the generated heat, resulting in the reduction of the MH bed temperature near the interface. Therefore, there is a heat transfer at the side from the interface of case 1 (PCM jacket), while there is a heat transfer at the side and bottom from case 2 (PCM pool bed) instead. Similarly, the heat is transferred from the MH to PCM at the side for case 3 (PCM jacket). More heat transfers are observed from case 4 where it has a PCM capsule that absorbs the heat from the top and bottom parts of the MH bed. However, there is also the additional heat transfer source from HTF from the case with SCHE-CR (case 3 and case 4). The lower MH bed temperature is observed around the wall of the HTF tube, where it has cooling fluid circulating inside. At 2000 s, the MH bed temperature is greatly lower at the side where is close to the PCM, while the PCM temperature is higher. This phenomenon occurs in case 1 and case 2. The MH bed temperature around the central area is still 654 K, while the minimum MH bed temperature near the interface is only 632 K for case 1 and 611 K for case 2. The minimum PCM temperature from these two cases is still the initial value of 573 K. The maximum PCM temperature at the interface from these two cases is 611 K. However, the MH bed temperature from case 3 and case 4 is significantly lower due to the SCHE-CR's effect. The MH bed temperature at the bottom part reduces to 589 K in these two cases. There are still some areas at the top part of case 3 that still has 654 K. The MH temperature at the top part from case 4 is less than 643 K. This is because the PCM capsule absorbs the heat from the top part. Furthermore, the MH bed temperature from the case with PCM capsule (case 4) is also lower at the top and bottom parts compared to the case with PCM jacket (case 3). The maximum PCM temperature near the interface from case 3 and case 4 is only 589 K, whereas the minimum PCM temperature is still the initial value at 573 K. Considering the PCM temperature at the middle part of MHHS from case 3 and case 4, the temperature variation around this area is less than other areas because the MH temperature at this area is lower than other areas. This is because this area is close to the HTF inlet and has more heat transfer surface areas from SCHE-CR structure. Although the bottom part of the MHHS is close to the HTF inlet, it has less heat transfer surface areas compared to the middle part. Therefore, the MH bed around the middle part is cooled down faster than in other areas. This leads to having less temperature difference around this area, resulting in having a less heat transfer rate.

At the end of the absorption process for each case, the centre part of MH bed from case 1 and case 2 still has a higher temperature as 654 K. The minimum PCM temperature at the outer wall is observed as 578 K. Therefore, the minimum PCM temperature increases from 573 K (initial value) to 578 K after reaching the end of the absorption process. However, the minimum PCM temperature from case 3 and case 4 still remains at 573 K. More temperature contours from various selected times after the hydrogen absorption are provided in the "Appendices: A2".

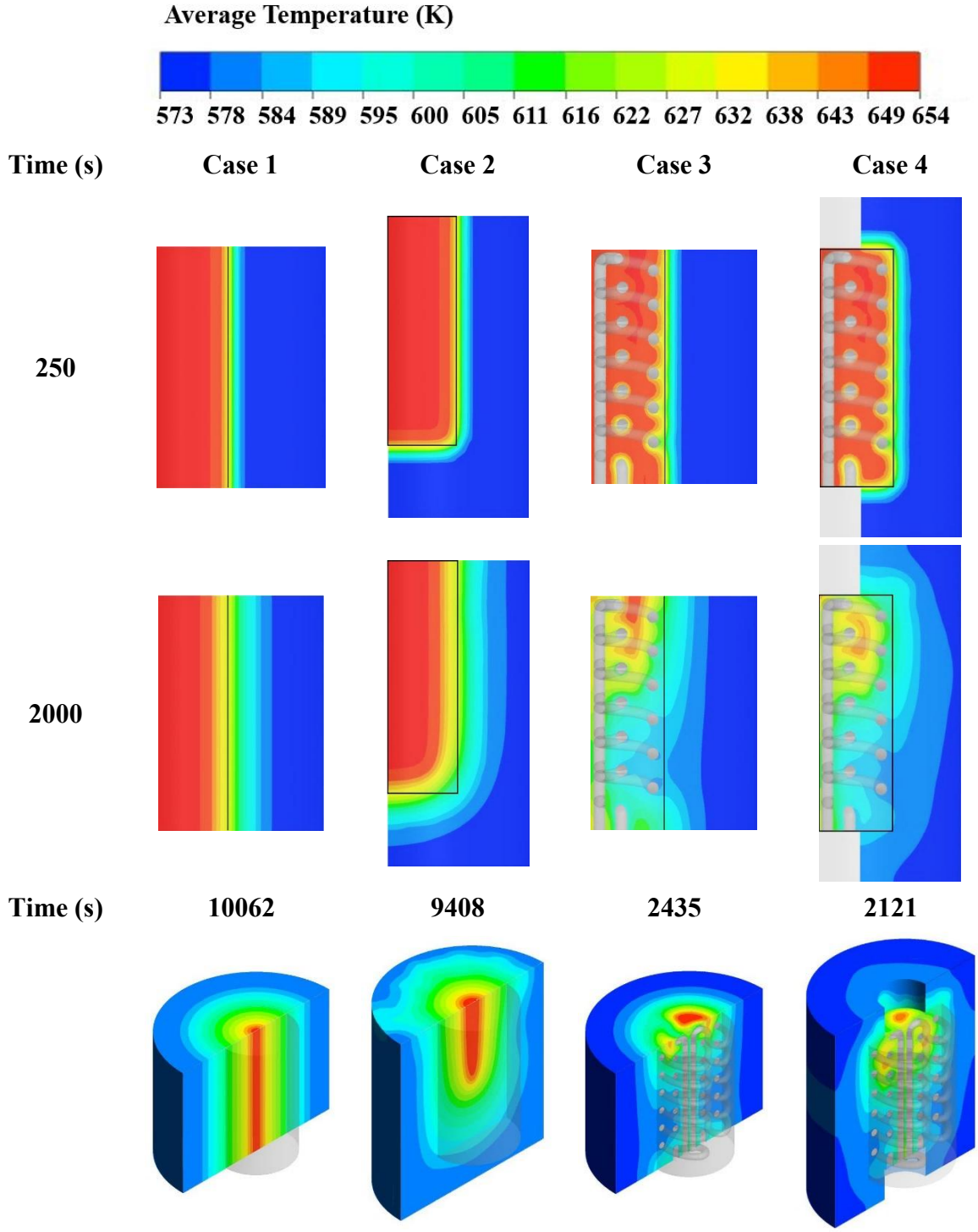

Figure 6.13 Average temperature of MH bed and PCM at 250 s, 2000 s, after starting the hydrogen absorption, and at the end of the absorption process from case 1 to case 4

The PCM liquid fraction during the absorption process for all cases is presented as the contours in Figure 6.14. At 250 s, the PCM solidus starts to transform to a liquid phase at the interface where it has a high MH temperature. At 2000s, the liquid fraction from all cases still remains the same patterns from the time at 250 s. However, at the end of the absorption process for each case, the case with the PCM pool bed (case 2) obtains more PCM liquidus compared to other cases. This is due to the fact that there are more heat transfers from the side and bottom parts of the MH bed from case 2 compared to case 1 which has only the side of PCM. Furthermore, there is no additional energy source from HTF in this case, when compared to case 3 and case 4 (with SCHE-CR). However, more PCM liquidus is observed from case 4 rather than case 3 due to the PCM capsule's effect. It should be noted that the PCM thickness at the side from case 1 and case 3 are constant due to having the same PCM configuration (PCM jacket). However, the PCM thickness at the side from case 2 and case 4 are less than another two cases due to having different PCM configurations. Case 2 (PCM pool bed) has full PCM at the bottom part, while case 4 (PCM capsule) has half PCM and the bottom and top parts. The purposes of these designs are to maintain the constant volume of PCM for all cases and enhance MHHS's performance by considering the enhancement of the heat transfer rate. More liquid fraction contours from various selected times after the hydrogen absorption can be found in the "Appendices: A2".

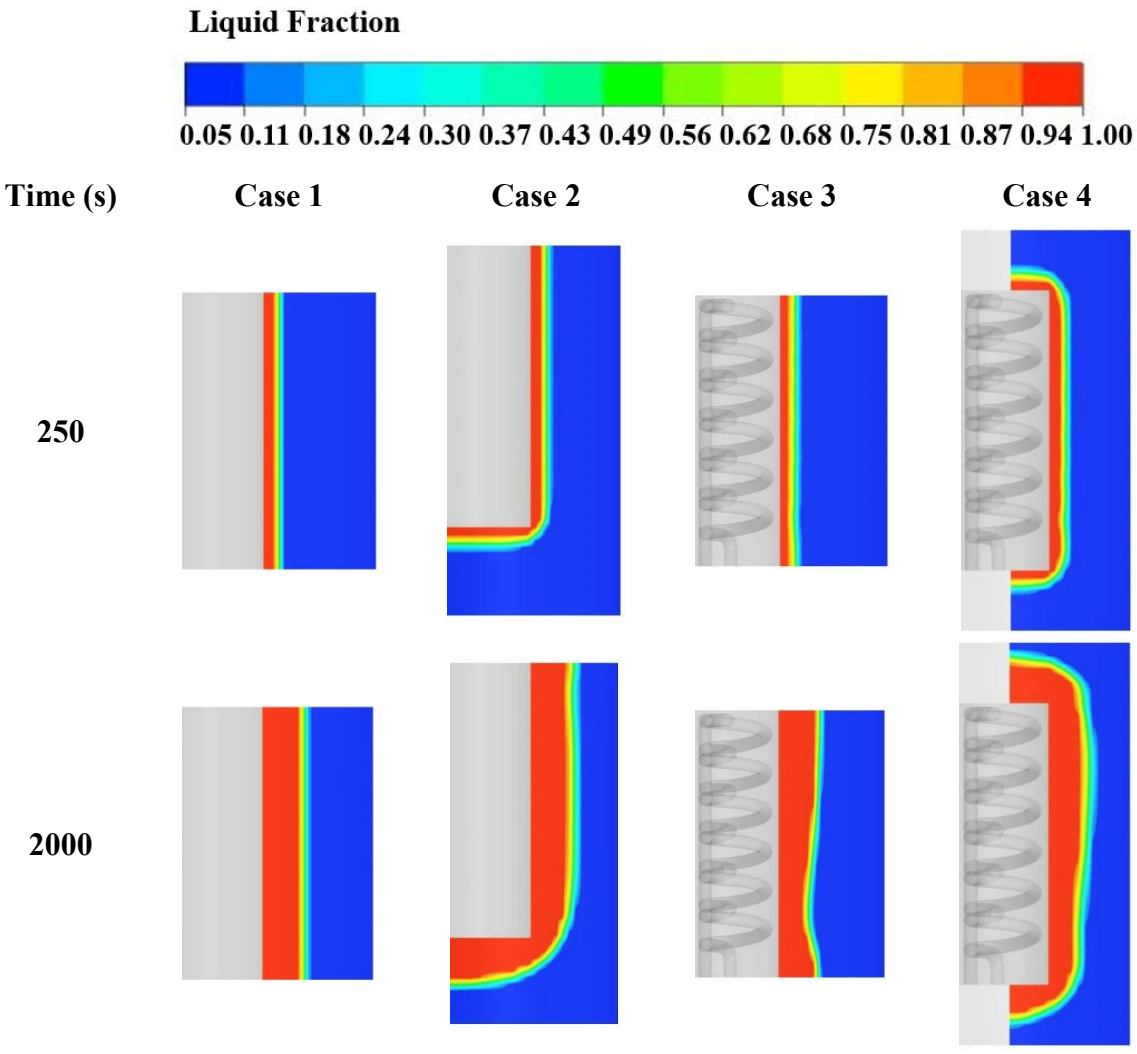

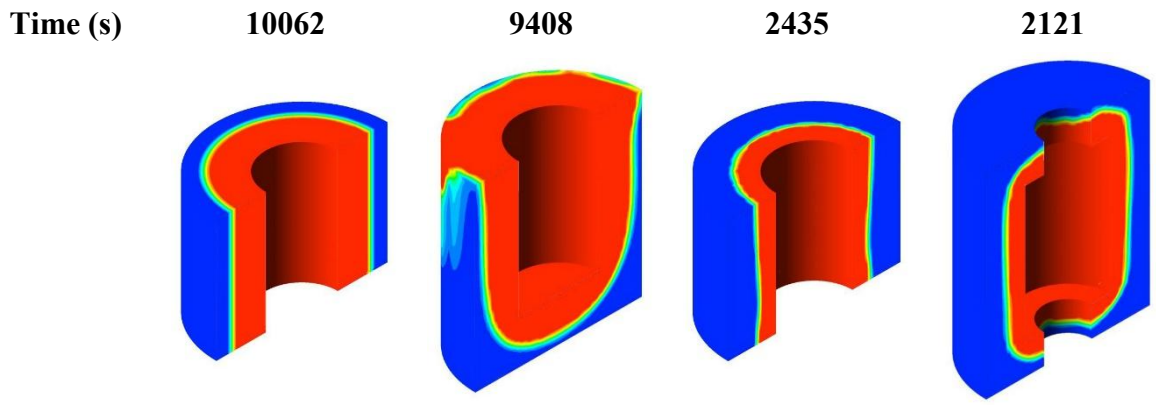

Figure 6.14 Liquid fraction of PCM at 250 s, 2000 s, after starting the hydrogen absorption, and at the end of the absorption process from case 1 to case 4

The hydrogen concentration contours at 2000 s and at the end of the absorption process for all cases are demonstrated in Figure 6.15. At 2000 s, a higher hydrogen concentration is found near the interface from case 1 and case 2. Furthermore, the bottom part of case 2 (PCM pool bed) also has a higher hydrogen concentration compared to case 1 (PCM jacket). However, the hydrogen concentration is significantly higher in case 3 and case 4 due to the SCHE-CR's effect. The PCM capsule (case 4) obtains better performance than the PCM jacket (case 3). There are high hydrogen concentrations at the top and bottom parts of the MH bed from case 4. The hydrogen concentration from most parts of case 1 and case 2 is still 11%, while the hydrogen concentration from most parts of case 3 and case 4 is 100%. At the end of the absorption process from each case (99% of overall hydrogen concentration), The lower hydrogen concentration is found at the central area of case 1 and case 2. However, there is only the middle and top parts of the central area from case 2 where it has a lower hydrogen concentration. The lower hydrogen concentration from case 3 is found at the top part and at the small areas from the bottom where it has less heat transfer surface areas. From case 4, there is only the top part that has the lower hydrogen concentration. More hydrogen concentration contours from various selected times after the hydrogen absorption are provide in the "Appendices: A2".

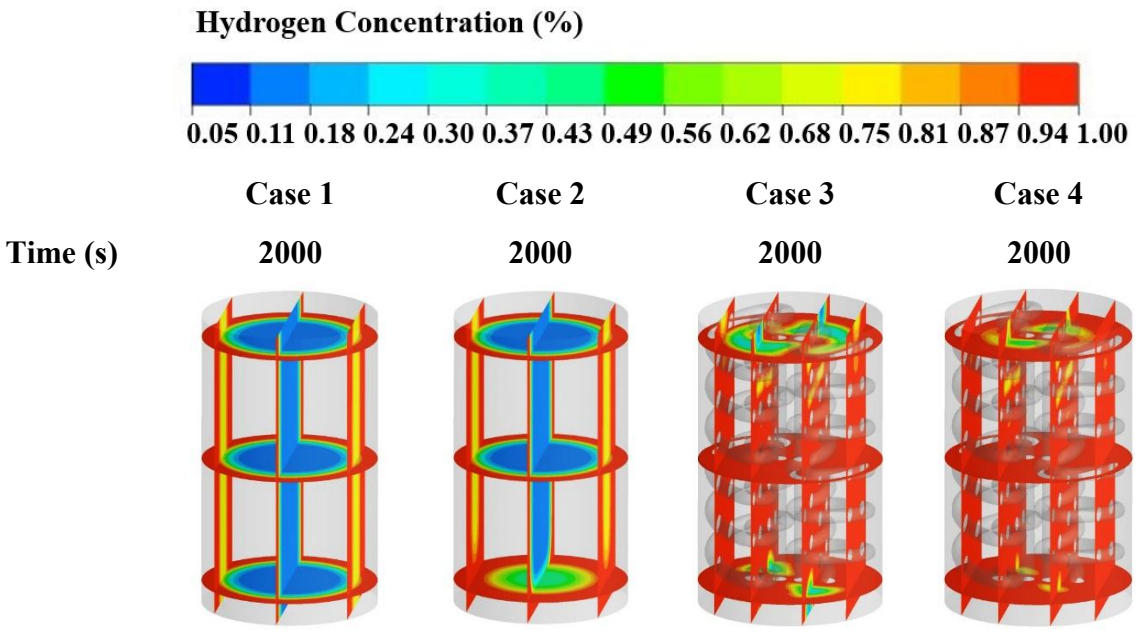

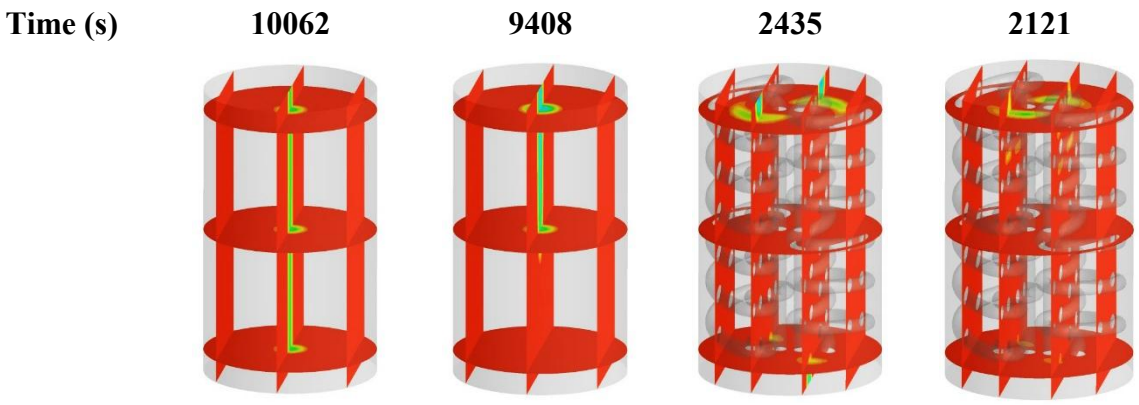

Figure 6.15 Hydrogen concentration at 2000 s and at the end of the hydrogen absorption process of each case (case 1 to case 4)

The temperature variations of the MH and PCM during the desorption process for all cases are presented in Figure 6.16. These include the selected time at 500 s and 7500 s after starting the desorption process. As mentioned earlier, the MH bed temperature is rapidly decreased due to the endothermic reaction. At 500 s, the minimum MH temperature from case 1 and case 2 is still 543 K, while there is only the top part of MHHS where it has a lower temperature at 543 K for case 3. However, the minimum MH temperature from case 4 is 548 K. At the interface of PCM and MH, the temperature from the MH side is higher while the temperature from the PCM side is lower for all cases. At this area, the maximum MH temperature from all cases at 500 s is 550 K, while the minimum PCM temperature is 570 K. From this process, the MH is heated up by receiving the heat from PCM, while the PCM is cooled down. The PCM temperature, where it is close to the interface, is lower than the melting point for all cases. It should be noted that the PCM temperature at the inner and central areas is higher than the outer side due to the effect of the absorption process, which leads the PCM near the MH having a higher temperature (refer to Figure 6.13).

From all cases, the case with SCHE-CR (case 3 and case 4) has a higher MH temperature compared to the case without SCHE-CR (case 1 and case 2). The significant change in temperature variations is observed from the temperature contours at 7500 s. The minimum MH temperature from case 1 and case 2 is still 543 K, while there are 560 K and 568 K of the minimum values from case 3 and case 4, respectively. Moreover, the maximum value of MH temperature from case 1 and case 2 is still 550 K but it is 570 K as the maximum value from case 3 and case 4. Focusing on PCM temperature for all cases, there is still heat transferring from the central area of PCM to the outer side of PCM as the PCM temperature at the outer side at 7500s is higher than at 500 s. This is due to the fact that at the end of the hydrogen absorption process, there is still a portion of the PCM, which remains in the solidification state (refer to the liquid fraction of PCM in Figure 6.14). The heat from melting PCM continually flows to solid PCM causing the increase in PCM temperature at the outer side. This fact is applied to all cases. For case 3 and case 4, the PCM temperature around the middle part of MHHS is higher than other parts due to the higher MH bed temperature around this area, which is caused by the heating HTF and its location. The HTF temperature from the bottom part is higher than the other parts as this part is close to the HTF inlet. More temperature contours from various selected times after the hydrogen desorption are provided in the “Appendices: A2”.

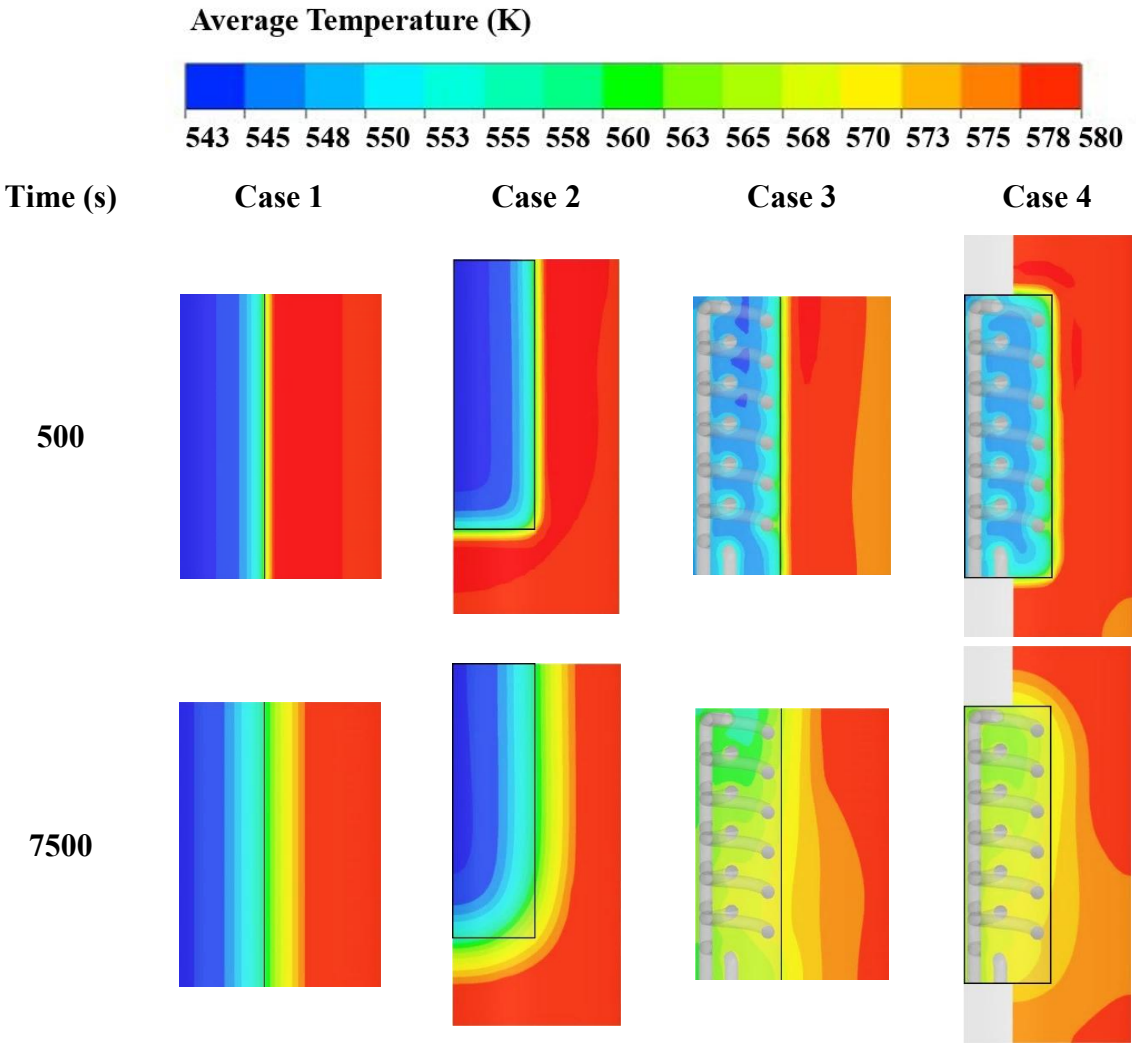

Figure 6.16 Average temperature of MH bed and PCM at 500 s and 7500 s after starting hydrogen desorption process from case 1 to case 4

Figure 6.17 illustrates the PCM liquid fraction after starting the desorption process at 500 s and 7500 s for all cases. For all cases, the PCM starts to release the heat and transform from liquid phase to solid phase at the interface between the MH and PCM. More amounts of PCM liquidus are observed around the outer side of PCM at 7500 s compared to at 500 s from case 1 and case 2. Although more PCM solidus is found from the interface side in these cases, the PCM liquidus from the outer side still increases as there is still the heat transferring from the central area of PCM to the outer side of PCM (see temperature contours in Figure 6.16). However, the PCM liquidus from case 1 and case 2 is still higher than case 3 and case 4. This is because the PCM liquidus from case 3 and case 4 is less than case 1 and case 2 at the end of the absorption process (see liquid fraction of PCM in Figure 6.14). This leads to having only 5-24% of PCM liquidus from case 3 and case 4, while there is still 94% of PCM liquidus from case 1 and case 2 at 7500 s. More liquid fraction contours from various selected times after the hydrogen desorption can be found in the "Appendices: A2".

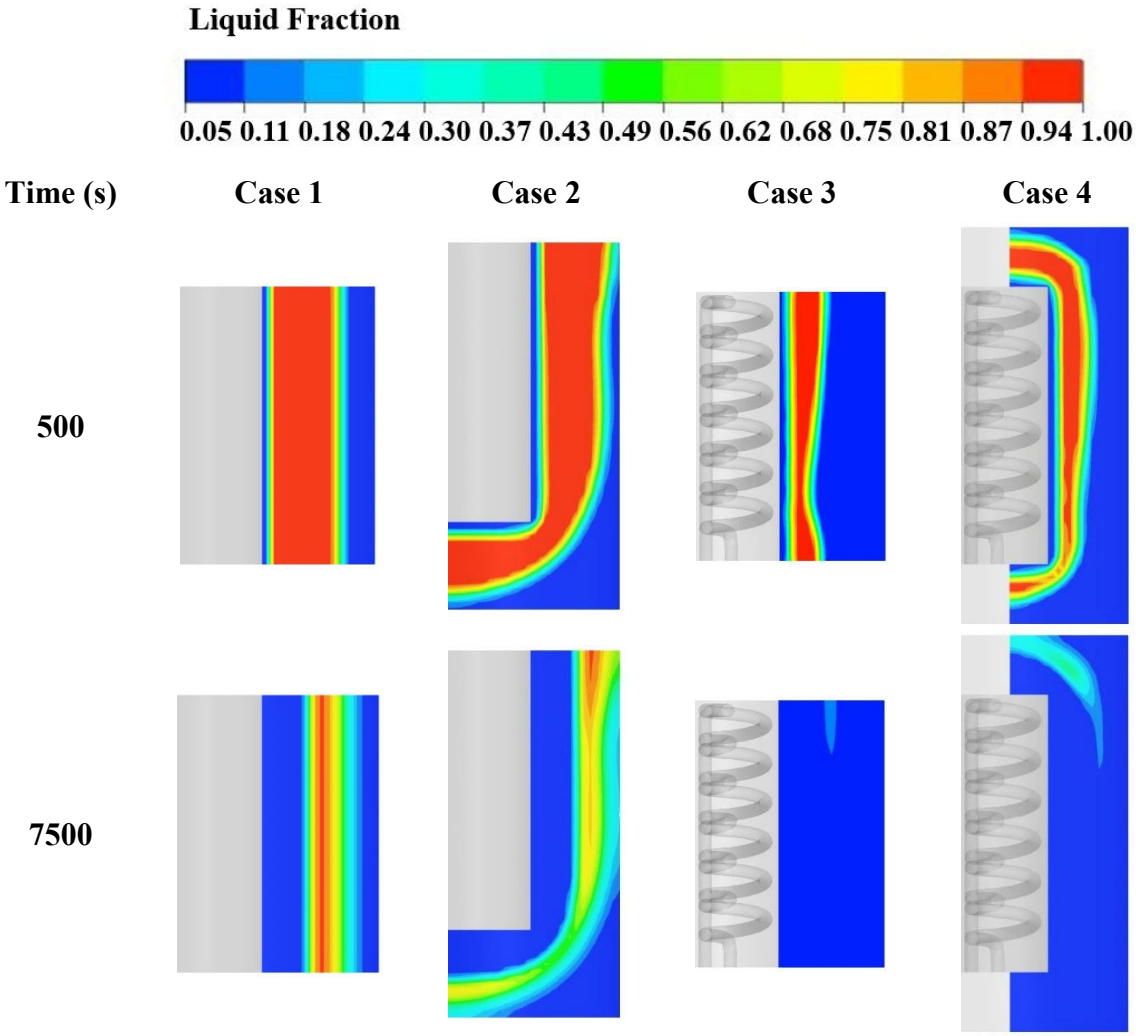

Figure 6.17 Liquid fraction of PCM at 500 s and 7500 s after starting the hydrogen desorption process from case 1 to case 4

The hydrogen concentration at 7000 s after starting the desorption process for all cases is presented in Figure 6.18. The hydrogen concentration from case 4 is less than 5% at 7000 s, while there is still an 18% of hydrogen concentration from some areas at the top and bottom parts for case 3. However, the hydrogen concentration from case 1 and case 2 is mostly 18-75%. It should be noted that the hydrogen concentration at the central area in these two cases (case 1 and case 2) is less than in other areas because of the effect of the absorption process. At the end of the absorption process (99% of overall hydrogen concentration), this area has less hydrogen concentration due to the PCM configurations (see hydrogen concentration contours in Figure 6.15). This results in a lower hydrogen concentration in this area during the hydrogen desorption. The hydrogen concentration at the bottom part of case 2 is still lower than case 1 due to the PCM pool bed configuration. More hydrogen concentration contours from various selected times after the hydrogen desorption are provide in the “Appendices: A2”.

However, the MHHS performance is significantly enhanced when using internal SCHE-CR incorporating the outer PCM, especially the PCM capsule. This is obvious from case 4, which obtains a faster hydrogen absorption and desorption compared to other cases. Therefore, the performance of MHHS configuration based on case 4 is then further analysed under the parametric study section.

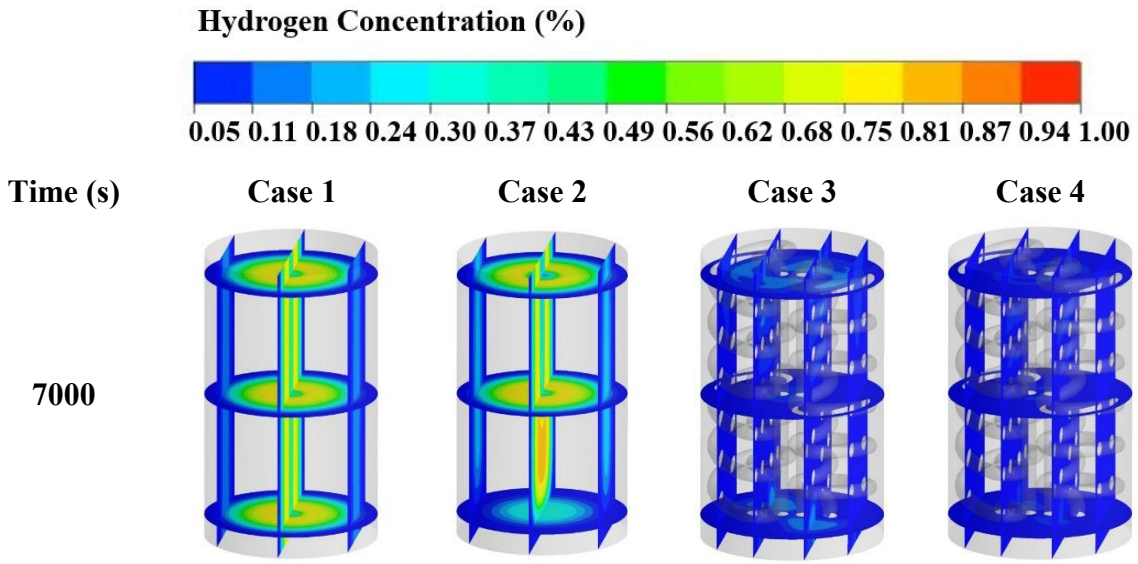

Figure 6.18 Hydrogen concentration at 7000 s after starting hydrogen desorption process from case 1 to case 4

6.6.3 Storage Weight and Heat Recovery

The overall storage weight is also an important parameter for the MHHS in compactable size. Figure 6.19 presents the effect of heat exchanger designs on the overall storage weight. There is only 0.59 kg of the MHHS when using the SCHE-CR (refer to case 0 in this figure). The original weight of the MH only is 0.45 kg with the total volume at 140 cm^3. This is only a 0.14 kg increase of additional weight from the SCHE-CR. It is worth mentioning that the SCHE weight is only 0.12 kg, which is 0.02 kg less than the weight of SCHE-CR. The duration of the absorption-desorption cycle is 17279 s, as mentioned earlier. When using the PCM as the heat exchanger instead of the SCHE-CR, the overall MHHS weight is 1.91 kg (case 1 and case 2). The PCM weight based on $NaNO_3$ from these two cases is 1.47 kg. However, the duration of the absorption-desorption cycle is increased with the use of PCM only. There are 29737 s and 28898 s of one complete duration in the absorption-desorption cycle from case 1 with the PCM jacket and case 2 with the PCM pool bed, respectively. The storage weight is then slightly increased when combining the PCM with SCHE-CR, as in case 3 and case 4. The overall storage weight from these two cases is 2.05 kg, which is increased by only 0.14 kg from the case with PCM only. The duration of the absorption-desorption cycle is then further reduced to 10587 s for case 3 with PCM jacket and 9546 s for case 4 with PCM capsule. From this combination, the duration of one complete cycle for absorption-desorption is reduced by 38.73% in case 3 and 44.75% in case 4, compared to the use of SCHE-CR only (case 0).

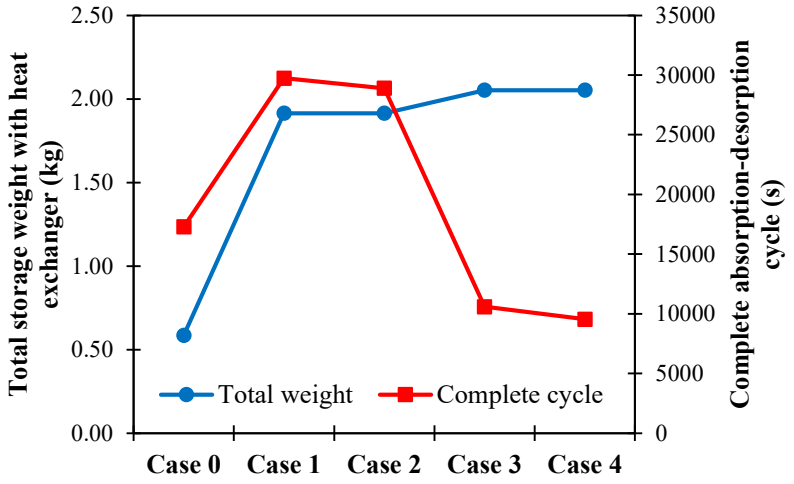

Figure 6.19 Comparison of total storage weight with heat exchanger and one complete absorption-desorption cycle from different heat exchanger designs

This section investigates energy exchange inside the MHHS under the different MHHS configurations. In the case with only MH and PCM (case 1 and case 2), the energy is exchanged only between the MH and PCM. Under the combination of PCM and SCHE-CR, the energy is exchanged among MH, HTF (from SCHE-CR), and PCM. For the analysis, the reaction heat (Q_r) of both hydrogen absorption and desorption is equal, while the heat loss in the energy exchange process is not considered (Ye et al., 2022). During the absorption process, the heat from the MH bed is transferred to the HTF (Q_{h1}) and PCM (Q_{p1}). Therefore, the reaction heat for the absorption process is $Q_{r,abs} = Q_{h1} + Q_{p1}$. For the desorption process, the stored heat in PCM is released to MH (Q_{p2}), while the heat is charged to MH by HTF (Q_{h2}). Therefore, the reaction heat for the desorption process is $Q_{r,des} = Q_{h2} + Q_{p2}$. It should be noted that $Q_{h1} = Q_{h2}$ and $Q_{p1} = Q_{p2}$. These conditions are applied to compare the performance of each MHHS design under the energy analysis only. The heat loss through the environment under absorption and desorption is not considered in this study. In reality, HTF requires to dissipate the heat (Q_{h1}) to the environment in order to maintain a constant inlet temperature (T_{in}), without considering the heat loss. For the desorption process, the HTF requires the additional heat sauce (Q_{h2}) to heat up the MH. Therefore, Q_{h2} is the main parameter for energy consumption in the MHHS. However, at the end of the hydrogen desorption process, the temperature of MH and PCM returns to the initial temperature of the absorption process (Ye et al., 2022). Therefore, the reaction heat for the MHHS with HTF only (case 0) is determined based on Equation 6.1. The reaction heat for the MHHS with PCM (case 1 and case 2) is expressed as Equation 6.2, while the reaction heat for the case with PCM and HTF (case 3 and case 4) is referred to as Equation 6.3 (Ye et al., 2022).

$$Q_r = Q_h = \frac{V_{MH} \times \rho_{MH} \times wt \times (1-\varepsilon)}{M} \Delta H \tag{6.1}$$

$$Q_r = Q_p = V_{PCM} \times \rho_{PCM} \left[L_{PCM} + c_{p,PCM} \times \left(T_{max,PCM} - T_0 \right) \right] \tag{6.2}$$

$$Q_h = Q_r - Q_p \tag{6.3}$$

where $T_{max,PCM}$ is the maximum temperature of the PCM during the hydrogen absorption or desorption process, while T_0 is the initial temperature of the PCM. The volumes of MH and PCM are V_{MH} and V_{PCM}, respectively.

Figure 6.20 presents the effect of PCM amount and its weight on the reaction heat and recovery rate of the reaction heat. The reaction heat from the HTF without PCM (case 0) is 255.37 kJ. It should be noted that the PCM amount from case 1 to case 4 is constant as 649 cm^3 or 1.47 kg of PCM weight, which is assumed to store all the heat released from the MHHS (refer to Equation 6.1). This amount is considered as the base case with 8/8 unit of the total PCM volume (100%). The other PCM amounts are reduced from the base case starting from 1/8 to 7/8 unit of the total PCM volume. From Figure 6.20a, the reaction heat from the PCM positively increases, corresponding to the reduction of HTF reaction heat, starting from the case with 1/8 unit to 4/8 unit. Under 1/8 of the total PCM volume, the reaction heat from the HTF (Q_h) is 233.56 kJ with the reaction heat from PCM (Q_p) at 21.82 kJ only. From the 4/8 of the total PCM volume, the Q_h is reduced to 146.71 kJ with an increase of the Q_p at 108.66 kJ. However, the PCM volumes from 5/8 to 8/8 units have less effect on reducing HTF reaction heat. Considering the reaction of heat recovery rate (Q_p/Q_r) from Figure 6.20b, this rate is increased from 8.54% to 42.55% when increasing the PCM volume from 1/8 unit to 4/8 unit. Although other higher PCM volumes, especially the case with 8/8 unit (the base case), have a higher reaction of heat recovery rate from 56.51% to 100%, these cases are useful with the use of MHHS and PCM only. The use of PCM and HTF is not effective under this condition. Moreover, the increase/decrease in PCM amount significantly affects the PCM weight, resulting in an increase/decrease in the overall MHHS weight. When using a PCM volume of 1/8 unit, there is only 0.12 kg of additional weight, compared to the case with SCHE-CR only. However, there is 0.59 kg of additional weight when using the PCM volume as 4/8 unit. There is a 50% increase in the overall MHHS weight from the additional PCM volume of 4/8 unit. Other higher PCM volumes result in a 57% to 72% increase in the overall MHHS weight. It can be summarised that the 4/8 of the total PCM volume or 1.47 kg of the PCM obtains the best performance when considering the reaction heat from HTF and PCM with an appropriate reaction of the heat recovery rate. It should be noted that this study only considers the effect of these PCM amounts on the energy and storage weight analysis. The effect of different PCM amounts on the hydrogen absorption/desorption duration is not considered in the present study.

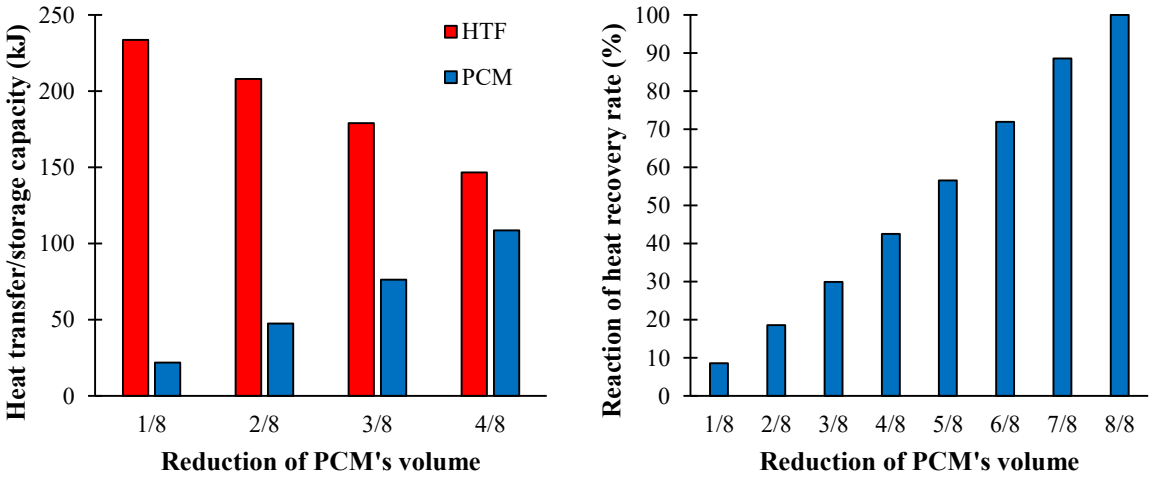

Figure 6.20 Effect of PCM's volumes on; (a) heat transfer/storage capacity and (b) reaction of heat recovery rate

6.6.4 Parametric Study of Operating Conditions

One of the main parameters that significantly affect the hydrogen kinetic reaction is HTF temperature. A lower HTF temperature will result in a higher heat removal rate during the absorption process. This leads to the reduction of absorption duration. In the opposite way, a higher HTF temperature will lead the storage system to be heated up during the desorption, resulting in the reduction of desorption duration. This section provides a more critical analysis regarding the effect of HTF temperature on hydrogen absorption and desorption. The MHHS with SCHE-CR and PCM capsule (case 4) is selected for this section as this case obtains the best performance for hydrogen absorption and desorption. For investigation purposes, various initial HTF temperatures are selected for both absorption and desorption and presented in Figure 6.21. The initial temperature of the MHHS is constant at 573 K with loading pressure at 1.8 MPa for the absorption process. For the desorption process, the ultimate temperature of the absorption process is the initial temperature of the MHHS (from the case with 573 K as the initial value) and hydrogen pressure at 0.1 MPa. Figure 6.21a refers to the absorption process with the HTF temperature varying from 473 K to 573 K. The absorption duration greatly reduces after using the lower HTF temperature. The final time of the absorption process is 2121 K with the initial HTF temperature at 573 K but it is only 1578 s when using 523 K as the HTF temperature. There is a 26% reduction in absorption duration from these cases. However, the absorption duration is further reduced to 1265 s and 1071 s when using the HTF temperature of 473 K and 423 K, respectively. There are 20% and 15% reductions in absorption duration when changing the HTF temperature from 523 K to 473 K and from 473 K to 423 K, respectively.

The effect of varying HTF temperatures on hydrogen desorption is presented in Figure 6.21b. The HTF temperatures vary from 573 K to 723 K for this process. It is evident that increasing the initial HTF temperature leads to the reduction of desorption duration. The final time of the desorption process from the case with HTF temperature at 573 K is 7425 s. However, there is a 38% reduction in desorption duration when changing the temperature from 573 K to 623 K. The final time from this case is 4573 s. The desorption duration is also further reduced by 28% and 25% when increasing the HTF temperature from 623 K to 673 K and from 673 K to 723 K, respectively. The duration of the desorption process from the cases with 673 K and 723 K is 3304 s and 2484 s, respectively.

The main reason to cause the significant improvement in heat transfer performance from these cases is that the greater temperature difference between the MH bed and cooling HTF leads to a greater convective heat transfer rate for the absorption process as the MH bed temperature is really high in this state. However, the MH bed temperature is low during the desorption, which leads to a greater temperature difference when increasing the HTF temperature. The higher convective heat transfer rate during the desorption comes from the higher HTF temperature.

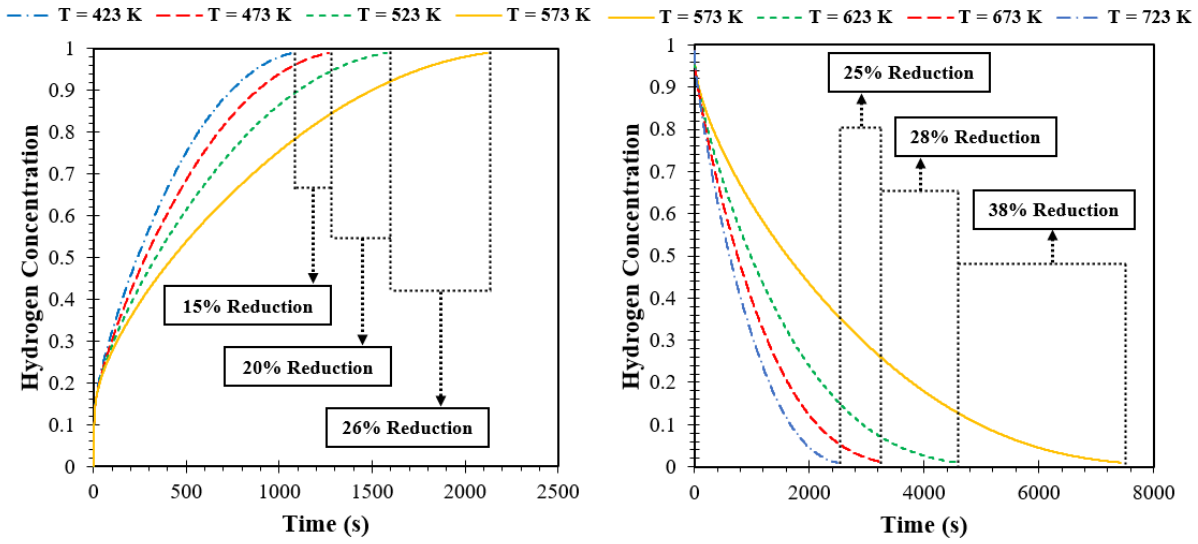

Figure 6.21 Hydrogen concentration for the different operating temperatures of the HTF in the case with SCHE-CR incorporating the PCM jacket (case 3). (a) hydrogen concentration during absorption and (b) hydrogen concentration during desorption

6.7 Conclusion

The metal hydride storage system (MHHS) performance with the use of semi-cylindrical coil heat exchanger with central return tube (SCHE-CR) is analysed for the completion of absorption-desorption cycle. The new MHHS configurations incorporating SCHE-CR and outer phase change material (PCM) are proposed in the present study to further enhance heat transfer rate. The MHHS with SCHE-CR is designed under different out PCM configurations. The metal hydride (MH) and PCM volumes are constant for all designs to provide a reasonable comparison. Furthermore, the initial operating condition of the heat transfer fluid (HTF) temperature is considered to investigate the new MHHS configuration under the absorption and desorption processes. The key findings are summarised as follows:

- There is a 31% reduction in the duration of the absorption-desorption cycle when using SCHE-CR instead of a semi-cylindrical coil heat exchanger (SCHE). There is at least a 50% reduction of this duration from SCHE-CR compared to the helical coil.
- The top part of the MH bed from the case with SCHE-CR obtains better heat transfer performance due to the well arrangement of itself, which increases more heat transfer surface areas compared to SCHE.
- The PCM configuration also affects the MHHS performance, especially the absorption process. The PCM capsule obtains better heat transfer improvement rather than the PCM jacket and PCM pool bed. More heat transfer surface areas are at the top and bottom parts of MHHS from the PCM capsule. The more PCM liquidus is observed from the case with the PCM capsule compared to other PCM configurations.
- The MHHS with SCHE-CR and PCM obtains greater improvement of heat transfer with at least a 39% reduction in the duration of absorption-desorption cycle, compared to SCHE-CR only. However, there is at least a 63% reduction in the duration of the completion time when using SCHE-CR and PCM, compared to the case with PCM only.
- The initial operating condition of the HTF temperature for the new MHHS configuration, which incorporates the SCHE-CR and PCM capsule, significantly influences the MHHS performance, especially the desorption process. The absorption duration is decreased by 15-26% when reducing the initial HTF temperature from 573 K to 423 K. However, the desorption duration

is significantly reduced by 25-38% when increasing the initial HTF temperature from 573 K to 723 K.

The comprehensive investigation of the magnesium-based hydrogen storage incorporating an internal heat exchanger and external PCM provides a better understanding of the heat transfer enhancement for hydrogen kinetic reaction during the absorption and desorption processes. This includes the investigation of a semi-cylindrical coil heat exchanger with central return tube when combining with different phase change material configurations. The findings of this study would improve the knowledge of the hydrogen storage for the fuel cell applications during the complete cycle of absorption-desorption. Moreover, the modelling principle, as well as the fundamental analysis of the heat exchanger designs and their performance, can be useful for several engineering applications.

Chapter 7 – The Enhancement of Metal Hydride Hydrogen Storage Performance Using Novel Triple-Branched Fin

Research Paper: **Larpruenrudee, P.,** Bennett, N.S., Fitch, R., Sauret, E., Gu, Y., Hossain, M.J., & Islam, M.S., (2025). The enhancement of metal hydride hydrogen storage performance using novel triple-branched fin. **Journal of Energy Storage**, 123, 116659. https://doi.org/10.3390/en18051291. **SJR: 1.456 [Q1], IF: 9.4**

7.1 Summary

Objectives to achieve the aim of this study:

- Propose the new storage configuration under the design of the new internal heat exchanger to enhance the storage thermal performance.
- The effect of pressure losses during the heat transfer fluid circulation inside the heat exchanger is considered as the key factor
- Identify an appropriate initial value of each operating parameter under the new storage configuration and heat exchanger

Achievements and innovations in this chapter:

- Propose the new fin design and enhance its performance under the hydrogen absorption and desorption processes
- Analyse the effect of pressure losses under the use of various heat exchanger designs
- Investigate the effect of fin materials on the hydrogen absorption-desorption cycle
- Investigate the initial values of the heat transfer fluid as well as the heat transfer coefficient on both hydrogen absorption and desorption processes

7.2 Abstract

The advantages of a high storage capacity and safety of metal hydride hydrogen storage (MHHS) have widely attracted people's interest in hydrogen storage. The improvement of the heat transfer performance is one of the key parameters to improve the overall MHHS performance. Various heat exchangers with complex structures have been developed for this purpose. However, the drawback of these heat exchangers is huge pressure losses. Therefore, this study aims to enhance the MHHS performance by considering the heat transfer improvement and maintaining the pressure loss inside the heat exchanger. To fulfil the requirement of heat transfer efficiency instead of using complex heat exchangers, a novel triple-branched fin is designed to attach to the simple straight tube heat exchanger. The effect of pressure losses due to the complex heat exchangers is analysed and compared with the simple straight tube. The novel fin heat exchanger's performance is also compared to conventional fins. Moreover, an enhancement of the novel fin geometries is considered with the parametric studies to achieve superior MHHS performance. The results indicate that the pressure losses are reduced by 31% when using the straight tube instead of other complex heat exchangers. The novel triple-branched fin obtains the best heat transfer performance compared to other fin designs, including the quadrilateral fin and Y-shaped fin. After the geometrical enhancement of this novel fin, the duration of the absorption-desorption cycle is reduced by 25% compared to the quadrilateral fin. Under the parametric study, heat transfer fluid temperature significantly affects the desorption process, while the heat transfer coefficient greatly affects the absorption process.

Keywords: Fins, Hydrogen absorption, Hydrogen desorption, Reaction time, Triple-branched fin, Y-shaped fin.

7.2.1 Graphical Abstract

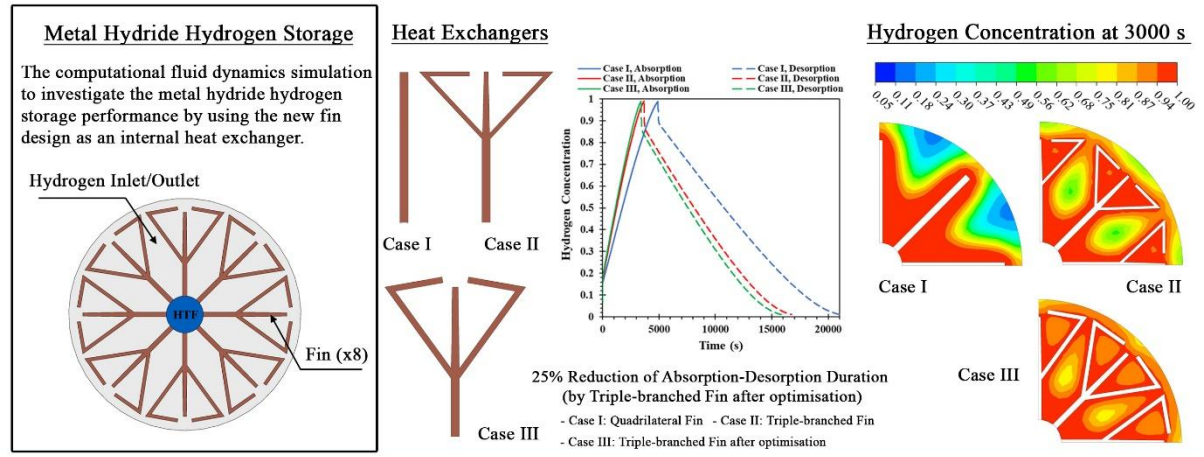

Figure 7.1 Graphical abstract for the fourth research paper

7.3 Introduction

The fin heat exchanger has been widely used for several engineering applications, such as thermal energy storage. The fin material with a high thermal conductivity is the key factor to increase the heat transfer rate. The main advantage of using fins as a heat exchanger is the simple installation and less maintenance during use, compared to other heat exchanger types (Eslami et al., 2021). For these purposes, several fin designs have been proposed for thermal energy storage with a cylindrical enclosure. Various fin parameters were considered for the radial fin design and optimisation. These included the fin thickness, fin height, fin number, fin length, fin width, and fin angle. The results from these fin parameters proved that increasing the fin number, height, and thickness improved the heat transfer performance by 20-23% enhancement of phase change duration (Zhang & Faghri 1996). Similarly, increasing the fin numbers and fin width reduces the discharging time (N´obrega et al., 2019). Beyond radial fins and annular fins, some studies also focused on heat transfer improvement based on the fin shape. These included the Y-shaped fin (Lohrasbi et al., 2016a; Sciacovelli et al., 2015), V-shaped fins (Lohrasbi et al., 2016b), and tree-shaped fins (Hosseinzadeh et al., 2019). From these fins, the V-shaped fin obtained better heat transfer improvement, compared to the simple radial fin and annular fin. The enhancement of phase change duration by using a V-shaped fin was 82%, while there were 74% and 72% enhancements of the phase change duration by using an annular fin and radial fin, compared to the case without fins (Lohrasbi et al., 2016b). For a Y-shaped fin, using this fin enhanced phase change duration by 81%, compared to the case without fins (Lohrasbi et al., 2016a). Increasing the length of the Y-shaped fin boosted thermal penetration in the storage medium with a 16.5% enhancement of the phase change duration (Sheikholeslami et al., 2019). From all fin designs, fin space had a favourable effect on the phase change duration for both the charging and discharging processes (Eslami et al., 2021). The fin number and fin length had a favourable effect on system performance rather than fin thickness (Eslami et al., 2021).

For the metal hydride hydrogen storage (MHHS), MHHS is a solid hydrogen storage technique that has recently attracted researcher interest due to its advantages that offer a high hydrogen capacity and high safety (Sakintuna et al., 2007; Jain et al., 2010). However, the main disadvantage of this technique is the low thermal conductivity of the metal hydride (MH) materials, which negatively affects the hydrogen kinetic reaction (Zhao et al., 2020). The enhancement of the heat transfer performance inside the MHHS is a key method to improve the hydrogen kinetic reaction rate. For this purpose, several heat exchangers have been used for heat transfer enhancement. Using fins as the internal heat exchanger is also another technique to improve heat transfer performance under the consideration of natural convection conditions (Keshari & Maiya 2018; Muthukumar et al., 2012). The fin arrangement also results in a more uniform temperature distribution inside the MHHS. The study from Muthukumar et al. (2012) indicated that increasing the heat transfer area by an internal fin leads to the improvement of the local thermal conductivity of the MH bed. Keshari & Maiya (2018) employed the internal copper pin fin for $LaNi_5$ MHHS. The pin fin was attached to each other at the centre to the centre and side-by-side. Their study proved that larger fin diameters and higher fin numbers increased heat transfer surface areas, resulting in a higher heat transfer efficiency. Krishna et al. (2024a) introduced the new fin efficiency concept based on the reverse engineering technique to optimise the MHHS. The number of fins and fin shape were considered for the study purpose. Appropriate selection of the fin's number significantly affects the heat transfer, while the precisely radial tapering had an insignificant impact on the heat transfer performance. The fin thickness of 3 mm was preferred for the use of precisely radial tapering (Krishana et al., 2024b). Some studies also combine internal fin heat exchangers with internal cooling tubes to increase the heat transfer performance and decrease the weight of the overall MHHS, as the main problem of using internal fins only is a higher weight of the overall MHHS. The multiple internal cooling tubes were combined with the fins and placed inside the MHHS (Ma et al., 2014; Mallik

& Sharma 2021). The results from these studies proved that the fin number was the key parameter that positively affected the hydrogen absorption rate, compared to fin radius and fin thickness. Bai et al. (2021) employed the tree-shaped fins incorporating the central cooling tube for the MHHS. This study indicated that the absorption duration was reduced by 20.7%, compared to the case with radial fins. This complex fin's structure was the key parameter to increase the heat transfer efficiency. A higher length ratio of these fins increased the heat transfer performance. However, the study from Ayub et al. (2020) stated that when using the annular truncated hollow conical fins with a central cooling tube, fin parameters significantly affected the MHHS performance. These fin parameters included fin angle, fin radius, number of fins, fin spacing, and fin thickness. Singh et al. (2017a) combined circular fins with a U-shape tube heat exchanger for MHHS. This study reported that the overall storage performance could improve when increasing the fin number as well as reducing the fin thickness at the same time. The study by Bai et al. (2020) combined both the inner and outer fins and placed them inside the MHHS with a cooling jacket. The uniformity of the temperature distribution in the MH bed was improved when increasing the fin number with the constant fin volume.

Some studies also combined internal fins with helical coil/spiral heat exchangers. Due to the structure of the helical coil heat exchanger, the annular/circular fins could be applied only. The hydrogen absorption duration from this combination was two times less than the case with helical coil heat exchanger only (Dhaou et al., 2011; Souahlia et al., 2014). Mellouli et al. (2010) proved that the absorption time was decreased by 66% with the use of a spiral-coil tube and circular fins, compared to the case with the spiral-coil tube only. Krisha et al. (2024) proposed a new heat exchanger design, namely a flat coil tube heat exchanger. A spiral fin was integrated with a flat coil tube. This integration obtained 35.3% and 16.7% of the hydrogen absorption time when compared to the case with a helical coil tube and double helical coil tubes, respectively. Shrivastav et al. (2024) combined the copper fin with phase change material to improve the hydrogen absorption/desorption rate. The copper fin was integrated into both MH and phase change material. This study proved that the hydrogen absorption rate significantly improved by at least 86.5% when using at least 10 fins, compared to the case without fins. Considering the performance between helical coil and straight tube, the helical coil/spiral coil heat exchanger with the heat transfer fluid (HTF) generally obtains better heat transfer performance compared to the straight tube heat exchanger. This is because the secondary circulation of the coil structure provides more heat transfer surface areas. However, the drawback of the coil heat exchanger is the pressure drop. The amount of pressure loss from the coil tube is higher than the straight tube due to the curvature ratio of itself. The study by Guan et al. (2014) stated that a coil tube caused pressure losses by 11-17% compared to a straight tube. For heat exchanger applications, a small amount of pressure drop is required for the fluid's movement inside the heat exchangers. However, a large amount of pressure drop can negatively affect the system's efficiency and can cause system failure. The heat exchange efficiency and pressure drop should be balanced to maintain the overall performance of the heat exchanger (Zhang & Liu 2022).

From the above mention, it can be summarised that the combination of the fin heat exchanger and other heat exchangers, which contain the HTF, significantly improves the heat transfer performance. However, the complex coil's structure significantly causes the pressure drop along the system. Furthermore, most studies only consider the improvement of heat transfer and hydrogen absorption/desorption based on the combination of fins and HTF tubes. The effect of the combination of these heat exchangers on the complete absorption-desorption cycle is still missing. Considering both processes, hydrogen absorption and desorption are one of the main parameters for the design of highly efficient MHHS (Wang & Brinjerhoff 2021a). As the hydrogen desorption durations are usually larger than the hydrogen absorption durations. This is because of the difference in initial pressure for each

process and the reaction-rate hysteresis (Wang & Brinjerhoff 2021b). Therefore, the duration of a complete hydrogen absorption-desorption cycle is significant for optimising the performance, safety, and cost-effectiveness of the storage systems (Klebanoff & Klebanoff 2012). Moreover, the comparison of the MH volumes with the HTF tube between with and without additional fins has still not been considered. As the overall volumetric and gravimetric of the MHHS should be prioritised, especially for mobile applications (Rahnama et al., 2019a). For the fin design, the fin number and fin length are the key parameters that positively affect the heat transfer performance due to increasing in heat transfer surface area (Yao & Huang 2021; Hickie-Bentzen et al., 2022). However, there are some limitations to increase these parameters, as the large number of fins or the longer length can suppress convective flows and limit the heat transfer enhancement level (Eslami et al., 2021). From the literature, the Y-shaped fin obtains better heat transfer performance compared to other conventional fins. However, when considering the MHHS without a cooling jacket, the heat transfer rate of the MH bed around the outer wall of the MHHS is lower than in other areas. This is because the MH bed around this area is far away from the HTF and fin branches. The complex fin's structure is also one of the key parameters that affect the heat transfer enhancement, as the well-arrangement of the fin mass distribution to the MH bed leads to a more uniform temperature distribution and less thermal resistance of the MH bed (Bai et al., 2021). In contrast, there are some limitations in the reality to manufacture the complex fin's structure by using conventional manufacturing techniques. The additive manufacturing is required instead (Zhang et al., 2023).

Therefore, the objective of this study is to further enhance the MHHS performance by considering the heat transfer improvement with the use of a fin heat exchanger, which is incorporated with the HTF tube. To achieve this, the simple straight tube of the HTF is used instead of other complex heat exchangers to maintain the pressure level. The effect of pressure losses due to the complex HTF tube's structure is analysed and compared with the simple straight tube. The novel triple-branched fin is first designed to fulfill the requirement of heat transfer efficiency instead of using other complex HTF tube designs by considering an increase in heat transfer surface area corresponding to the appropriate arrangement of fin mass distribution to the MH bed. This design is developed from the conventional Y-shaped fin to further enhance the Y-shaped fin performance under the consideration of the complexity of the fin structure. This new fin structure is also designed to meet the requirements of conventional manufacturing techniques by considering not too much complexity of fin structure. Furthermore, based on the literature, the fin parameters also have a greater influence on the heat transfer performance. Consequently, the effect on various fin parameters is also considered to further enhance the triple-branched fin performance by considering the fin/MH volume. The expectation of this study is to improve hydrogen kinetic reaction and heat transfer performance, especially around the middle area between the Y-shaped fin and the top area, which is close to the outer MHHS wall. To investigate the triple-branched fin performance, several fin designs are provided to compare the performance of these fins with the novel fin design. The average bed temperature of the MHHS as well as hydrogen concentration in the hydrogen absorption/desorption process, are investigated to verify this hypothesis. Moreover, the duration of one complete hydrogen absorption-desorption cycle based on these new designs is estimated in this study. The parametric study based on the operating conditions of the HTF and material of the fin/HTF tube is also considered to investigate the triple-branched fin performance on the heat transfer efficiency as well as the hydrogen kinetic reaction for both processes.

7.4 System Description

The MHHS performance is analysed under the fin geometric study as well as the parametric study. The effect of four different fin designs on the average bed temperature of the MHHS and the hydrogen concentration are compared in this study. The best fin performance is then selected for further improvement under the geometric study and parametric study. The MHHS contains internal 8 fins, which connect to the internal straight tube for the HTF. The angle between each fin is 45°. The height and outer diameter of the MHHS are 80 mm and 50 mm, respectively (Larpruenrudee et al., 2023; Larpruenrudee et al., 2024). The HTF tube's diameter is fixed at 8 mm (Bai et al., 2021). Both the fin and HTF tube are made of copper. The same dimensions and materials are applied for all cases. For the parametric study, the effect of initial HTF temperatures, heat transfer coefficients between the HTF and MH bed, as well as materials of fin and HTF tube are considered in this section.

7.4.1 Comparison between the Heat Exchangers

The schematic diagram of the MHHS with heat exchanger tube and fins designs is presented in Figure 7.2. From Figure 7.2a, the inlet and outlet for the hydrogen are at the top of the MHHS, while the HTF is released from the bottom surface of the HTF tube. Figure 7.2b to Figure 7.2e represent the fin characteristics from four fin designs, including the quadrilateral fin, which is considered as the original fin design or case A (Figure 7.2b), Y-shaped fin design I as case B (Figure 7.2c), Y-shaped fin design II as case C (Figure 7.2d), and triple-branched fin design as case D (Figure 7.2e). Fin characteristics and dimensions from these four cases are provided in Figure 7.2 and Table 7.1, respectively. The fin height (H) and width (W) are 18 mm and 1 mm (Bai et al., 2021), which are constant for all cases. Due to the simple design from case A, there are only fin height and width. However, the other specific parameters of the other three models are various depending on the fin characteristics. L is the length of the Y-shaped fin from the left branch to the right branch, α_y is the angle of the Y-shaped fin section, and α_b is the angle of the middle branch fin from the triple-branched fin section. Other specific parameters are included H_1, L_1, W_1, W_2, and α_1. The MH volume from case A is 140.2 cm^3, while the fin volume from this case is 12.9 cm^3. It should be noted that the reduction of the MH volume from other cases is between 1-5%, compared to case A as the base case. Among these four designs, the best design, that obtains the best heat transfer and hydrogen kinetic reaction performances, is selected to further enhance the fin performance under the fin geometry section.

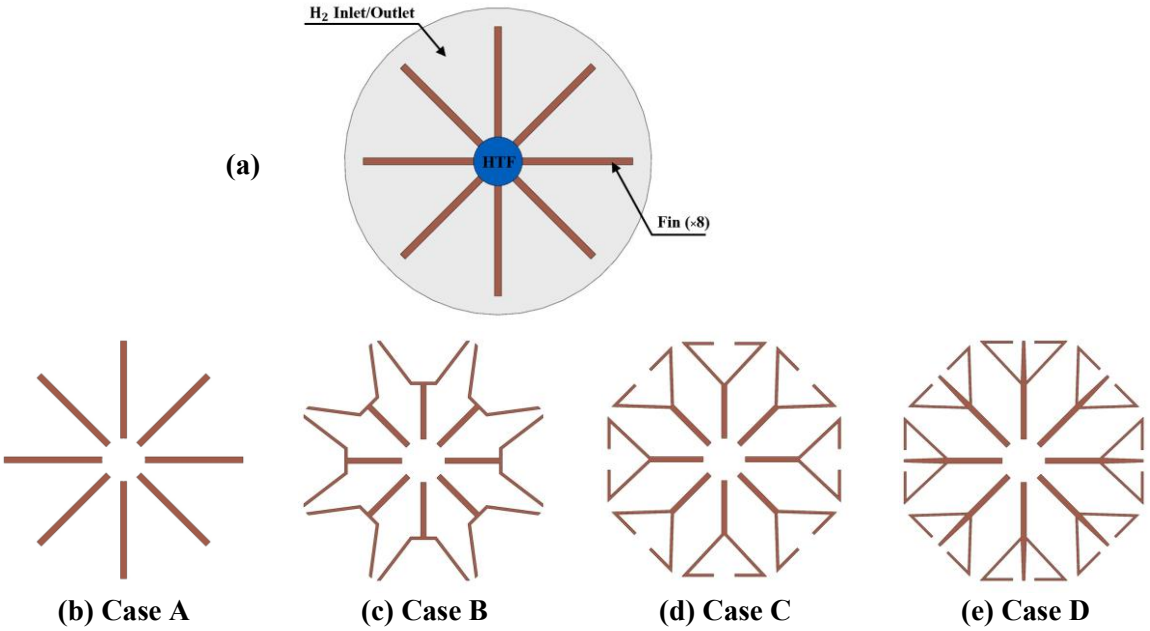

Figure 7.2 Storage tanks and fin designs; (a) schematic diagram of storage tanks with heat exchanger tube incorporating fins, (b) quadrilateral fin (case A), (c) Y-shaped fin design I (case B), (d) Y-shaped fin design II (case C), and (e) triple-branched fin design (case D)

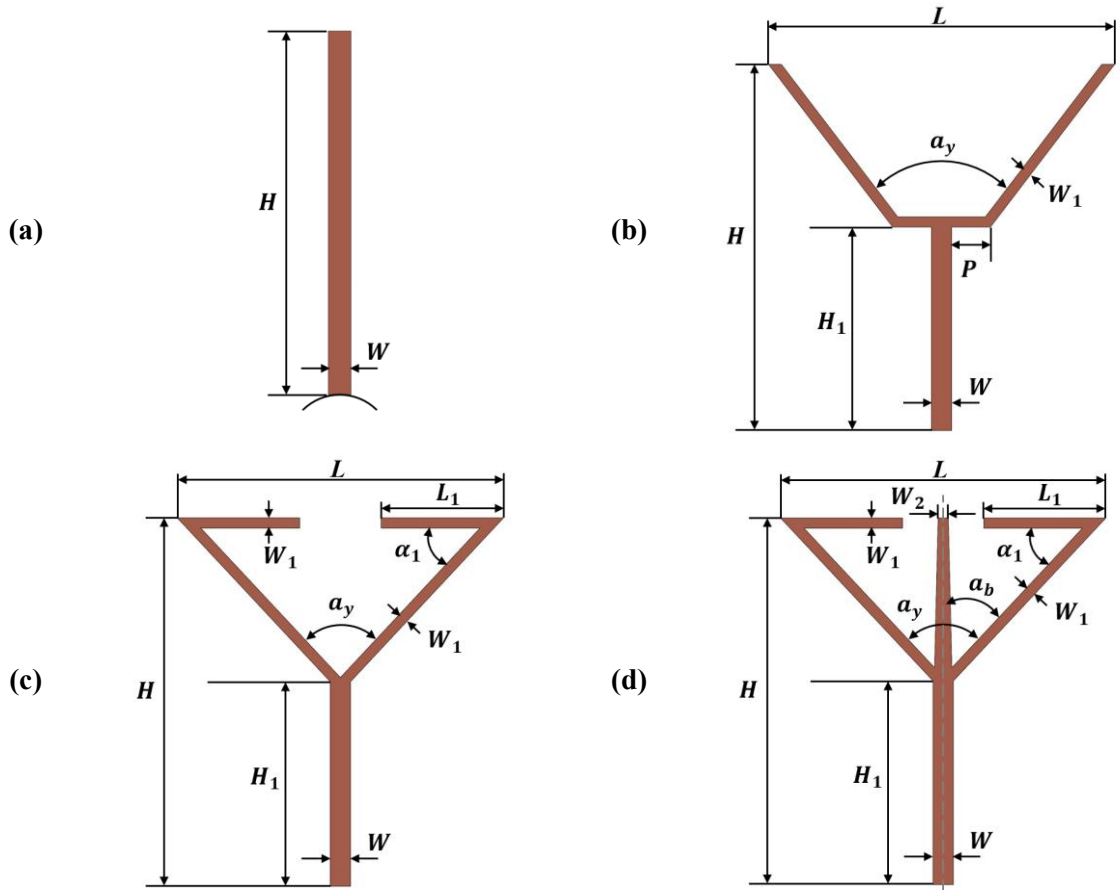

Figure 7.3 Characteristics of storage tanks with fin designs; (a) original fin design (case A), (b) Y-shaped fin design I (case B), (c) Y-shaped fin design II (case C), and (d) triple-branched fin design (case D).

Table 7.1 Characteristic of MH tanks with various fin designs; the original fin design (case A), Y-shaped fin design I (case B), Y-shaped fin design I (case C), and triple-branched fin design (case D)

Case No.	H (mm)	W (mm)	L (mm)	P (mm)	α_y (°)	α_b (°)	α_1 (°)	H_1 (mm)	L_1 (mm)	W_1 (mm)	W_2 (mm)
A	18.0	1.0	-	-	-	-	-	-	-	-	-
B	18.0	1.0	17.0	1.9	75	-	-	10.0	-	0.4	-
C	18.0	1.0	16.0	-	86	-	47	10.0	6.0	0.4	-
D	18.0	1.0	16.0	-	86	43	47	10.0	6.0	0.4	0.5

7.4.2 Geometric Study of Triple-Branched Fin Design

From our present study, the new fin design from case D (triple-branched fin) obtains the best performance to enhance the heat transfer efficiency and hydrogen kinetic reaction. The results for four different fin designs can be found in the result and discussion section under "7.4.2 Performance comparison between different fin designs" Therefore, the fin design case D is selected for further enhancement under the fin parameters. Table 7.2 provides the fin dimensions with various specific parameters from case D. These include 15 cases, which are from case D and case D-1 to case D-14. The main parameters include fin height, fin angle, fin width, and fin thickness. To study the effect of these

parameters, the constant value of each specific parameter from case D is then increased and decreased for comparison purposes. To consider the overall volumetric and gravimetric of the MHHS, the variation of each fin parameter is selected by considering the reduction of the MH volume. The maximum reduction of the MH volume from each parameter is fixed at 1%. Based on this constraint, the overall MH volume from case D to case D-14 is reduced by less than 5%. By considering the selected parameters and heat transfer efficiency, the best fin performance is selected for further investigation under the parametric study. The results of the comparison between four different fin designs (case A to case D) are provided under the results and discussion section.

Table 7.2 Characteristic of fin geometry and selected parameters for case D

Case No.	H (mm)	W (mm)	L (mm)	α_y (°)	α_b (°)	α_1 (°)	W_1 (mm)	W_2 (mm)	L_1 (mm)	H_1 (mm)
D	18.0	1.0	16.0	86	43	47	0.5	0.5	6.0	10.0
D-1	18.0	1.0	16.0	86	43	47	0.5	0.3	6.0	10.0
D-2	18.0	1.0	16.0	86	43	47	0.5	0.7	6.0	10.0
D-3	18.0	1.0	16.0	86	43	47	0.5	0.7	5.0	10.0
D-4	18.0	1.0	16.0	86	43	47	0.5	0.7	7.0	10.0
D-5	18.0	1.0	16.0	86	43	37	0.5	0.7	7.0	10.0
D-6	18.0	1.0	16.0	86	43	57	0.5	0.7	7.0	10.0
D-7	18.0	1.0	16.0	86	43	49	0.5	0.7	7.0	12.0
D-8	18.0	1.0	16.0	80	40	60	0.5	0.7	7.0	9.0
D-9	18.0	1.0	16.0	74	37	63	0.5	0.7	7.0	8.0
D-10	18.0	1.0	16.0	69	34	66	0.5	0.7	7.0	7.0
D-11	18.0	1.0	15.0	65	32	62	0.5	0.7	7.0	7.0
D-12	18.0	1.0	17.0	72	36	64	0.5	0.7	7.0	7.0
D-13	18.0	1.0	17.0	72	36	64	0.3	0.7	7.0	7.0
D-14	18.0	1.0	17.0	72	36	64	0.7	0.7	7.0	7.0

7.4.3 Parametric Study for Operating Conditions

A parametric study is performed only for the MHHS with the best fin design among case D to case D-14. The parametric study includes the operating conditions of the HTF as well as materials of the fin and HTF tube. Under this section, the initial HTF temperature at 573 K and heat transfer coefficient between the HTF and MH at 500 W m^{-2} K^{-1}, are set as the base values for both absorption and desorption. For all cases, copper is used as the fin and HTF tube materials. Various operating conditions of the HTF are presented in Table 7.3. These include the HTF temperature from 423 K to 573 K for the absorption and from 573 K to 723 K for the desorption. The heat transfer coefficient between the HTF and MH varies from 250 W m^{-2} K^{-1} to 1000 W m^{-2} K^{-1}. Under fin and HTF tube material, four different materials are selected to compare the performance of heat transfer during hydrogen absorption and desorption. These materials include aluminium, copper, nickel, and steel. Table 7.4 presents thermos-physical properties of these materials.

Table 7.3 Operating values for the HTF

Parameters	Base value	Sensitivity value
HTF inlet temperature for absorption (K)	573	423, 473, 523
HTF inlet temperature for desorption (K)	573	623, 673, 723
Heat transfer coefficient of HTF for absorption and desorption (W m^{-2} K^{-1})	500	250, 750, 1000

Table 7.4 Thermo-physical properties of different materials for fin and HTF tube

Material	Density ($kg\ m^{-3}$)	Specific heat ($J\ kg^{-1}\ K^{-1}$)	Thermal conductivity ($W\ m^{-1}\ K^{-1}$)
Aluminum	2719	871.0	202.4
Copper	8978	381.0	387.6
Nickel	8900	460.6	91.7
Steel	8030	502.5	16.3

7.5 Mathematical Model

This section provides all related equations for the numerical simulation. The related equations include the governing equations for both hydrogen absorption and hydrogen desorption processes as well as the governing equations for the HTF and fins. The initial and boundary conditions, numerical schemes, grid independency, and model validation are also included in this section.

7.5.1 Governing Equations

The appropriate selection of MH material for the use of this thesis are provided in "Chapter 3 – Methodology" section. The governing equations regarding the absorption and desorption processes as well as the heat transfer fluid and fins can be found in the same chapter as "Chapter 3 – Methodology". For the absorption and desorption processes, the governing equations are provided in 3.1.1 Absorption Process and Desorption Process. The governing equations of heat transfer fluid and fins can be found in "3.1.4 Heat Transfer Fluid and Fins".

7.5.2 Initial and Boundary Conditions

The initial conditions of the MHHS for the hydrogen absorption are 573 K of the temperature ($T_{MH,abs} == T_{0,abs}$) and 1.8 MPa of the loading pressure ($P_{0,abs}$). From the experiment study of Muthukumar et al., (2008), the maximum hydrogen storage capacity of the Mg_2Ni storage is obtained when using the initial MHHS temperature as 573 K. Using hydrogen pressure at 1.8 MPa obtains the better absorption performance, comparing with other values (Larpruenrudee et al., 2022a). For the hydrogen desorption process, the initial conditions of the MHHS are the ultimate temperature of the absorption ($T_{MH,des} = T_{ultimate,abs} = T_{0,des}$) and 0.1 MPa of the hydrogen pressure ($P_{0,des} = P_a$). The HTF temperature from the internal straight tube heat exchanger is fixed as 573 K for both absorption and desorption ($T_{HTF,abs} = T_{HTF,des}$). The heat transfer coefficient (h_f) between the HTF and the HTF tube is constant at 500 $W\ m^{-2}\ K^{-1}$ for both absorption and desorption. It should be noted that the same conditions are applied for all simulation cases under the fin designs and optimisation. However, the values of HTF temperature and h_f are varied under the parametric study.

Adiabatic wall of the storage:

$$\frac{\partial T_{MH}}{\partial \vec{n}} = 0 \tag{7.1}$$

Wall of the heat exchanger tube:

$$\lambda_e \frac{\partial T_{MH}}{\partial \vec{n}} = h_f\left(T_f - T_{MH}\right) \tag{7.2}$$

7.5.3 Numerical Schemes, Grid Independency, and Model Validation

- Numerical Schemes and Grid Independency

Due to the similar setup conditions for the pre-processing process, the numerical schemes for all chapters are summarised and provided in "3.3.2 Numerical Schemes" under "Chapter 3 – Methodology section". For the grid independency, a typical 1/4 unit of the whole storage container is used for all numerical simulations due to the symmetry structure of the MHHS, allowing a reduction of computation time. Grid refinement tests were performed for different grid sizes for hydrogen absorption process to achieve accurate simulation results. Due to the same MHHS and heat exchangers, case B is selected. The same meshing techniques are then applied to the other cases. From Table 7.5, it is obvious that the average bed temperature and absorption time become stable and have minor changes at 436,416 element numbers for case B. Based on these elements, the average bed temperature is 620.19 K, with the absorption time at 4297 s. Therefore, these element numbers are chosen for further studies.

Table 7.5 Effect of different grid numbers on the hydrogen absorption time and average bed temperature for case B

No.	Number of elements	Average bed temperature (K)	Absorption time (s)
1	172837	620.77	4361
2	221973	620.57	4317
3	436416	620.19	4297
4	622554	619.29	4292

- Code Validation for Metal Hydride Storage System

The model validation for the use of metal hydride storage system based on Mg_2Ni are provided in "3.3.1 Model Validation" under "Chapter 3 – Methodology" section.

7.6 Results and Discussion

The effect of heat exchanger types on pressure variation along the inlet throughout the outlet is analysed in this section. The investigation of this effect is based on the use of HTF and pressure loss due to the heat exchanger's structure. The best heat exchanger performance is then selected to integrate with the fin heat exchanger to further heat transfer enhancement. Furthermore, the simulated results of the MHHS based on various fin designs for hydrogen absorption/desorption are then provided. The average bed temperature of the MHHS and the hydrogen concentration based on these fin designs are also included in this section for comparison purposes. The best fin performance, which obtains the best heat transfer efficiency and hydrogen kinetic reaction rate, is selected to further enhance the fin efficiency under various selected parameters. Finally, the best fin geometry with appropriately selected parameters is then chosen to analyse its performance in the parametric study section.

7.6.1 Pressure Variation along the Heat Exchangers

The effect of heat exchanger types on the pressure variation from the inlet throughout the outlet is analysed and presented in Figure 7.4 under the pressure contour. The comparison is provided under the same boundary conditions, which include the inlet flow velocity as 76.86 m s^{-1} and air as the HTF. In this section, the selected material of the HTF tube is stainless steel. The heat exchanger types in this study include the straight tube heat exchanger (STHE), helical coil heat exchanger (HCHE), semi-cylindrical coil heat exchanger (SCHE), and semi-cylindrical coil heat exchanger with central return tube (SCHE-CR). The heat transfer performance based on these heat exchangers was analysed in our previous study (Larpruenrudee et al., 2022a, b; Larpruenrudee et al., 2023; Larpruenrudee et al., 2024). The HCHE and SCHE (×2) are designed under the constant volume at 15.34 cm^3, while the SCHE-CR

(×2) has the volume at 17.12 cm^3. The volume of the STHE is 1.01 cm^3. The tube diameter of all heat exchangers is fixed at 4 mm for comparison purposes. Under the same fluid velocity at the inlet, the pressure contour from Figure 7.4 indicates that the cases with coil tube structure have higher pressures, especially at the inlet. The inlet pressure from these cases is over 147646 Pa. However, the pressure decreases along the coil tube from the inlet throughout the outlet, which has a pressure of 98738 Pa. This is due to the effect of the curvature ratio of the coil tube, which requires more power to inject the HTF from the inlet and circulate throughout the heat exchanger. In contrast, the pressure difference from the STHE is very small. The inlet pressure is only around 109218 Pa, while the outlet pressure is around 98738 Pa.

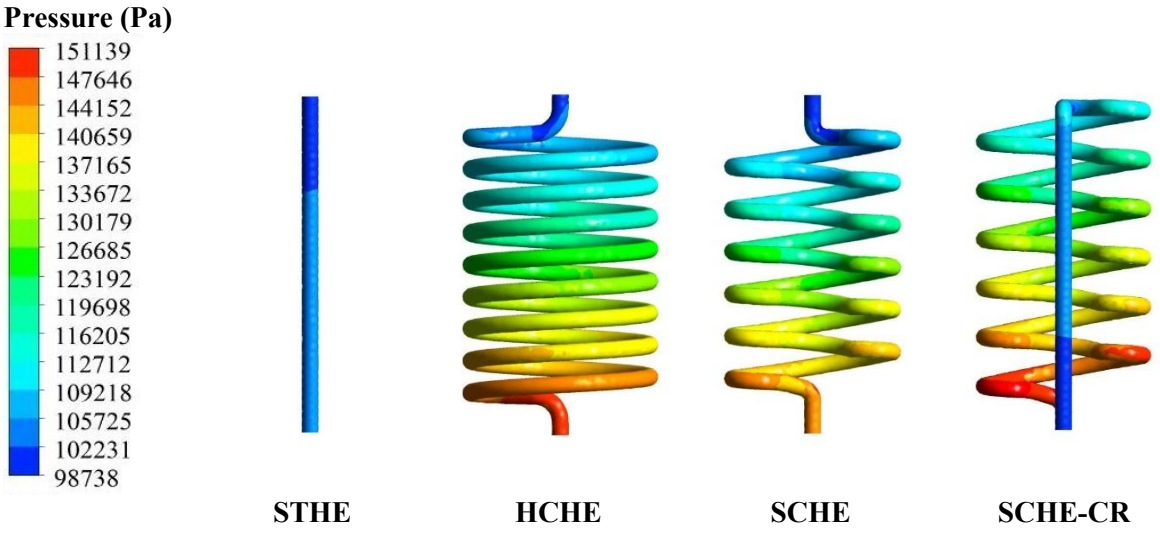

Figure 7.4 Pressure variation from various heat exchangers

More analysis regarding the effect of heat exchanger types is provided in Figure 7.5 and Figure 7.6. This includes the range of skin friction coefficient from each design along the heat exchanger tube (Figure 7.5a) and the effect of heat exchanger type on pressure losses from the inlet throughout the outlet (Figure 7.5b). It should be noted that the percentage is calculated based on the maximum pressure between the inlet and the outlet of each heat exchanger. Figure 7.6 refers to the heat transfer surface area from each heat exchanger type (Figure 7.6a) and the hydrogen absorption/desorption duration from various heat exchangers (Figure 7.6b). From Figure 7.5a, the minimum skin friction coefficients from all heat exchanger types are less than 10. However, the maximum skin friction coefficients at the inlet of these heat exchangers are different. The maximum values from STHE, HCHE, SCHE, and SCHE-CR are 28, 31.51, 35.64, and 43.76, respectively. The skin friction coefficient refers to the ratio of the wall shear stress and the reference dynamic pressure. The equation of skin friction coefficient is as follows,

$$C_f = \frac{\tau_\omega}{\frac{1}{2}\rho U_\infty^2}, \tag{7.3}$$

where C_f is the skin friction coefficient, τ_ω is the wall shear stress, ρ is fluid density, and U is the free-stream velocity (at the inlet). Based on the boundary conditions from this study, the density of fluid and inlet velocity are constant for all designs. However, the results from Figure 7.5a are different. This means that the wall shear stress is only the one parameter that affects the difference in the skin friction coefficients between different designs. In general, the wall shear stress depends on the fluid velocity when moving from the tube wall toward the centre of the tube. Due to the complex design of all coil cases, it generates a turbulent flow inside the tube. The results of the turbulent level of fluid flow inside the tube can be found in our previous study (Larpruenrudee et al., 2023). Therefore, a higher velocity

magnitude from these cases obtains a higher wall shear stress, which leads to a higher skin friction coefficient. During fluid flowing in the tube, there is a combination of the tangential force at the wall and the viscous shear stress at the wall, which acts in the opposite direction to the direction of fluid motion (Bird et al., 2002). A higher pressure at the tube inlet is required when these parameters have higher values (Bird et al., 2002). As a result, this phenomenon affects the amount of pressure drop inside the tube. The results from Figure 7.5b prove that there are more pressure losses from the coil tube structure compared to the straight tube. There is around 34% pressure loss between the inlet and outlet from these complex heat exchangers. However, there is only a 3% pressure loss from the inlet to the outlet from the case with the straight tube. In general, the pressure drop is the result of the friction which is caused by the HTF rubbing against the inner wall of the tube. The HTF will require more power to overcome the friction inside the longer tube, compared to the shorter tube. In other words, a longer tube will obtain a higher pressure drop than a short tube (Zhang & Liu 2022). This is obvious in the results from Figure 7.6a, as the STHE has a shorter length with only 10 cm^2 of heat transfer surface area, while the other cases have a longer length due to the coil's effect with the range of 150-172 cm^2 of heat transfer surface area. It should be noted that the difference in the percentage of the pressure loss and heat transfer surface area in coil cases can be because of the difference in the curvature ratio of each coil design. A higher curvature ratio can obtain a higher pressure loss. Considering the effect of heat exchanger types on the one complete cycle of hydrogen absorption-desorption from Figure 7.6b, the duration of the one complete cycle from the HCHE, in this case, is 38646 s. When using the SCHE, this duration is reduced to 25147 s. However, when using the central return tube as the SCHE-CR, this duration is further reduced to 17279 s. Therefore, using the coil tube significantly improves the heat transfer rate inside the storage system, leading to a reduction in hydrogen absorption/desorption duration. This is because of an increase in the heat transfer surface area of the coil tube from the secondary circulation of itself (Wu et al., 2014). The STHE case has less heat transfer surface area leading to less heat transfer efficiency, compared to the coil tube cases. This negatively affects the hydrogen absorption/desorption duration. The final time of this one complete cycle from this case is 116723 s. From these results, it is obvious that there are 67%, 78%, and 85% reductions in duration for one complete cycle when using HCHE, SCHE, and SCHE-CR instead of STHE. It should be noted that the absorption and desorption from these cases are obtained based on the stainless steel tube of the HTF. Other materials with a high thermal conductivity, such as copper, aluminium, and nickel, can enhance the rate of hydrogen kinetic reaction, resulting in faster hydrogen absorption/desorption. Although the straight tube has less heat transfer efficiency, the straight tube has minor pressure losses compared to the coil tube. As the excessive pressure drops (from inlet to outlet) will significantly result in a negative system's efficiency and excessive energy consumption (Zhang & Liu 2022). The straight tube is then selected for further study by combining itself with the fin heat exchangers. The effect of this combination on the heat transfer efficiency and hydrogen absorption-desorption duration is provided in the next section.

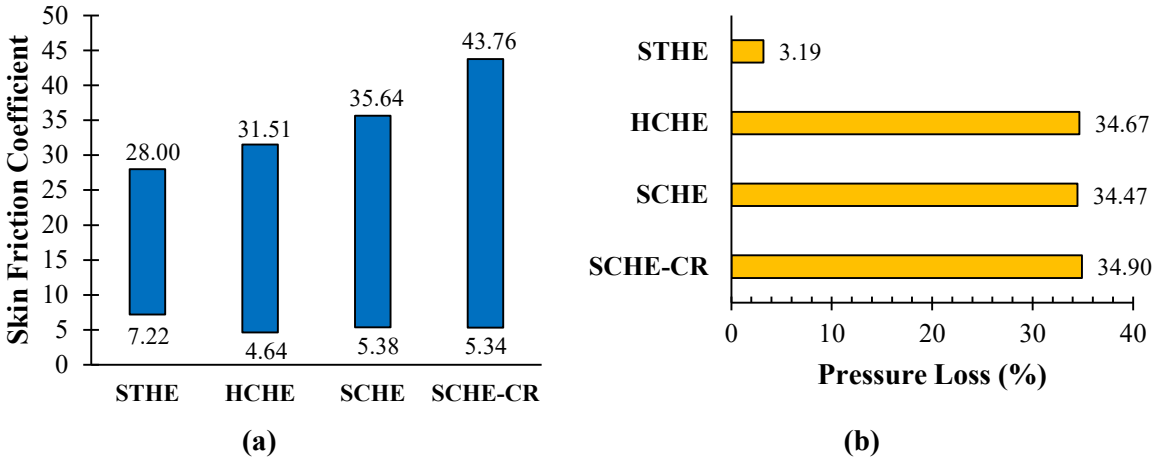

Figure 7.5 Skin friction coefficient and pressure losses from various heat exchangers; (a) skin friction coefficient and (b) pressure loss

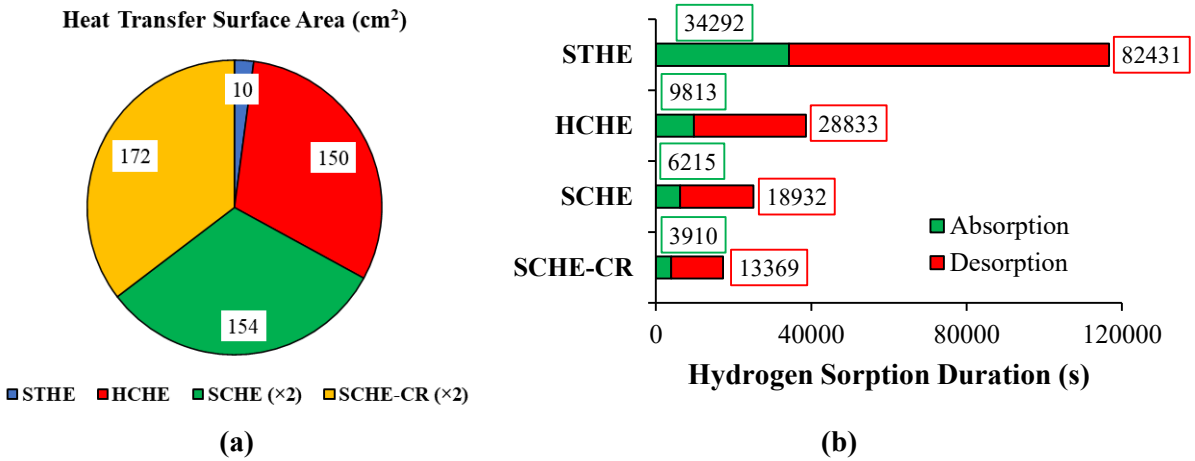

Figure 7.6 Heat transfer surface area and hydrogen sorption duration from various heat exchangers; (a) heat transfer surface area and (b) hydrogen absorption/desorption duration

In general, air and water are commonly selected as the HTFs for the MHHS due to their advantages that they offer low cost and less environmental impact, compared to other HTFs. However, due to a high operating temperature range of Mg2Ni, air is selected as the HTF for this study. Furthermore, air also offers better flow characteristics when compared to other liquid metals and molten salt (Ward et al., 2016). Considering the effect of pressure loss due to the HTF, the use of air as the HTF significantly causes huge pressure losses, especially when using complex heat exchangers. However, the effect of pressure loss might be insignificant when employing other HTFs with different thermal-physical properties.

7.6.2 Comparison between the Fin Designs

The comparison of average bed temperature and hydrogen concentration during the hydrogen absorption under four different fin designs is presented in Figure 7.7. Case A refers to the MHHS with a quadrilateral fin, while case B and case C are for the MHHS with Y-shaped fin design I and Y-shaped fin design II. Case D refers to the MHHS with the new fin design, namely the triple-branched fin. For all cases, the MHHS temperature is fixed as 573 K with loading pressure at 1.8 MPa. The HTF temperature is constant at 573 K with the heat transfer coefficient at 500 W m^{-2} K^{-1}. From this figure, there is an interaction between the metal alloy and hydrogen when the hydrogen is initially injected into the MHHS. This leads to a rapid increase in MH bed temperature and slowly increase to reach the maximum point. The MH bed temperature then continually decreases due to the heat transfer effect from the HTF and fins. The generated heat during this stage must be removed from the system to control

the desired charging rate during this stage (Ardahaie et al., 2021). A faster MH bed temperature reduction causes a faster hydrogen kinetic reaction, resulting in faster hydrogen absorption (Ardahaie et al., 2021). The more fin mass distribution to the MH bed leads to the more uniform temperature distribution to the MH bed (Bai et al., 2021). The results from Figure 7.7 also support this fact. The average MH bed temperature from case A reduces slower than case B, resulting in slower hydrogen absorption from case A, compared to case B. The final time of the absorption process from case A is 4919 s, while it is only 4297 s from case B. Due to more fin mass distribution to the MH bed from case C and case D, the heat is transferred faster than in the first two cases. However, the absorption duration from case D is still shorter than case C due to the effect of the new fin design, which provides more fin mass distribution. The absorption duration from case C is 3848 s, while it is 3680 s from case D. More discussion regarding the temperature difference is provided in the next section.

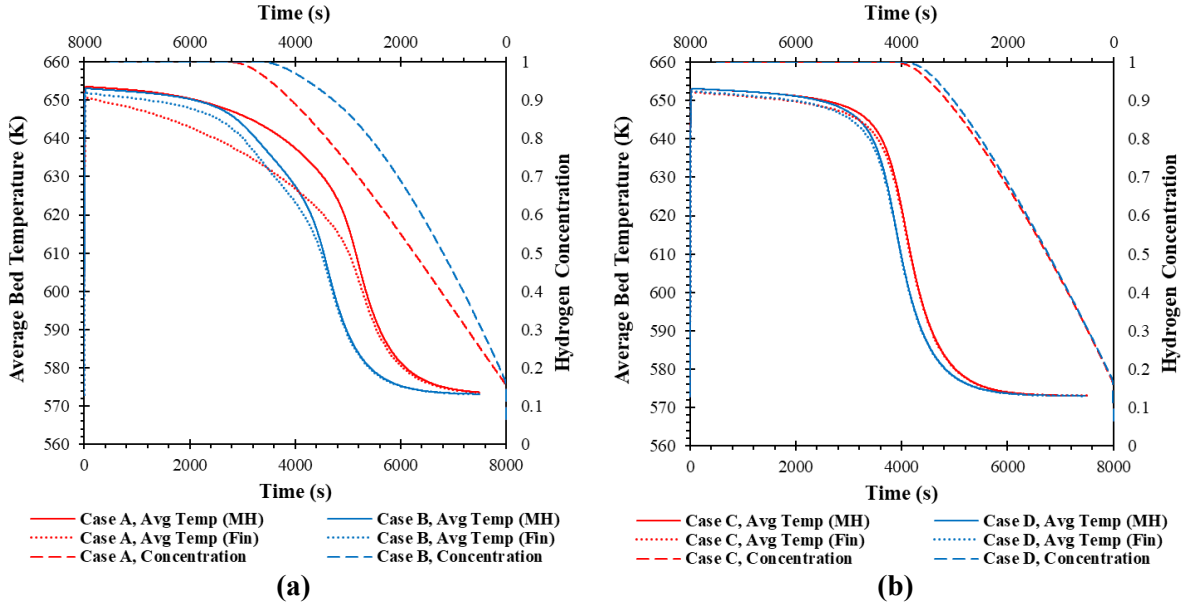

Figure 7.7 Average bed temperature and hydrogen concentration from all cases; (a) case A, case B and (b) case C, case D. (The solid line is for average bed temperature, the large dashed line is for hydrogen concentration, and the small dashed line is for average fin temperature)

For more analysis, temperature contours and hydrogen concentration contours along the MHHS with different fin designs are presented in Figure 7.8. The selected times, including 2500 s and 3500 s, after starting the hydrogen absorption, are provided in this figure. From Figure 7.8a, the central area from all designs has the lower temperature because it directly connects with the HTF tube, which is located at the central area of the MHHS. The MH, which is close to the fin area, also has a lower temperature. This is due to the metal fin ability, which conducts and transfers the heat between the HTF and MH. At 2500 s, the fin temperature from case A is significantly lower than the fin temperatures from other cases. This is due to the complex fin structure from other cases, which has more fin mass distribution in the MH bed around the outer part of the MHHS. This requires longer times to conduct and transfer the heat between the HTF tube and copper fins. In other words, the heat is then further transferred from the MH beds to the HTF tube via the copper fins (Bai et al., 2021). The MH bed temperature from most areas around the outer wall of the MHHS from case A is still higher, compared to other cases. Similarly, most outer areas from case B still have a higher temperature, compared to case C and case D. This is due to the complex fin design. The more fin mass distribution leads to the reduction in heat conduction resistance of the MH bed, resulting in a more uniform MH bed temperature (Bai et al., 2021). It is obvious that at the top parts of the Y-shaped fin from case C and D, more uniform temperature distributions occur around these parts. However, due to the complex fin design from case D, which

increases more fin areas, especially at the centre of the Y-shaped fin, the outer areas of the MHHS have lower temperatures compared to case C. The significant changes in the temperature variation between these four cases are observed at 3500 s. A high MH bed temperature, especially around the outer areas, is still observed from case A and case B. The MH bed temperature from case D is more uniform and significantly lower than in other cases. It is obvious that increasing the fin areas from the Y-shaped fin (case B) obtains better heat transfer performance inside the MHHS, especially from the tripled-branched fin (case D). In hydrogen absorption, faster heat removal from the system causes a faster hydrogen absorption. In other words, lower MH temperatures mean higher hydrogen concentrations. The hydrogen concentration contours from Figure 7.8b can support this fact, as around the HTF and fin areas usually have a higher hydrogen concentration. This is because these areas have lower temperatures, compared to other areas (refer to temperature contours from Figure 7.8a). Due to the complex fin structure from case C and case D, the concentration at the outer areas from these cases is always higher than another two cases (case A and case B). The significant difference in hydrogen concentration is observed at 3500 s as case A and case B still have less hydrogen concentration around the outer areas of the MHHS.

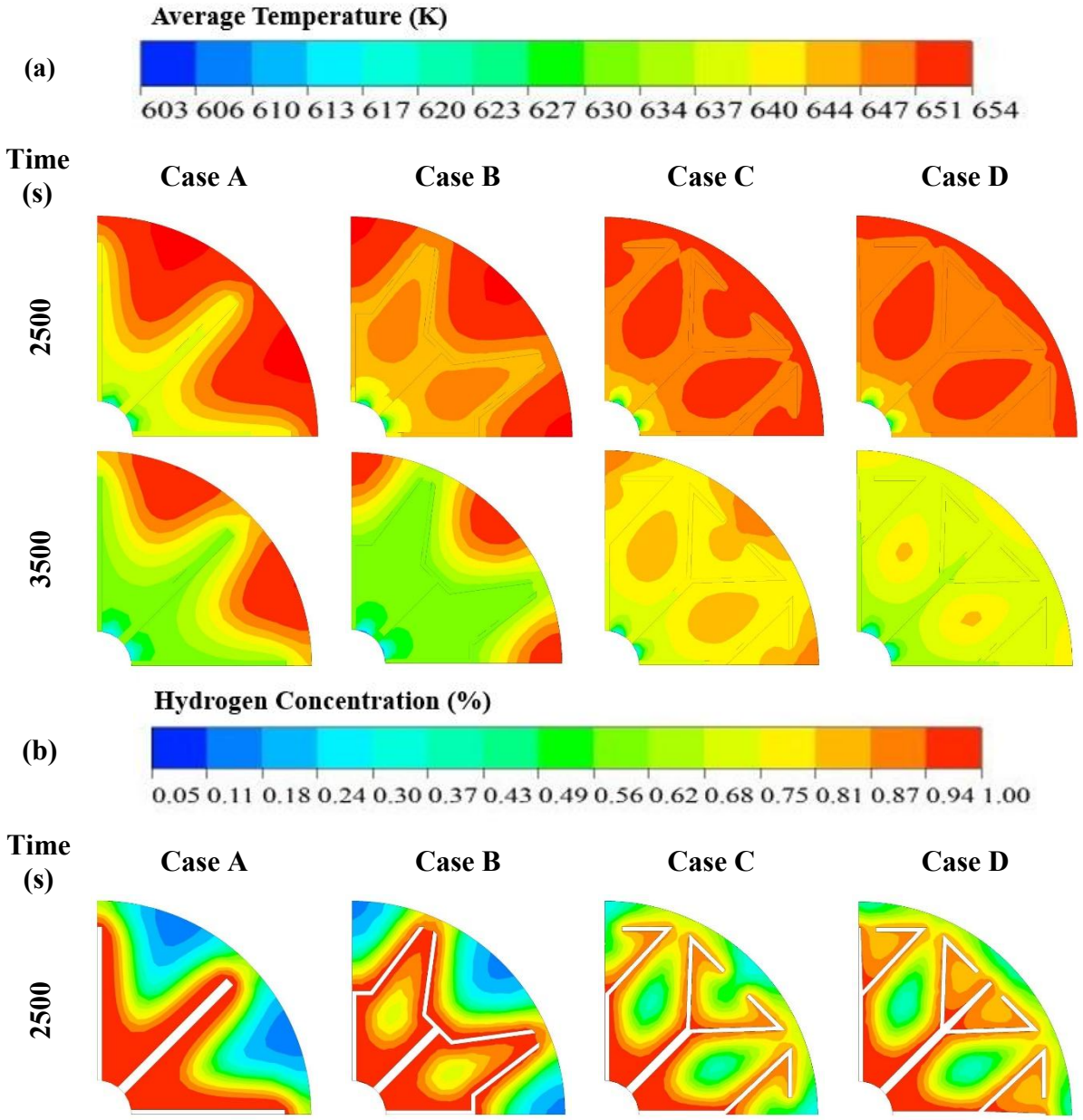

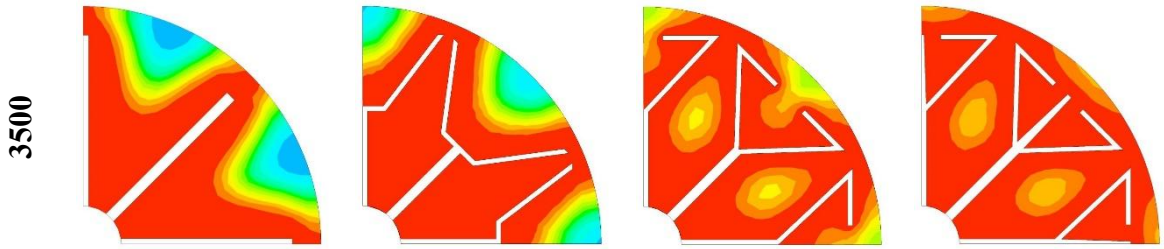

Figure 7.8 Average temperature and hydrogen concentration of MH bed and fins at 2500 s and 3500 s after starting hydrogen absorption process in all cases; **(a)** average temperature and **(b)** hydrogen concentration.

Figure 7.9 presents the comparison of MH volume/fin volume and its effects on the absorption duration from all cases. From Figure 7.9a, there is a 0.9% reduction of MH volume from case A (base case) to case B, while there are 2.7% and 5.2% reductions of MH volume from case A to case C and from case A to case D, respectively. However, considering the absorption duration from all cases from Figure 7.9b, (refer to the discussion from Figure 7.7), the reductions of absorption duration from case A to case D are 12.6%, 21.8%, and 25.2%, respectively. It is obvious that case D obtains the best performance in terms of heat transfer efficiency and hydrogen absorption, compared to the other cases. Therefore, case D is selected for further investigation to enhance its performance.

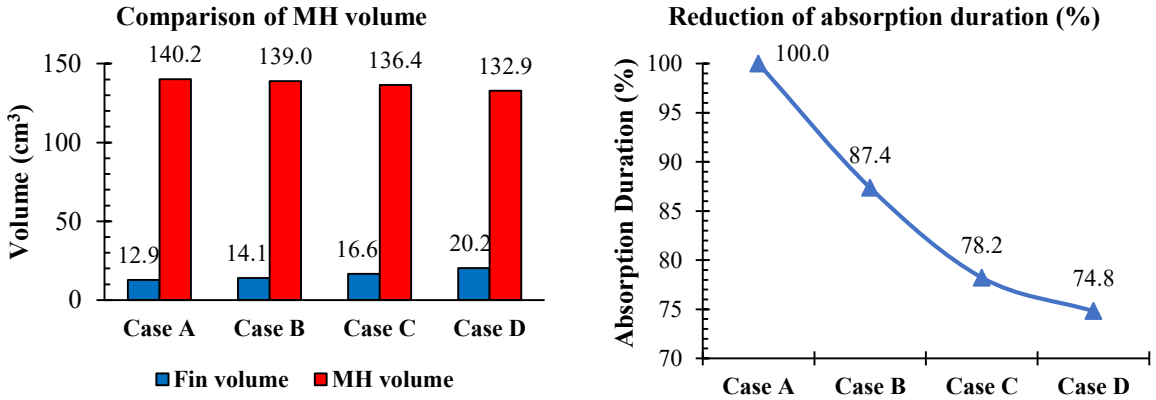

Figure 7.9 Comparison of MH and fin volume on the hydrogen absorption duration for all four cases. (a) comparison of MH volume and (b) reduction of absorption duration

7.6.3 Geometric Study of Triple-Branched Fin Designs (Case D)

This section provides a comprehensive study of the fin geometry for the triple-branched fin (case D) based on the constant operating conditions. The fin performance based on various fin parameters is investigated under the comparison of MH temperature at selected locations during the hydrogen absorption. These various fin parameters and values are defined into 15 cases (case D, and case D-1 to case D-14). Figure 7.10 presents the selected locations to compare the MH temperature based on various fin parameters. It should be noted that these locations are randomly selected to obtain the best comparison for the temperature variation.

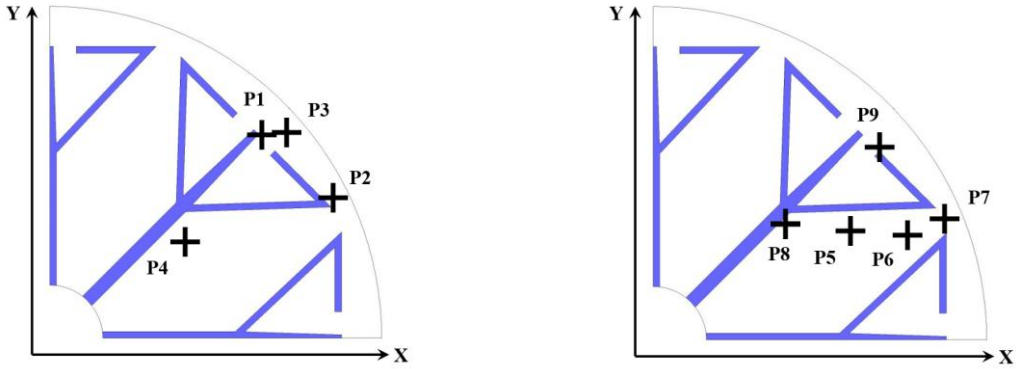

(a) **(b)**

Figure 7.10 Selected points for the comparison of storage bed temperature during the hydrogen absorption; (a) at P1 to P4 and (b) at P5 to P9

- *Influence of fin thickness at the middle branch (W_2) and fin width at the top branch (L_1)*

Effects of fin thickness at the middle branch (W_2) and fin width at the top branch (L_1) on the temperature at the selected points along the MHHS are presented in Figure 7.11. From Figure 7.11a, the MH temperature at P1 is reduced when increasing the fin thickness at the middle branch (W_2). The comparison from this parameter is made based on three different fin thicknesses at this branch from case D (0.5 mm thickness), case D-1 (0.3 mm thickness), and case D-2 (0.7 mm thickness). From Figure 7.11b, the MH temperature at P1 is also reduced faster when increasing the fin width at the top branch (L_1). The three different values are selected for the comparison, including 6 mm for case D-2, 5 mm for case D-3, and 7 mm for case D-4. From these two parameters, the temperatures from these cases have minor differences due to the minor differences in the fin thickness in this area and fin width at the top branch. One of the main reasons is that the tapering of fin thickness (W_2) is distributed to a larger amount of the MH, compared to the other side (Krishna et al., 2024a). However, the difference in MH volume from these three cases is still less than 1%.

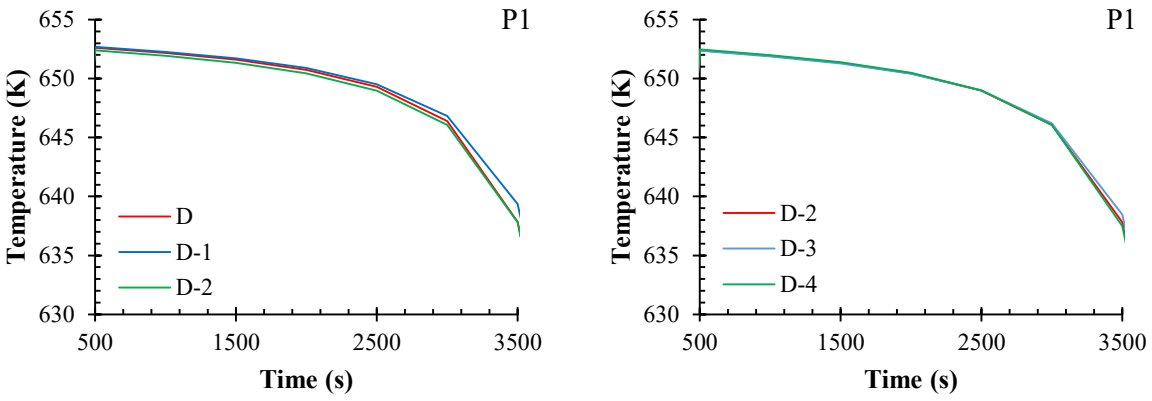

(a) **(b)**

Figure 7.11 Temperature at selected point, P1 based on the fin parameters (from case D to case D-4); (a) fin thickness at second branch and (b) fin width at top branch

- *Influence of fin angle (α_1), fin height (H_1) and fin width (L) for triple-branched section*

The effects of the fin angle of the top branch (α_1), fin height (H_1) and fin width (L) for the triple-branched section on the temperature variation are presented and compared in Figure 7.12 based on the selected points at P2 to P7. Three different values of the fin angle include 47° (case D-4), 37° (case D-5), and 57° (case D-6). From Figure 7.12a, it can be seen that the fin angle (α_1) only slightly affects the

MH bed temperature at P2. However, the greater fin angle at 57° (case D-6) causes a greater MH temperature reduction at P3 from Figure 7.12b. The MH temperature at 3500 s in this case is greatly lower than in other cases. The difference in MH temperature between the lowest angle and the highest angle is 6 K. Based on this parameter, there is only a 1% reduction of MH volume from case D-6, compared to other cases. Therefore, fin angle significantly affects the improvement of heat transfer inside the MHHS, especially around the outer wall of the MHHS. This is due to more fin mass distribution to this area. Considering the fin height, five different values of fin height are selected for this study, including 10 mm (case D-6), 12 mm (case D-7), 9 mm (case D-8), 8 mm (case D-9), and 7 mm (case D-10). From Figure 7.12c, d, it is obvious that reducing the fin height (H_1) results in a faster MH temperature reduction. This is because it increases the triple-branched area. The length of the left and right branches from this fin design is increased because of this height. The effect of branching becomes advantageous due to the greater thermal penetration depth into the system (Klebanoff & Klebanoff 2012). This results in a more uniform temperature distribution along these fin areas. Comparing between the highest fin height and the lowest fin height at 3500 s of absorption time, the MH temperatures at P4 are 5 K in difference, while the MH temperatures at P5 are 9 K in difference. The MH volume from all cases only reduces by around 1%, comparing between case D-7 and case D-10. Therefore, the fin height for the triple-branched section also greatly affects the heat transfer performance inside the MHHS. Considering the fin width (L) from Figure 7.12e, f, the different fin widths for the triple-branched section include 15 mm (case D-11), 16 mm (case D-10), and 17 mm (case D-12). At 3500 s, the MH temperature at both P6 and P7 from the lowest fin width is 637 K, while the MH temperature at these points from the highest fin width is 633 K. The MH temperature from these points indicates that the larger fin width at the triple-branched section positively affects the heat transfer performance. Similar to the fin height, the larger fin width leads to an increase in the overall length at the Y-shaped branch section, resulting in more fin mass distribution to the MH bed. Under this parameter, the difference in MH volume is only less than 0.5%.

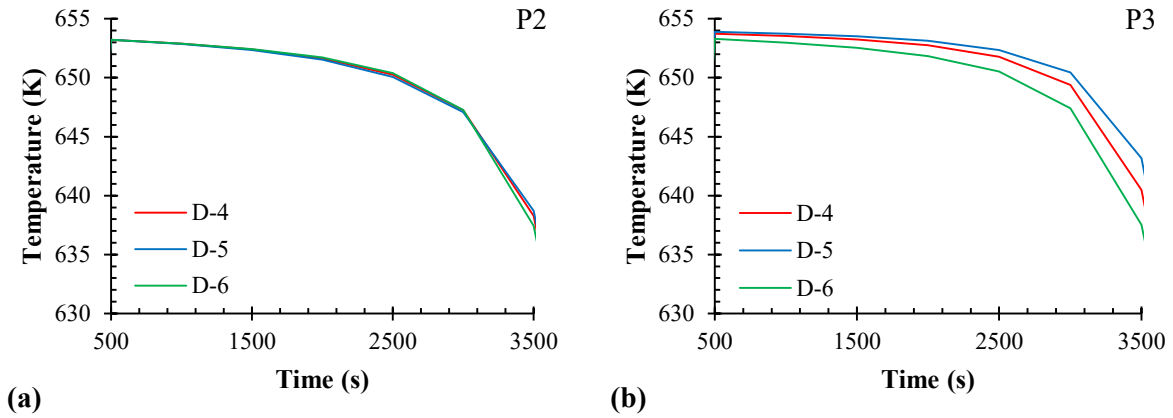

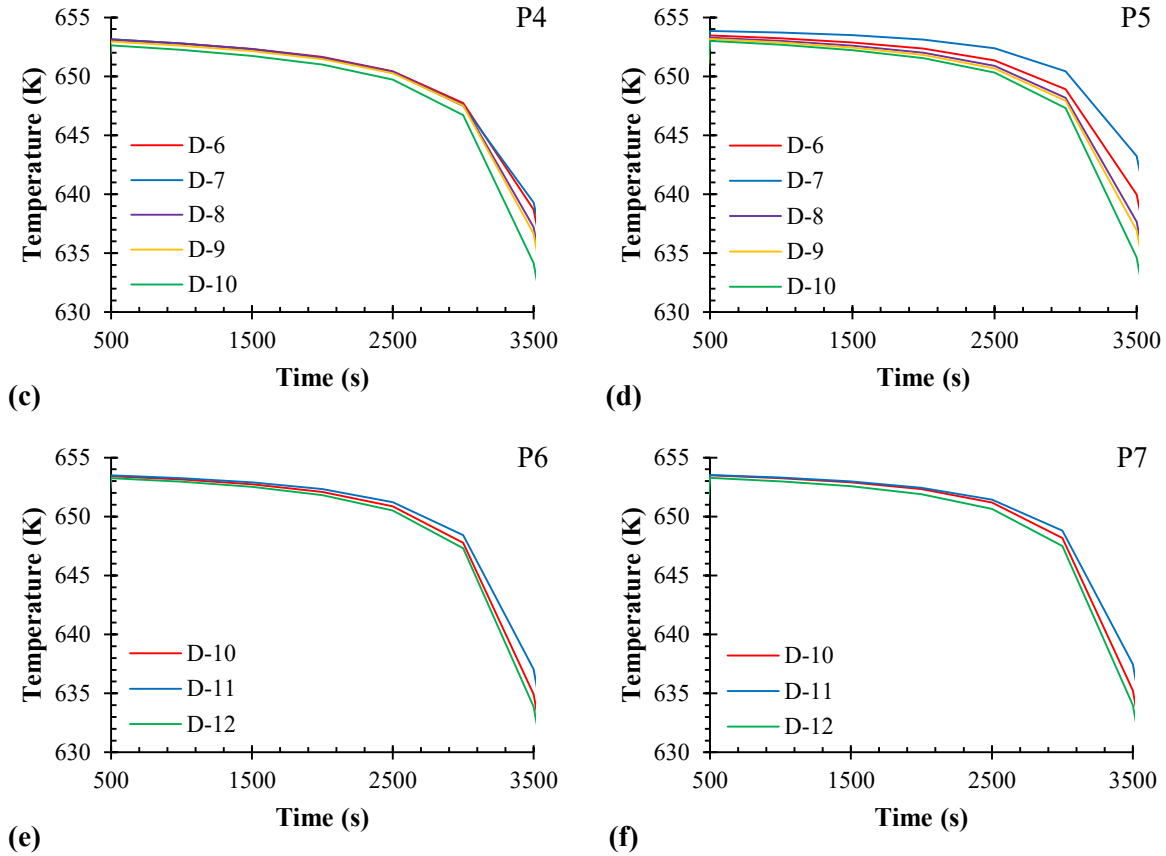

Figure 7.12 Temperature at selected point based on the influences of fin angle, fin height, and fin width for triple-branched section (from case D-4 to case D-6, case D-6 to case D-10, and from case D-10 to case D-12); (a) at P2, (b) at P3, (c) at P4, (d) at P5, (e) at P6, and (f) at P7.

- *Influence of fin thickness at side branches (W_1)*

Figure 7.13 demonstrates the MH temperature at P8 (Figure 7.13a) and P9 (Figure 7.13b) under the influence of fin thickness at the first and third branches (W_1). Three different fin thicknesses are selected in this section. These include 0.3 mm (case D-13), 0.5 mm (case D-12), and 0.7 mm (case D-14). Although fin thickness is not the critical fin parameter, there is an optimal thickness. The thicker fin can reduce the rate of enhancement effect (Low et al., 2024). From Figure 7.13, it is obvious that increasing the thickness of the triple-branched fin significantly enhances the heat transfer rate. The MH temperature from a higher fin thickness is usually lower than the lower fin thickness. Increasing the fin thickness leads to an increase in heat transfer surface areas. At 3500 s, the MH temperature at P8 from the thickness of 0.7 mm is 14 K less than the case with 0.3 mm thickness, while it is 15 K less than 0.3 mm thickness at P9. Therefore, the fin thickness of 0.7 mm still positively affects the heat transfer rate. However, the MH volume is reduced by 6%, comparing between 0.3 mm and 0.7 mm thickness.

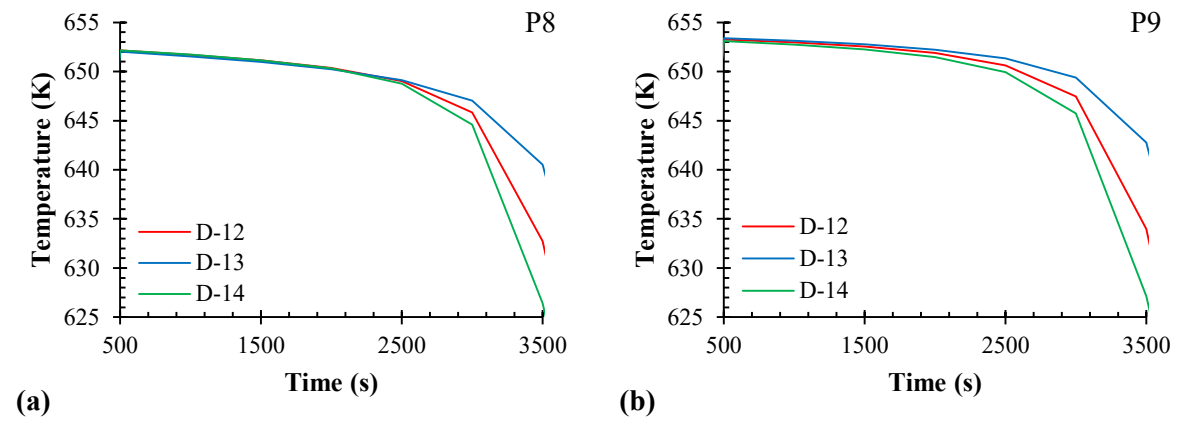

Figure 7.13 Temperature at selected point based on the influence of fin thickness at first and third branches (from case D-12 to case D-14); **(a)** at **P8** and **(b)** at **P9**.

Figure 7.14 shows the hydrogen concentration contours for the hydrogen absorption process between case D (before enhancement) and case D-14 (after enhancement). In both cases, around the central area has a higher hydrogen concentration as this area is close to the HTF tube. Other areas close to the fin also have a higher hydrogen concentration, but this concentration is still lower than the central area. It is obvious that case D-14 obtains a faster hydrogen absorption as this case always has a higher hydrogen concentration, especially around the fin domain. At 3500 s, there is full hydrogen absorption (100% concentration) from case D-14, where it is still at 81% concentration from some areas in the middle and the top corner areas of the MHHS from case D. The hydrogen concentration contours from Figure 7.14 prove that the fin angle, fin width, and fin height of the triple-branched fin, significantly affect the heat transfer mechanism, leading to a faster hydrogen kinetic reaction.

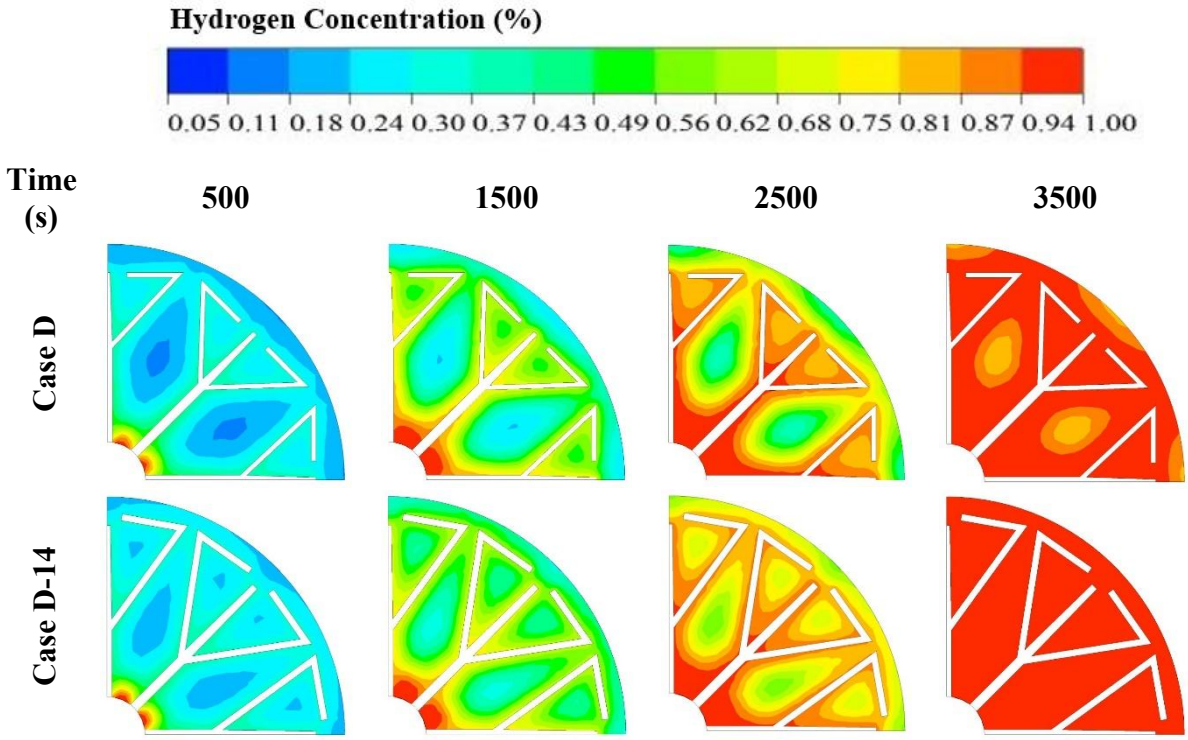

Figure 7.14 Hydrogen concentration at 500 s, 1500 s, 2500 s, and 3500 s after starting hydrogen absorption process from case D and case D-14.

- *Influence of fin designs on hydrogen absorption-desorption cycle*

The comparison of the hydrogen absorption-desorption cycle based on various fin designs is presented in Figure 7.15. From this figure, the final times of one complete cycle from case A to case D are 21047 s, 18675 s, 17440 s, and 16782 s, respectively. Considering the reduction of absorption-desorption duration from case A (as the base case), there are 11% reduction from case B, 17% reduction from case C, and 20% reduction from case D. After the development of case D, the duration of one complete cycle from case D-14 is only 15869 s, which is less than 16000 s. Comparing to case A, case D-14 obtains a 25% reduction of one complete cycle. Considering the volumetric and gravimetric of the MHHS, these two are the main factors for the compact MHHS (Rahnama et al., 2019a). The weight of heat exchangers should be optimised for the use of compact MHHS, such as automobile applications. To achieve a reasonable driving range, the MHHS must suit the size of the vehicle without adding too much weight (Rahnama et al., 2019a). Focusing on the MH volume from case D-14, it has only a 10% reduction of MH volume when comparing with case A. There is only a 20% reduction in MH volume compared to the MHHS without any heat exchangers. Therefore, it is obvious that the new fin design (case D), especially after the development (case D-14), obtains better heat transfer mechanisms compared to the original fin design as a straight-shaped fin and a Y-shaped fin. Therefore, case D-14 is then selected for further analysis of its performance under the parametric study section. Focusing on the reduction of absorption and desorption duration from Figure 7.15, the development of fin design is more effective in the hydrogen kinetic reaction during the hydrogen absorption rather than the hydrogen desorption. This is obvious in the reduction percentage from each case. However, this is only applied in the case of having the same HTF temperature as 573 K for both processes. Selecting a higher HTF temperature for the hydrogen desorption can cause faster hydrogen desorption. The effect of various initial HTF temperatures is then analysed and presented under the parametric study.

Furthermore, the results from case D-14 prove that this case, which contains the straight tube and triple-branched fins, obtains better heat transfer efficiency and shorter hydrogen absorption/desorption duration. The hydrogen absorption-desorption duration from this case is less than 16000 s, while the final time from the SCHE-CR is 17270 s. It should be noted that there is a 15% increase in heat exchanger volume when using the design from case D-14, compared to the SCHE-CR case. This results in a reduction of MH volume from case D-14. In contrast, there is only 3% pressure loss from the case with a straight tube, while there is over 34% pressure loss from the case with coil tubes. However, the difference in hydrogen absorption-desorption duration from these two cases is because of the difference in material use of each heat exchanger. The material used for SCHE-CR is stainless steel, which offers a low thermal conductivity, compared to other materials. The material used in all fin designs in this study is copper, which offers a high thermal conductivity. These can cause a major difference in heat transfer performance. Under the use of stainless steel as the SCHE-CR material, this material was selected at the beginning from our previous studies due to its advantages, which offer more resistance in damage and superior corrosion resistance. It is worth mentioning that this present study only focuses on the fin geometric design and its performance. The comparison between the use of different heat exchanger materials for SCHE-CR and others are not considered in this study.

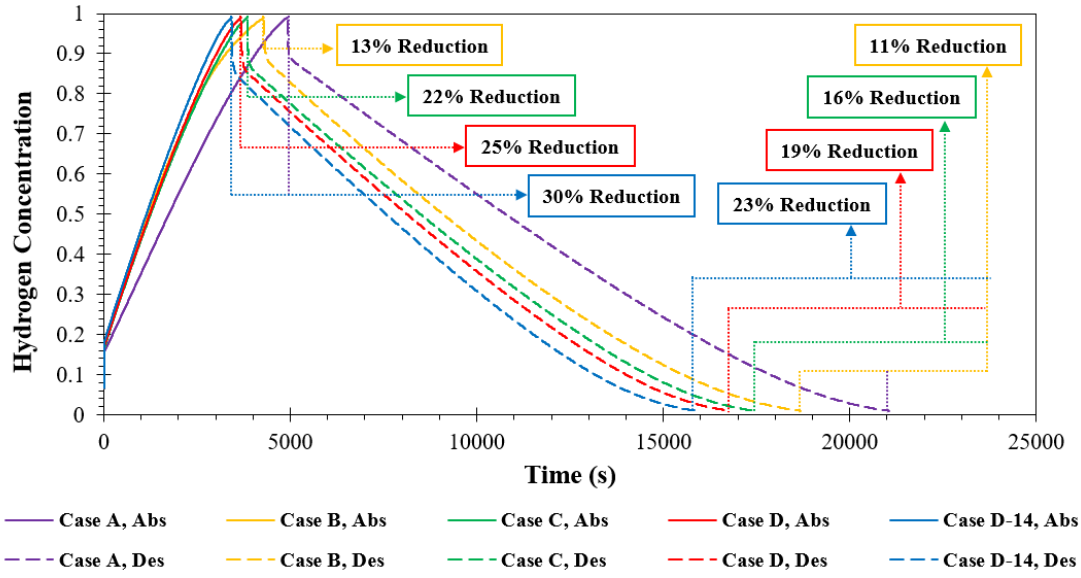

Figure 7.15 Average hydrogen concentration for hydrogen absorption-desorption cycle from various fin designs.

7.6.4 Parametric Study for Operating Conditions

The parametric study in this study focuses on three operating parameters. The MHHS temperature is set as 573 K for all cases of hydrogen absorption, while the initial MHHS temperature for the desorption is set as the ultimate temperature at the end of the absorption process. The loading pressure is set as 1.8 MPa during hydrogen absorption, whereas the pressure of 0.1 MPa is used for hydrogen desorption.

- Heat Transfer Fluid Temperature

The initial HTF temperature plays a significant role in the improvement of the hydrogen kinetic reaction during absorption/desorption. Reducing the HTF temperature obtains faster hydrogen absorption as the MHHS must be cooled down during this stage. In contrast, the MHHS must be heated up for faster hydrogen desorption purposes. In general, the range of temperature for hydrogen absorption and desorption are varied depending on the MH materials (Kanti et al., 2024). Therefore, the choice of HTF is based on the selected MH material (Kanti et al., 2024). From our present study, air is selected as the HTF due to the high operating temperature range of magnesium-based alloy (Larpruenrudee et al., 2022a). Figure 7.16 presents the effect of various HTF temperatures during the hydrogen absorption/desorption. The heat transfer coefficient between the HTF and MH bed is set as 500 W m^{-2} K^{-1} for all cases. From Figure 7.16a, a greater reduction of initial HTF temperature obtains faster hydrogen absorption. The absorption durations from these cases are 3427 s for 573 K, 2164 s for 523 K, 1595 s for 473, and 1271 s for 423 K. Comparing to the base value of 573 K, there is a 37-63% reduction of the absorption time when the temperature decreases from 573 K to 423 K. From Figure 7.16b, increasing the HTF temperature significantly reduces the hydrogen desorption duration. The hydrogen desorption durations from these cases are 12442 s for 573 K, 4717 s for 623 K, 2917 s for 673 K, and 2115 s for 723 K. Comparing to the base HTF temperature at 573 K, there is a 62-83% reduction of hydrogen desorption duration when increasing the HTF temperature from 573 K to 723 K. It can be seen that changing the HTF temperature significantly affects the hydrogen kinetic reaction rate, especially during the desorption process. The initial HTF temperature during the desorption process should be higher than 623 K.

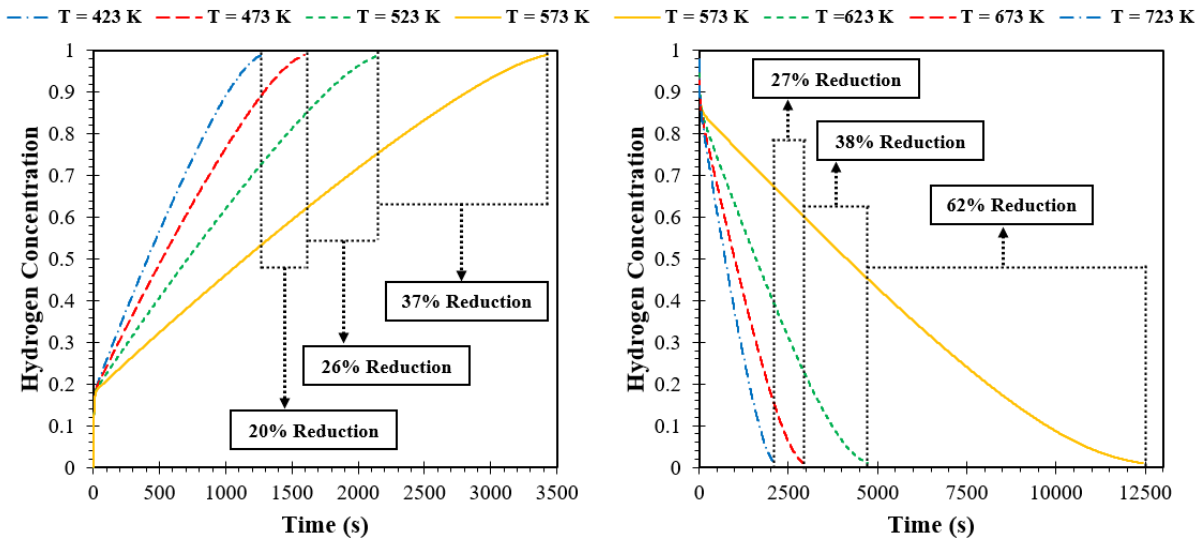

Figure 7.16 Hydrogen concentration based on various initial temperatures of HTF from case D-14; (a) during hydrogen absorption and (b) during hydrogen desorption

- Heat Transfer Coefficient between Heat Transfer Fluid and Metal Hydride

This section provides the investigation of the heat transfer coefficient (h_f) between the HTF and MH bed on the heat transfer performance. Figure 7.17 indicates the effect of various h_f values on hydrogen absorption (Figure 7.17a) and hydrogen desorption (Figure 7.17b). The initial HTF temperature is set as 573 K for both hydrogen absorption and desorption. From Figure 16a, the absorption durations from these cases are 5794 s for 250 W m^{-2} K^{-1}, 3427 s for 500 W m^{-2} K^{-1}, 2602 s for 750 W m^{-2} K^{-1}, and 2167 s for 1000 W m^{-2} K^{-1}. Comparing to the base value at 250 W m^{-2} K^{-1}, there is a 41-63% reduction of hydrogen absorption duration when increases the h_f value from 250 W m^{-2} K^{-1} to 1000 W m^{-2} K^{-1}. From Figure 7.17b, the desorption duration from these cases are 19415 s for 250 W m^{-2} K^{-1}, 12442 s for 500 W m^{-2} K^{-1}, 9985 s for 750 W m^{-2} K^{-1}, and 8685 s for 1000 W m^{-2} K^{-1}. Comparing to the base value at 250 W m^{-2} K^{-1}, it obtains a 36-55% reduction of hydrogen absorption duration when increases the h_f value from 250 W m^{-2} K^{-1} to 1000 W m^{-2} K^{-1}. In general, the amount of heat transfer in the MH bed is directly proportional to the h_f (Eisapour et al., 2021a). Increasing the h_f between the HTF and MH bed positively affects the hydrogen kinetic reaction for both hydrogen absorption and desorption processes (Eisapour et al., 2021a). This is because of the fast reduction in MH bed temperature during the absorption and the fast increase in MH bed temperature during the desorption. It can be summarised that the h_f has a better effect on hydrogen absorption rather than hydrogen desorption. However, this is only applied to the case when using the initial HTF temperature of 573 K for both absorption and desorption.

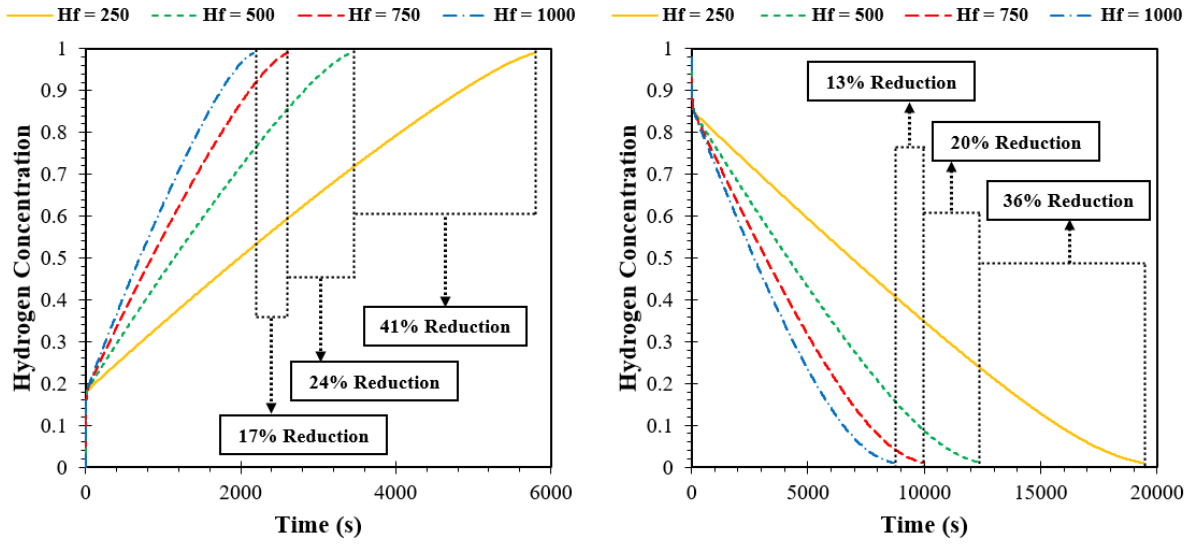

Figure 7.17 Hydrogen concentration based on various heat transfer coefficients between HTF and HTF tube from case D-14; (a) during hydrogen absorption and (b) during hydrogen desorption

- Material Used for Heat Exchanger Tube and Fin

Appropriate selecting material for the heat exchanger tube and fin also plays a significant role in heat transfer management. Four different materials are selected and analysed for their performances under hydrogen absorption and desorption, which are presented in Figure 7.18. These four materials include copper, aluminum, nickel, and steel. For all cases, the initial temperature of the HTF and the h_f between the HTF and MH bed are set as 573 K and 500 W m^{-2} K^{-1}. In general, thermal efficiency, cost, corrosion resistance, compatibility fabrication, and durability are general factors, that should be considered when choosing material for heat exchanger purposes. The material should have a high thermal conductivity to offer more effective to conduct and transfer heat (Cengel & Boles 2015). When using the material with a high thermal conductivity of the HTF tube and fin, the heat transfer efficiency is much higher, compared to the material with low thermal conductivity. From Figure 7.18, it can be seen that steel obtains the longest time to complete the hydrogen absorption and desorption processes. The final time for the hydrogen absorption-desorption cycle based on steel is 21697 s. However, the final time for one cycle from other materials is less than 17000 s as these materials have a higher thermal conductivity compared to steel (refer to Table 7.4 for thermal-physical properties of each material). The final time for one cycle based on nickel, aluminum, and copper is 16748 s, 16265 s, and 15869 s, respectively. A higher thermal conductivity causes a shorter time to complete the hydrogen absorption-desorption cycle. This is because the greater heat transfer efficiency significantly affects the hydrogen kinetic reaction as the faster heat reduction results in a faster hydrogen absorption, while the faster heat addition leads to faster hydrogen desorption (Ardahaie et al., 2021). Therefore, the duration of one complete cycle from nickel, aluminum, and copper reduces by 23-27% when compared to the case with steel. However, copper obtains faster hydrogen absorption/desorption, compared to other materials. This is because the thermal diffusivity and effusivity of copper are better than other materials (Hashain et al., 2021). When considering the hydrogen absorption-desorption duration from the new fin design, nickel, aluminum, and copper are recommended to be used as the material of the HTF tube and fin. The difference in hydrogen absorption-desorption duration between these three materials is less than 5%. However, it should be noted that this study only considers the thermal performance of heat exchanger based on thermal conductivity from different materials and its effect on the hydrogen absorption-desorption duration. Other factors, such as cost, compatibility fabrication, and durability, are not considered in this study.

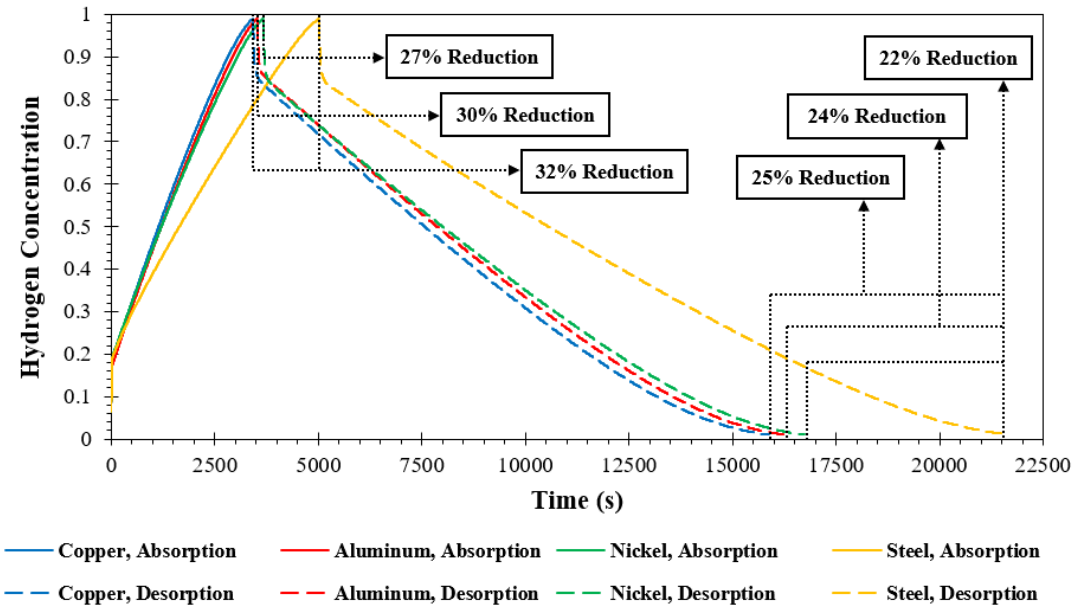

Figure 7.18 Hydrogen concentration during absorption-desorption cycle based on various materials of HTF tube and fin from case D-14.

7.7 Conclusion

The present study proposes a new MHHS configuration incorporating a cooling tube and fin heat exchanger. The simple straight tube is used as a cooling tube instead of other complex heat exchangers to maintain the pressure level. The effect of pressure loss due to the complex HTF tube's structure is investigated to support the selection of a cooling tube to integrate with the new fin design. The novel triple-branched fin design is proposed to fulfil the requirement of heat transfer efficiency instead of using the complex HTF tube. The fin geometry is analysed by considering the increase in heat transfer surface area and fin mass distribution. Various fin designs are also proposed in this study to compare the fin performance under the average MH bed temperature and hydrogen absorption/desorption. Furthermore, the overall MH bed volumes before and after enhancing the fin performance are also investigated in this study. In the parametric study during hydrogen absorption and desorption, the three main selected parameters include the effect of various initial HTF temperatures, the influence of the heat transfer coefficient between the HTF and MH, and the effect of different materials of the fin and HTF tube. The key findings are summarised in the following points:

- There is a 3% pressure loss from the inlet throughout the outlet of the straight tube heat exchanger, while there is over a 34% pressure loss throughout the coil heat exchangers.
- Under four different fin designs, the MHHS with the novel triple-branched fin obtains the best performance with a 25% reduction of absorption duration and less than a 5% reduction of the MH volume, compared to the case with a quadrilateral fin.
- After enhancing the fin performance, the durations of absorption and desorption are reduced by 30% and 23%, compared to the case with quadrilateral fin. For one complete cycle, the duration for this complete cycle from the triple-branched fin after the enhancement is reduced by 25%, compared to the conventional quadrilateral fin. Due to the complex fin structure, which obtains more fin distribution inside the MHHS, there is more uniform temperature distribution along the MH bed and lower thermal resistance. This results in a faster hydrogen kinetic reaction. In other words, it results in faster hydrogen absorption/desorption.

- Considering the MH volume reduction, the fin height and width of the triple-branched section, as well as the fin angle at the top branches, are the key parameters to increase the heat transfer efficiency.
- The HTF temperature for the new MHHS configuration significantly affects the MHHS performance, especially for the hydrogen desorption process. The absorption duration reduces by up to 63% when the HTF temperature is reduced from 573 K to 423 K. However, the desorption duration further reduces by up to 83% when the HTF temperature increases from 573 K to 723 K.
- The heat transfer coefficient between the HTF and MH bed has a more positive effect on the hydrogen absorption process rather than the hydrogen desorption process with up to 63% reduction of absorption duration and up to 55% reduction of desorption when changing the heat transfer coefficient from 250 W m^{-2} K^{-1} to 1000 W m^{-2} K^{-1}.
- Using steel as the fin and HTF tube material obtains less effect on the hydrogen absorption/desorption, compared to other materials, including nickel, aluminium, and copper. The duration of one complete cycle from these materials is 23-27% less than the case with steel.

This study proposes a new magnesium-based hydrogen storage configuration incorporating the internal fin with the cooling tube. The comprehensive investigation of this new configuration on the heat transfer performance and the hydrogen kinetic reaction during the hydrogen absorption/desorption process, is also provided in this study. Furthermore, the effect of fin geometry based on the selected fin parameters is analysed under the temperature variation along the metal hydride bed. It should be noted that the purpose of this study is to introduce the novel triple-branched fin design with the use of a simple cooling tube. The effect of fin parameters on the heat transfer improvement is performed by basic investigations. More analysis of the novel fin design will be considered in future studies by focusing on the effect of different fin ratios, such as fin length, fin width, and fin angle, on the heat transfer enhancement and fin efficiency. Moreover, the future studies will also focus on the fin structure and its strength to withstand the impact of the hydride. To avoid lengthy analog computation for multi-parameter studies, the intelligent algorithms such as artificial neural network (ANN) will be considered in future studies. However, experiment studies regarding this storage configuration are required to obtain concrete, practical results and ensure that this configuration can be applied to industrial settings and supported advancements in hydrogen storage applications.

Chapter 8 – Conclusions

The aim and objectives of this study are achieved by considering various aspects. The primary aim of this study is to enhance thermal performance of the MHHS based on the heat exchangers. The objectives are divided into several main points for the aim achievement purpose. This section summarises the aim/objectives that are achieved during the PhD thesis completion. Furthermore, the improvement of the overall MHHS performance by the storage design is also considered for future work.

8.1 Research Problem Synopsis

The MHHS has been widely used for several engineering applications due to its advantages that offer a high hydrogen storage capacity and high safety. However, the main disadvantage of this MHHS is the low thermal conductivity of the MH materials, resulting in slow hydrogen absorption/desorption. In other words, the key problem of this MHHS is the slow hydrogen kinetic reaction. This significantly affects the overall MHHS performance in terms of the time-consuming purpose. For the hydrogen absorption process, the MHHS temperature is rapidly increased due to a chemical reaction between the hydrogen injection and MH material. The MHHS must be cooled down to control the hydrogen charging flow at the desired rate with the maximum storage capacity. For this purpose, the faster heat removal from the storage system results in faster hydrogen absorption. For the hydrogen desorption process, the MHHS temperature is rapidly decreased due to the release of hydrogen. The MHHS must be heated up to achieve maximum storage performance. Therefore, the faster additional heat supply results in faster hydrogen desorption. For these reasons, the improvement of thermal performance inside the MHHS is one of the most effective ways to improve the hydrogen kinetic reaction. The thermal performance of the MHHS can be enhanced by several techniques. These include the improvement of the thermal performance inside the MHHS by considering the structure, the selection of the MH materials and HTF, and the appropriate selection of operating conditions for the MHHS.

For the improvement of thermal performance, several internal and external heat exchangers have been designed and proposed. From the study, using an internal heat exchanger obtains better heat transfer performance, compared to an external heat exchanger. The key point of the internal heat exchanger design, which significantly affects the heat transfer improvement, is the well arrangement of the heat exchanger structure. This can increase the heat transfer surface area and reduce the temperature variation along the MH bed. The selection of initial operating conditions as well as the selection of MH materials also play an important role in terms of the overall MHHS performance. The activation temperature of the MH and hydrogen loading pressure are basically based on the selected MH material. Furthermore, the initial operating condition of the HTF is also one of the important factors. Increasing the HTF flow rate greatly increases the heat transfer rate as the heat is transferred faster due to the higher turbulent HTF flow. Moreover, decreasing/increasing the initial HTF temperature also significantly improves the heat transfer rate, resulting in the improvement of the hydrogen kinetic reaction during the hydrogen absorption/desorption process. However, the operating conditions and their performances are varied due to the difference in the MHHS configurations. Therefore, it is important to understand the effect of these parameters when applying them to the new MHHS configurations based on the new heat exchanger designs.

8.2 Research Aims/Objectives and Main Achievements

The aim of this study is to enhance the thermal performance of the MHHS by considering the use of heat exchanger under the CFD method. Several new heat exchangers are designed and proposed to achieve the aim. The objectives are divided into several points for this purpose. Each objective and the main achievement are summarised as follows;

Research Aim/Objective i: Proposing the new internal heat exchanger design to enhance the storage thermal performance

Achievement i: The new heat exchanger, namely the semi-cylindrical coil heat exchanger (SCHE) is first designed and proposed in this study. This SCHE is developed from the original helical coil heat exchanger (HCHE), which is known as one of the best heat exchanger designs, compared to other heat exchanger types. This SCHE offers more heat transfer surface areas due to the well arrangement of the heat exchanger structure, compared to the HCHE. The design of the SCHE is performed under the investigation of the effect of the coil pitch size on the heat transfer performance.

Research Aim/Objective ii: Further enhancing thermal performance of the storage system and heat exchanger by further developing the new internal heat exchanger structure from the objective i.

Achievement ii: The SCHE is then further developed to enhance the heat transfer performance by combining itself with the central return tube (SCHE-CR). The purpose is to further enhance the heat transfer performance, especially at the central area of the storage. This area is far away from the heat transfer fluid, resulting in lower heat transfer rates in this area when using SCHE only. The design of this SCHE-CR is performed under the investigation of the effect of the tube size (diameter) on the heat transfer performance.

Research Aim/Objective iii: Further enhancing thermal performance of the storage system and heat exchanger by combining the new internal heat exchanger (from objective ii) with the external heat exchanger under an active thermal management technique

Achievement iii: The new heat exchanger from objective ii, namely SCHE-CR is used to combine with the external heat exchanger, namely cooling jacket. The heat transfer fluid is used for both heat exchangers under the active thermal management technique. The purpose is to further enhance the heat transfer performance of the storage system. The heat is then transferred from the outer side of the storage to the cooling jacket and from the inner side to the SCHE-CR.

Research Aim/Objective iv: Further enhancing thermal performance of the storage system and heat exchanger by combining the new internal heat exchanger (from objective ii) with the external heat exchanger under passive thermal management technique

Achievement iv: The new heat exchanger from objective ii, namely SCHE-CR is used to combine with the external heat exchanger under the passive thermal management technique. Phase change material (PCM) is employed for this purpose. The effect of PCM configuration after combining with the new heat exchanger is comprehensively analysed under the liquid fraction and average bed temperature of the MH and PCM. The new PCM configuration, namely the PCM capsule is proposed to combine with the SCHE-CR. The PCM capsule is designed to further improve the heat transfer performance from all the surface sides of the storage system.

Research Aim/Objective v: Proposing the new storage configuration under the design and the enhancement of its performance of the new internal heat exchanger to enhance the storage performance. The effect of pressure losses during heat transfer fluid circulating inside the heat exchanger is considered as the key factor

Achievement v: The new internal fin, namely the triple-branched fin, is designed and enhanced its performance. This is to be used with an internal straight tube heat exchanger to reduce the pressure losses during the use of heat transfer fluid. The design and the enhancement of its performance of this triple-branched fin are performed under the effect of fin thickness, fin width, fin angle, and fin height on the heat transfer improvement.

Research Aim/Objective vi: Identifying an appropriate initial value for each operating parameter of the metal hydride storage system under the new storage configurations and heat exchangers. The operating parameters include;

- **Operating condition of the metal hydride storage system under the activation temperature and hydrogen pressure**
- **Operating condition of the heat transfer fluid (HTF) under the flow rate, initial temperature, and heat transfer coefficient**

The main purpose of identifying an appropriate initial value for each operating parameter is to ensure that the maximum storage performance is achieved when employing the new heat exchangers. In general, an appropriate initial value for each operating parameter must be defined when having the new storage configuration, which also includes the internal/external heat exchangers.

Achievement vi: The considerations of operating conditions for the new MHHS configuration are as follows;

- Operating condition of the MHHS with the SCHE under the activation temperature and hydrogen loading pressure
- Operating condition of the HTF under flow rate for the MHHS with SCHE and SCHE-CR
- Operating condition of the HTF under initial temperature during the hydrogen absorption/desorption process for the MHHS with SCHE, the MHHS with SCHE-CR, the MHHS with SCHE-CR incorporating PCM capsule, and the MHHS with triple-branched fin
- Operating condition between the HTF and MH bed under heat transfer coefficient during the hydrogen absorption/desorption for the MHHS with SCHE-CR incorporating cooling jacket and the MHHS with triple-branched fin.

8.3 Thesis Conclusions

In this thesis, several studies have been done to achieve the aim regarding the enhancement of the MHHS thermal performance by considering the use of heat exchangers. The several objectives have been achieved for this purpose. The hydrogen kinetic reaction during the hydrogen absorption/desorption process has been investigated under the new MHHS configurations/heat exchangers. Under the investigation of the hydrogen kinetic reaction, the hydrogen absorption/desorption duration as well as the duration of one complete hydrogen absorption-desorption cycle have been considered as the main parameter. The faster completion of each process refers to better thermal performance of the heat exchanger and the MHHS. This is due to the enhancement of the heat transfer rate inside the MHHS. Therefore, another important parameter in this study is the average bed temperature of the MHHS. These two parameters are considered as the main parameters to determine the MHHS performance under the various MHHS configurations. The key findings from all research works are summarised and presented in the following section;

The effect of a semi-cylindrical coil heat exchanger (SCHE) on the MHHS thermal performance

- The use of SCHE significantly improves the heat transfer performance due to having a more uniform heat distribution in the MHHS, compared to the conventional helical coil heat exchanger (HCHE). The thermal performance of the heat exchanger is also enhanced when using the SCHE instead of the HCHE. This reduces the temperature variation along the MH bed, resulting in a faster hydrogen absorption/desorption process. Under the constant MH bed and heat exchanger, there is a 59% reduction of the hydrogen absorption duration when using the SCHE instead of HCHE.
- Considering the tube parameter, the pitch size of the coil heat exchanger also affects the heat transfer performance. Reducing the pitch size from 15 mm to 10 mm significantly reduces the hydrogen absorption duration. With 10 mm of pitch size, the MH volume only reduces by 5%, compared to the base pitch size of 15 mm. The absorption duration is further reduced from 59% to 61% when changing the pitch size. This is due to the increase in heat transfer surface area from the secondary circulation of the HTF tube structure.
- The operating conditions of the MHHS with SCHE also have a great effect on the overall MHHS thermal performance, in terms of the reduction in hydrogen absorption duration. Increasing the hydrogen loading pressure from 1.2 MPa to 1.8 MPa results in a 32% reduction in hydrogen absorption duration. The suitable activation temperature of the MHHS based on Mg2Ni with SCHE is 573 K. The MHHS can achieve the maximum hydrogen storage capacity at 3.6 *wt%* based on this temperature.
- The operating conditions of the heat transfer fluid (HTF) are also one of the main parameters that significantly affect the MHHS thermal performance when incorporating the SCHE. A higher Reynolds number or a higher HTF flow rate positively influences hydrogen absorption duration. The lower initial HTF temperature also greatly improves the convective heat transfer between the MH bed and cooling fluid. The absorption duration greatly reduces by 50-60% when changing these two parameters.

The effect of a semi-cylindrical coil heat exchanger with a central return tube (SCHE-CR) on the MHHS thermal performance

- The use of SCHE-CR further enhances the thermal performance inside the MHHS, especially at the central area of the upper part of MHHS. The more uniform heat distribution is observed in this specific area of the MHHS. The absorption and desorption durations from the case with SCHE-CR are reduced by 30% and 29%, compared to the case with SCHE only. There is a 31% reduction in the duration of the absorption-desorption cycle when using the SCHE-CR instead of the SCHE only. Moreover, there is at least a 50% reduction of this duration from the case with SCHE-CR, compared to the case with HCHE.
- For the tube parameter, the tube diameter also affects the MHHS thermal performance. A larger tube size of the SCHE-CR positively influences the hydrogen absorption reaction, resulting in the reduction of hydrogen absorption duration. The main reason for this reduction is the increase of heat transfer surface area from the larger tube size. The absorption duration is decreased by 40% when changing the tube size from 3 mm to 4 mm.
- Considering the effect of the operating conditions of the HTF on the new MHHS configuration with SCHE-CR, the Reynolds number of HTF at 9000 is the best value. This is considered under the investigation of the turbulent flow on the average turbulence kinetic energy and average heat transfer coefficient for the use of SCHE-CR. The absorption duration is reduced by 24% when increasing the Reynolds number from 6400 to 9000. Other higher values have less effect on the absorption duration. For the initial HTF temperature, reducing the HTF temperature from 573 K to 423 K results in the reduction of hydrogen absorption duration by 19-36%.

The effect of a semi-cylindrical coil heat exchanger with a central return tube incorporating the cooling jacket (SCHE-CR+CJ) on the MHHS thermal performance

- Combining the SCHE-CR with a cooling jacket as the external heat exchanger also greatly improves the thermal performance of the MHHS. From this technique, the generated heat during the absorption process is transferred to the internal SCHE-CR and external cooling jacket. The absorption duration is further decreased by 51% when using the SCHE-CR with a cooling jacket, compared to the use of SCHE-CR only.
- Operating condition between the HTF and MH bed has less effect when using the SCHE-CR with a cooling jacket. The increasing heat transfer coefficient between this HTF and MH bed from 250 W/m2K to 500 W/m2K improves the heat transfer performance, resulting in only 8% reduction of the absorption duration. Other higher heat transfer coefficient values improve the absorption duration by only 1-3%.

The effect of a semi-cylindrical coil heat exchanger with a central return tube incorporating the phase change material (PCM) as the capsule configuration on the MHHS thermal performance

- The combination between the SCHE-CR and PCM as the external heat exchanger greatly obtains the better thermal performance of the MHHS. There are more heat transfers between the PCM surface and MH bed around the MHHS which is covered by the PCM. When using the PCM jacket, the heat can transfer between the side of the PCM surface and the MH bed. However, when using the PCM capsule, the heat can transfer between the side, top, and bottom parts of the PCM surface and MH bed. There is at least a 39% reduction in the duration of the absorption-desorption cycle when using SCHE-CR with PCM, compared to the use of SCHE

only. However, there is at least a 63% reduction in the duration of the completion process when using SCHE-CR incorporating PCM, instead of using PCM only.

- Considering the use of MHHS with PCM only, the PCM configuration also affects the MHHS thermal performance. The PCM configuration greatly enhances the heat transfer performance during the hydrogen absorption process rather than the desorption process. The PCM capsule obtains the best heat transfer improvement rather than the PCM jacket and PCM pool bed. This is due to the more heat transfer surface areas at the top and bottom parts of the MHHS from the PCM capsule. The more PCM liquidus is observed from the PCM capsule during the absorption process, compared to other PCM configurations. This means that there are more heat transfers from the MH bed to the PCM capsule as the PCM is changing from the solid stage to the liquid stage.
- For the operating conditions of the HTF under the use of MHHS with SCHE-CR and PCM capsule, the initial HTF temperature significantly influences the MHHS performance, especially the desorption process. The absorption duration is decreased by 15-26% when reducing the HTF temperature from 573 K to 423 K. Under the desorption process, increasing the HTF temperature from 573 K to 723 K results in the reduction of desorption duration by 25-38%.
- Under the study of PCM heat recovery when combined with SCHE-CR, using only 4/8 of the total PCM volume obtains the best performance in terms of the consideration of the reaction heat from the HTF and PCM and the overall MHHS weight. Based on this PCM volume, the heat recovery rate is 43% with the 1.47 kg of the PCM.

The effect of triple-branched fin on the MHHS thermal performance

- Using the triple-branched fin obtains the best thermal performance, compared to the original straight fin and Y-shaped fin. The hydrogen absorption duration is reduced by 25% when using the triple-branched fin instead of the conventional straight fin. The MH volume between these two designs is only less than 5%.
- After the enhancement of the triple-branched fin structure, the hydrogen absorption duration is reduced by 30%, compared to the original straight fin. The desorption duration is reduced by 23% between these two designs. This results in a 25% reduction in the hydrogen absorption-desorption cycle when using a triple-branched fin after the enhancement, compared to the case with the original straight fin. This is due to the complex fin structure of the triple-branched fin. The complex fin structure obtains more fin distribution inside the MHHS, resulting in a more uniform temperature distribution along the MH bed as well as lower thermal resistance. The hydrogen kinetic reaction is significantly improved, resulting in faster hydrogen absorption/desorption.
- The key parameters for enhancing the heat transfer performance under the fin design and the enhancement of its performance are the fin height, fin width, and fin angle. These parameters are evaluated under the consideration of the MH volume reduction.
- Under the operating condition of the HTF based on the MHHS with a triple-branched fin, the HTF temperature greatly affects the MHHS performance, especially during the hydrogen desorption process. The absorption duration is reduced by 37-63% when reducing the HTF temperature from 573 K to 423 K. However, when increasing the HTF temperature from 573 K to 723 K, the desorption duration is further reduced by 62-83%. Under the same HTF temperature, the heat transfer coefficient has a more positive effect on the hydrogen absorption process rather than the desorption process. Increasing the heat transfer coefficient from 250

W/m^2K to 500 W/m^2K results in the reduction of hydrogen absorption duration by 41-63% and reduction by 36-55% of the desorption duration.

- There is a 3% pressure loss from the inlet through the outlet of the straight tube heat exchanger, while there is over a 34% pressure loss throughout the coil heat exchangers.
- Appropriate selection of fin material and HTF tube material also plays an important role in terms of heat transfer enhancement. This is due to the difference in thermal conductivity of each material. Using steel as the tube and fin material obtains less effect on the hydrogen absorption/desorption duration, compared to other materials, including nickel, aluminum, and copper. When using copper instead of steel as the heat exchanger material, the absorption duration is reduced by 32%, while the desorption duration is reduced by 25%.

8.4 Selection of input parameters for the proposed designs on the realistic and practical applications

The selected input parameters for the current works are as the following points;

- The initial temperature of storage for the absorption process = 573 K (This value is selected based on the experimental study from Muthukumar et al., 2008. Based on this value, it obtains the highest hydrogen storage capacity for Mg_2Ni material)
- The initial temperature of storage for the desorption process = Ultimate temperature from the absorption process (The ultimate temperature from the absorption process is generally used as the initial temperature of the desorption process)
- The supply pressure of hydrogen absorption = 1.8 MPa (The results from my first paper prove that using 1.8 MPa as supply pressure obtains the better hydrogen absorption rate compared to other lower values. The other higher values have less effect on the absorption rate)
- The supply pressure of hydrogen desorption = 0.1 MPa (This value is selected based on the experimental results from Chaise et al., 2010. At the initial process of hydrogen desorption, the temperature is found to be homogeneously distributed, the exhaust valve is opened, and hydrogen is released at atmospheric pressure)
- Initial velocity of the heat transfer fluid = The heat transfer coefficient at 800 W/m^2K. (The initial velocity is calculated based on the Reynolds number and tube diameter). The comparison of changing the Reynolds number is provided in the first paper and the second paper. From the comparison, using 800 W/m^2K as the heat transfer coefficient obtains better hydrogen absorption/desorption compared to other higher and lower values.
- Initial temperature of the heat transfer fluid = 573 K (This value is selected based on the initial temperature of the storage)
- The effect of changing the initial temperature of the heat transfer fluid on the hydrogen absorption/desorption is provided in all of the research papers. In reality, there is a limitation in the initial value of inlet temperature when applying to the cyclic application, including absorption and desorption processes.

8.5 Limitations and Future Study

The aim and objectives of this study have been achieved through the PhD studying. However, the main works from this study focus on the heat exchanger structure and its effect on thermal performance only. There are still some limitations in this study. The specific limitations and future study are summarised as following points.

- The works from Chapter 6 (Research Paper 3) only consider the effect of SCHE-CR and PCM on the heat transfer and overall MHHS performance. The total PCM volume is calculated by assuming that this volume can fully absorb and store the heat from the MH bed without considering the SCHE-CR effect. An appropriate PCM volume selection on the heat recovery when incorporating the SCHE-CR is investigated in this study. However, the final time of absorption and desorption based on an appropriate PCM volume selection is not considered in this study. This parameter is further considered in the next study.
- Although the well arrangement/layout of the internal heat exchanger structure is the key factor in increasing the heat transfer distribution inside the MHHS, there are some limitations for manufacturing in reality as all of these present studies are only based on numerical simulation. An experimental study is required for this purpose.
- The effect of the turbulent flow of the HTF (from all research chapters) on heat transfer improvement is investigated in this study. However, this study does not consider the effect of this turbulent flow on the oscillations. In reality, there might be oscillations due to the high-speed flow of the HTF and the design of the HTF tube in some cases. This can positively affect the heat and mass transfer rates. In contrast, these changes can also induce flow instabilities in equipment due to the fluctuation of flow and pressure drop. This oscillation will be considered in the future study.
- The works from the current study only focus on the effect of the structure of the new heat exchanger designs on the heat transfer performance. The effect of roughness in the tube on the heat transfer efficiency is not considered in this study. In reality, Increasing the surface roughness will increase the turbulence flow and disrupt the thermal boundary layer. This will result in the improvement of the heat transfer performance. However, this enhancement will increase the pressure drop, which negatively affects the overall storage system performance. The balance between the improvement of the heat transfer by surface roughness and the increase in pressure drop must be considered in the future study.
- This study only focuses on the hydrogen kinetic reaction based on the improvement of heat transfer performance. The hydrogen storage capacity is constant at 3.6 *wt%* for all research papers. The effect of using different input parameters or different storage designs on the hydrogen storage capacity is not considered in the current study. The change in hydrogen storage capacity will be considered in the future study.
- The comparison of different fin materials on the hydrogen absorption-desorption duration is performed under the research work in Chapter 7. The materials include aluminum, copper, nickel, and steel. The comparison is only based on the thermal-physical properties of each material on the heat transfer performance in terms of hydrogen absorption-desorption duration. Other factors such as cost, compatibility fabrication, and durability are not considered in this study.
- The selected material used for HCHE, SCHE, and SCHE-CR (from the first three research papers under Chapter 4 to Chapter 6) is stainless steel. This material is selected because of its advantages which offer more resistance in damage and superior corrosion resistance. This is the key factor when considering the material selection under the use of the HTF. However, the

selected material used for triple-branched fin and all fin designs from the last research paper (Chapter 7) is copper. This material is selected for this study because of its thermal-physical properties, which offer a high thermal conductivity. The stainless steel usually has a low thermal conductivity, compared to copper. This causes a major difference in heat transfer performance. The difference in hydrogen absorption-desorption duration between these two materials is because of the difference in material use of each heat exchanger. From all research works in this thesis, the comparison between these heat exchanger designs, including the triple-branched under the same material, is still not considered. The future study will focus on this aspect to predict the final time of the hydrogen absorption-desorption cycle.

References

Abdellaoui, M., Cracco, D., & Percheron-Guegan, A., (1998). Structural characterization and reversible hydrogen absorption properties of Mg2Ni rich nanocomposite materials synthesized by mechanical alloying. *Journal of Alloys Compounds*, 268, 233–240.

Abdellaoui, M., Mokbli, S., Cuevas, F., Latroche, M., Guegan-Percheron, A., & Zarrouk, H., (2006). Structural, solid–gas and electrochemical characterization of Mg2Ni-rich and MgxNi100−x amorphous-rich nanomaterials obtained by mechanical alloying. *International Journal of Hydrogen Energy*, 31, 247–250.

Abe, J.O., Popoola, A.P.I., Ajenifuja, E. & Popoola, O.M., (2019). Hydrogen energy, economy and storage: Review and recommendation. *International Journal of Hydrogen Energy*, 44, 15072-15086.

Aburto, A., & Orgaz, E., (2007). Ab initio structural and electronic investigation of magnetic R Ni Sn (R¼La, Ce, Pr, Nd) intermetallics and their hydrides. *Physical Review B*, 75, 045130.

Adilkhanova, I., Memon, S.A., Kim, J., & Sheriyev, A., (2021). A novel approach to investigate the thermal comfort of the lightweight relocatable building integrated with PCM in different climates of Kazakhstan during summertime. *Energy*, 217, 119390.

Afzal, M., Mane, R. & Sharma, P. (2017). Heat transfer techniques in metal hydride hydrogen storage: A review. *International Journal of Hydrogen Energy*, 42, 30661–30682.

Afzal, M., & Sharma, P., (2018). Design of a large-scale metal hydride based hydrogen storage reactor: simulation and heat transfer optimisation. *International Journal of Hydrogen Energy*, 43, 13356-13372.

Afzal, M., & Sharma, P., (2021a). Design and computational analysis of a metal hydride hydrogen storage system with hexagonal honeycomb based heat transfer enhancements-part A. *International Journal of Hydrogen Energy*, 46, 13116-13130.

Afzal, M., & Sharma, P., (2021b). Experimental analysis of a metal hydride hydrogen storage system with hexagonal honeycomb-based heat transfer enhancements-part B. *International Journal of Hydrogen Energy*, 46, 13131-13141.

Ahluwalia, R.K., (2007). Sodium alanate hydrogen storage system for automotive fuel cells. *International Journal of Hydrogen Energy*,32, 1251-1261.

Alqahtani, T., Mellouli, S., Bamasag, A., Askri, F., & Phelan, P.E., (2020a). Thermal performance analysis of a metal hydride reactor encircled by a phase change material sandwich bed. *International Journal of Hydrogen Energy*, 45, 23076-23092.

Alqahtani, T., Mellouli, S., Bamasag, A., Askri, F., & Phelan, P.E., (2020b). Cyclic behaviors of a novel design of a metal hydride reactor encircled by cascaded phase change materials. *International Journal of Hydrogen Energy*, 45, 32285-32297.

Anbarasu, S., Muthukumar, P., & Mishra, S.C., (2014a). Thermal modeling of LmNi4. 91Sn0. 15 based solid state hydrogen storage device with embedded cooling tubes. *International Journal of Hydrogen Energy*, 39, 15549-62.

Anbarasu, S., Muthukumar, P., & Mishra, S.C., (2014b). Tests on LmNi4. 91Sn0. 15 based solid state hydrogen storage device with embedded cooling tubes - Part A: absorption process. *International Journal of Hydrogen Energy*, 39, 3342-3351.

Anbarasu, S., Muthukumar, P., & Mishra, S.C., (2014c). Tests on LmNi4. 91Sn0. 15 based solid state hydrogen storage device with embedded cooling tubes - Part B: desorption process. *International Journal of Hydrogen Energy*, 39, 4966-4972.

Anbarasu, S., Muthukumar, P., & Mishra, S.C., (2014d). Thermal modeling of Mg2Ni-based solid-state hydrogen storage reactor. *Heat Transfer Engineering*, 35, 1354-1362.

Andreasen, G., Melnichuk, M., Ramos, S., Corso, H.L., Visintin, A., Triaca, W.E., & Peretti, H.A., (2013). Hydrogen desorption from a hydride container under different heat exchange conditions. *International Journal of Hydrogen Energy*, 38, 13352-13359.

Aoyagi, H., Aoki, K., & Masumoto, T., (1995). Effect of ball milling on hydrogen absorption properties of FeTi, Mg2Ni and LaNi5. *Journal of Alloys Compounds*, 231, 804–809.

Ardahaie, S.S., Hosseini, M.J., Eisapour, M., Eisapour, A.H., & Ranjbar, A.A., (2021). A novel porous metal hydride tank for hydrogen energy storage and consumption assisted by PCM jackets and spiral tubes. *Journal of Cleaner Production*, 311, 127674.

Askri, F., Miled, A., Mellouli, S., & M^aad, H.B., (2019). Numerical investigation of high temperature metal hydride water pumping system. *International Journal of Hydrogen Energy*, 44, 16777-16792.

Askri, F., Salah, M.B., Jemni, A., & Nasrallah, S.B., (2009). Optimisation of hydrogen storage in metal-hydride tanks. *International Journal of Hydrogen Energy*, 34, 897-905.

Ayub, I., Nasir, M.S., Liu, Y., Munir, A., Wu, Z., Yang, F., & Zhang, Z., (2020). Numerical modeling and performance comparison of high-temperature metal hydride reactor equipped with bakery system for solar thermal energy storage. *International Journal of Hydrogen Energy*, 45, 31612-31631.

Bai, X.S., Yang, W.W., Tang, X.Y., Yang, F.S., Jiao, Y.H., & Yang, Y., (2021). Optimisation of tree-shaped fin structures towards enhanced absorption performance of metal hydride hydrogen storage device: A numerical study. *Energy*, 220, 119738.

Bai, X.S., Yang, W.W., Zhang, W.Y., Yang, F.S., & Tang, X.Y., (2020). Hydrogen absorption performance of a novel cylindrical MH reactor with combined loop-type finned tube and cooling jacket heat exchanger. *International Journal of Hydrogen Energy*, 45, 28100-28115.

Balachandar, C., Arunkumar, S., & Venkatesan, M., (2015). Computational heat transfer analysis and combined ANN–GA optimization of hollow cylindrical pin fin on a vertical base plate, *Sadhana*,40, 1845–1863.

Bao, Z., Wu, Z., Nyamsi, S.N., Yang, F., & Zhang, Z., (2013a). Three-dimensional modeling and sensitivity analysis of multitubular metal hydride reactors. *Applied Thermal Engineering*, 52, 97-108.

Bao, Z., Yang, F., Wu, Z., Cao, X., & Zhang, Z., (2013b). Simulation studies on heat and mass transfer in high-temperature magnesium hydride reactors. *Applied Thermal Engineering*, 112, 1181–1189.

Beigzadeh, R., Rahimi, M., Jafari, O., & Alsairafi, A.A., (2016). Computational fluid dynamics assists the artificial neural network and genetic algorithm approaches for thermal and flow modeling of air-

forced convection on interrupted plate fins, *Numerical Heat Transfer, Part A: Applications*, 70:546–565.

Bergman, T.L., Lavine, A.S., Incropera, F.P., & Dewitt, D.P., (2011). Fundamentals of heat and mass transfer 7th edn. John Wiley & Sons, Incorporated.

Bhogilla, S., Pandoh, A., & Singh, U.R., (2024). Cogeneration system combining reversible PEM fuel cell, and metal hydride hydrogen storage enabling renewable energy storage: Thermodynamic performance assessment. *International Journal of Hydrogen Energy*, 52(Part D), 1147-1150.

Bhogilla, S.S., (2017). Design of a AB2-metal hydride cylindrical tank for renewable energy storage. *Journal of Energy Storage*, 14, 203-210.

Bhouri, M., Burger, I., & Linder, M., (2015). Numerical investigation of hydrogen charging performance for a combination reactor with embedded metal hydride and coolant tubes. *International Journal of Hydrogen Energy*, 40, 6626-6638.

Bird, R., Stewart, W., & Lightfoot, E., (2002.) Transport Phenomena. 2nd Edition, John Wiley and Sons, New York.

Cengel, Y.A. & Boles, M.A., (2015) *Thermodynamics: An Engineering Approach*. 8th Edition, McGraw Hill, New York.

Chaise, A., Marty, P., Rango, P.D., & Fruchart, D., (2009). A simple criterion for estimating the effect of pressure gradients during hydrogen absorption in a hydride reactor. International Journal of Heat and Mass Transfer, 52, 4564–4572.

Chaise, A., Rango, P.D., Marty, P., & Fruchart, D., (2010). Experimental and numerical study of a magnesium hydride tank. *International Journal of Hydrogen Energy*, 35, 6311–6322.

Chandra, D., Chien, W.M., & Talekar, A., (2011). Rare earths – crucial elements of advanced technology. *Material Matters*, 6, 51.

Christopher, M.D., (2006). Application of the transient hot-wire technique for measurement of effective thermal conductivity of catalyzed sodium alanate for hydrogen storage. *Virginia Tech*.

Chung, C., & Lin, C.S., (2009). Prediction of hydrogen desorption performance of Mg2Ni hydride reactors, *International Journal of Hydrogen Energy*, 34, 9409–9423.

Chung, C.A., & Ho, C.J., (2009). Thermal-fluid behavior of the hydriding and dehydriding processes in a metal hydride hydrogen storage canister. *International Journal of Hydrogen Energy*, 34, 4351-4364.

Claman, M., & Minton, P., (1977). An experimental investigation of flow in an oscillating pipe. *Journal of Fluid Mechanics,* 81, 421-431.

Colozza, A.J., (2002). Hydrogen storage for aircraft applications overview. Technical Report, Brook Park, OH United States: *Analex Corp*.

Corgnale, C., Hardy, B., Motyka, T., Zidan, R., Teprovich, J., & Peters, B., (2014). Screening analysis of metal hydride based thermal energy storage systems for concentrating solar power plants. *Renewable and Sustainable Energy Reviews*, 38, 821-833.

Corre, S., Bououdina, M., Fruchart, D., & Adachi, G.Y., (1998). Stabilisation of high dissociation pressure hydrides of formula La1−xCexNi5 with carbon monoxide. *Journal of Alloys Compounds*, 275, 99–104.

Cui, Y., Zeng, X., Xiao, J., & Kou, H. (2022). The comprehensive review for development of heat exchanger configuration design in metal hydride bed. *International Journal of Hydrogen Energy*, 47, 2461-2490.

Dagdougui, H., Sacile, R., Bersani, C., & Ouammi, A., (2018). Hydrogen storage and distribution: Implementation scenarios. In: Dagdougui H, Sacile R, Bersani C, Ouammi A, editors. Hydrogen infrastructure for energy applications. *Academic Press*, 37–52.

Dai, H., Chen, Z., Cao, H., Tian, Z., Zhang, M., Wang, X., He, S., Wang, W., & Gao, M. (2024). Effect of partition arrangement of metal hydrides and phase change materials on hydrogen absorption performance in the metal hydride reactor. *International Journal of Hydrogen Energy*, 84, 780-792.

Darzi, A.A.R., Afrouzi, H.H., Moshfegh, A., & Farhadi, M. (2016). Absorption and desorption of hydrogen in long metal hydride tank equipped with phase change material jacket. *International Journal of Hydrogen Energy*, 41, 9595-610.

Darzi, A.R., Farhadi, M., Sedighi, K., Aallahyari, S. & Delavar, M.A., (2013). Turbulent heat transfer of Al2O3ewater nanofluid inside helically corrugated tubes: numerical study. *International Communications in Heat and Mass Transfer*, 41, 68-75.

Dedrick, D., Kanouff, M., Replogle, B., & Gross, K., (2005). Thermal properties characterization of sodium alanates. *Journal of Alloys Compounds*, 389, 299-305.

Deng, S., Nie, C., Wei, G., & Ye, W.B., (2019). Improving the melting performance of a horizontal shell-tube latent-heat thermal energy storage unit using local enhanced finned tube. *Energy and Buildings*, 183, 161–73.

Dhaou, H., Khedher, N.B., Mellouli, S., Souahlia, A., Askri, F., Jemni, A., & Nasrallah, S.B., (2011). Improvement of thermal performance of spiral heat exchanger on hydrogen storage by adding copper fins. *International Journal of Thermal Sciences*, 50, 2536-2542.

Dhaou, H., Souahlia, A., Mellouli, S., Askri, F., Jemni, A. & Nasrallah, S.B. (2010). Experimental study of a metal hydride vessel based on a finned spiral heat exchanger. *International Journal of Hydrogen Energy* 35, 1674-1680.

Dieterich, M., Pohlmann, C., Bürger, I., Linder, M. & R€ontzsch, L. (2015). Long-term cycle stability of metal hydride-graphite composites. *International Journal of Hydrogen Energy*, 40, 16375–16382.

DOE: US Department of Energy. Metal hydride storage materials: Hydrogen and fuel cell technologies office, https://www.energy.gov/eere/fuelcells/metal-hydride-storage-materials (accessed 05 January 2023)

Dong, D., Humphries, T.D., Sheppard, D.A., Stansby, B., Paskevicius, M., Sofianos, M.V., Chaudhary, A.L., Dornheim, M., & Buckley, C.E., (2017). Thermal optimisation of metal hydride reactors for thermal energy storage applications. *Sustainable Energy & Fuels*, 1, 1820-1829.

Eisapour, A.H., Eisapour, M., Talebizadehsardari, P., & Walker, G.S., (2021b). An innovative multi-zone configuration to enhance the charging process of magnesium based metal hydride hydrogen storage tank. *Journal of Energy Storage*, 36, 102443.

Eisapour, A.H., Naghizadeh, A., Eisapour, M., & Talebizadehsardari, P., (2021a). Optimal design of a metal hydride hydrogen storage bed using a helical coil heat exchanger along with a central return tube during the absorption process. *International Journal of Hydrogen Energy*, 46, 14478-14493.

El Mghari, H., Huot, J., & Xiao, J., (2019). Analysis of hydrogen storage performance of metal hydride reactor with phase change materials. *International Journal of Hydrogen Energy*, 44, 28893-28908.

El Mghari, H., Huot, J., Tong, L., & Xiao, J., (2020). Selection of phase change materials, metal foams and geometries for improving metal hydride performance. *International Journal of Hydrogen Energy*, 45, 14922-1439.

Erek, A., lken, Z., & Acar, M.A., (2005). Experimental and numerical investigation of thermal energy storage with a finned tube. *International Journal of Energy Research*, 29, 283–301.

Esapour, M., Hosseini, M.J., Ranjbar, A.A., Pahamli, Y., & Bahrampoury, R., (2016). Phase change in multi-tube heat exchangers. *Renewable Energy*, 85, 1017–1025.

Eslami, M., Khosravi, F., & Fallah Kohan, H.R., (2021). Effects of fin parameters on performance of latent heat thermal energy storage systems: A comprehensive review. *Sustainable Energy Technologies and Assessments*, 47, 101449.

Fadonougbo, J.O., Kim, H., Suh, B., Yim, C.D., Na, T., Park, H. & Suh, J. (2022). On the long-term cyclic stability of near-eutectic Mg-Mg_2Ni alloys. *International Journal of Hydrogen Energy*, 47, 3939–3947.

Ferekh, S., Gwak, G., Kyoung, S., Kang, H-g., Chang, M-h., Yun, S-h., Oh, Y-h., Kim, W., Kim, D., Hong, T. & Ju, H., (2015). Numerical comparison of heat-fin-and-metal-foam-based hydrogen storage beds during hydrogen charging process. *International Journal of Hydrogen Energy*, 40, 1440-1450.

Fernández, R.Á., Caraballo, C.S., Cilleruelo, B.F., & Lozano, J.A., (2018). Fuel optimization strategy for hydrogen fuel cell range extender vehicles applying genetic algorithms. *Renewable and Sustainable Energy Reviews*, 81, 655-668.

Fernandez-Seara, J., Pi neiro-Pontevedra, C. & Dopazo, J.A. (2014). On the performance of a vertical helical coil heat exchanger. Numerical model and experimental validation. *Applied Thermal Engineer* 62, 680-689.

Flueckiger, S., Voskuilen, T., Pourpoint, T., Fisher, T.S., & Zheng, Y., (2010). In situ characterization of metal hydride thermal transport properties. *International Journal of Hydrogen Energy*, 35, 614-621.

Førde, T., Eriksen, J., Pettersen, A.G., Vie, P.J.S., & Ulleberg., (2009). Thermal integration of a metal hydride storage unit and a PEM fuel cell stack. *International Journal of Hydrogen Energy*, 34, 6730-6739.

Freni, A., Cipiti, F., & Cacciola, G., (2009). Finite element-based simulation of a metal hydride-based hydrogen storage tank. *International Journal of Hydrogen Energy*, 34, 8574-8582.

Friedlmeier, G., & Groll, M., (1996). *Proceedings International Symposium on Metal Hydrogen Systems 1996*, Switzerland, August 25–30, 497–507.

Gambini, M., (1994). Metal hydride energy systems performance evaluation. Part A: dynamic analysis model of heat and mass transfer. *International Journal of Hydrogen Energy*, 19, 67-80.

Gambini, M., Stilo, T., & Vellini, M., (2019). Hydrogen storage systems for fuel cells: comparison between high and low-temperature metal hydrides. *International Journal of Hydrogen Energy*, 44, 15118-15134.

Garrier, S., Delhomme, B., De Rango, P., Marty, P., Fruchart, D., & Miraglia, S., (2013). A new MgH_2 tank concept using a phase-change material to store the heat of reaction. *International Journal of Hydrogen Energy*, 38, 9766-9771.

Garrison, S.L., Hardy, B.J., Gorbounov, M.B., Tamburello, D.A., Corgnale, C., Mosher, D.A., & Anton, D.L., (2012). Optimisation of internal heat exchangers for hydrogen storage tanks utilising metal hydrides. *International Journal of Hydrogen Energy*, 37, 2850-2861.

Goodell, P., (1980). Thermal conductivity of hydriding alloy powders and comparisons of reactor systems. *Journal of Less Common Metals*, 74, 175-84.

Guan, F., Ma, W., Tu, Y., Zhou, C., Zhou, B. (2014). An experimental study of flow behavior of coiled tubing drilling system. *Advance in Mechanical Engineering*, 6.

Guarino, A., & Spagnuolo, G., (2021). Automatic features extraction of faults in PEM fuel cells by a Siamese artificial neural network. *International Journal of Hydrogen Energy*, 46, 34854-34866.

Hahne, E., & Kallweit, J., (1998). Thermal conductivity of metal hydride materials for storage of hydrogen: experimental investigation. *International Journal of Hydrogen Energy*, 23, 107-14.

Hameed, G., Ghafoor, M.A., Yousaf, M., Imran, M., Zaman, M., Elkamel, A., Haq, A., Rizwan, M., Wilberforce, T., Abdlkareem, M.A., & Olabi, A.G., (2022). Low temperature phase change materials for thermal energy storage: Current status and computational perspectives. *Sustainable Energy Technologies and Assessments*, 50, 101808.

Hardy, B.J. & Anton, D.L. (2009). Hierarchical methodology for modelling hydrogen storage systems. Part II: detailed models. *International Journal of Hydrogen Energy*, 2992-3004.

Harries, D.N., Paskevicius, M., Sheppard, D.A., Edward, T., Price, C. & Buckley, C.E. (2012). Concentrating solar thermal heat storage using metal hydrides. *Proceedings of the IEEE* 100, 539-549.

Hasnain, F., Irfan, M., Khan, M.M., Khan, L.A., & Ahmed, H.F., (2021). Melting performance enhancement of a phase change material using branched fins and nanoparticles for energy storage applications. *Journal of Energy Storage*, 38, 102513.

Hassanpouryouzband, A., Wilkinson, M. & Haszeldine, R.S. (2024). Hydrogen energy futures foraging or farming? *Chemical Society Reviews. R. Soc. Chem.*, 53, 2258–2263.

Hassanpouryouzband, A., Veshareh, M.J., Wilkinson, M., Nick, H.M., Ngwenya, B.T. & Haszeldine, R.S. (2025). In situ hydrogen generation from underground fossil hydrocarbons. *Joule*, 9, 101809.

Hickie-Bentzen, A., Elsharqawy, M., Tasnim, S.H. & Mahmud, S. (2022). Parametric investigation of internal Y-shaped fin configurations under natural convection in a concentric annulus. *Results in Engineering*, 16, 100692.

Hirscher, M., Yartys, V.A., Baricco, M., von Colbe, J.B., Blanchard, D., Bowman, Jr.R.C., Broom, D.P., Buckley, C.E., et al., (2020). Materials for hydrogen-based energy storage – past, recent progress and future outlook. *Journal of Alloys and Compounds*, 827, 153548.

Hosseini, M.J., Rahimi, M., & Bahrampoury, R., (2014). Experimental and computational evolution of a shell and tube heat exchanger as a PCM thermal storage system. *International Communications in Heat and Mass Transfer*, 50,128–136.

Hosseinzadeh, K., Alizadeh, M., & Ganji, D.D., (2019). Solidification process of hybrid nanoenhanced phase change material in a LHTESS with tree-like branching fin in the presence of thermal radiation. *Journal of Molecular Liquids*, 275, 909–925.

Hwang, J.J., & Chang, W.R., (2012). Characteristic study on fuel cell/ battery hybrid power system on a light electric vehicle. *Journal of Power Sources*, 207, 111-119.

Ishido, Y., Kawamura, M., & Ono, S., (1982). Thermal conductivity of magnesium-nickel hydride powder beds in a hydrogen atmosphere. *International Journal of Hydrogen Energy*, 7, 173-182.

Jain, I., Lal, C., & Jain, A., (2010). Hydrogen storage in Mg: a most promising material. *International Journal of Hydrogen Energy*, 35, 5133-5144.

Jemni, A., Ben-Nasrallah, S., & Lamloumi, J., (1999). Experimental and theoretical study of a metal–hydrogen reactor. *International Journal of Hydrogen Energy*, 24, 631–644.

Jiang, Y., Zhang, G., Wang, J., & Vaferi, B., (2021). Hydrogen solubility in aromatic/cyclic compounds: prediction by difference machine learning techniques. *International Journal of Hydrogen Energy*, 46, 23591-23602.

Jin, D.J., Uhm, H.S., & Cho, G., (2013). Influence of the gas-flow Reynolds number on a plasma column in a glass. *Physics of Plasmas*, 20, 083513.

Jiao, K., Li, X., Yin, Y., Zhou, Y., Yu, S. & Du, Q. (2012). Effects of various operating conditions on the hydrogen absorption processes in a metal hydride tank. *Appl. Energy*, 94, 257–269.

Kalbasi, R., (2021). Introducing a novel heat sink comprising PCM and air - adapted to electronic device thermal management. *International Journal of Heat and Mass Transfer*, 169, 120914.

Kanti, P.K., Shrivastav, A.P., Sharma, P. & Maiya, M.P., (2024). Thermal performance enhancement of metal hydride reactor for hydrogen storage with graphene oxide nanofluid: Model prediction with machine learning. *International Journal of Hydrogen Energy*, 52, 470-484.

Kaplan, Y., (2009). Effect of design parameters on enhancement of hydrogen charging in metal hydride reactors. *International Journal of Hydrogen Energy*, 34, 2288-2294.

Karmakar, A., Mallik, A., Gupta, N., & Sharma, P., (2021). Studies on 10kg alloy mass metal hydride based reactor for hydrogen storage. *International Journal of Hydrogen Energy*, 46, 5495-5506.

Kazemi, M., Hosseini, M., Ranjbar, A.A.A., & Bahrampoury, R., (2018). Improvement of Longitudinal Fins Configuration in Latent Heat Storage Systems. *Renew Energy*, 116 (Part A), 447–457.

Kempf, A., & Martin, W., (1986). Measurement of the thermal properties of TiFe0. 85Mn0. 15 and its hydrides. *International Journal of Hydrogen Energy*, 11, 107-116.

Keshari, V., & Maiya, M.P., (2018). Design and investigation of hydriding alloy based hydrogen storage reactor integrated with a pin fin tube heat exchanger. *International Journal of Hydrogen Energy*, 43, 7081-7095.

Keshari, V., & Maiya, M.P., (2020). Numerical study of solid state hydrogen storage system with finned tube heat exchanger. *Heat Transfer Engineering*, 41, 484-496.

Khaitan, S.K., & Raju, M., (2012). Discharge dynamics of coupled fuel cell and metal hydride hydrogen storage bed for small wind hybrid systems. *International Journal of Hydrogen Energy*, 37, 2344-2352.

Kim, K., Kang, M., Lee, G., Jung, K., Kharangate, C.R., Asheghi, M., Goodson, K.E., & Lee, H., (2022). A machine learning approach for predicting heat transfer characteristics in micro-pin fin heat sinks. *International Journal of Heat and Mass Transfer*, 194, 123087.

Klebanoff, L., & Klebanoff, L. (2012). *Hydrogen Storage Technology: Materials and Applications*, 1st Edition, CRC Press.

Klopcic, N., Grimmer, I., Winkler, F., Sartory, M. & Trattner, A. (2023). A review on metal hydride materials for hydrogen storage. *Journal of Energy Storage*, 72, 108456.

Kojima, Y., Kawai, Y., Towata, S.I., Matsunaga, T., Shinozawa, T., & Kimbara, M., (2006). Development of metal hydride with high dissociation pressure. *Journal of Alloys Compounds*, 419, 256-261.

Koroneos, C., Dompros, A., Roumbas, G., & Moussiopoulos, N., (2004). Life cycle assessment of hydrogen fuel production processes. *International Journal of Hydrogen Energy*, 29, 1443-1450.

Krisha, K.V., Kanti, P.K., & Maiya, M.P. (2024). A novel flat coil heat exchanger for metal hydride hydrogen storage reactors. *International Journal of Hydrogen Energy*, 64, 98-108.

Krishna, K.B, Kanti, P.K., & Maiya, M.P., (2024a). A novel fin efficiency concept to optimize solid state hydrogen storage reactor. *Energy*, 288, 129789.

Krishna, K.B., Kanti, P.K., & Maiya, M.P., (2024b). Design optimization of metal hydride-based hydrogen storage reactor using fin efficiency concept. 38th ISTANBUL International Conference on Advances in "Science, Engineering & Technology" (IASET-24) May 13-15, 2024 Istanbul (Turkiye)

Krishnayatra, G., Tokas, S., & Kumar, R., (2020). Numerical heat transfer analysis & predicting thermal performance of fins for a novel heat exchanger using machine learning. *Case Studies in Thermal Engineering*, 21, 100706.

Kumar, A., Raju, N.N., Muthukumar, P., & Selvan, P.V., (2019). Experimental studies on industrial scale metal hydride based hydrogen storage system with embedded cooling tubes. *International Journal of Hydrogen Energy*, 44, 13549-13560.

Kumar, E.A., Maiya, M.P., & Murthy, S.S., (2011). Measurement and analysis of effective thermal conductivity of $MmNi_{4.5}Al_{0.5}$ hydride bed. *Industrial & Engineering Chemistry Research*, 50, 12990-12999.

Kumar, V., Saini, S., Sharma, M., & Nigam, K.D.P., (2006). Pressure drop and heat transfer study in tube-in-tube helical heat exchanger. *Chemical Engineering Science*, 61, 4403–4416.

Larpruenrudee, P., Bennett, N.S., Fitch, R., Sauret, E., Gu, Y.T., & Islam, M.S., (2024). Investigation of metal hydride hydrogen storage performance using phase change materials. *International Journal of Hydrogen Energy*, 60, 996-1019.

Larpruenrudee, P., Bennett, N.S., Gu, Y.T., Fitch, R., & Islam, M.S., (2022a). Design optimization of a magnesium-based metal hydride hydrogen energy storage system. *Scientific Reports*, 12, 13436.

Larpruenrudee, P., Bennett, N.S., Hossain, M.J., Fitch, R., & Islam, M.S. (2022b). *Hydrogen energy storage system: how does the semi-cylindrical helical coil heat exchanger affect metal hydride beds' thermal conductivity?*. In Proceeding of the 23rd Australasian Fluid Mechanics Conference., eds C. Lei, B. Thornber, and S. Armfield. Sydney, Australia.

Larpruenrudee, P., Bennett, N.S., Luo, Z., Fitch, R., Sauret, E., & Islam, M.S., (2023). A novel design for faster hydrogen storage: A combined semi-cylindrical and central return tube heat exchanger. *Journal of Energy Storage*, 71, 108018.

Laurencelle, F., & Goyette, J., (2007). Simulation of heat transfer in a metal hydride reactor with aluminium foam. *International Journal of Hydrogen Energy*, 32, 2957-2964.

Lee, H., Kang, M., Jung, K.W., Kharangate, C.R., Lee, S., Iyengar, M., Malone, C., Asheghi, M., Goodson, K.E., & Lee, H., (2021). An artificial neural network model for predicting frictional pressure drop in micro-pin fin heat sink. *Applied Thermal Engineering*, 194, 117012.

Lewis, S.D. & Chippar, P. (2020). Numerical investigation of hydrogen absorption in a metal hydride reactor with embedded embossed plate heat exchanger. *Energy* 194, 116942.

Lewis, S.D., & Chippar, P., (2021). Analysis of heat and mass transfer during charging and discharging in a metal hydride - phase change material reactor. *Journal of Energy Storage*, 33, 102108.

Li, H., Wang, Y., He, C., Chen, X., Zhang, Q., Zheng, L., et al., (2015). Design and performance simulation of the spiral mini-channel reactor during H2 absorption. *International Journal of Hydrogen Energy*, 40, 13490-13505.

Liang, G., (2004). Synthesis and hydrogen storage properties of Mg-based alloys. *Journal of Alloys Compounds*, 370, 123-128.

Lin, C.X., & Ebadian, M.A., (1997). Developing turbulent convective heat transfer in helical pipes. *International Journal of Heat and Mass Transfer*, 40, 3861-3873.

Ling, Z., Zhang, Z., Shi, G., Fang, X., Wang, L., Gao, X., et al., (2014). Review on thermal management systems using phase change materials for electronic components, Li-ion batteries and photovoltaic modules. *Renewable and Sustainable Energy Reviews*, 31, 427-438.

Liu, J., Li, K., Cheng, H., Yan, K., Wang, Y., Liu, Y., Jin, H. & Zheng, Z. (2017). New insights into the hydrogen storage performance degradation and Al functioning mechanism of LaNi5-xAlx alloys. *International Journal of Hydrogen Energy*, 42, 24904–24914

Liu, Y., Wang, H., Ayub, I., Yang, F., Wu, Z., & Zhang, Z., (2021). A variable cross-section annular fins type metal hydride reactor for improving the phenomenon of inhomogeneous reaction in the thermal energy storage processes. *Applied Energy*, 295, 117073.

Lohrasbi, S., Bandpy, M.G., & Ganji, D.D., (2016b). Response surface method optimization of V-shaped fin assisted latent heat thermal energy storage system during discharging process. *Alexandria Engineering Journal*, 55, 2065–2076.

Lohrasbi, S., Sheikholeslami, M., & Ganji, D.D., (2016a) Discharging process expedition of NEPCM in fin-assisted latent heat thermal energy storage system. *Journal of Molecular Liquids*, 221, 833–41.

Low, Z.H., Qin, Z. & Duan, F., (2024) A review of fin application for latent heat thermal energy storage enhancement. *Journal of Energy Storage*, 85, 111157.

Lundin, C.E., Lynch, F.E., & Magee, C.B., (1977). A correlation between the interstitial hole sizes in intermetallic compounds and the thermodynamic properties of the hydrides formed from those compounds. *Journal of Less Common Metals*, 56, 19-37

Luts, A.E., Bradshaw, R.W., Bromberg, L., & Rabinovich, A., (2004). Thermodynamic analysis of hydrogen production by partial oxidation reforming. *International Journal of Hydrogen Energy*, 29, 808-816.

Ma, J., Wang, Y., Shi, S., Yang, F., Bao, Z., & Zhang, Z., (2014). Optimisation of heat transfer device and analysis of heat & mass transfer on the finned multi-tubular metal hydride tank. *International Journal of Hydrogen Energy*, 39, 13583-13595.

Maad, H.B., Askri, F., & Nasrallah, S.B., (2016a). Heat and mass transfer in a metal hydrogen reactor equipped with a phase-change heat-exchanger. *International Journal of Thermal Sciences*, 99, 271-278.

Maad, H.B., Askri, F., Virgone, J., & Nasrallah, S.B., (2018). Numerical study of high temperature metal-hydrogen reactor (Mg2Ni-H2) with heat reaction recovery using phase change material during desorption. *Applied Thermal Engineering*, 140, 225–234.

Maad, H.B., Miled, A., Askri, F., & Nasrallah, S.B., (2016b). Numerical simulation of absorption-desorption cyclic processes for metal-hydrogen reactor with heat recovery using phasechange material. *Applied Thermal Engineering*, 96, 267-276.

MacDonald, B.D., & Rowe, A.M., (2006). Impacts of external heat transfer enhancements on metal hydride storage tanks. *International Journal of Hydrogen Energy*, 31, 1721-1731.

Malleswararao, K., Aswin, N., Murthy Srinivasa, S., & Dutta, P., (2020). Performance prediction of a coupled metal hydride based thermal energy storage system. *International Journal of Hydrogen Energy*, 45, 16239-16253.

Malleswararao, K., Aswin, S., Murthy, S.S., & Dutta, P., (2021). Studies on a dynamically coupled multifunctional metal hydride thermal battery. *Journal of Alloy Compounds*, 866, 158979.

Mallik, A., & Sharma, P., (2021). Modeling and numerical simulation of an industrial scale metal hydride reactor based on CFD-Taguchi combined method. *Energy Storage*, 3, 227.

Marnellos, G.E., Athanasiou, C., Makridis, S.S., & Kikkinides, E.S., (2008). Integration of hydrogen energy technologies in autonomous power systems. In: Hydrogen-based autonomous power systems: Techno-economic analysis of the integration of hydrogen in autonomous power systems 2008. London: Springer London, 23–81.

Mathew, A., Nadim, N., Chandratilleke, T.T., Humphries, T.D., Paskevicius, M., & Buckley, C.E., (2021). Performance analysis of a hightemperature magnesium hydride reactor tank with a helical coil heat exchanger for thermal storage. *International Journal of Hydrogen Energy*, 46, 1038-1055.

Mazzucco, A., Dornheim, M., Sloth, M., Jensen, T.R., Jensen, J.O., & Rokni, M., (2014). Bed geometries, fueling strategies and optimisation of heat exchanger designs in metal hydride storage systems for automotive applications: a review. *International Journal of Hydrogen Energy*, 39, 17054-17074.

Mellouli, S., Abhilash, E., Askri, F., & Nasrallah, S.B., (2016). Integration of thermal energy storage unit in a metal hydride hydrogen storage tank. *Applied Thermal Engineering*, 102, 1185-1196.

Mellouli, S., Askri, F., Abhilash, E., & Nasrallah, S.B., (2017). Impact of using a heat transfer fluid pipe in a metal hydride-phase change material tank. *Applied Thermal Engineering*, 113, 554-565.

Mellouli, S., Askri, F., Dhaou, H., Jemni, A., & Nasrallah, S.B., (2007). A novel design of a heat exchanger for a metal-hydrogen reactor. *International Journal of Hydrogen Energy*, 32, 3501-3507.

Mellouli, S., Askri, F., Dhaou, H., Jemni, A., & Nasrallah, S.B., (2010). Numerical simulation of heat and mass transfer in metal hydride hydrogen storage tanks for fuel cell vehicles. *International Journal of Hydrogen Energ*, 35, 1693-1705.

Mellouli, S., Dhaou, H., Askri, F., Jemni, A., & Nasrallah, S.B., (2009). Hydrogen storage in metal hydride tanks equipped with metal foam heat exchanger. *International Journal of Hydrogen Energy*, 34(23), 9393-401.

Mellouli, S., Khedher, N.B., Askri, F., Jemni, A., & Nasrallah, S.B., (2015). Numerical analysis of metal hydride tank with phase change material. *Applied Thermal Engineering*, 90, 674-682.

Mendelsohn, M.H., Gruen, D.M., & Dwight, A.E., (1979). The effect of aluminum additions on the structural and hydrogen absorption properties of AB5 alloys with particular reference to the LaNi5-xAlx ternary alloy system. *Journal of Less Common Metals*, 63, 193-207.

Meng, X., Wu, Z., Bao, Z., Yang, F., & Zhang, Z., (2013). Performance simulation and experimental confirmation of a minichannel metal hydrides reactor. *International Journal of Hydrogen Energy*, 38, 15242-15253.

Miled, A., Mellouli, S., Ben Maad, H., & Askri, F., (2017). Improvement of the performance of metal hydride pump by using phase change heat exchanger. *International Journal of Hydrogen Energy*, 42, 26343-26361.

Minko, K.B., Artemov, V.I., & Yan'Kov, G.G., (2015). Numerical study of hydrogen purification using metal hydride reactor with aluminium foam. *Applied Thermal Engineering*, 76, 175-184.

Mirabile Gattia, D., Montone, A., Di Sarcina, I., Nacucchi, M., De Pascalis, F., Re, M., Pesce, E. & Vittori Antisari, M. (2016). On the degradation mechanisms of Mg hydride pellets for hydrogen storage in tanks. *International Journal of Hydrogen Energy*, 41, 9834–9840.

Mocanu, E., Nguyen, P.H., Gibescu, M., & Kling, W.L., (2016). Deep learning for estimating building energy consumption. *Sustainable Energy, Grids and Networks*,6, 91-99.

Mohan, G., Maiya, M.P., & Murthy, S.S., (2007). Performance simulation of metal hydride hydrogen storage device with embedded filters and heat exchanger tubes. *International Journal of Hydrogen Energy*, 32, 4978-4987.

Moradi, R., & Groth, K.M., (2019). Hydrogen storage and delivery: Review of the state of the art technologies and risk and reliability analysis. *International Journal of Hydrogen Energy*, 44, 12254–69.

Mou, X., Bao, Z., & Huang, W., (2023). Performance investigation of metal hydride reactor equipped with helically coiled heat exchanger during hydrogen absorption and desorption. *Thermal Science and Engineering Progress*, 38, 101656.

Musharavati, F., & Khanmohammadi, S., (2022). Design and exergy based optimization of a clean energy system with fuel Cell/MED and hydrogen storage option. *International Journal of Hydrogen Energy*, 47, 26715-26727.

Muthukumar, P., Kumar, A., Raju, N.N., Malleswararao, K., & Rahman, M.M., (2018). A critical review on design aspects and developmental status of metal hydride based thermal machines. *International Journal of Hydrogen Energy*, 43, 17753-17779.

Muthukumar, P., Prakash Maiya, M., Srinivasa Murthy, S., Vijay, R., & Sundaresan, R., (2008). Tests on mechanically alloyed Mg2Ni for hydrogen storage. *Journal of Alloys and Compounds*, 452, 456–461.

Muthukumar, P., Singhal, A., & Bansal, G., (2012). Thermal modeling and performance analysis of industrial-scale metal hydride based hydrogen storage container. *International Journal of Hydrogen Energy*, 37, 14351-14364.

N´obrega, C.R.E.S., Ismail, K.A.R., & Lino, F.A.M., (2019). Enhancement of ice formation around vertical finned tubes for cold storage applications. *International Journal of Refrigeration*, 99, 251–263.

Nam, J., Ko, J., & Ju, H., (2012). Three-dimensional modeling and simulation of hydrogen absorption in metal hydride hydrogen storage vessels. *Applied Energy*, 89, 164-175.

Nemukula, E., Mtshali, C.B. & Nemangwele, F. (2025). Metal hydrides for sustainable hydrogen storage: A review. *Int. J. Energy Res.*, 6300225.

Nguyen, H.Q., & Shabani, B., (2020). Metal hydride thermal management using phase change material in the context of a standalone solar-hydrogen system. *Energy Conversion and Management*, 224, 113352.

Nguyen, H.Q., & Shabani, B., (2021). Review of metal hydride hydrogen storage thermal management for use in the fuel cell systems. *International Journal of Hydrogen Energy*, 46(62), 31699–31726.

Ni, M., Leung, M.K.H., & Leung, D.Y.C., (2008). Energy and exergy analysis of hydrogen production by a proton exchange membrane (PEM) electrolyser plant. *Energy Conversion and Management*, 49, 2748-2756.

Nunes, V.M.B., Lourenco, M.J.V., Santos, F.J.V., & Nieto de Castro, C.A., (2006). Viscosity of molten sodium nitrate. *International Journal of Thermophysics*, 27, 1638-1649.

Nuss, P. & Eckelman, M.J. (2014). Life cycle assessment of metals: A scientific synthesis. *PLoS ONE*, 9, e101298

Nyamsi, S.N., Tolj, I., & Lototskyy, M., (2019). Metal hydride beds-phase change materials: dual mode thermal energy storage for medium-high temperature industrial waste heat recovery. *Energies*, 12, 3949.

Nyamsi, S.N., Yang, F., & Zhang, Z., (2012). An optimization study on the finned tube heat exchanger used in hydride hydrogen storage system – analytical method and numerical simulation. *International Journal of Hydrogen Energy*, 37, 16078-16092.

Omrani, R., Nguyen, H.Q., & Shabani, B., (2020). Thermal coupling of an open-cathode proton exchange membrane fuel cell with metal hydride canisters: an experimental study. *International Journal of Hydrogen Energy*, 45, 28940-28950.

Ostanek, J.K., (2014). Improving pin-fin heat transfer predictions using artificial neural networks, *Journal of Turbomachinery*, 136, 051010

Pahamli, Y., Hosseini, M.J., Ranjbar, A.A., & Bahrampoury, R., (2018). Inner pipe downward movement effect on melting of PCM in a double pipe heat exchanger. *Applied Mathematics and Computation*, 316, 30–42.

Paskevicius, M., Sheppard, D.A., Williamson, K., & Buckley, C.E., (2015). Metal hydride thermal heat storage prototype for concentrating solar thermal power. *Energy*, 88, 469-77.

Patil, S.D., & Gopal, M.R., (2013). Analysis of a metal hydride reactor for hydrogen storage. *International Journal of Hydrogen Energy*, 38, 942-951.

Pendyala, R., Jayanti, S., & Balakrishnan, A.R., (2008). Convective heat transfer in single-phase flow in vertical tube subjected to axial low frequency oscillations. *Heat Mass Transfer*, 44, 857-864.

Pons, M., & Dantzer, P., (1994). Determination of thermal conductivity and wall heat transfer coefficient of hydrogen storage materials. *International Journal of Hydrogen Energy*, 19, 611-616.

Pons, M., Dantzer, P., & Guilleminot, J., (1993). A measurement technique and a new model for the wall heat transfer coefficient of a packed bed of (reactive) powder without gas flow. *International Journal of Heat and Mass Transfer*, 36, 2635-2646.

Principi, G., Agresti, F., Maddalena, A., & Russo, S.L., (2009). The problem of solid state hydrogen storage. *Energy*, 34, 2087-2091.

Qu, Y., Zhou, D., Xue, F., & Cui, L., (2021). Multi-factor analysis on thermal comfort and energy saving potential for PCM-integrated buildings in summer. *Energy and Buildings*, 241, 110966.

Rahnama, A., Zepon, G., & Sridhar, S., (2019a). Machine learning based prediction of metal hydrides for hydrogen storage, part I: prediction of hydrogen weight percent. *International Journal of Hydrogen Energy*, 44, 7337-7344.

Rahnama, A., Zepon, G., & Sridhar, S., (2019b). Machine learning based prediction of metal hydrides for hydrogen storage, part II: prediction of material class. *International Journal of Hydrogen Energy*, 44, 7345-7353.

Raju, M., & Kumar, S., (2011). System simulation modeling and heat transfer in sodium alanate based hydrogen storage systems. *International Journal of Hydrogen Energy*, 36, 1578-1591.

Raju, M., & Kumar, S., (2012). Optimisation of heat exchanger designs in metal hydride based hydrogen storage systems. *International Journal of Hydrogen Energy* 2012;37:2767-2778.

Raju, N.N., Kumar, A., Malleswararao, K., & Muthukumar, P., (2019a). Parametric studies on LaNi4. 7Al0. 3 based hydrogen storage reactor with embedded cooling tubes. *Energy Procedia*, 158, 2384-2390.

Raju, N.N., Muthukumar, P., Selvan, P.V., & Malleswararao, K., (2019b). Design methodology and thermal modelling of industrial scale reactor for solid state hydrogen storage. *International Journal of Hydrogen Energy*, 44, 20278-20292.

Reilly, J., & Wiswall, R.H., (1972). Jr. Hydrogen Storage and Purification Technical Report for Brookhaven National Laboratory: 1972.

Reilly, J.J., Adzic, G.D., Johnson, J.R., Vogt, T., Mukerjee, S., & McBreen, J., (1999). The correlation between composition and electrochemical properties of metal hydride electrodes. *Journal of Alloys Compounds*, 293-295, 569-582.

Reiser, A., Bogdanovic, B. & Schliche, K. (2000). The application of Mg-based metal-hydrides as heat energy storage systems. *International Journal of Hydrogen Energy* 25, 425–430.

Ren, Q., Guo, P., & Zhu, J., (2020). Thermal management of electronic devices using pin-fin based cascade microencapsulated PCM/expanded graphite composite. *International Journal of Heat and Mass Transfer*, 149, 1-16.

Rödl, A., Wulf, C., & Kaltschmitt, M., (2018). Assessment of selected hydrogen supply chains—Factors determining the overall GHG emissions. *In: Azzaro-Pantel C, editor. Hydrogen supply chains. Academic Press; 2018*, 81–109.

Ron, M., Bershadsky, E., & Josephy, Y., (1991). The thermal conductivity of porous metal matrix hydride compacts. *Journal of Less Common Metals*, 172, 1138-1146.

Rusman, N., & Dahari, M., (2016). A review on the current progress of metal hydrides material for solid-state hydrogen storage applications. *International Journal of Hydrogen Energy*, 41, 12108–12126.

Sakintuna, B., Lamari-Darkrim, F., & Hirscher, M., (2007). Metal hydride materials for solid hydrogen storage: a review. *International Journal of Hydrogen Energy*, 39, 1121-1140.

Sandrock, G., & Thomas, G., (1997). Compilation of IEA/DOE/SNL databases Technical Report for International Energy Agency (IEA): 1997.

Sandrock, G. (1997). State-of-the Art Review of Hydrogen Storage in Reversible Metal Hydrides for Military Fuel Cell Applications. *Final Report Contract*, pp. 1–159.

Sandrock, G., (1999). A panoramic overview of hydrogen storage alloys from a gas reaction point of view. *Journal of Alloys and Compounds*, 293-295, 877-888.

Sandrock, G.D., (1979). Development of low cost nickel-rare earth hydrides for hydrogen storage. In Proceedings of the 2nd World Hydrogen Energy Conference., Vol.3, eds T.N. Veziroglu an W. Seifritz. Pergamon, Oxford, 1979, 1625-1656.

Schlichting, H., (1979). Boundary layer theory, 7th edn. McGraw-Hill, New York.

Sciacovelli, A., Gagliardi, F., & Verda, V., (2015). Maximization of performance of a PCM latent heat storage system with innovative fins. *Applied Energy*, 137, 707–715.

Sekhar, B.S., Lototskyy, M., Kolesnikov, A., Moropeng, M.L., Tarasov, B., & Pollet, B., (2015). Performance analysis of cylindrical metal hydride beds with various heat exchange options. *Journal of Alloys Compounds*, 645, S89-95.

Shafiee, S., & McCay, M.H., (2016). Different reactor and heat exchanger configurations for metal hydride hydrogen storage systemsea review. *International Journal of Hydrogen Energy*, 41, 9462-9470.

Shao, H., Liu, T., Wang, Y., Xu, H., & Li, X., (2008). Preparation of Mg-based hydrogen storage materials from metal nanoparticles. *Journal of Alloys Compounds*, 465, 527-533.

Sheikholeslami, M., Haq, R., Shafee, A., Li, Z., Elaraki, Y.G., & Tlili, I., (2019). Heat transfer simulation of heat storage unit with nanoparticles and fins through a heat exchanger. *International Journal of Heat and Mass Transfer*, 135,470–478.

Shtivastav, A.P., Kanti, P.K., Mohan, G., & Maiya, M.P. (2024). Design and optimization of metal hydride reactor with phase change material using fin factor for hydrogen storage. *Journal of Energy Storage*, 77, 109975.

Singh, A., Maiya, M.P., & Murthy, S.S., (2017a). Performance of a solid state hydrogen storage device with finned tube heat exchanger. *Internal Journal of Hydrogen Energy*, 42, 26855-26871.

Singh, A., Maiya, M.P., Murthy, S.S, (2015). Effects of heat exchanger design on the performance of a solid state hydrogen storage device. *International Journal of Hydrogen Energy*, 40, 9733-9746.

Singh, A., Maiya, M.P., Murthy, S.S, (2017b). Experiments on solid state hydrogen storage device with a finned tube heat exchanger. *International Journal of Hydrogen Energy*, 42, 15226-15235.

Singh, A.K., Singh, A.K., & Srivastava, O.N., (1995). On the synthesis of the Mg2Ni alloy by mechanical alloying. *Journal of Alloys Compounds*, 227, 63–68.

Sodhi, G.S., & Muthukumar, P., (2021). Experimental and numerical investigations on the charging and discharging performances of high-temperature cylindrical phase change material encapsulations. *Solar Energy*, 224, 411-424.

Souahlia, A., Dhaou, H., Mellouli, S., Askri, F., Jemni, A., & Nasrallah, S.B., (2014). Experimental study of metal hydride-based hydrogen storage tank at constant supply pressure. *International Journal of Hydrogen Energy*, 39, 7365-7372.

Sreeraj, R., Aadhithiyan, A.K., Anbarasu, S., (2022). Integration of thermal augmentation methods in hydride beds for metal hydride based hydrogen storage systems: Review and recommendation. *Journal of Energy Storage*, 52, 105039.

Suda, S., (1985). Recent development of hydride energy systems in Japan. *International Journal of Hydrogen Energy*, 10, 757-765.

Suda, S., Kobayashi, N., & Yoshida, K., (1981). Thermal conductivity in metal hydride beds. *International Journal of Hydrogen Energy*, 6, 521-528.

Suda, S., Kobayashi, N., Yoshida, K., Ishido, Y., & Ono, S., (1980). Experimental measurements of thermal conductivity. *Journal of Less Common Metals*, 74, 127-36.

Suissa, E., Jacob, I., & Hadari, Z., (1984). Experimental measurements and general conclusions on the effective thermal conductivity of powdered metal hydrides. *Journal of Less Common Metals*, 104, 287-295.

Sun, D.W., & Deng, S.J., (1990). Theoretical descriptions and experimental measurements on the effective thermal conductivity in metal hydride powder beds. *Journal of Less Common Metals*, 160, 387-395.

Sun, K., Esnaola, I., Okorie, O., Charnley, F., Moreno, M., & Tiwari, A., (2021). Data-driven modeling and monitoring of fuel cell performance. *International Journal of Hydrogen Energy*, 46, 33206-33217.

Suwarno, S., Dicky, G., Suyuthi, A., Effendi, M., Witantyo, W., Noerochim, L., & Ismail, M., (2022). Machine learning analysis of alloying element effects on hydrogen storage properties of AB_2 metal hydrides. *International Journal of Hydrogen Energy*, 47, 11938-11947.

Tange, M., Maeda, T., Nakano, A., Ito, H., Kawakami, Y., Masuda, M., et al. (2011). Experimental study of hydrogen storage with reaction heat recovery using metal hydride in a totalised hydrogen energy utilisation system. *International Journal of Hydrogen Energy*, 36, 11767-11776.

Tao, Y.B., & He, Y.L., (2015). Effects of natural convection on latent heat storage performance of salt in a horizontal concentric tube. *Applied Energy*, 143, 38-46.

Tiwari, S., & Sharma, P., (2021). Optimisation based methodology to design metal hydride reactor for thermal storage application. *Journal of Energy Storage*, 41, 102845.

Tong, L., Xiao, J., B´enard, P., & Chahine, R., (2019a). Thermal management of metal hydride hydrogen storage reservoir using phase change materials. *International Journal of Hydrogen Energy*, 44, 21055–21066.

Tong, L., Xiao, J., Yang, T., B´enard, P., & Chahine, R., (2019b). Complete and reduced models for metal hydride reactor with coiled-tube heat exchanger. *International Journal of Hydrogen Energy*, 44, 15907–15916.

Tong, L., Yuan, Y., Yang, T., Benard, P., Yuan, C., & Xiao, J., (2021). Hydrogen release from a metal hydride tank with phase change material jacket and coiled-tube heat exchanger. *International Journal of Hydrogen Energy*, 46, 32135-32148.

Urunkar, R.U., & Patil, S.D., (2021). Enhancement of heat and mass transfer characteristics of metal hydride reactor for hydrogen storage using various nanofluids. *International Journal of Hydrogen Energy*, 46, 19486-19497.

Valizadeh, M., Aghajani-Delavar, M., & Farhadi, M., (2016). Numerical simulation of heat and mass transfer during hydrogen desorption in metal hydride storage tank by Lattice Boltzmann method. *International Journal of Hydrogen Energy*, 41, 413-424.

Veerraju, C., & Gopal, M.R., (2010). Heat and mass transfer studies on plate fin-and-elliptical tube type metal hydride reactors. *Applied Thermal Engineering*, 30, 673-82.

Versteeg, H.K., & Malalasekera, W., (2007). An introduction to computational fluid dynamics: the finite volume method 2nd edn. Pearson/Prentice Hall.

Vignarooban, K., Xu, X., Arvay, A., Hsu, K., Kannan, A.M., (2015). Heat transfer fluids for concentrating solar power systems – a review, *Applied Energy*, 146, 383–396.

Vija, R., Sundaresan, R., Maiya, M.P., & Murthy, S.S., (2005). Comparative evaluation of Mg–Ni hydrogen absorbing materials prepared by mechanical alloying. *International Journal of Hydrogen Energy*, 30, 501–508.

Vijay, R., Sundaresan, R., Maiya, M.P. & Srinivasa Murthy, S. (2005). Comparative evaluation of Mg-Ni hydrogen absorbing materials prepared by mechanical alloying. *International Journal of Hydrogen Energy* 30, 501–508.

Visaria, M., & Mudawar, I., (2012a). Coiled-tube heat exchanger for high pressure Metal Hydride hydrogen storage systemse Part 1. Experimental study. *International Journal of Heat and Mass Transfer*, 55, 1782-1795.

Visaria, M., & Mudawar, I., (2012b). Coiled-tube heat exchanger for high pressure metal hydride hydrogen storage systemse Part 2. Computational model. *International Journal of Heat and Mass Transfer*, 55, 1796-1806.

Visaria, M., & Mudawar, I., (2012c). Experimental investigation and theoretical modeling of dehydriding process in highpressure metal hydride hydrogen storage systems. *International Journal of Hydrogen Energy*, 37, 5735-5749.

Vo, N.D., Kang, J.H., Oh, D.H., Jung, M.Y., Chung, K., & Lee, C.H., (2021). Sensitivity analysis and artificial neural network-based optimization for low-carbon H2 production via a sorption enhanced steam methane reforming (SESMR) process integrated with separation process. *International Journal of Hydrogen Energy*, 47, 820-847.

Wang, C.S., & Brinjerhoff, J. (2021a). Is there a general time scale for hydrogen storage with metal hydrides or activated carbon?. *International Journal of Hydrogen Energy*, 46, 12031-12034.

Wang, C.S., & Brinjerhoff, J. (2021b). Predicting hydrogen adsorption and desorption rates in cylindrical metal hydride beds: Empirical correlations and machine learning. International Journal of Hydrogen Energy, 46, 24256-23270.

Wang, D., Li, S., Huang, Z., Liu, Z., Wang, Y., Yang, F., Wu, Z., Zhang, Z., Wu, J., Shi, L., & Yuan, J., (2020). Design optimisation, sensitivity analysis and operational comparison of a duplex helical elliptical tube metal hydride reactor. *Sustain Energy & Fuels*, 4, 5851-5868.

Wang, D., Wang, Y., Huang, Z., Yang, F., Wu, Z., & Zheng, L., (2019). Design optimisation and sensitivity analysis of the radiation minichannel metal hydride reactor. *Energy*, 173, 443-456.

Wang, D., Wang, Y., Wang, F., Zheng, S., Guan, S., Zheng, L., Wu, L., Fang, T., Yang, X., & Lv, M., (2021). Hydrogen storage in branch mini-channel metal hydride reactor: optimisation design, sensitivity analysis and quadratic regression. *International Journal of Hydrogen Energy*, 46, 25189-25207.

Wang, H., Prasad, A.K., & Advani, S.G., (2012). Hydrogen storage system based on hydride materials incorporating a helical-coil heat exchanger. *International Journal of Hydrogen Energy*, 37, 14292-14299.

Wang, Y., Adroher, X.C., Chen, J., Yang, X.G., & Miller, T., (2009). Three dimensional modeling of hydrogen sorption in metal hydride hydrogen storage beds. *Journal of Power Sources*, 194, 997-1006.

Ward, P.A., Corgnale, C., Teprovich, J.A., Motyka, T., Hardy, B., Sheppard, D., Buckley, C. & Zidan, R. (2016). Technical challenges and future direction for high-efficiency metal hydride thermal energy storage systems. *Applied Physics A,* 122, 462.

Weiss-Ungethum, J., Burger, I., Schmidt, N., Linder, M., & Kallo, J., (2014). Experimental investigation of a liquid cooled high temperature proton exchange membrane (HT-PEM) fuel cell coupled to a sodium alanate tank. *International Journal of Hydrogen Energy*, 39, 5931-5941.

Witman, M., Ling, S., Grant, D.M., Walker, G.S., Agarwal, S., Stavila, V., et al., (2020). Extracting an empirical intermetallic hydride design principle from limited data via interpretable machine learning. *Journal of Physical Chemistry Letters*, 11, 40-47.

Wu, Z., Yang, F., Zhang, Z., & Bao, Z., (2014). Magnesium based metal hydride reactor incorporating helical coil heat exchanger: simulation study and optimal design. *Applied Energy*, 130, 712-722.

Wu, Z., Yang, F., Zhu, L., Feng, P., Zhang, Z., & Wang, Y., (2016). Improvement in hydrogen desorption performances of magnesium based metal hydride reactor by incorporating helical coil heat exchanger. *International Journal of Hydrogen Energy*, 41, 16108–16121.

Yang, W., Ye, Y., Cheng, H., Liu, J., Yan, K., & Miao, H. (2025). Performance optimization of a U-tube heat exchanger type hydrogen storage reactor with a novel fin structure. *International Journal of Hydrogen Energy*, 82, 272-280.

Yang, F.S., Wang, G.X., Zhang, Z.X., & Rudolph, V., (2010) Investigation on the influences of heat transfer enhancement measures in a thermally driven metal hydride heat pump. *International Journal of Hydrogen Energy*, 35, 9725-9735.

Yang, F.S., Zhang, Z.W., & Bao, Z.W., (2012). An extensive parametric analysis on the performance of a single-state metal hydride heat transformer. *International Journal of Hydrogen Energy*, 37, 2623-2634.

Yang, S.M., & Tao, W.Q., (1998). *Heat transfer theory* (3rd ed.) Beijing: Chinese Higher Education Press.

Yao, J., Zhu, P., Guo, L., Duan, L., Zhang, Z., Kurko, S., & Wu, Z., (2020a). A continuous hydrogen absorption/desorption model for metal hydride reactor coupled with PCM as heat management and its application in the fuel cell power system. *International Journal of Hydrogen Energy*, 45, 28087-28099.

Yao, J., Zhu, P., Qian, C., Hamidullah, U., Kurko, S., Yang, F., Zhang, Z., & Wu, Z., (2020b). Study of an autothermal-equilibrium metal hydride reactor by reaction heat recovery as hydrogen source for the application of fuel cell power system. *Energy Conversion and Management*, 213, 112864.

Yao, S., & Huang, X. (2021). Study on solidification performance of PCM by longitudinal triangular fins in a triplex-tube thermal energy storage system. *Energy*, 227, 102527.

Ye, Y., Ding, J., Wang, W., & Yan, J., (2021a). The storage performance of metal hydride storage tanks with reaction heat recovery by phase change materials. *Applied Energy*, 299, 117255.

Ye, Y., Lu, J., Ding, J., Wang, W., & Yan, J., (2020). Numerical simulation on the storage performance of a phase change materials based metal hydride hydrogen storage tank. *Applied Energy*, 278, 115682.

Ye, Y., Lu, J., Ding, J., Wang, W., & Yan, J., (2022). Performance improvement of metal hydride storage tanks by using phase change materials. *Applied Energy*, 320, 119290.

Ye, Y., Yue, Y., Lu, J., Ding, J., Wang, W., & Yan, J., (2021b). Enhanced hydrogen storage of a $LaNi_5$ based reactor by using phase change materials. *Renewable Energy*, 180, 734-743.

Yehui, C., Xiangguo, Z., Junfeng, X., & Huaqin, K., (2022). The comprehensive review for development of heat exchanger configuration design in metal hydride bed. *International Journal of Hydrogen Energy*, 47, 2461-2490.

Yiotis, A.G., Kainourgiakis, M.E., Charalambopoulou, G.C., Stubos, A.K., (2015). A generic physical model for a thermally integrated high-temperature PEM fuel cell and sodium alanate tank system. *International Journal of Hydrogen Energy*, 40, 14551-14561.

Yoo, H., Kim, W., & Ju, H., (2014). A numerical comparison of hydrogen absorption behaviors of uranium and zirconium cobaltbased metal hydride beds. *Solid State Ionics*, 262, 241-247.

Yu, X., Shen, Y., Guan, Z., Zhang, D., Tang, Z., & Li, W., (2021). Multi-objective optimization of ANN-based PSA model for hydrogen purification from steam-methane reforming gas. *International Journal of Hydrogen Energy*, 46, 11740-11755.

Yue, M., Lambert, H., Pahon, E., Roche, R., Jemei, S., & Hissel, D., (2021). Hydrogen energy system: A critical review of technologies, applications, trends and challenges. *Renewable and Sustainable Energy Reviews*, 146, 111180.

Zaluski, L., Zaluska, A., & Strom-Olsen, J.O., (1995). Hydrogen absorption in nanocrystalline Mg_2Ni formed by mechanical alloying. *Journal of Alloys Compounds*, 217, 245-249.

Zhang, S., Mancin, S., & Pu, L. (2023). A review and prospective of fin design to improve heat transfer performance of latent thermal energy storage. *Journal of Energy Storage*, 62, 106825.

Zhang, Y., & Faghri, A., (1996). Heat transfer enhancement in latent heat thermal energy storage system by using the internally finned tube. *International Journal of Heat and Mass Transfer*, 39, 3165–73.

Zhang, Z., & Liu, H., (2022). Research on the thermal performance of a helical coil heat exchanger. *In Proceedings of the International Conference of Fluid Power and Mechatronic Control Engineering.,* Atlantis Highlights in Engineering.

Zhao, W., Yang, Y., Bao, Z., Dong, Y., & Zhu, Z., (2020). Methods for measuring the effective thermal conductivity of metal hydride beds: a review. *International Journal of Hydrogen Energy*, 45, 6680-6700.

Zheng, S., Wang, Y., Wang, D., Guan, S., Liu, Y., Wang, F., Zheng, L., Wu, L., Gao, X., & Zhang, Z. (2023). Design and performance study on the primary & secondary helical-tube reactor. *Energy*, 263, 125840.

Appendices

A1: Supplementary Info for Chapter 4

A1.1 Metal hydride reactor with helical coil heat exchanger and semi-cylindrical coil heat exchanger

Figure A1.1 presents a schematic diagram of MH reactors with a helical tube (Figure A1.1a) and two semi-cylindrical tubes (Figure A1.1b). From this supplementary figure., air as the HTF is injected from

the bottom part into the porous MH reactor through a helical tube/two semi-cylindrical tubes, while hydrogen is injected from the upper surface of the reactor.

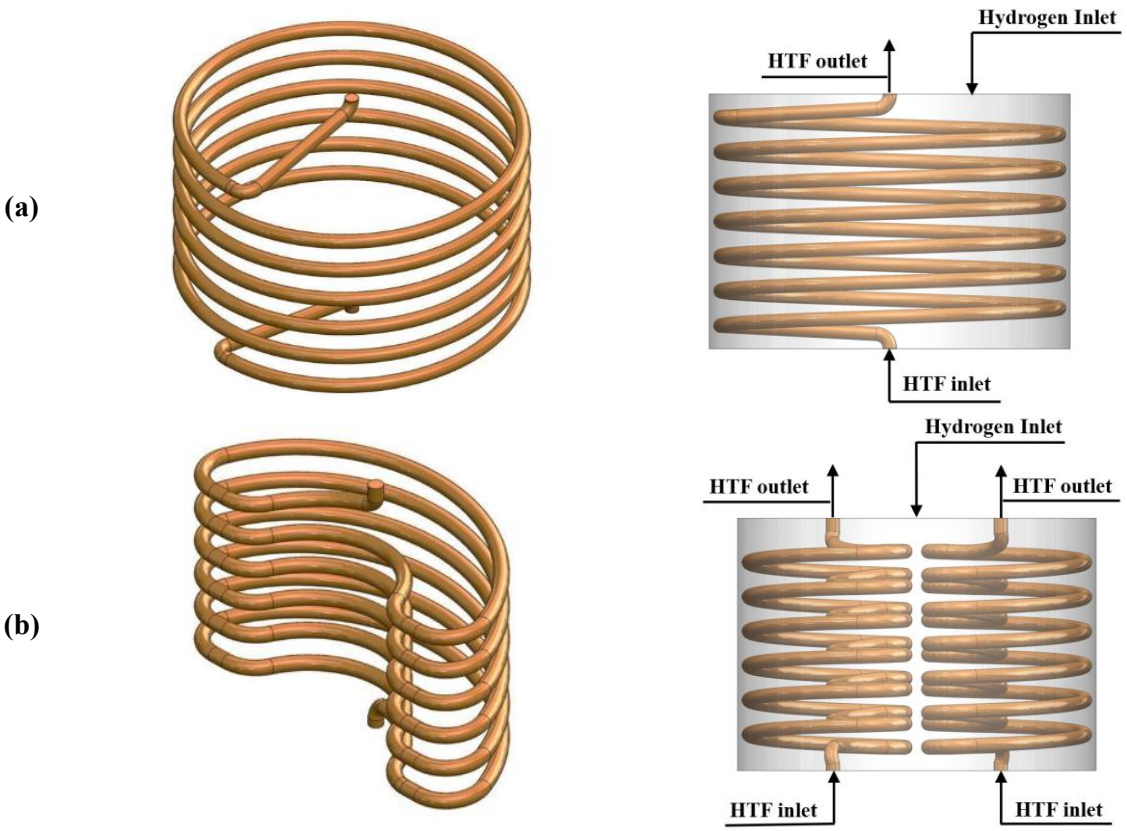

Figure A1.1 Schematic diagram of MH reactors and characteristics of selected geometries for MH reactors. (a) With helical coil tub heat exchanger, and (b) With semi-cylindrical tube heat exchanger

A1.2 Mathematical Model

- *Grid independency*

The average bed temperature for the hydrogen absorption process for various mesh sizes are presented in Figure 1.2a, b for case 1 and case 4, respectively. The average bed temperature of the absorption process after the element numbers 428891 (Figure 1.2a for case 1) and 430599 (Figure A1.2b for case 4) do not vary. Hence, these grid sizes are selected for further computational calculations. Figure A1.3 presents the successively refined grids for case 1 and case 4.

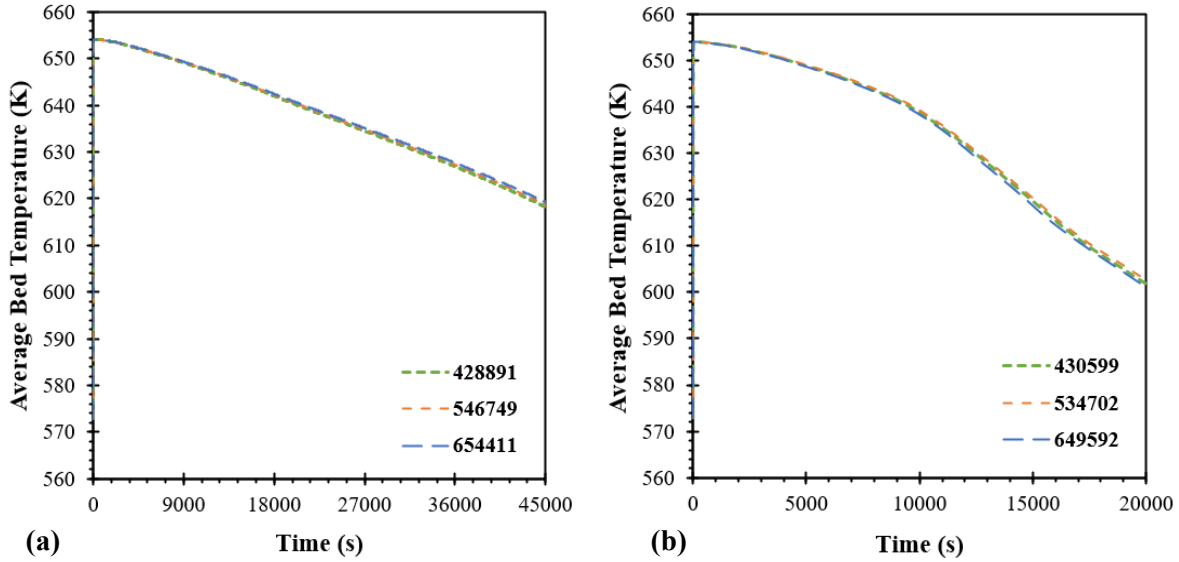

Figure A1.2 Average bed temperature for the hydrogen absorption process in the MH reactor under various grid numbers. (a) average bed temperature for case 1, and (b) average bed temperature for case 4

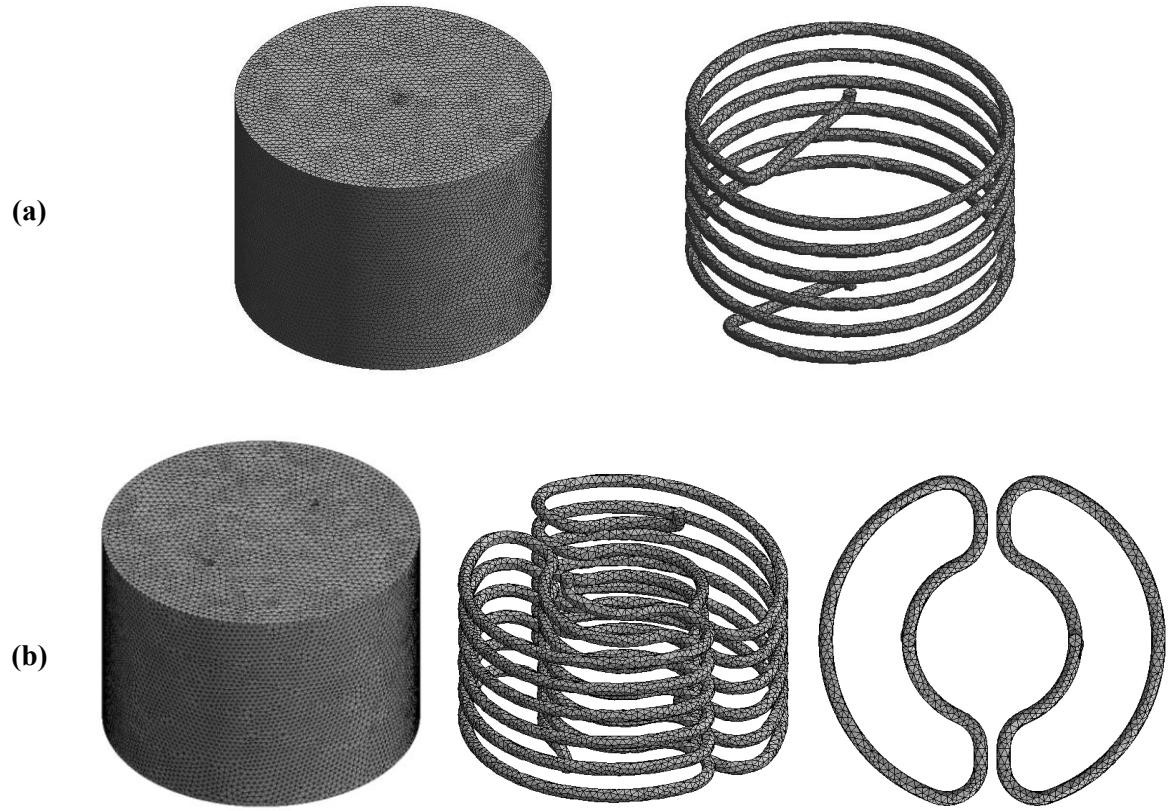

Figure A1.3 Computational meshing of MH reactor and HTF tube. (a) case 1, and (b) case 4

A1.3 Results and discussion

- *Effect of helical coil pitch*

Figure A1.4 shows the temperature contours at three selected locations of the MH bed for 500 s, 25000 s, and 45000 s. From this figure, the lower bed temperature was found at the bottom plane for all cases where it is near the HTF inlet. Nearly the HTF wall, the temperature significantly reduces while higher temperature locates at the center where it has no contact area with the HTF. For comparison, reducing pitch values results in greater heat transfer improvement, especially for case 3. Figure A1.5 demonstrates the hydrogen concentration at selected times for three pitch sizes. At 500 s, from Figure A1.5, it can be seen that the hydrogen begins to get absorbed at the bottom part where it is around the HTF inlet. Similarly, higher hydrogen concentration was found around the HTF area at 25000 s and 45000 s. This is because of the conductive heat transfer mechanism between the HTF and MH reactor. Therefore, the center area of the reactor has less hydrogen concentration due to having less conductive heat transfer from the HTF.

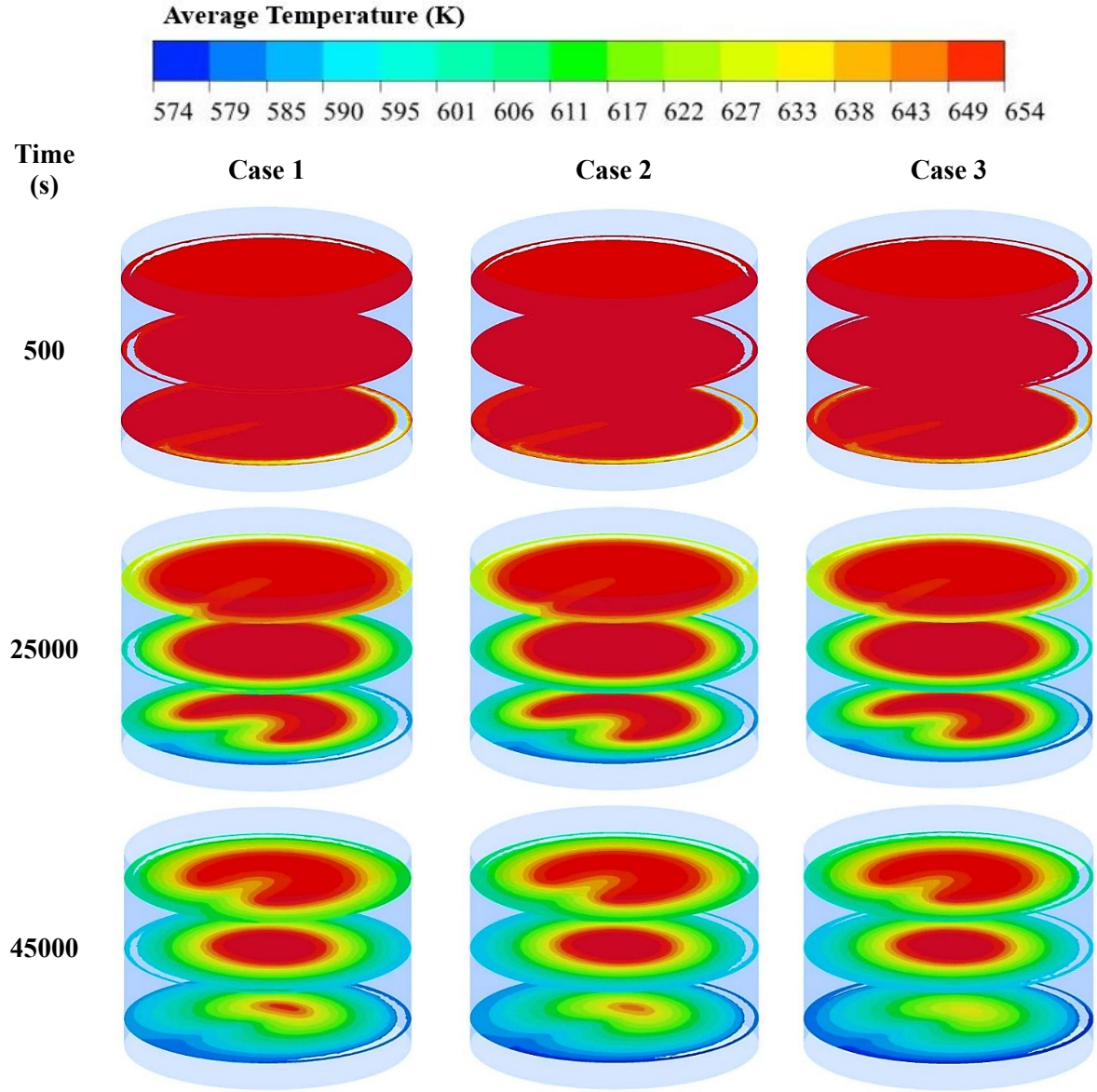

Figure A1.4 Distribution of bed temperature at 500 s, 25000 s, and 45000 s after the start of the hydrogen absorption process in the MH reactor

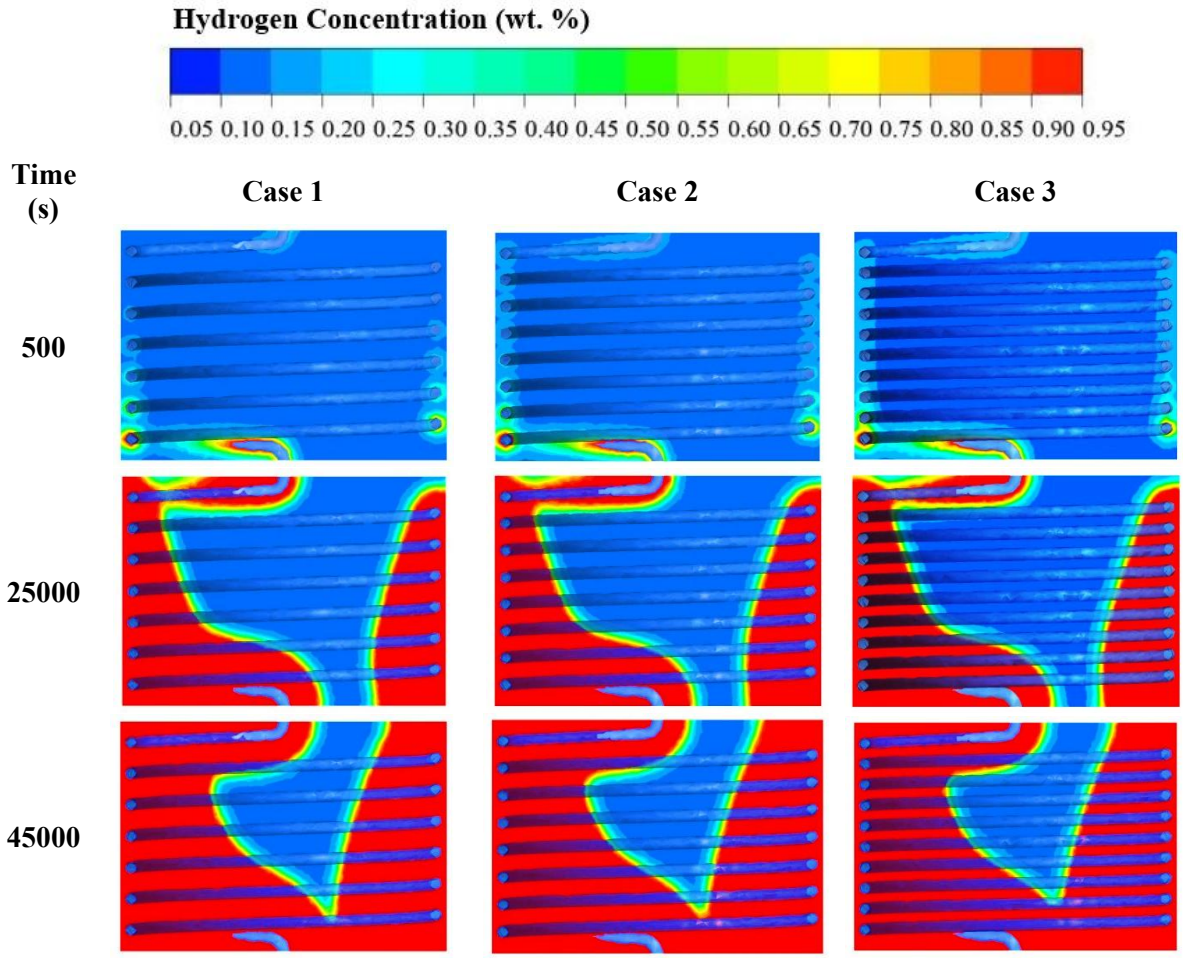

Figure A1.5 Hydrogen concentration in the MH bed after 500 s, 25000 s, and 45000 s of the hydrogen absorption process in the MH reactor for different helical coil pitches

- *Effect of semi-cylindrical coil pitch*

Figure A1.6 and Figure A1.7 demonstrate the average bed temperature and hydrogen concentration, respectively. The selected times as 500 s, 9000 s, and 18000 s for both bed temperature and concentration are provided for all three cases. From these two figures, a lower bed temperature and higher hydrogen concentration were found at the bottom section for all cases due to better conductive heat transfer. A higher temperature is also located at the center of MH reactor and the top, close to hydrogen injection. This results in lower hydrogen absorption in these areas. Similar to HCHE, higher hydrogen concentration was observed around the HTF area especially at the bottom reactor, where it has an HTF inlet.

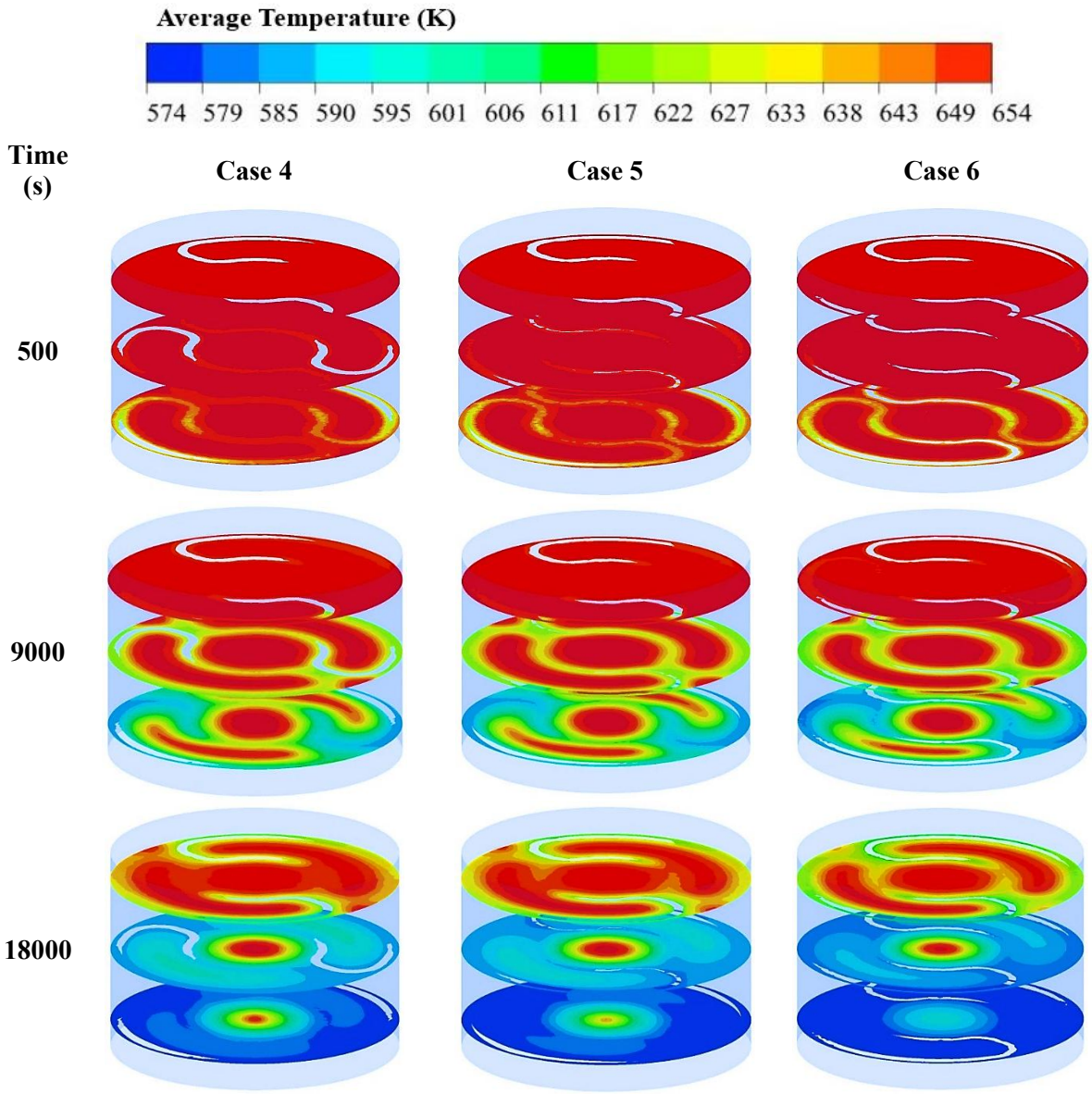

Figure A1.6 Distribution of bed temperature at 500 s, 9000 s, and 18000 s after the start of the hydrogen absorption process in the MH reactor

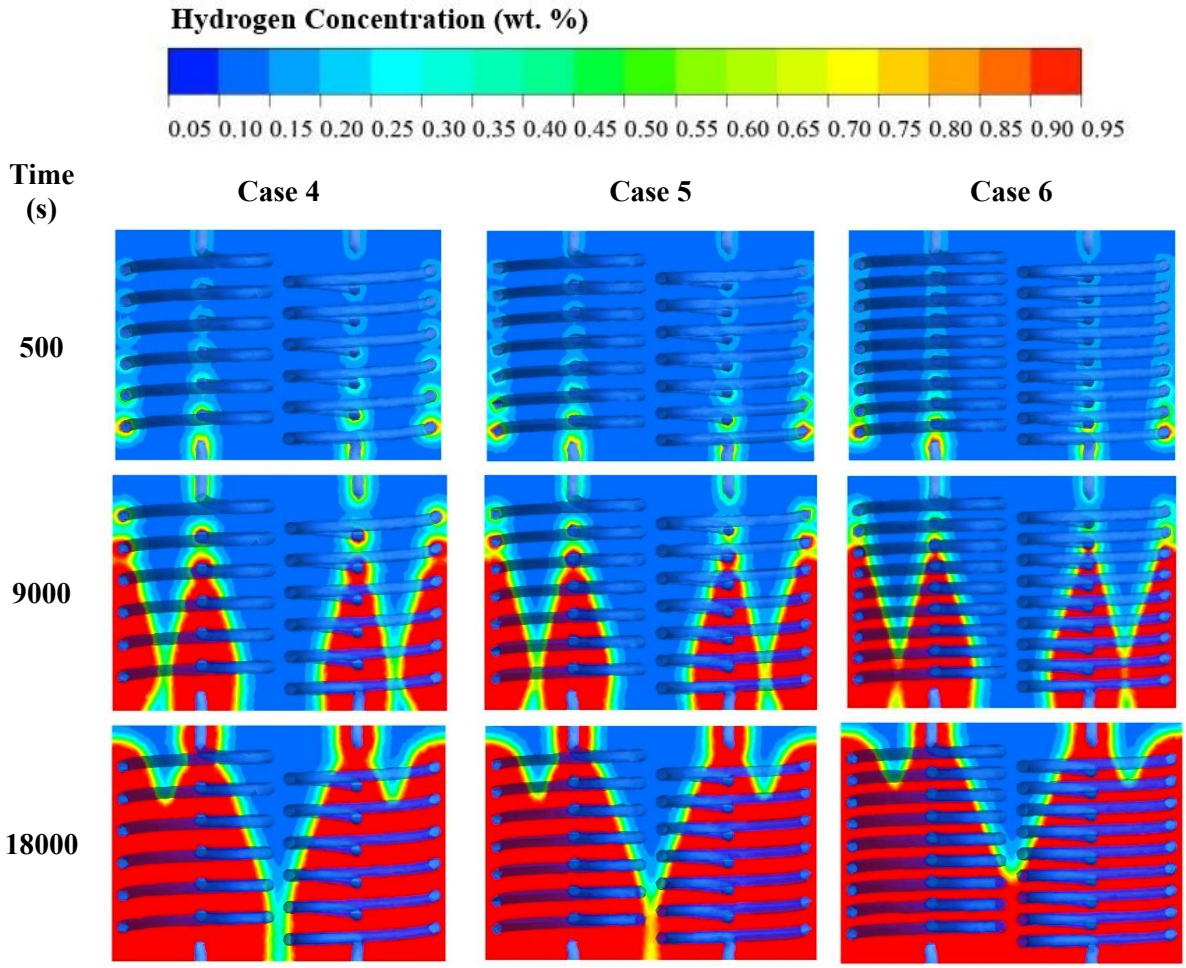

Figure A1.7 Hydrogen concentration in the MH bed after 500 s, 9000 s, and 18000 s of the hydrogen absorption process in the MH reactor for different semi-cylindrical pitches

- *Performance comparisons between the MH reactors with helical coil heat exchanger and semi-cylindrical coil heat exchanger*

The comparison of the average temperature of the MH bed and the HTF tube between case 3 and case 4 is presented in Figure A1.8 in order to provide a better understanding of the relationship between the HTF and the MH bed in a systematic way. Various selected times after the start of the absorption process are included. For the HTF tube, the air as a cooling fluid is injected from the bottom and then flows towards the tube to the outlet at the top of the MH reactor. At the beginning, the average HTF around the upper part is higher than the lower part due to exposure to the reaction heat generated during the hydrogen absorption process from the top surface of the MH reactor. This results in higher average bed temperature of the MH reactor. Regarding the exothermic behavior of hydrogen absorption, the initial temperature of the reactor rapidly increases and is significantly higher than the HTF temperature. This will generate a high heat transfer rate between the HTF and MH bed. The average HTF temperature then continually decreases, which is related to absorption times. Therefore, conductive heat transfers between the MH bed and the HTF is occurring. A larger difference in temperature rates between the MH reactor and the HTF causes a higher heat transfer rate. At 10000 s and 20000 s, the bed temperature at the bottom and middle sections are reduced and close to the HTF average temperature. However, this is only for case 4. The average bed temperature inside the MH reactor with HCHE from case 3 is still high, even the bottom part of the reactor. The bed temperature difference between center and outer areas from case 3 is significantly higher than case 4. The existence of temperature gradients between these areas negatively affects mass transfer mechanisms and the overall MH reactor performance.

Furthermore, the difference in heat transfer performance between these two configurations is mainly because of having less space between the HTF and the MH bed for SCHE that, leads to having more uniform temperature distribution as well as lower thermal resistance inside the reactor.

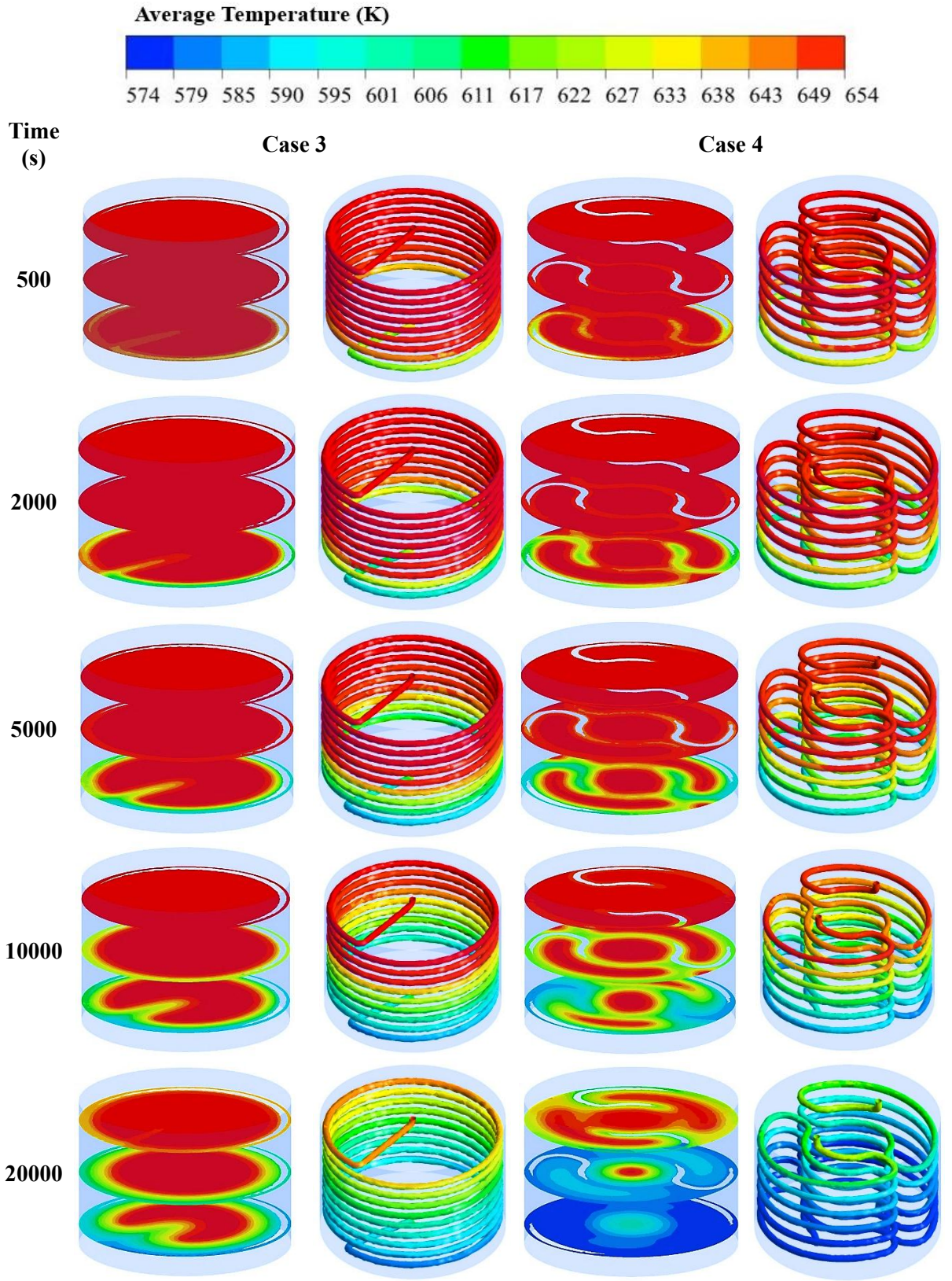

Figure A1.8 Average temperature of MH bed and HTF tube at 500 s, 2000 s, 5000 s, 10000 s, and 20000 s after the start of the hydrogen absorption process in the MH reactor for case 3 and case 4

A1.4 Sensitivity analysis of operating conditions

- *Effect of the loading pressure on the hydrogen absorption process*

Figure A1.9 illustrates the hydrogen concentration at 15500 s for all loading pressures. It can be seen that there is a significantly different concentration between 1.2 MPa and 3.0 MPa.

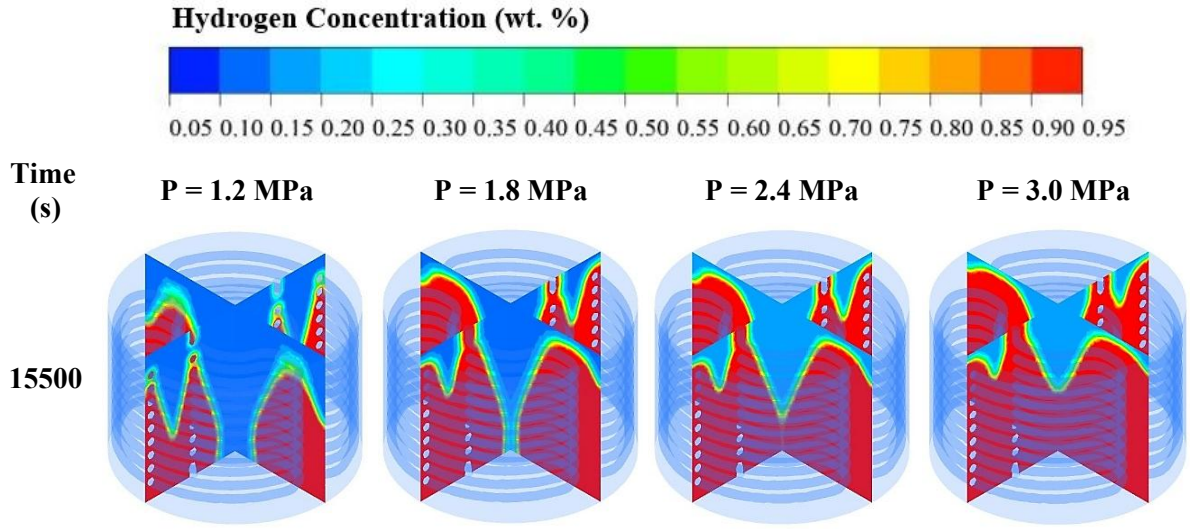

Figure A1.9 Hydrogen concentration at 15500 s after start of the hydrogen absorption process for various loading pressures

- *Effect of the initial temperature on the hydrogen absorption process*

Figure A1.10 illustrates the hydrogen concentration contours at 15500 s. It can be seen that the decreasing an initial temperature of MH bed also influences hydrogen concentration.

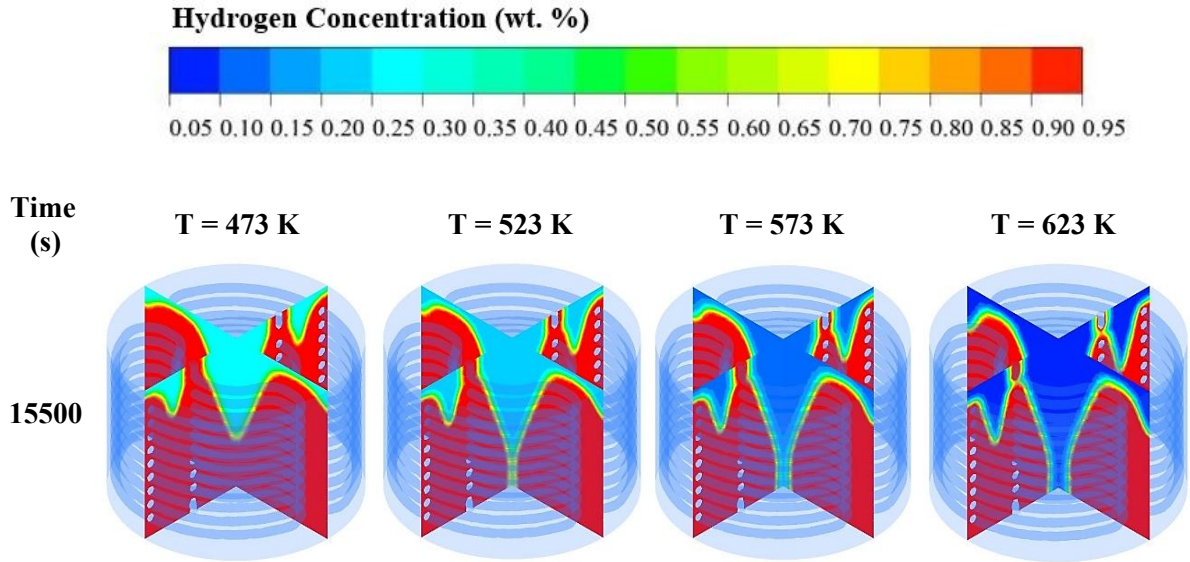

Figure A1.10 Hydrogen concentration at 15500 s after start of the hydrogen absorption process for various initial bed temperature

- *Effect of the Reynolds Number of the heat transfer fluid on the hydrogen absorption process*

Figure A1.11 presents the hydrogen concentration at 12500 s for all Reynolds numbers. Similar to other operating parameters, increasing the Reynolds number results in faster hydrogen absorption, especially for the case of Reynolds number as 22000 compared to 10000.

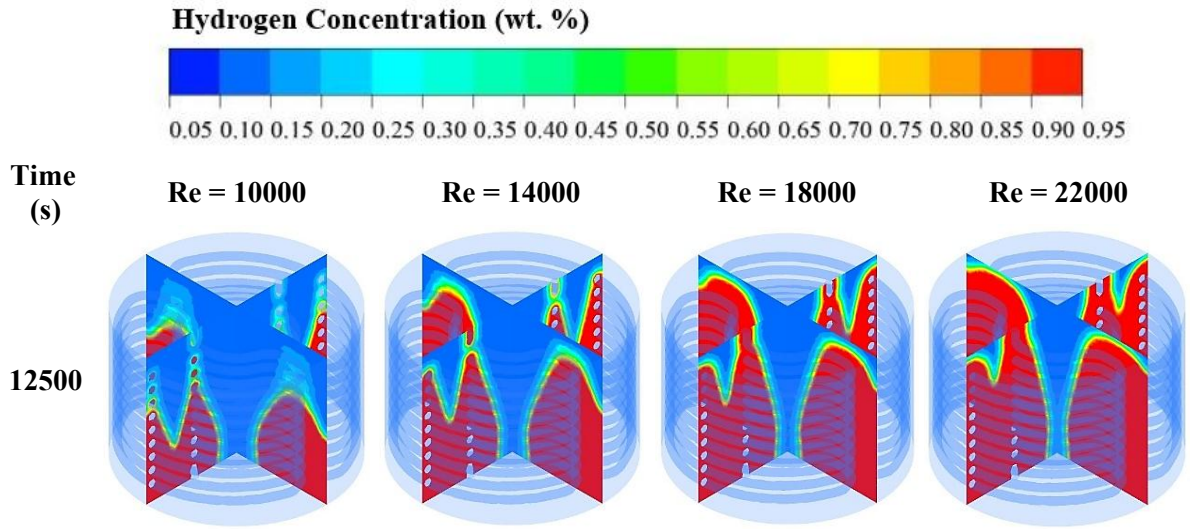

Figure A1.11 Hydrogen concentration at 12500 s after start of the hydrogen absorption process for various Reynolds numbers of heat transfer fluid

Effect of the initial temperature of the heat transfer fluid on the hydrogen absorption process

Figure A1.12 illustrates the hydrogen concentration at 7000 s for all inlet HTF temperatures. It can be seen that over 90% of hydrogen is stored in the reactor with the inlet temperature at 373 K, whereas there is around 50% hydrogen stored in the reactor from 573 K inlet temperature.

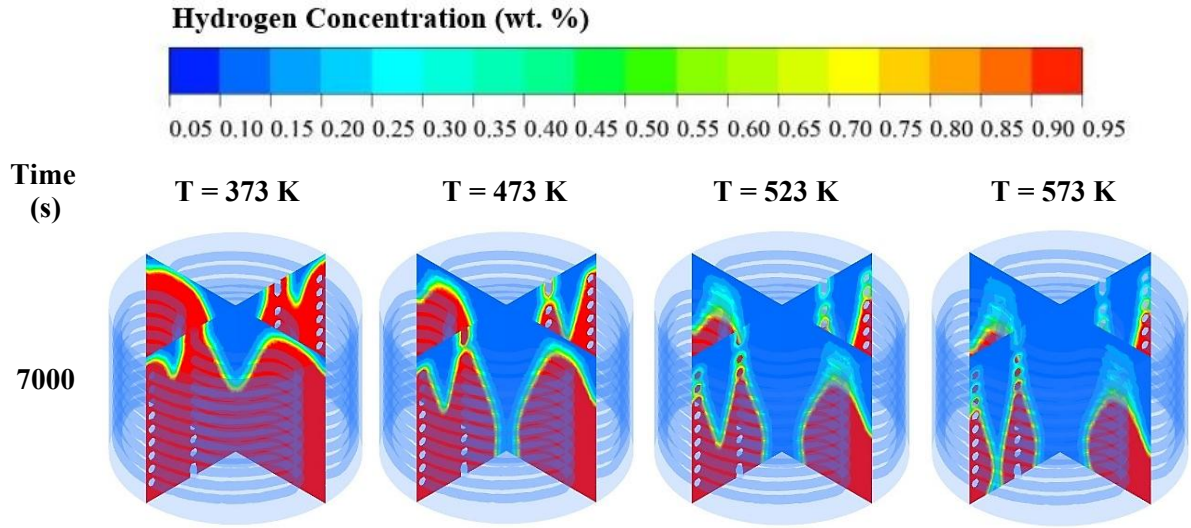

Figure A1.12 Hydrogen concentration at 7000 s after start of the hydrogen absorption process for various inlet temperatures of heat transfer fluid

A2: Supplementary Info for Chapter 6

A2.1 Mathematical Model

- Grid independency

Figure A2.1 presents the successively refined grids for case 1 and case 3. Figure A2.1a is for case 1, while Figure A2.1b is for case 3. These include the successively refine grids for PCM jacket, MH bed, and two SCHE-CR.

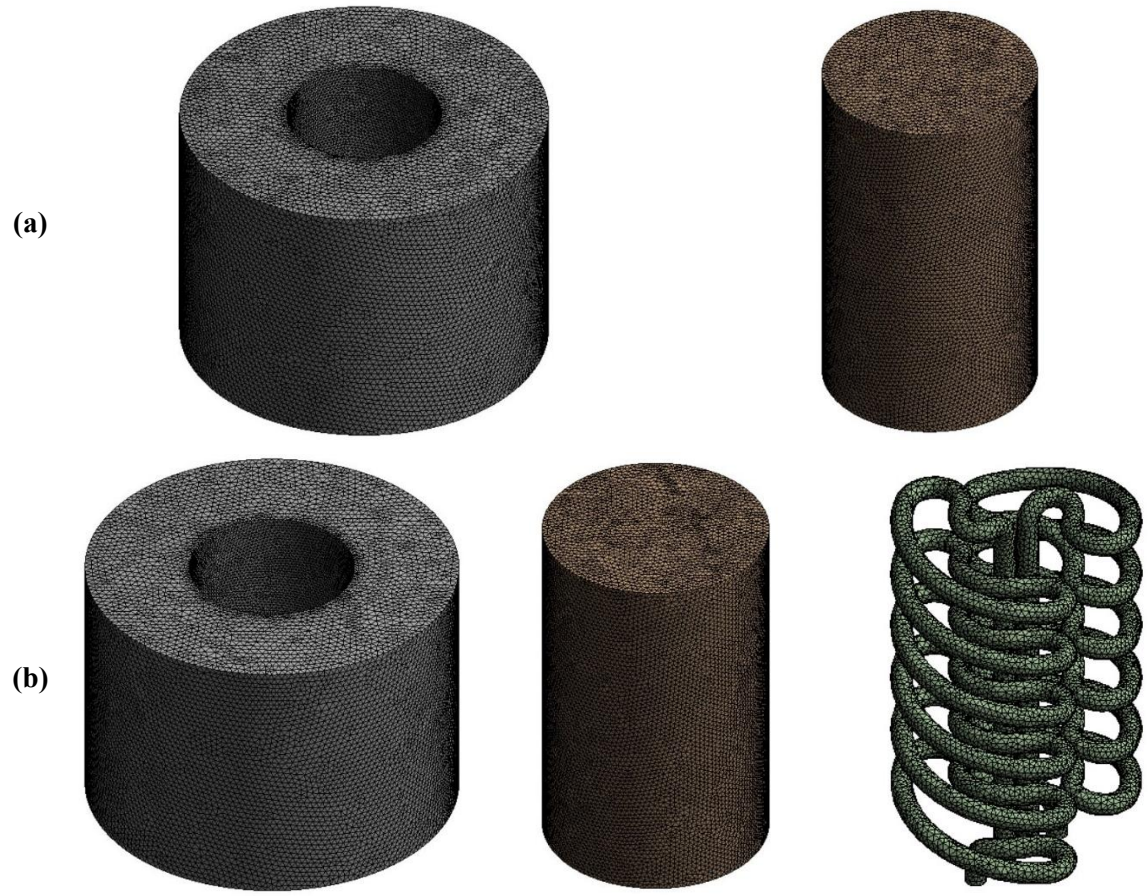

Figure A2.1 Computational meshing of MH storage and HTF tube. (a) case 1, and (b) case 3

A2.2 Result and discussion

- Temperature contours of metal hydride bed and phase change materials during the absorption process

Figure A2.2 shows the temperature contours of the MH bed and PCM for 250 s, 500 s, 10000 s, 1500 s, and 2000 s after starts the hydrogen absorption process. At 250 s, the MH temperature near the interface between the MH and PCM is lower than in other areas due to the PCM effects. The PCM near the interface starts to absorb the generated heat, resulting in the reduction of the MH bed temperature near the interface. This is applied at the surface of the interface in all cases. More heat transfers are found from the case with PCM pool bed (case 2) and PCM capsule (case 4), which have the PCM at the bottom, and both bottom top parts of the MH bed. The lower MH bed temperature is found around the wall of the HTF tube, where it has cooling fluid circulating inside. The greater MH temperature reduction corresponds to the greater hydrogen absorption duration (from 250 s to 1500 s). At 2000 s, the MH bed temperature is greatly lower at the side where is close to the PCM, while the PCM temperature is higher. This phenomenon occurs in case 1 and case 2. The MH bed temperature around the central area still remains the same as the initial value (654 K). However, the MH bed temperature

from case 3 and case 4 is significantly lower due to the SCHE-CR's effect. The MH bed temperature at the bottom part reduces to 589 K in these two cases. There are still some areas at the top part of case 3 that still has 654 K. The MH temperature at the top part from case 4 is less than 643 K. This is because the PCM capsule absorbs the heat from the top part. Furthermore, the MH bed temperature from the case with PCM capsule (case 4) is also lower at the top and bottom parts compared to the case with PCM jacket (case 3). Considering the PCM temperature at the middle part of MHHS from case 3 and case 4, the temperature variation around this area is less than in other areas because the MH temperature at this area is lower than in other areas. The MH bed around this area is close to the HTF inlet. The MH bed around this area is cooled down faster than in other areas. Therefore, there is less temperature difference around this area, resulting in having a less heat transfer rate.

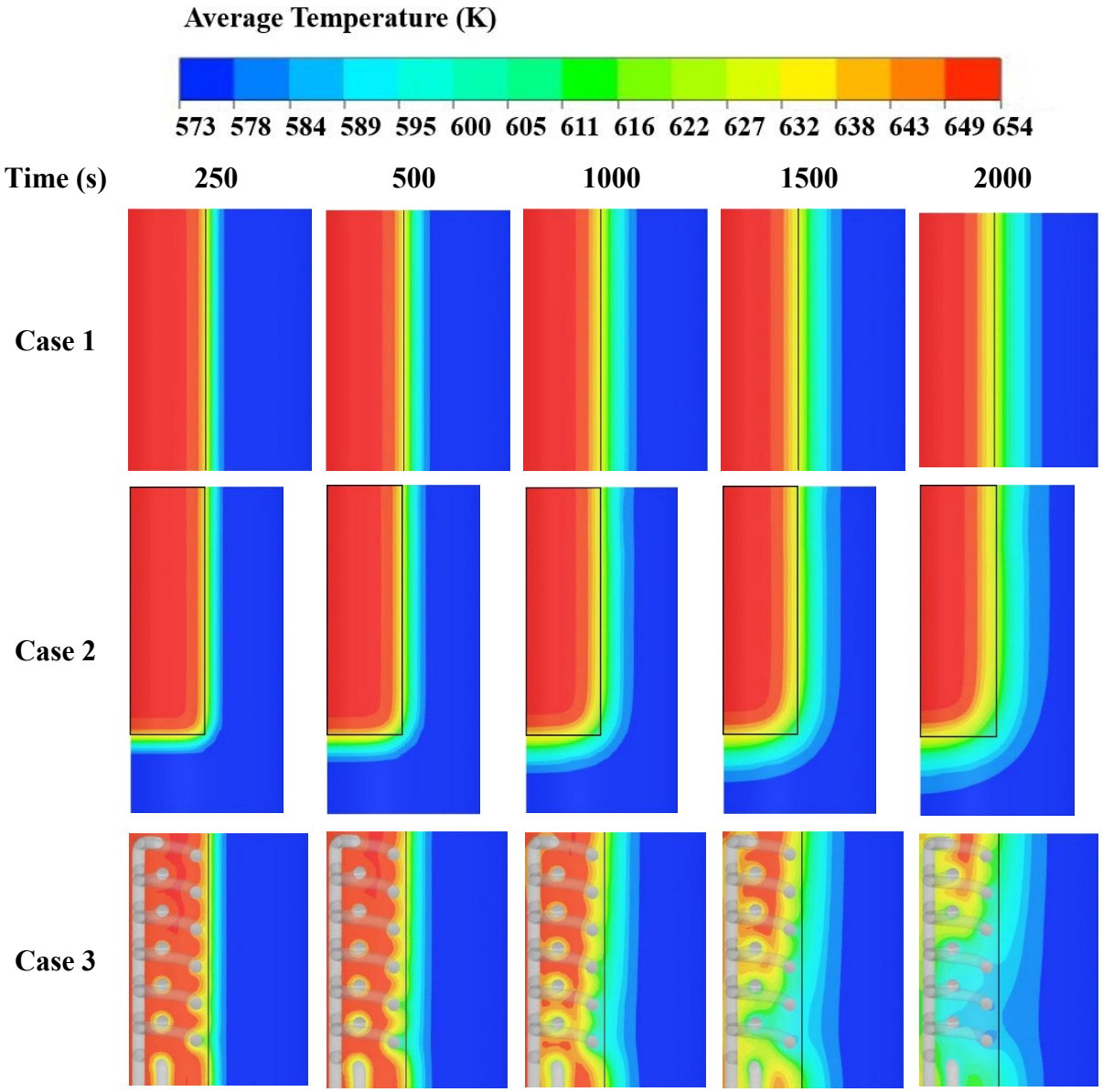

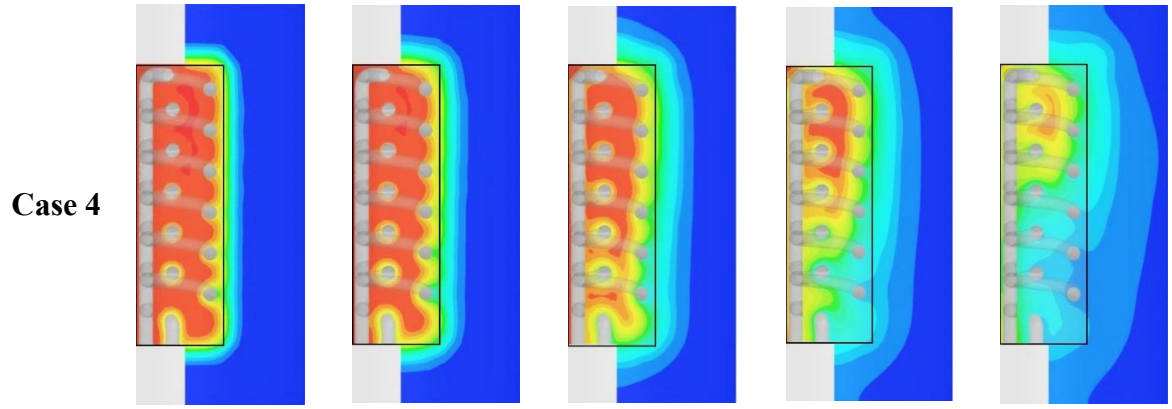

Figure A2.2 Average temperature of MH bed and PCM at 250 s, 500 s, 1000 s, 1500 s, and 2000 s after starting hydrogen absorption process from case 1 to case 4

- *Liquid fraction contours of phase change materials during the absorption process*

Figure A2.3 presents the liquid fraction contours of the PCM at 250 s, 500 s, 10000 s, 1500 s, and 2000 s after starts the hydrogen absorption process. At 250 s, the PCM solidus starts to transform to a liquid phase at the interface where it has a high MH temperature. More PCM liquidus is observed from all cases after 250 s until the time at 2500 s. At 2000s, the liquid fraction from all cases still remains the same patterns from the time at 250 s.

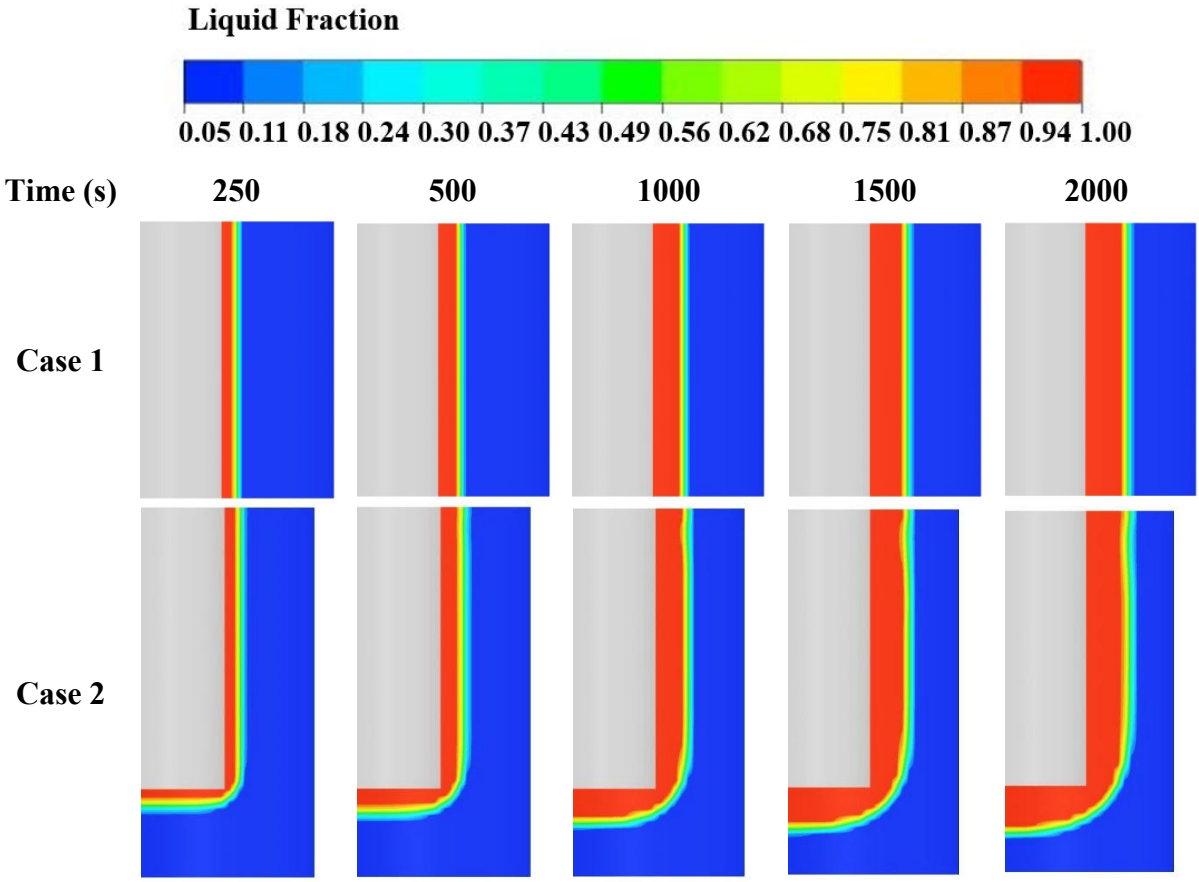

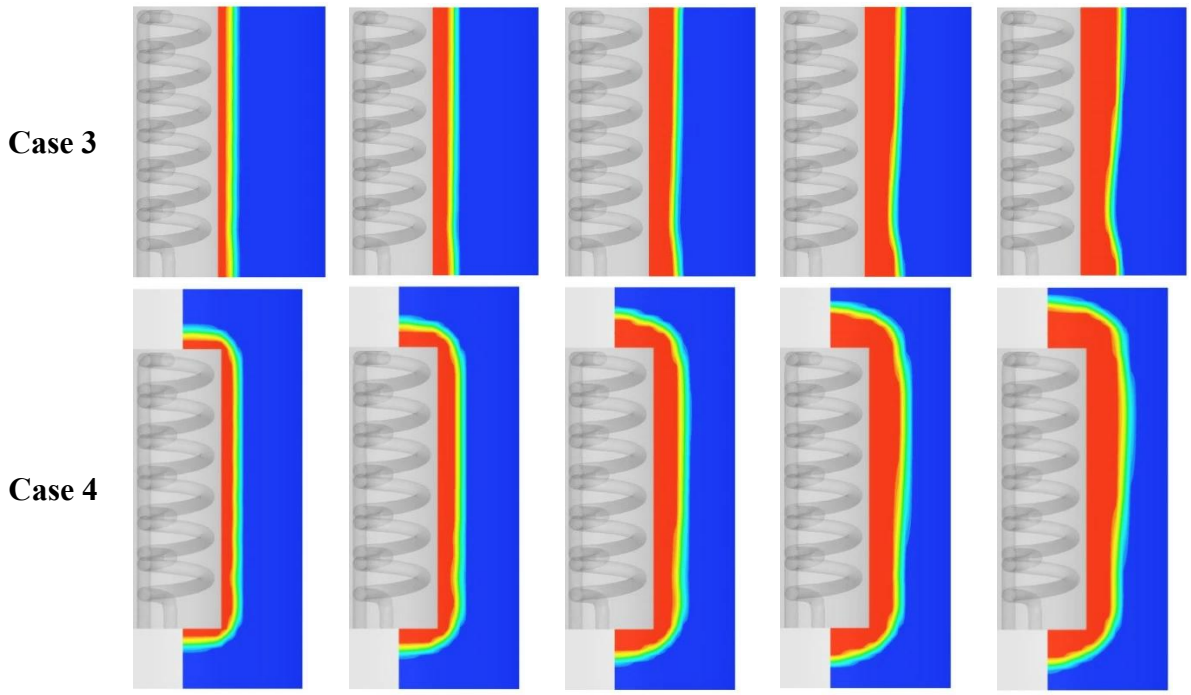

Figure A2.3 Liquid fraction of PCM at 250 s, 500 s, 1000 s, 1500 s, and 2000 s after starting hydrogen absorption process from case 1 to case 4

- *Hydrogen concentration contours of metal hydride bed during the absorption process*

Figure A2.4 provides the hydrogen concentration contours of the MH bed for 250 s, 500 s, 10000 s, 1500 s, and 2000 s after starts the hydrogen absorption process. At 250 s to 500 s, the hydrogen concentration from most parts of MHHS for case 1 and case 2 is still 11%. A similar concentration is also found from case 1 at 1000 s to 1500 s. However, case 2 has a higher hydrogen concentration (18-24%) at the bottom part from the time at 1000 s to 1500 s. For case 3 and case 4, there are still some areas that have the hydrogen concentration at 11% at 250 s as these areas are far away from the HTF tube. At 500, more variation of hydrogen concentration is found in these two cases (case 3 and 4). The hydrogen concentration from most parts of these two cases is 56% at 1000 s. The more hydrogen concentration at 100% is found in these cases at 1500 s. At 2000 s, a higher hydrogen concentration is found near the interface from case 1 and case 2. Furthermore, the bottom part of case 2 (PCM pool bed) also has a higher hydrogen concentration compared to case 1 (PCM jacket). However, the hydrogen concentration is significantly higher in case 3 and case 4 due to the SCHE-CR's effect. The PCM capsule (case 4) obtains better performance than the PCM jacket (case 3). There are more hydrogen concentrations at the top and bottom parts of the MH bed. The hydrogen concentration from most parts of case 1 and case 2 is still 11%, while the hydrogen concentration from most parts of case 3 and case 4 is 100%.

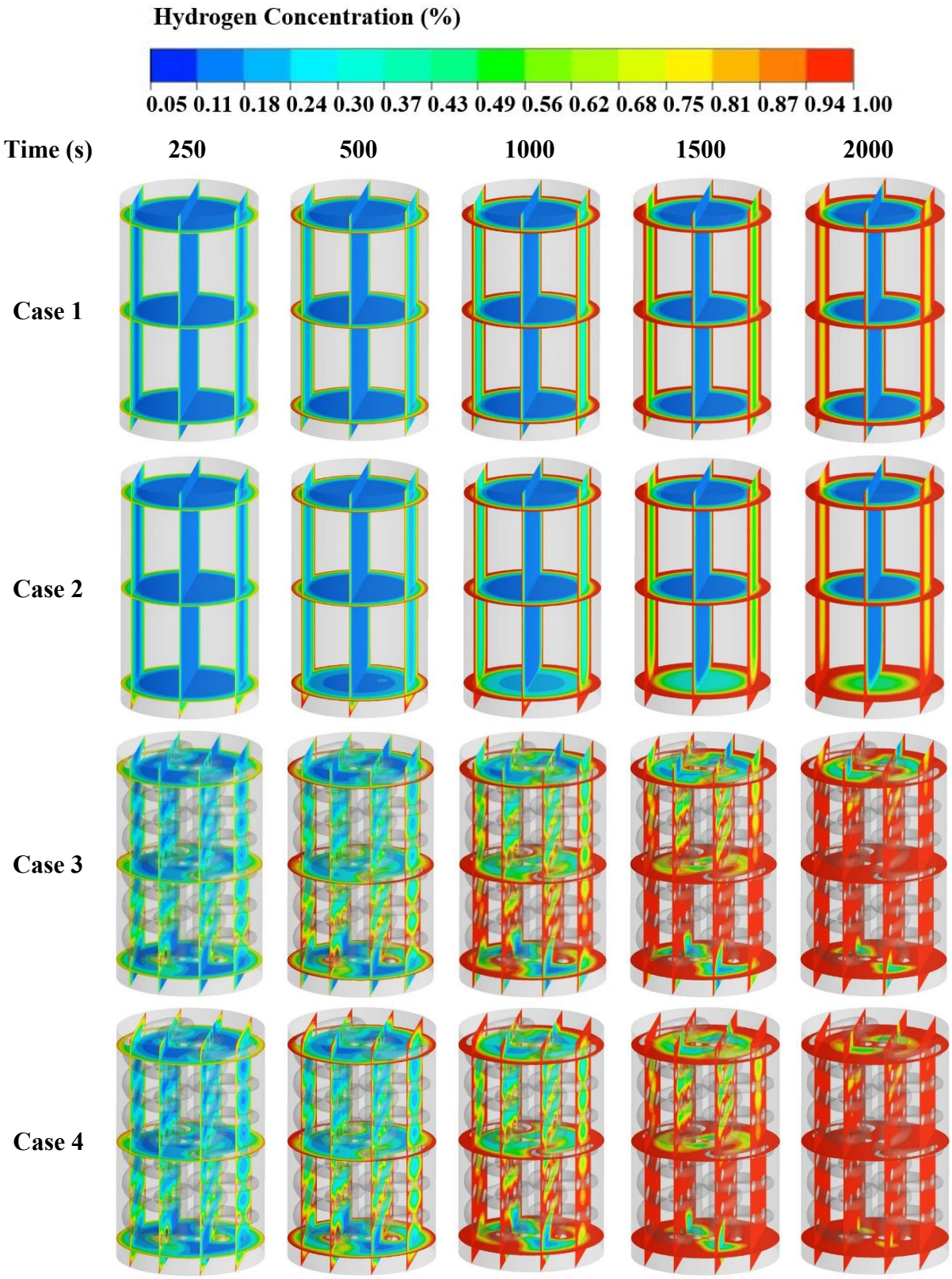

Figure A2.4 Hydrogen concentration at 250 s, 500 s, 1000 s, 1500 s, and 2000 s after starting hydrogen absorption process from case 1 to case 4

- *Temperature contours of metal hydride bed and phase change materials during the desorption process*

Figure A2.5 shows the temperature contours of the MH bed and PCM for 250 s, 500 s, 10000 s, 1500 s, and 2000 s after starts the hydrogen desorption process. At 500 s, the minimum MH temperature from case 1 and case 2 is still 543 K, while there is only the top part of MHHS where it has a lower temperature at 543 K for case 3. However, the minimum MH temperature from case 4 is 548 K. At the interface of PCM and MH, the temperature from the MH side is higher, while the temperature from the PCM side is lower for all cases. From this process, the MH is heated up by receiving the heat from PCM while the PCM is cooled down. The PCM temperature, where it is close to the interface, is lower than the melting point for all cases. It should be noted that the PCM temperature at the inner and central areas is higher than the outer side due to the effect of the absorption process, which leads the PCM near the MH to have a higher temperature (refer to Figure A2.2). The higher MH bed temperature is observed when increasing the desorption duration (from 500 s to 5500 s). Similarly, more PCM temperature reduction corresponds to greater desorption time. From all cases, the case with SCHE-CR (case 3 and case 4) has a higher MH temperature compared to the case without SCHE-CR (case 1 and case 2). A significant change in temperature variations is observed from the temperature contours at 7500 s. Focusing on PCM temperature for all cases, there is still heat transferring from the central area of PCM to the outer side of PCM as the PCM temperature at the outer side at 1500 s is higher than at 500 s. This is due to the fact that at the end of the hydrogen absorption process, there is still a portion of the PCM that remains in the solidification state (refer to the liquid fraction of PCM in Figure A2.3). The heat from melting PCM continually flows to solid PCM, causing an increase in PCM temperature at the outer side. This fact is applied to all cases. For case 3 and case 4, the PCM temperature around the middle part of MHHS is higher than other parts due to the higher MH bed temperature around this area, which is caused by the heating HTF and its location. The HTF temperature from the bottom part is higher than the other parts as this part is close to the HTF inlet.

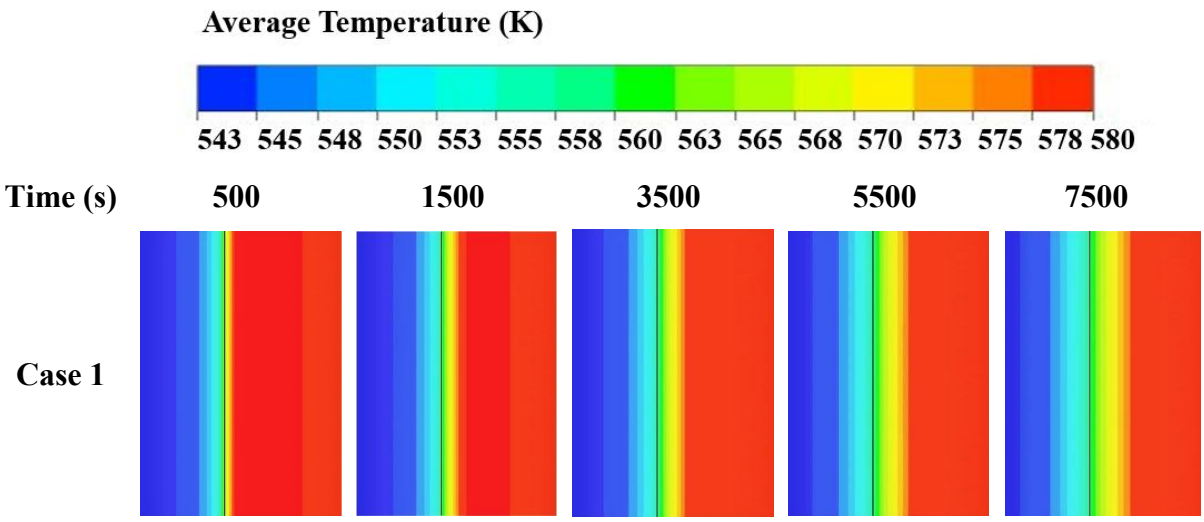

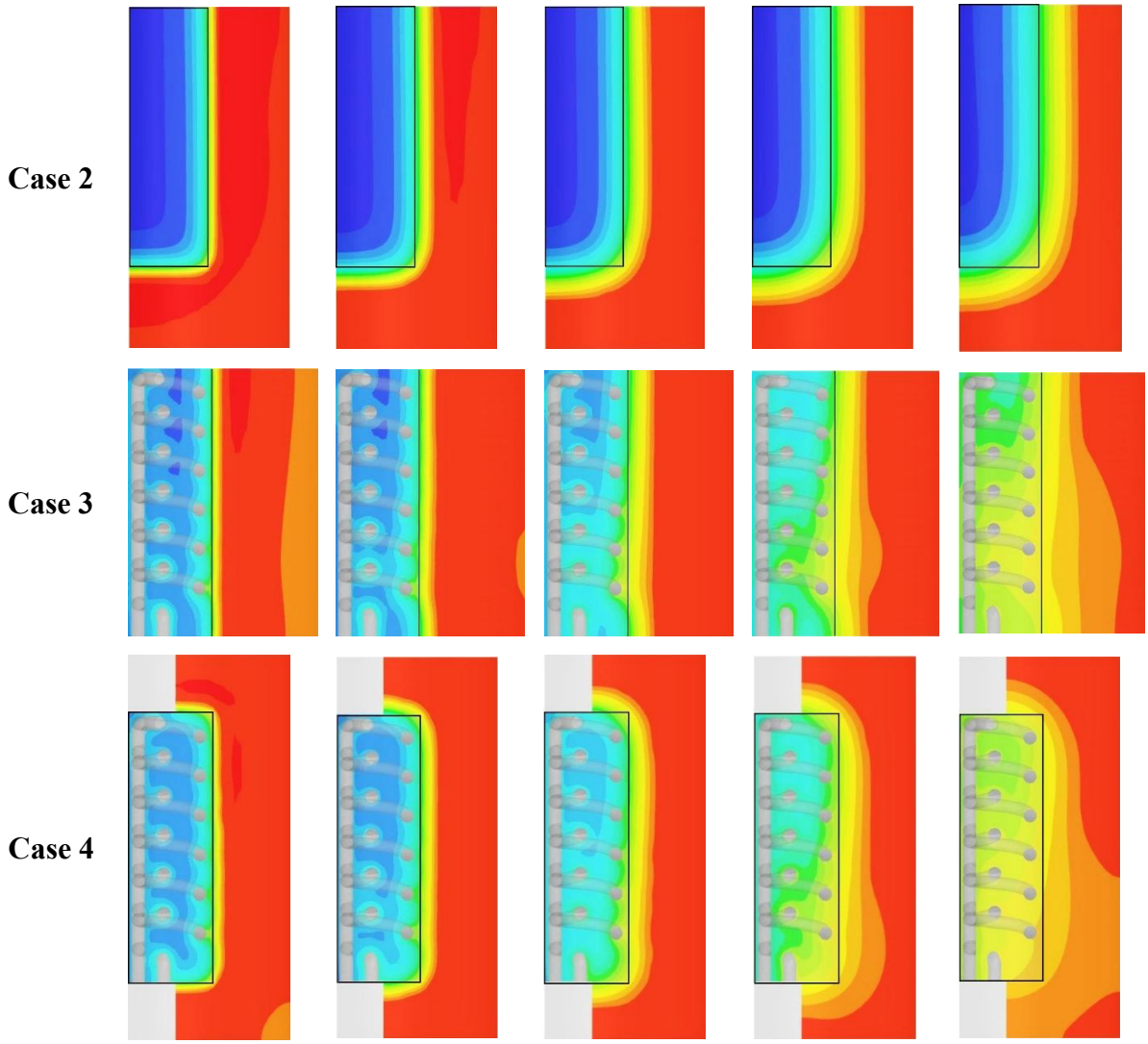

Figure A2.5 Average temperature of MH bed and PCM at 500 s, 1500 s, 3500 s, 5500 s, and 7500 s after starting hydrogen desorption process from case 1 to case 4

- *Liquid fraction contours of phase change materials during the absorption process*

Figure A2.6 presents the liquid fraction contours of the PCM at 250 s, 500 s, 10000 s, 1500 s, and 2000 s after starts the hydrogen desorption process. For all cases, the PCM starts to release the heat and transform from liquid phase to solid phase at the interface between the MH and PCM. More amounts of PCM liquidus are observed around the outer side of PCM at 7500 s compared to at 500 s from case 1 and case 2. Although more PCM solidus is found from the interface side in these cases, the PCM liquidus from the outer side still increases as there is still the heat transferring from the central area of PCM to the outer side of PCM (see temperature contours in Figure A2.5). However, the PCM liquidus from case 1 and case 2 is still higher than case 3 and case 4. This is because the PCM liquidus from case 3 and case 4 is less than case 1 and case 2 from the absorption process. This leads to having only 5-24% of PCM liquidus from case 3 and case 4, while there is still 94% of PCM liquidus from case 1 and case 2 at 7500 s.

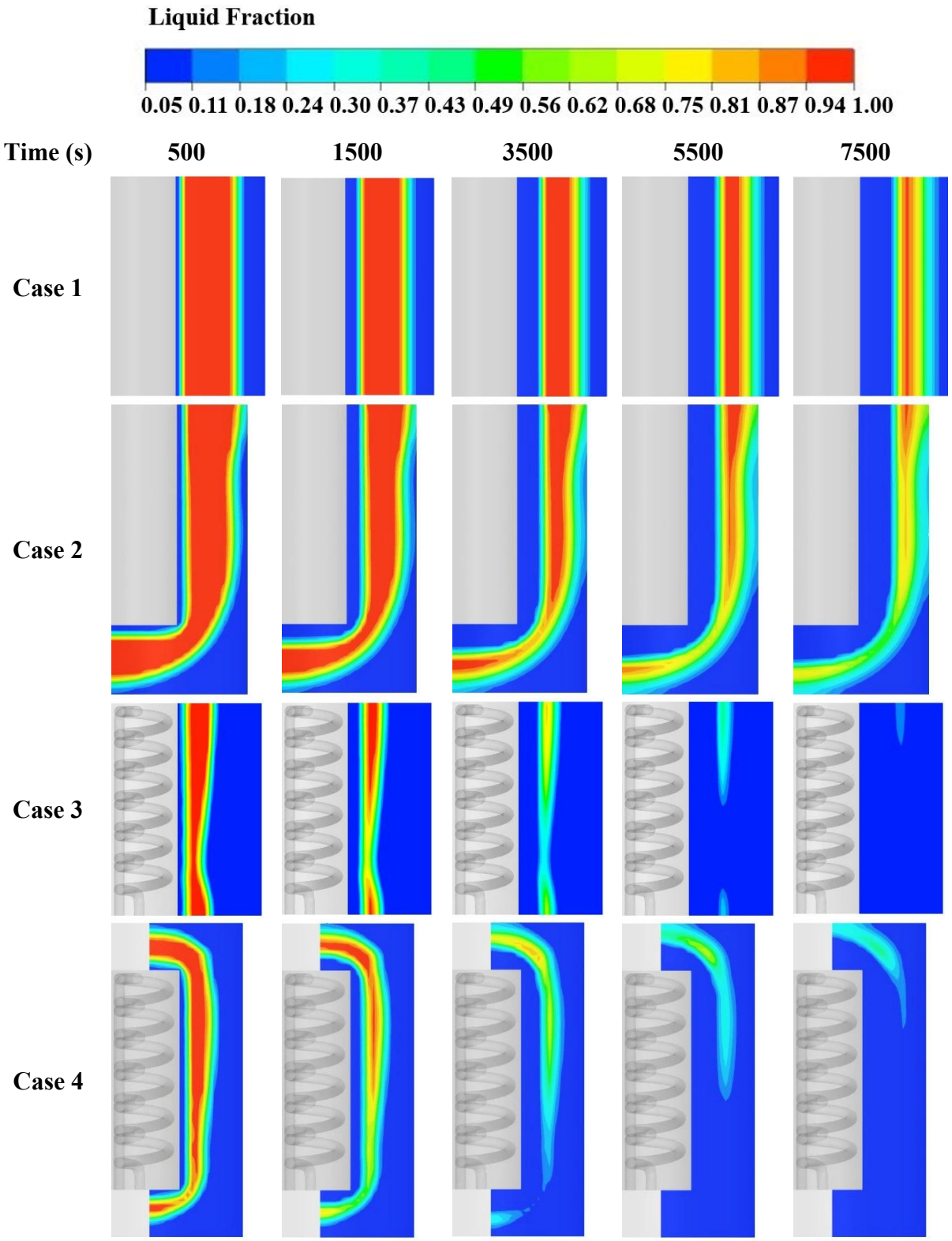

Figure A2.6 Liquid fraction of PCM at 500 s, 1500 s, 3500 s, 5500 s, and 7500 s after starting hydrogen desorption process from case 1 to case 4

- *Hydrogen concentration contours of metal hydride bed during the desorption process*

Figure A2.7 provides the hydrogen concentration contours of the MH bed for 250 s, 500 s, 10000 s, 1500 s, and 2000 s after starts the hydrogen desorption process. The hydrogen concentration from case 3 and case 4 is significantly lower than case 1 and case 2 after the time at 3500 s. The maximum hydrogen concentration in the central area from case 3 and case 4 is 49%, while there is still an 81% of hydrogen concentration in this area from case 1 and case 2. The less hydrogen concentration is also found in most parts of the MH bed for case 3 and case 4 at 5500 s. However, the maximum hydrogen concentration from case 3 is still 24% for most parts, while there is only 11% of the maximum hydrogen concentration from case 4. At 7500 s, the hydrogen concentration from case 4 is less than 5%, while there is still an 11% of hydrogen concentration from some areas at the bottom part for case 3. However, the hydrogen concentration from case 1 and case 2 is mostly 11-75%. It should be noted that the hydrogen concentration at the central area in these two cases is less than in other areas because of the effect of the absorption process. At the end of the absorption process (99% of overall hydrogen concentration), this area has less hydrogen concentration due to the PCM configurations. This results in a lower hydrogen concentration in this area during the hydrogen desorption. The hydrogen concentration at the bottom part of case 2 is still lower than case 1 due to the PCM pool bed configuration.

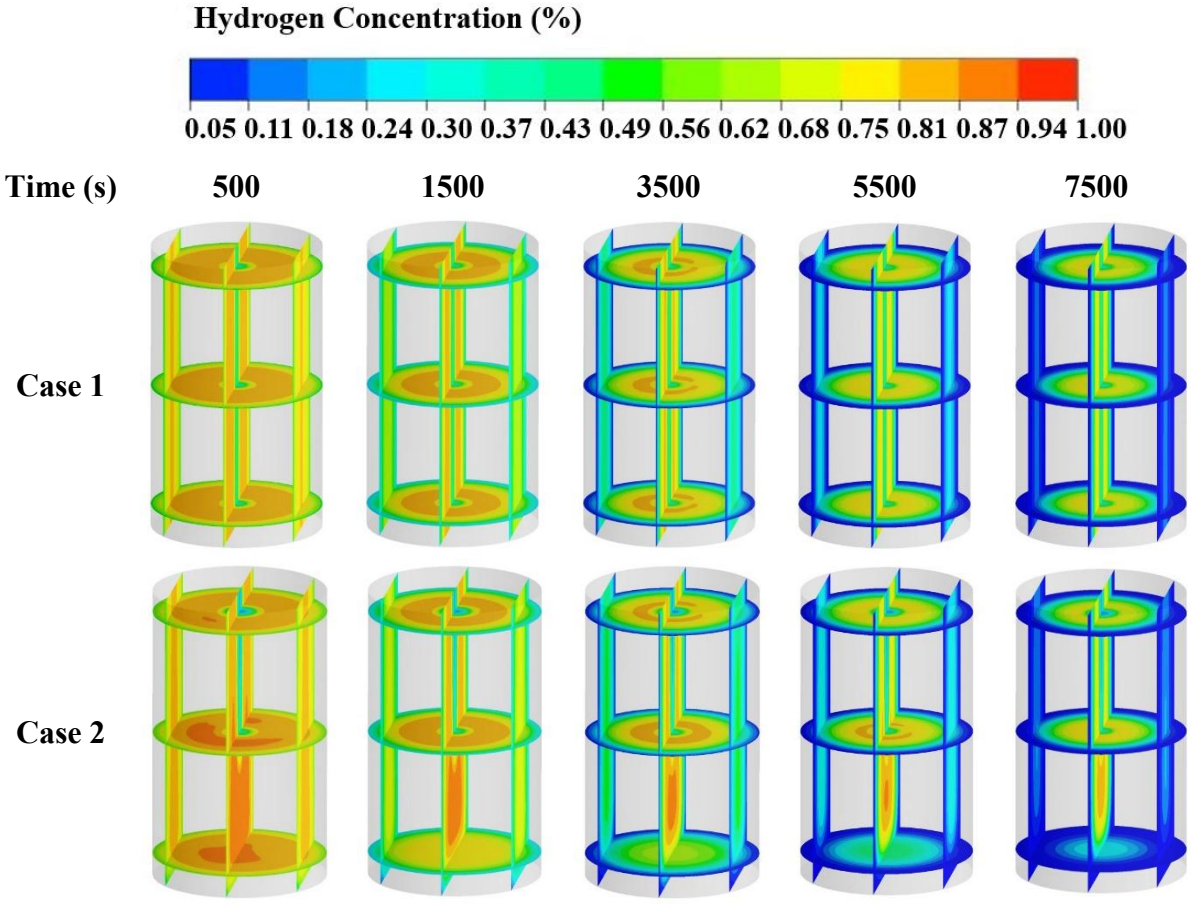

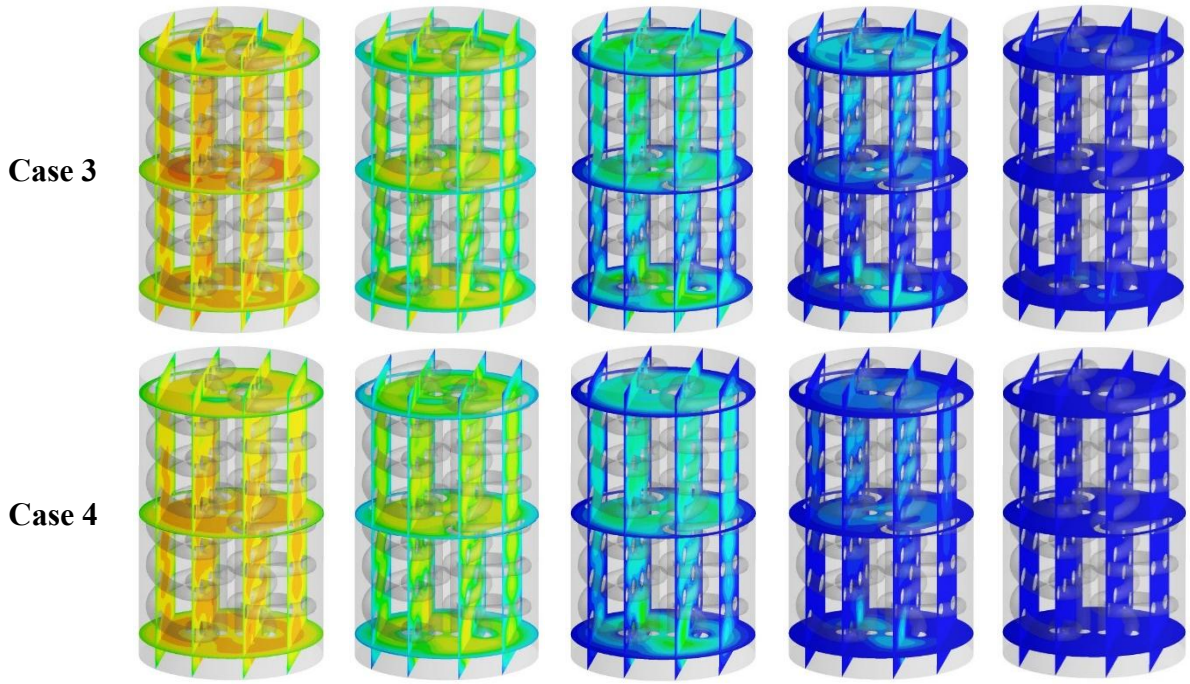

Figure A2.7 Hydrogen concentration at 500 s, 1500 s, 3500 s, 5500 s, and 7500 s after starting hydrogen desorption process from case 1 to case 4